IMPROVEMENT TO THE SURFACE FINISH OF ADDITIVE LAYER MANUFACTURED PARTS MADE BY SELECTIVE LASER MELTING

BY

KAHALID ALRBAEY

A THESIS IN PARTIAL FULFILMENT OF THE REQUIREMENTS FOR

THE DEGREE DOCTOR OF PHILOSOPHY

Submitted to

De Montfort University

2014

Student ID: - P09001899

ABSTRACT

The Selective Laser Melting (SLM) process has been used since the end of last decade for different applications in the industrial sector. The priority of the technique is to produce fully dense and functional metallic parts of very complex design, but it is limited by a few issues such as quality of surface finish and porosity.

The current study focuses on improving the surface finish of parts built on an SLM machine through two different approaches of post processing technique, laser re-melting followed by electropolishing.

In this investigation Renishaw's SLM 125 was employed to produce 3Dimensional (3D) parts by using stainless steel 316L material with powder particle size ranges from 15 to 45 microns. Samples with different inclinations were constructed in order to generate samples with different surface roughness; the parts were measured and inspected for surface finish by measuring *Ra*. The initial surface roughness ranges from 10 to 20µm *Ra.*

Due to the poor surface quality, laser re-melting was implemented as a first stage in order to eliminate the initial surface roughness. Laser re-melting as a post-processing technique was employed for re-melting procedure employing the RECLAIM machine at Manufacturing Technology Centre (MTC) Coventry. Different setups of process were analysed to optimize the parameters for re-melting. The results proved that the best results are conducted with laser energy density ranges between 2160 to 2700 J/cm^2 to give exceptional results of surface roughness of about 1.4 µm±15% *Ra*. In such case it's possible to say that laser re-melting has the capacity to improve surface finish by about 80% compared to the initial surface roughness created by SLM.

In the second stage, improvement was carried out by implementing green process to reduce the waste, pollution and high toxicity using a suitable room temperature ionic liquid (RTLs) as a solution in order to eliminate the secondary surface roughness that comes after re-melting. Physical properties such as shininess and reflectivity were significantly improved, due to the capacity of the process to improve the surface roughness and remove the oxide film created during re-melting. The method proved that the best results were obtained when the specimens were anodically kept at current densities associated with potential ranges between (4 to 5.5 volt), maintained at (40 C°) to give roughness (*Ra*) less than 0, 5µm. These levels of voltage can be facilitated to operate and avoid any passivation of material dissolving, which can lead to pitting of the surface.

ACKNOWLEDGMENT& DEDICATION

First I would like to thank the Department of Technology (Innovation centre) at De Montfort University that gave me the opportunity to obtain a degree of PhD of Technology.

Second, I would like to offer my most sincere thanks and gratitude to my supervisors Dr. Adam Moroz, Dr. Yong Sun and Prof. David Wimpenny for their guidance, constructive remarks, and valuable suggestions from which I benefited and learned throughout the stages of this project. Also special thanks go to the Manufacturing Technology Centre (MTC) and Chemistry department at Leicester University for their assistance.

Finally, I dedicate this wok to

- *My father and my mother*
- *My wife and my children*
- *My brothers and my sisters*

TABLE OF CONTENTS

LIST OF FIGUERS

LIST OF TABLES

ABBREVIATION

AFM	**Atomic Force Microscope**
AM	**Additive manufacture**
CAD	**Computer- Aided Design**
CAM	**Computer Aided Manufacturing**
CAM	**Computer- Aided Manufacture**
CNC	**Computer numerical control**
DES	**Deep eutectic solvent**
DMLS	**Direct metal laser sintering**
EBM	**Electron Beam Melting**
ECP	**Electro chemical polishing**
ECP	**Electro chemical process**
EDX	**Electron Dispersive X-ray**
EOS	**Electro optical system**
GPES	**General Purpose Electrochemical System**
HCF	**High cycle fatigue**
HIP	**Hot Isostatic Pressing**
ILs	**Ionic Liquids**
LM	**Laser Melting**
LS	**Laser Sintering**
MPIF	**Metal powder industry federation**
MTT	**Manufacture technology group**
PBF	**Powder bed fusion**
RM	**Rapid manufacture**
RP	**Rapid Prototyping**
RRM	**Rapid Response to Manufacturing**
RTILs	**Room temperature ionic liquids**
SEM	**Scan Electron Microscope**
SLM	**Selective Laser Melting**
SLP	**Selective laser polishing**
SLR	**Selective Laser Re-melting**
STL	**Standard Triangulation Language**
TGM	**Temperature gradient method**
UV	**Ultraviolet**
VP	**Virtual Prototype**
AMF	**Additive manufacture file format**

1.0. Introduction

1.1 Background of the project

Additive Manufacturing (AM) has the ability to produce complex parts direct from Computer Aided Design (CAD) information without the aid of tooling. The method was basically used as a technique for making models required for design verification and marketing purposes however, it is increasingly being used for producing end use parts.

According to Wohler's Report of 2010 & 2012, the AM sector is estimated to be worth $1.2 billion per year growing over the previous years at about 14% and showed impressive growth in 2011 which was about 26.5% over 2010, to be worth $1.7 billion. [1, 2] Generally, AM of metal parts is divided into laser cladding (Directed Energy Deposition in the F42 classification) and powder bed methods. Laser cladding is basically the melting of a stream of powder using laser power and is used to repair worn out parts such as gas turbine blades etc. In powder bed processes a layer of powder is selectively melted using energy from either an electron or laser beam and the remaining powder is used as support for the part. Metal powder bed processes are still in their infancy because of the recent development of high power fibre lasers. Arcam produces powder bed machines that use an electron beam which provides a faster production rate but at the expense of surface finish.

There are four major SLM technology providers, namely MTT technologies which is now Renishaw, Concept Laser, Phenix Systems and EOS. EOS has the largest market share (~50% of annual sales) and other companies roughly share the remainder of the market. [1]

Although, AM technology has the ability to produce strong and durable parts direct from CAD data without tooling, but the major disadvantage is that the manufactured parts have steps in their surface texture. In addition SLM, used for producing metallic parts, has a granular surface finish and residual porosity which may cause significant problems in some applications where high strength is required. In order to overcome these problems several approaches can be used, relating to part set-up, starting from CAD programme, controlling and monitoring machine parameters (in-process techniques), or using post-processing methods as sub-stage to improve and enhance the surface quality of the part such as mechanical, electrochemical and thermal methods. [3]

1.2 The current gap of knowledge

AM has been utilized in various industrial fields such as medical, aerospace, automotive and in research centres. AM methods are used to manufacture parts of complex shapes directly from CAD data, which are fully dense with generally good mechanical properties, but the processes still suffer from some drawbacks such as insufficient surface finish, porosity, dendritic surfaces and thermal cracks. The degradation caused by the defects is probably dependant on laser parameters and entrapment of gas shielding during the process, leading to variability of powder bed melting, solidification and generating more residual stress. It is worth mentioning that all AM techniques develop parts with different surface roughness (*Ra*) ranging from 10 to 30µm based on the machine parameters, CAD model orientation and metal powder specifications. Several efforts have been made in this field (AM) from in-process (machine parameters setup), to implementing any finishing techniques (post-processing) to obtain the final finish. The results from these techniques have shown significant improvement compared with the initial surface and the best results of surface roughness (*Ra*) about 1 to 1.25µm have been achieved. However, these surfaces need further improvement due to the necessity of mechanical properties (costumes need). [4 - 7]

1.3 Aims and objectives

The study of surface finish and its characterisation are very vital for SLM parts due to their significant influence on the mechanical properties when under load. The mechanical failure starts first from the surface affected, during exposure to dynamic stress. [4]

The aim of this project is a novel two-stage combination: to employ laser re-melting as a precursor to electropolishing. It was expected to be possible to achieve the desired surface finish and maintain the tolerance accuracy of parts in (Stainless Steel 316L) produced by SLM 125.

The study focuses on the follows objectives

1- General literature survey on (SLM) to achieve a comprehensive knowledge about the laser melting process and its applications.
2- To evaluate current post-processing techniques used to improve surface finish, particularly those available on the market today.
3- Conduct laboratory trials to analyse the characteristics of SLM parts such as surface roughness, surface topography, density and identify the most common parameters that cause poor surface finish during the build process (in-process parameters). Also to ensure that the machine output is repeatable.
4- The study will focus on the use of post processing methods; specifically those that are suitable for automation and assess the efficacy of the methods to improve surface finish as well as comparing these results with those obtained from in-process methods.
5- To address the limitations of the current methods and contribute to the efficiency of these methods to improve surface roughness with less harmful effects.
6- To employ different surface assessment techniques, such as stylus profilometer, digital microscope and scanning electron microscope (SEM) to assess the surface roughness and morphologies as well.

1.4 Thesis structure

This section lays out the thesis in a progressive manner. In chapter one the background has been demonstrated, taking in to consideration the current gap of knowledge and the aims and objectives of the project.

A review of metal powder AM methods, in particular Selective Laser Melting (SLM) taking into consideration the basic principle of this process, applications, advantages, machine providers, component quality (part characterisation) and cost effects are demonstrated in chapter two.

The stages of surface finish improvement (in-processing and post-processing) were taken into the same consideration and are presented in chapters three and four respectively. The methodology (outline of experiment), materials used and equipment are presented in chapter five.

In chapter six some experiments were undertaken to analyse the part characteristics after manufacture in order to ensure that the machine output is repeatable.

In chapter seven laser re-melting procedure (as post-processing), was obtained, in order to optimize parameters and evaluate the capabilities of the optimal parameters to overcome any dendrite connected with SLM manufactured parts. Also the selection of optimal parameters for good surface finish and topography are demonstrated in this chapter by (DOE) analysis.

Chapter eight has been divided in two sections, the first one focuses on electropolishing as a second approach after re-melting, in order to eliminate the secondary surface roughness and improve the physical and mechanical properties of SLM parts. The second section focuses on generating reverse bending fatigue tests, in order to assess the fatigue life of SLM components subjected in two different stages of surface improvement and compare this with the initial results.

Chapter nine is the overall conclusion and recommendation for future work.

1.5 Contribution to science

This work is the first systematic study of the use of laser re-melting and electropolishing in combination for the improvement of the surface texture of additively manufactured parts and specifically stainless steel 316L parts made by SLM. Unlike other research to date, the re-melting was conducted on a dedicated machine as opposed to using the SLM machine that made the parts, which allowed more control over the process variables.

The electropolishing process used an organic deep eutectic ionic electrolyte (Ethaline) which has not been used before with additively manufactured parts. Ethaline is significantly better for the environment than the electrolytes currently used in industry, such as sulphuric and phosphoric acids. Furthermore, no previous literature on combining laser re-melting and electropolishing for surface texture improvement was found by the author.

In this research, the use of laser re-melting as a post-processing technique has shown the capability to improve the surface texture of stainless steel parts. The microstructure (dendrites such as balling, agglomeration, waviness and shrinkage cavities, open and closed pores) can be substantially modified, when the optimal parameters are employed. An improvement of up to 80% was obtained for an average roughness (*Ra*) in comparison to the original SLM part. In addition, external and internal (open and closed) porosity was completely eliminated, leaving the melting zone with almost 100% density. The results also show that further improvement of the surface texture can be obtained by electropolishing following re-melting. The final roughness can be optimised by changing voltage and temperature. Also, the residual oxide film formed during the re-melting process can be removed. The measured improvement of the parts' roughness by the electropolishing process alone (after re-melting) was approximately 65%.

Overall, the combination of laser re-melting followed by electropolishing improved of the parts' surface texture by up to 95% compared to the as-built condition. This was evidenced by the measured improvement in the fatigue life of the samples.

This work also showed that DOE optimisation software can be useful for design, analysis and optimization of parameters for both re-melting and electropolishing processes and also two models have been developed and written up based on the DOE analysed results. Furthermore, the low values obtained for average roughness are achieved with the help of optimization, using statistical data.

2.0. Additive manufacture

2.1 Definition of Additive Manufacturing

Additive manufacturing is an overall term that is used to describe all the technologies that are used to manufacture parts by the addition of material layer-by-layer to obtain the final model, as opposed to the traditional subtractive methods or processes that involve the removal of material [8].

In the past, AM technology was limited to the manufacturing of prototypes and models and hence the term Rapid Prototyping (RP) was coined as the original generic term for AM. The advance of processes, machine hardware and materials meant that the parts could be developed with mechanical properties which permit functional application.

This has led to the adoption of Rapid Manufacturing (RM), a term used to show the differences between the fully functional characteristics of the sections being manufactured from the prototypes and RP models. Additive Manufacturing is the overall term that is used to describe Rapid Manufacturing and Rapid Prototyping [9]. The combination of this technology with advanced CAD packages allows design freedoms that are not available with other processes. Several operations are reduced while the overall manufacturing efficiency is increased. Complex models with sophisticated shapes can be fabricated (up to a certain size of model) compared to conventional manufacturing methods, such as conformal cooling channels in injection molds [10 -12].

2.2 Basic principle of Additive Manufacturing

The AM technologies develop parts through polymerization, sintering or fusion of material in predetermined layers that do not require tools as opposed to the conventional subtractive processes in which material is removed from the stock base. Utilization of AM enables the development of geometries that are nearly impossible to be produced by conventional methods such as forming and machining. The process is independent of predetermined tool paths and internal part details, undercuts or draft angles can be designed and developed. The layers of AM parts are developed by specialist CAD software through the slicing of the STL file data and sent to the AM machine to obtain the final product. All the AM systems utilize this principle; however, the layer thickness is dependent on the system and the parameters used. Commercially used machine for various applications utilize layers with a thickness of 16 to 200μm [13]. In all the AM processes, the layers are clearly visible on the part surface, which influences the quality

of the surface finish section, it is known as the staircase effect and it is a relationship between the orientation of the surface and the thickness of the layer. As a result, a thinner layer helps obtain a smooth surface quality[14]. **Figure 2-1** and **Figure 2-2** illustrate the basic principle of this technique.

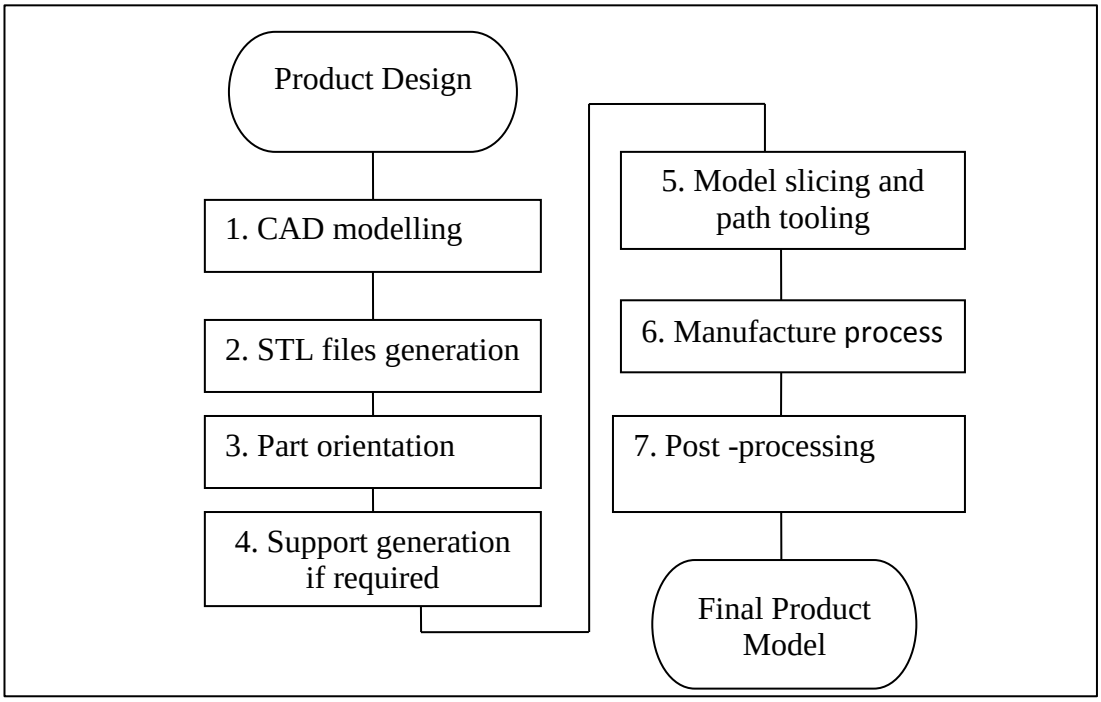

Figure 2-1: Flow chart diagram(RP & RM).[3]

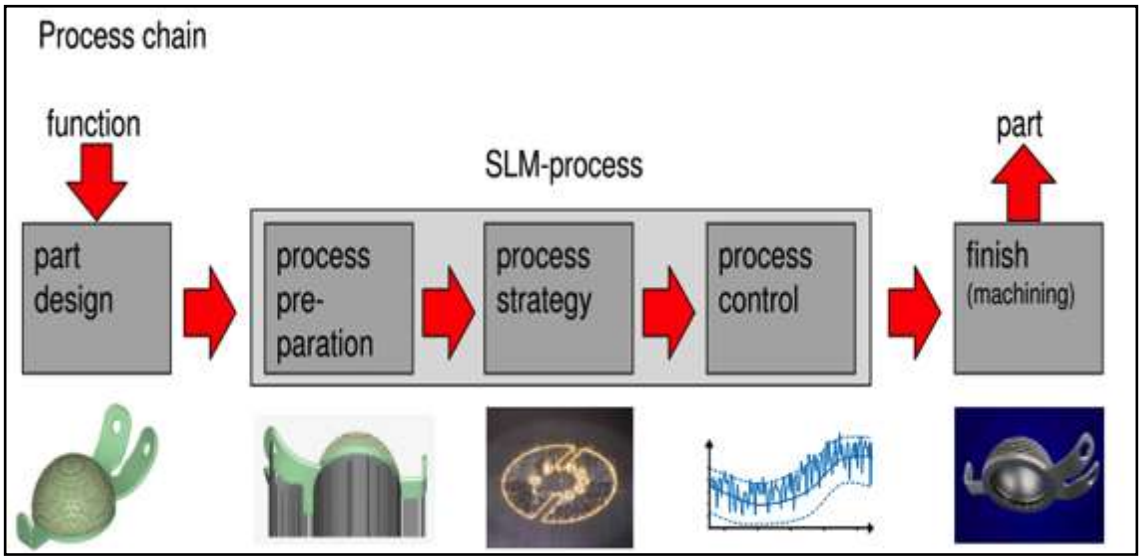

Figure 2-2: Chain diagram of rapid manufacture.[13]

2.3 Classification of Additive Manufacturing According to Material used

There are many types of AM classification; the most significant of them can be classified based on the material used, such as polymers, ceramic and metal etc. The form of the material used can be divided into three categories as are shown below:

1- Liquid-based systems, such as Stereolithography (SLA).
2- Powder-based systems, such as Selective Laser Sintering (SLS/M) and EBM).
3- Solid-based systems, such as (Fused Deposition Modelling). [15]

The worth mention there are more than 30 techniques for additive manufacturing have been commercialized during the past of 25 years, to be used as techniques to produce direct parts by different material, but all build the objective form with the same principle, layer by layer. [16] **Figure 2-3** shows the classification of metallic rapid manufacture processes.

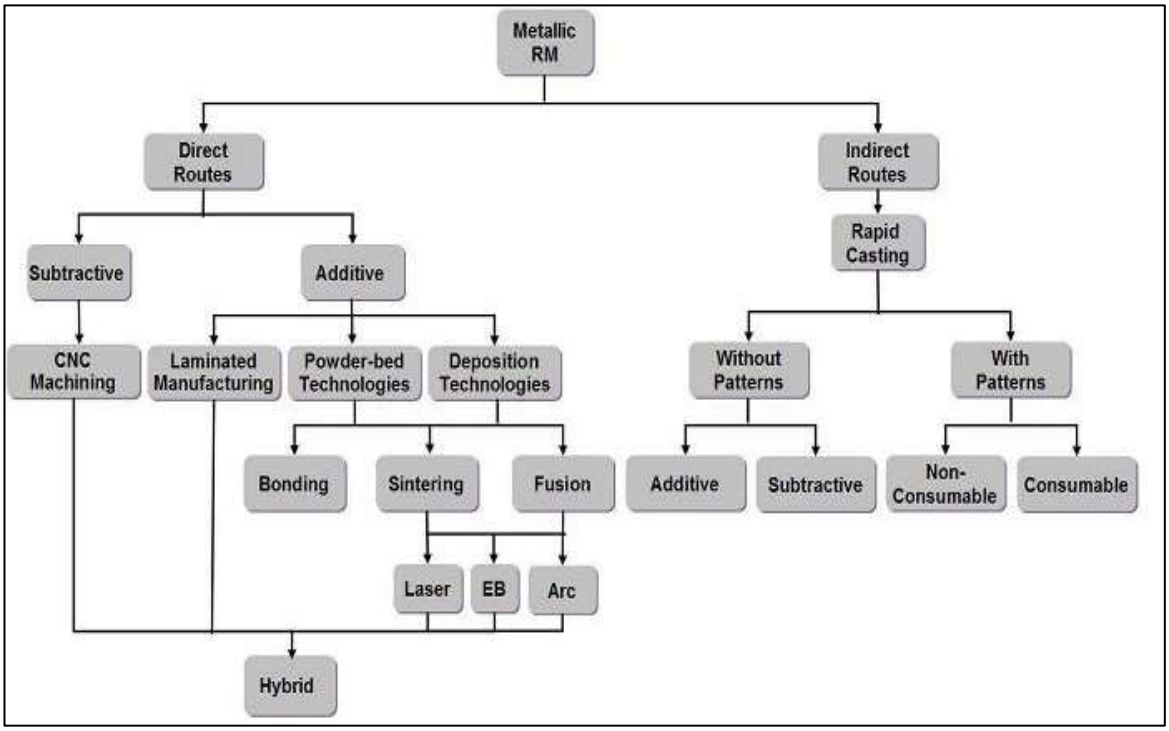

Figure 2-3: Classification of metallic rapid manufacture. [17]

This work will focus on the metal powder bed based system and specifically on selective laser melting as a main technique in order to produce fully dense parts.

2.4 Selective Laser Melting (SLM)

2.4.1 SLM background

The market trend is for shorter and shorter product life cycles with increasing technological complexity. The success of a company can only be made safe if they can respond quickly to the ever changing needs of the customer by using innovative technologies. This way, companies can have an advantage over their competitors by offering a wide range of goods with high performance. Since the end of the last century, a new generation of customers have had more influence on the organizations to do more research in technology development and practice, thereby improving their business processes and their manufacturing development cycle.

This has resulted in factories being forced to apply a new philosophy of engineering called the Rapid Response to Manufacturing (RRM). This technique uses previously designed products to enhance the development of new ones. The system of RRM was established by utilizing technologies such as CAD-based modelling and both together form an integrated system of direct production, involving product and process management. Direct production uses rapid manufacturing technologies for prototyping and tooling and for testing the design and building the parts quickly. [18]

Among the RRM technologies are Rapid Prototyping (RP) and Virtual Prototyping (VP) which are rapidly changing the way products are designed. Rapid Prototyping technology involves a range of processes, which can develop parts directly from CAD models with very little human interaction. Hence the designers can create real and complex prototypes in an efficient and simple way which allows them to assess the component's fit and functions early in the design and development process.

This has the benefit of catching errors before they have a big impact on product lead times and costs. [19]

Like other RP technologies, selective laser sintering (SLS) technology was developed to provide a prototype technique to reduce the cost and time of the product development cycle. It involves building the object layer-by-layer by selectively sintering or partially melting a powder bed using laser energy.

Different powder binding mechanisms are necessary for obtaining high density, for use as functional prototypes, or for bridge tooling. Thus, SLM was developed as one of the additive manufacturing technologies, which employs a high power fibre laser to scan specific area of fine powder through a series of 2D (two-dimensional) tracks to generate 3D parts direct from 3D CAD data. [20]

In 1999, the first SLM machine was produced by Fockele and Schwarze (F&S) in Germany, in order to produce full dense metal powder parts. This system was developed with cooperation of the institute of laser technology (Fraunhofer). Later (F&S) teamed up with the manufacturing technology group (MTT) in order to commercialize the first direct powder metal system called the SLM Realizer 250 in 2004. Subsequently in 2008 MTT announced distribution of their products in America, and also revealed their new SLM 125 and SLM 250 in the UK instead of Germany. Apart from MTT, several other companies have been involved in this scope of technology and commercialised several types of SLM machine such as Concept Laser, Phenix Systems (now owned by 3DS) and EOS. [1, 21]

2.4.2 SLM process

Generally, the SLM machine works by first distributing a metal powder on a base platform. A laser beam follows an outline so only the required powder is melted. The platform is lowered, to allow distribution of a new layer of powder to be ready for scanning. The laser beam again traces another outline and also joins the second layer to the first. This procedure is repeated until the final model is constructed. The following **Figure 2-4** clarifies the entire process to create a 3D model part. [22]

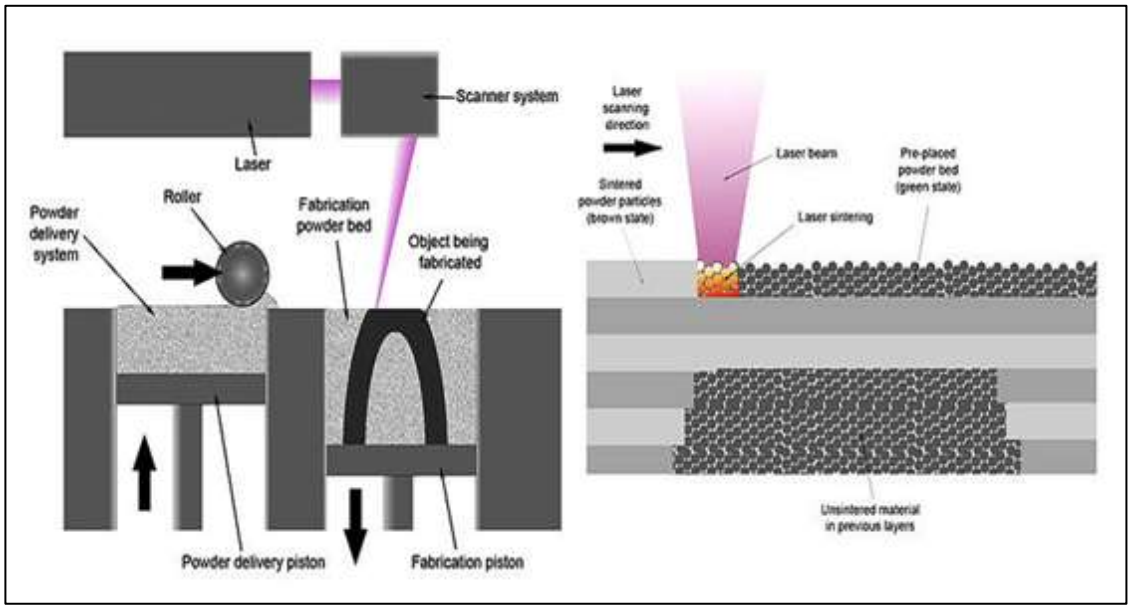

Figure 2-4: Selective laser melting system schematic.

The work-piece has to be enclosed in a vacuum chamber; the vacuum chamber vacuumed the air first and followed by high purity argon during laser processing. This helps to protect the molten metal and initial powder against oxidisation. `

By use of SLM it is possible to manufacture metal parts that are almost fully dense. Some difficulties are normally encountered in the control of the factors in this process and if not handled well they can lead to some defects in and on the part's surface. [23, 14]

However, good control of these factors can give rapid manufacturing metallic parts that are quite complex for application by end-users. Such materials will not require post-processing and may need very little treatment of their surface.

A broad variety of material grades can be used in the process. Numerous companies have produced commercially available materials such as 316L stainless steel, Ti-6Al-4V, tool steel, aluminium, as well as cobalt-chromium related alloys. The characteristics of the materials differ but still the process is the same. [24]

2.4.3 Advantages of SLM

There are many merits that come with the use of SLM technology. Most of these advantages, such as the following, are a result of the process itself:

- Easy and a fully automatic production procedure.
- Avoids the distortion /stresses associated with processing of parts in furnaces.
- Ability to create light parts with a function of complex geometric structures such as internal curved channels, which are not possible to be produced by conventional machining.
- SLM uses a relatively efficient fibre laser hence being energy-efficient and in turn cost effective.
- Finally, parts have the ability to be finished with normal or conventional techniques applied in polishing.

In brief, the advantages of this technology might be summarized in the following main points which are:

- Resource savings; reduction in time, waste, labour and energy. This technique is efficient because it uses the required amount of material instead of a solid block of material as with the conventional process in which the block is then machined to obtain the final object: the amount of wastage is approximately (80-90)%. On

the other hand, by utilizing AM it is possible to produce parts with about 10% of metal wastage.

- Support tooling for manufacturing is not required as with conventional techniques.
- Eco-design optimization: AM plays a significant role in decreasing the causes of pollution, because this technology utilizes natural resources in order to protect the environment against harmful materials, for instance toxic chemical reactions and vapour are reduced as well. [25 - 27]

The advancements in these technologies have made AM be of great use in many industries including fabrications, biomedical, and repairs of metallic forms of components, since they have the capacity to deposit metal material on set substrates.

2.4.4 Applications of SLM

The SLM process has been used in many applications in industry such as production of tooling, short-run components, and general functional prototypes. Because it allows parts to be created (through a powder base) instead of by subtraction, the waste to develop the final object is reduced. So, the process has been applied in:

- Medical implants, by using biocompatible materials to bond with the soft tissues with proper strength.
- Aerospace and automotive applications where the lightness and strength are considered important.
- Restorations in dental operations.
- Tooling of dies in combination with cooling channels.
- General industrial applications. [13]

The suitability of these applications to SLM methods comes from various attributes, namely medium to very high levels of complexities in terms of geometries accompanied by low quantity requirements. For instance, freedoms in geometrical structures and mass customization have given very excellent prospects when it comes to medically related applications such as implants that are individualized, or bone scaffolds and prostheses involving dental operations. [28 - 30]

2.4.5 Machine providers

There are many technical companies worldwide which work in the field of (RM) as technical providers, based on SLM technologies. The most common of them are as shown in the **Table 2:1**.

Company	Machines	Maximum envelope (mm)	Maximum build rate (cm^3/hr)	Layer thickness (µm)	Laser type	Laser power (Watt)	Beam focus diameter (µm)
EOS	M 270	250x250x215	20	20-100	Fibre	200	100-500
	M 280	250x250x235	28	20-100	Fibre	200-400	100-500
Renishaw	SLM 125	125x125x125	20	20-100	Fibre	100-200	35
	SLM250	250x250x230	20	20-100	Fibre	200-400	70
Phenix systems (now part of 3DS)	PM100	100x100x80		20-100	Fibre	100-500	
	PM250	300x250x250		20-100	Fibre	100-500	
Concept Laser	M1	250x250x250	20	20-80	Fibre		70-200
	M2	250x250x280	20	20-50	Fibre		70-200
	M3	300x350x300	20	20-80	Fibre	100-200	70-200

Table 2:1: Details of different SLM machines.

2.4.6 Materials available

Materials for additive manufacturing have presented great opportunities and a significant challenge. In the past, AM materials have proven not satisfactory for end use products due to lack of suitable material grades.

This challenge is opening the door to development of several types of material grades and alloys, to be providing a solution to control parts' properties such as porosity, surface finish and mechanical properties. [1]

Nowadays enormous volumes of material can be processed by SLS/M, but the actual numbers of these processed materials are limited. Applications using similar materials have increased while the types of materials processed are roughly constant.

Thus, almost of the materials are developed specifically to be oriented for specific applications. [16] Many materials are offered from different companies of manufacturing systems to be used to gain the final part features according to process parameters steeps. It is worth mentioning that each company has its own list of material powders which can be summarised as shown in **Table 2:2.**

Material	Available from			
	EOS	**Renishaw**	**Phenix**	**Concept**
Aluminium				
AlSi10Mg	√			
AlSi12				√
Cobalt Chrome, various	√	√		√
Nickel-Bronze composite	√			
Stainless Steel 316L	√	√	√	√
Steels, Various	√	√	√	√
Ti6Al4V	√	√		√
Titanium other		√		√
Gold 18 carat	√			
Inconels, various	√	√		√
Precious metals (unspecified)			√	
Ferrous alloys (unspecified)			√	
Super alloys (unspecified)			√	

Table 2:2 : Materials available for SLM

Information available online from. [31-34]

2.5 Component quality (characterization of SLM parts)

This section demonstrates that additive manufacturing techniques can produce fully functional parts with controlled microstructure, in order to get the desired properties and grain structure. Investigation of SLM parts, microstructural characterisation and links to the material characteristics have been among the top subjects of intense research in most of the additive manufacturing groups.

2.5.1 Surface roughness and quality

In additive manufacturing, surface quality is considered as one of the foremost disadvantages since parts are produced with high surface roughness. Apart from this issue, surface accuracy is one of the other concerns with costumer. However, there are a number of techniques available on the market to improve the surface texture.

In AM surface roughness is mostly a result of the parameters set by the machine operator during the fabrication process and the powder specification, according to Senthilkumaran and co-authors. Also has recommended that the SLM process and other additive manufacture techniques have an extensive range of parameters that can be adjusted and controlled by the operator such as laser power, powder characterisation, layer thickness, scan speed, hatch spacing and environmental conditions. [5]

In recent years many studies have been carried out in this field. However, the ability to produce acceptable surface quality is still considered as one of drawbacks of this process. Researchers have noted that utilizing fine particles powder results in better surface finish quality and density results compared to coarse powder. In all cases fine powder is very significant factor which is required in order to enhance part properties such as surface quality, mechanical strength and density. [35 - 37]

Also Contuzzi [38] has studied the capability of the SLM process and its performance for building small feature parts. The results showed that the process has good accuracy for features that have dimensions over 0.4mm, while the dimensional error increases with decreased the value of dimension below 0.4mm because it is influence by laser spot diameter, scanning strategy and the range powder particle size.

Campanelli [20] has reported that the effect of beam spot size on the ability to build small features and came to the conclusion that good accuracy for small feature size (less than 0.3 mm) is achieved with a beam diameter of 20μm. Thus, the study presents that the efficiency of building accurate small feature sizes is related to the beam diameter rather than the material particle size or its specification.

The accuracy of surface and thin walled features are very vital, especially with some applications such as aerospace, automotive, and medical implants because of the weight effect and the mechanical properties required. Research has been done by Thomas [39], on small thin walls ranging between 0.2 and 0.4mm. The results show that the accuracy of the wall is dependent on the material particle size, beam diameter (spot size) and scanning strategy.

2.5.1.1 Surface roughness effect on fatigue life

Surface roughness parameters describe all the surface texture features in terms of various parameters. The most commonly used parameter is the arithmetic average roughness (*Ra*), which is also referred to as the centre line through the given sample length. Among other parameters are the average summation of the highest five peaks and lowest valleys through the cut length (*Rz*) and (*Rt*) which is the distance between the lowest valley and highest peak through the cut length. [40, 41]

Generally fatigue behaviour has been proven to vary under the varying surface finishes for traditional materials, but for additive manufacture the behaviour is still not fully known due to the process variables. For instance, localised surface scale defects are usually found with forged metals. These dendrites and the increase in the surface roughness can lead to rapidity of fatigue failure, specifically in the high cycle fatigue (HCF) region. In the low cycle fatigue regions, surface roughness has less effect. Also the results of heat treatment on the forged parts may facilitate a reduction of the hardness and increase in fatigue life.

The fatigue results of as-forged surface finish will be improved through surface cleaning treatments such as sand blasting and vapour blasting. These techniques will remove scale defects along with some of the decarburized layers to improve the surface properties. In some case, a compressive residual stress will also be induced at the surface which is recommended in some cases, especially for fatigue application.

The literature related to the effects of the machined surface topography on fatigue life was reviewed by Novovic [42] and co-author who studied various roughness parameters. Their study found that the most commonly applied parameter was *Ra* in describing the fatigue behaviour of the material. But specimens with the same *Ra* value showed fatigue results with a typical 20% scatter. It was hence suggested that the *Rt* and *Rz* should be preferred in comparison to *Ra*, when determining the fatigue performance.

A comparison study was done by Spierings and co-authors, to compare the behaviour of conventional materials and SLM fabricated materials under dynamic fatigue testing. The results demonstrated that the fatigue life for SLM SS316L samples is about 25% less than that of conventional materials at lower stress, even under differing surface conditions for the two tests. Also the endurance limits for SLM samples were demonstrated to be 20% lower than conventional materials at lower stress. At higher stress (higher amplitudes) the materials showed a similar lifetime. [43]

2.5.2 Density issue

Density is another significant factor to look at in the SLM additive manufacturing process. It is considered as a major factor on parts mechanical properties. [4] Although the main objective of SLM is to obtain fully dense functional parts, it is difficult to achieve because of the interaction of parameters during the fabrication process and also because the mechanical pressure used in moulding (which helps remove porosities) is absent in SLM. [4, 44]

The mechanical properties of the metal component are significantly influenced by the part density which consequently affects the performance of the object according to Morgan and co-authors [45]. In the SLM process, gas bubbles can be located inside the part during the layer construction and solidification process. At the end, the porosity can be observed in the final part which is a biggest challenge than with conventional methods such as die casting. In fact if the laser energy is insufficient to melt the deposited layer completely, the region will be weaker and have voids. Research has found that rough surfaces can be caused by gas entrapment when a new layer is deposited. [46]

Kruth [4] and co-authors have suggested that the usual porosity of SLM components is approximately 0.77% while improvements by re-melting obtain components with a porosity of 0.032%. Thus, laser re-melting plays a significant rule in reduction of porosity in SLM components as well as helping to lower surface roughness and residual stress, demonstrating a positive effect on the part properties. [4]

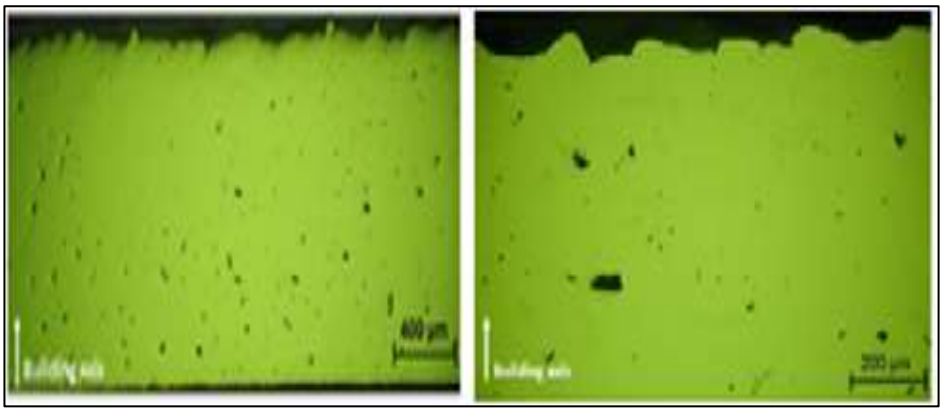

Figure 2-5: Cross-section of a SLM part magnified by 40X and 100X. [4]

Figure 2-5 shows a cross-section of an SLM part produced from stainless steel powder observed using a microscope. All the black spots in the micrograph show non-homogeneously distributed pores or holes, produced during the SLM process.

Porosity is a very significant issue with SLM parts; post processing techniques like re-melting may be required to get rid of porosity issues caused by many factors like laser beam density and environmental conditions etc.

Also, the rapid cooling at room temperature associated with powder additive manufacture techniques is reported as another key factor causing an increase in the porosity in SLM components. [47, 48]

Hot Isostatic Pressing (HIP) is a method which is used to reduce the porosity in ceramics and metal casting, and this method can also be used on SLM parts, but it will not remove open porosities on the surface.

Another method is impregnation with another metal that has a lower melting point to impregnate the base one for a specific purpose such as improved mechanical properties and reduced surface roughness. [49, 50]

2.5.3 Mechanical properties

The mechanical properties obtained in parts made by SLM techniques are currently being examined by many researchers worldwide. In fact, the static load capacity characteristics of layer manufactured parts such as tensile strength, hardness and elongation are well understood and published. Kruth [37] and co-authors have concluded that SLM part properties are comparable to those of bulk materials, apart from properties like ductility which is very low in SLM manufactured parts. Also it has been reported that bulk materials are tougher than SLM parts. Lower toughness in additive manufactured parts is caused by the presence of impurities, of oxygen in the build chamber and the lack of pressure, which cause porosities, especially with reactive materials such as titanium alloys. [37]

It has been identified that the mechanical properties of AM technology are not only determined by the composition of the alloy, but also depend on the number of defects that are created by the process and its parameters during the build.

Thus, in terms of mechanical characteristics a lot of issues remain to be addressed. A typical example is fatigue properties at high temperature which demonstrate the relation between the microstructure of the component and its mechanical properties. [37]

Wang [51] and co-authors analysed the effects of laser parameters on the features shrinkage during the SLS process. They found out that the percentage of shrinkage is increased, by decreasing hatch spacing and scanning speed. On the other hand, shrinkage decreases when the part temperature or layer thickens increase. Also, beam offset, positioning errors in hatching and the inertia of the scanning mirror are found to be causes of shrinkage problems but part orientation and exposure strategies can influence whether the correct size is produced. [51]

The mechanical properties of SLM parts are expected to be non-homogenous, because the parts built by SLM are influenced by many adjacent melted tracks and melted layers on top of each other. The strength properties of SLM parts depend on the solidification microstructure, whereas the good solidification of parts depends on the local solidification in the metal component. [52] Another researcher proposed that significant thermal stresses are present in the sample part because of the sudden temperature reduction due to the rapid cooling of the SLM process. Thermal strain in parts and buckling deformation can take place due to the thermal stresses and the buckling deformation may lead to a reduction in dimensional accuracy of the part and surface accuracy as well. [53]

A few researchers have suggested that dividing the scanning spot into many small scanning regions are important to reduce the temperature gradient and the rescanning method is used to reduce and eliminate the buckling deformation. The layer of powder is scanned twice; in the first scan the phase the powder in selected region is melted completely and the rescanning process is completed perpendicular to the first direction. The rescanning method can be used to avoid buckling deformation and reduce the residual stress by approximately 55%. [54, 55]

AM processes produce non-homogenous damaging residual stresses and surface roughness, which need to be homogenised. An investigation was conducted by Sanz [49] and co-authors on cobalt chrome alloy (CoCr), maraging steel and Inconel as shown in **Figure 2-6**. Parts were exposed to different thermal treatment and mechanical finishing techniques in particular shot peening, abrasive flow machine (AFM) and a vibratory method, aiming to demonstrate the influence of different treatments on the residual stress and hardness properties.

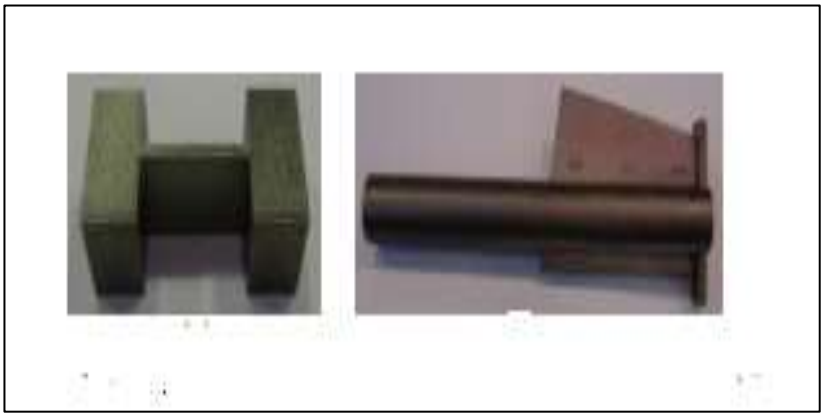

Figure 2-6: Samples manufactured by DMLS, H-geometry samples and prototyped guide vanes. [49]

Through the experiments carried out, the average porosity was quite low and the different treatments were not comparable in terms of porosity improvement. The results showed that shot peening, and other similar finishing techniques can be used to normalise the surface finish of the samples. Shot peening techniques achieve a greater reduction of surface porosity than heat treating does, and also demonstrate an improvement of surface hardness comparable with the initial properties (as-manufactured). [49]

The quantities of residual stress were also measured longitudinally on four different areas of each sample to assess the process of manufacture. The results showed that

direct metal laser sintering (DMLS), without additional treatment, generated non-homogeneous residual stress on the surface of maraging steel (H-geometry) samples. DMLS is an EOS trademarked name, used to describe their SLM process; despite the use of the word ‘sintering’ the process is an SLM process and the parts are fully melted. Application of shot peening provided homogeneous compressive stress which is an important advantage to relieve the residual stress and improve other properties such as fatigue life and hardness. In addition, thermal treatment of Inconel 718 by the same authors showed less improvement of residual stress comparable with shot peening, probably due to it not creating compressive stresses.

Other polishing treatments such as abrasive flow machine (AFM) and vibratory polishing demonstrated some compressive residual stress, implying that the mechanical polishing technique is more important than thermal technique. [49]

2.5.4 Microstructure

The microstructure of parts made by SLM and other additive manufacturing processes can be enhanced by employing ideal parameters during the manufacturing process. A layer-wise building technique is employed in the SLM process and so a part's microstructure may differ in different directions. A study was carried out by Murr and co-authors on a titanium part manufactured using optimized process parameters to get maximum density. Laser power was 42W, scan speed 200mm/s and scan spacing 75µm and a bi-directional scanning strategy was used. Due to the high temperature gradients used during the process, the microstructure was expected to be very fine and have the same direction on all sides. The results showed that the grain microstructure of the front surface was finer than on the other sides. [56, 57]

Kempen [58] and Yasa recently studied the effect of various parameters during the SLM process such as layer thickness, scan speed and laser power on both mechanical properties and microstructure of 18Ni-300 steel. The results demonstrated that a fully functional dense part can be generated by using SLM with mechanical properties comparable to those obtained by conventional techniques. [58]

As a result fully dense parts can be prepared without the necessity of further post-processing, although surface finishing is required. Parameters such as a large layer thickness and high scan speed lead to a reduction in density and also a decrease in the micro hardness. These process parameters can influence the macro-hardness due to their influence on the part density. In addition, results showed that the re-melting after each

layer led to high density and improved other mechanical properties such as hardness, smoothness, wear resistance and fatigue life. Also Young's Modulus had a significant improvement due to the exchange of matrix formation properties influenced by the re-melting process. [58, 59]

Research by Hasan [60] and co-authors on the characterisation of titanium alloy (Ti-6A14V) layer manufactured parts; produced using the SLM process was conducted at the University of Liverpool. The results showed that the titanium parts' micro lattice experiences brittle fracture failures although it has reasonable strength. In addition, it was also reported that titanium alloy (Ti-6A14V), especially the micro-lattice, is quite competitive with aluminium honeycomb impact failure particularly if the energy density is high during the SLM process. On the other hand, the combination of high laser power and high exposure time for the micro-lattice structure core, results in a more brittle material. The following micro lattice part (**Figure 2-7, Figure 2-8 and Figure 2-9)** was built for this investigation. [60]

Figure 2-7: Shows 20x20x20 BCC Ti-6A1-4V micro-lattice strut model. [60]

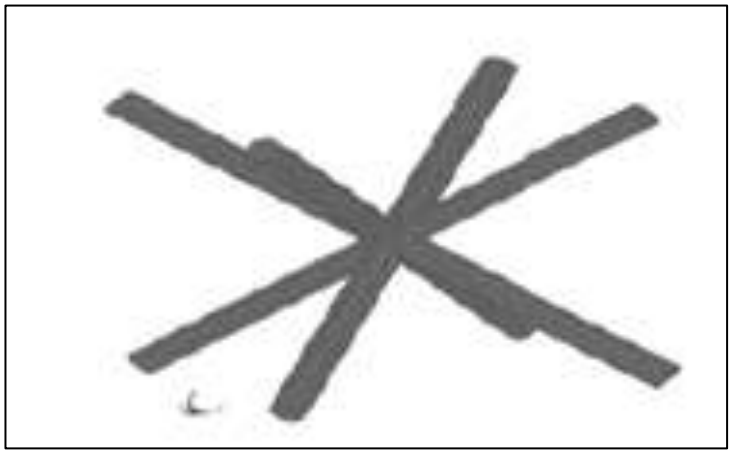

Figure 2-8: Shows a BCC unit cell with eight struts. [60]

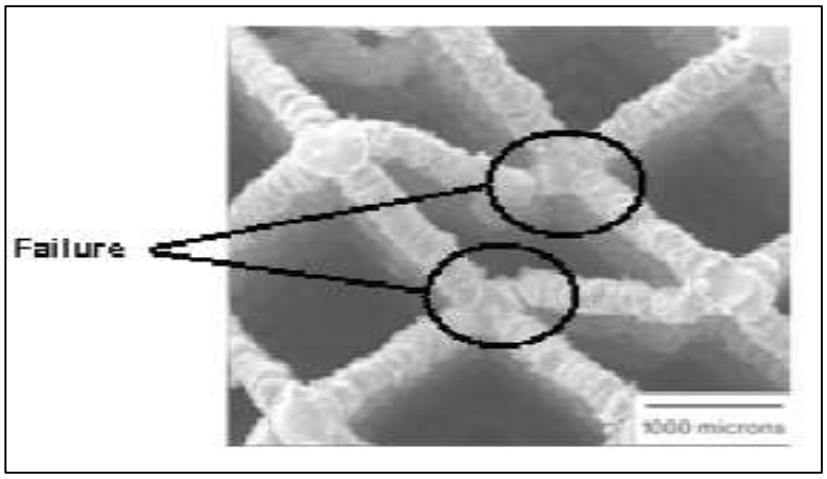

Figure 2-9: SEM micrograph of SLM Ti-6A1-4V micro lattice block shows failure on the node. [60]

When the micro lattice strut model was exposed to an impact load, a fracture occurred at the end of the part, specifically around the node area recorded.

As shown in the SLM (Ti-6A1-4V) micrograph above, the lattice model failed on the 45^{o} diagonal plane. In the same way, many researchers have also noted that the microstructure of SLM processed stainless steel gives less ductile behaviour. It was suggested that similar problem could also happen to Ti-6A1-4V. [60]

2.5.5 Residual stresses and curls

Residual stresses and distortions are some of the major concerns in SLM metal parts according to Kruth other researchers. Residual stress is caused by localised heating, complex thermal gradients and phase transformation during the SLM process. Also the solidification of layer after layer and cooling down procedure helping to generate extensive thermal stress and gradients can exceed the limits of material strength. Residual stresses can also cause the part to deform, fracture and decrease in strength.

According to the authors, the cooling rate of a part is affected by the melt pool and the temperature in the chamber, which finally affect grain formation and mechanical properties of the part. The final properties of the part are depended upon the successful bonding of adjacent layers and it is very important to use correct parameters for the given material. [37]

When the constructed layer is completed and starts cooling, the heat diffuses into the surrounding powder and new successive layer being formed. The difference in cooling rates between the finished layer and powder can lead to thermal stress. In such cases, the thermal stress is formed in the finished layers because of the exposed surface and

the layer under the exposed surface leading to curl in some cases, as shown in **Figure 2-10**. Supports are added to the part in the pre-build stage to prevent curling and they absorb some residual stresses that could lead to damage during the construction process. [61]

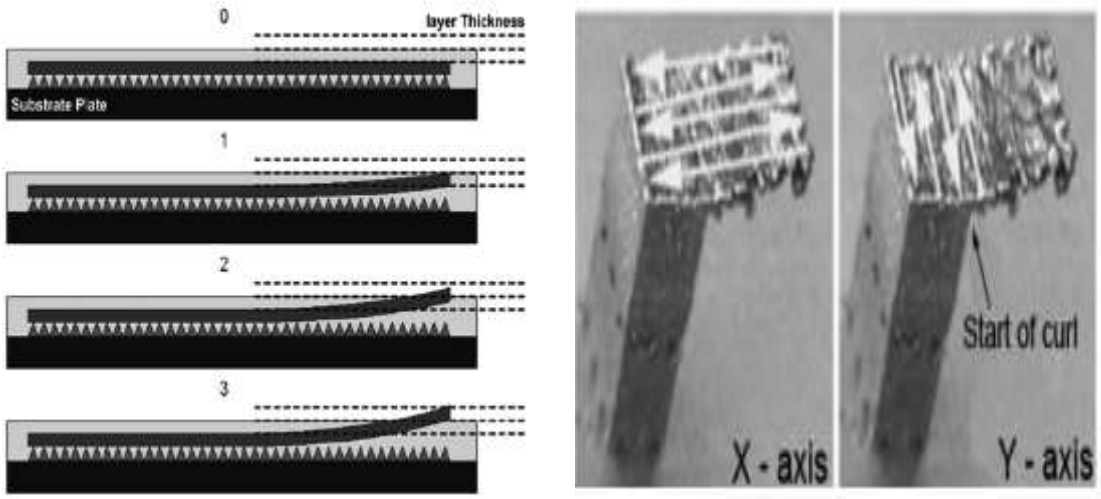

Figure 2-10 : Curling occurring during the SLM process. [61]

The residual stresses in the part can be caused by shrinkage while the layers cool and it also been proven experimentally that the residual stresses are influenced by the build platform and the best suitable position to build the part is on centre of the substrate because the laser is perpendicular to the powder on substrate. [19]

An investigation into residual stresses on SLM models were performed using the temperature gradient method (TGM) by Vollersten. The results showed that a high reduction of residual stress occurred on the surface in comparison with the standard build process and also noted that removing the part from the base plate leads to reduced residual stresses within the part as well. [62]

Many techniques are used today in the market to reduce the residual stress including:-

- The raw powder is maintained at a certain temperature to reduce the difference in temperature between raw material and molten material (pre heat of powder).
- The scanning is done longitudinally along the thin walls instead of using a stochastic strategy for the scan.
- The parts are heat treated to overcome any residual stress.
- The laser re-melting method is used to re-scan the same path many times to re-melt the layer, refine the grain size and relieve stress. [63 - 65,49]

2.5.6 Cost components

The factors to be considered in the cost of the part are based on the machine time and cost of the material. In all cases the raw material used will be in the form of powder and is always very expensive compared to bar or other stock. Powder material is sold in kilograms and also in different particle sizes e.g. the cost price of stainless steel powder is approximately £50 per Kg and titanium about £500. This presents a major obstacle to the growth of AM production applications and the prices are about 50 to 100 times greater than the price of materials used for injection moulded parts. [1]

Running time of the equipment needs to be taken into consideration; some of time needs to be spent on building the supports in addition to the actual time of model construction. Other time is spent on removal of the supports and cleaning both the machine and the part after creating it. The maximum build rates are approximately 30cm^3/hr, and more often are around 20 cm^3/hr

Apart from the running time of the machine and the cost of the material used, we also need to consider the indirect savings such as less powder material used to fabricate the final part as compared the other subtractive conventional techniques. Most of the excess powder can be reused to fabricate other parts, depending on the quality required and this brings decreases the typical cost of parts from 10:1 to 1:1 for SLM. [13, 66]

The other advantages that can offset the cost are related to the fact that there is no tooling required during the process:

- The complexity or shape of the component does not affect fabrication time.
- The manufacturing of components using difficult materials such as Inconel is no longer a problem with any other alloys.
- Ready-made assemblies can be manufactured during the processes and no assembling costs are then required.
- Manufacturing drawings are no longer essential, only for inspection of the component and for configuration management.
- Nesting parts on the platform also minimises the machine time cost per part and several parts can be manufactured at the same time. [67]

3.0. Surface finishing methods

Surface finish methods are very important due to their effect on the majority of mechanical properties of parts. In AM, surface roughness is considered as a major drawback of the technology. Thus, these surfaces are required to be improved. Surface improvement can be accomplished during the production of the components, or alternatively by some post-processing which is already on the market today, to obtain an improved final finish. Many attempts have been made to improve the surface finish quality of SLM parts. [68 - 76]

These attempts are varied and can be divided into two types as follows:

- CAD program and machine parameters adjustment (in-process methods).
- Post-processing methods to modify the final surface finish.

These stages have been divided in two chapters. In-process procedures are in chapter **3** and post-processing techniques in chapter **4**.

3.1 In-Process Procedures

SLM has been relatively recently begun to be used to manufacture complex metal parts with less treatment, directly layer-by-layer that are fully dense and functional. On the other hand, the parts coming through this method still suffer from some problems such as residual porosity and rough surfaces, which are related to the CAD programme or in-process parameters or material specification. Thus, these parameters need careful adjustment to obtain a good final result. These parameters can be divided into four groups as follows:

1- Laser parameters such as laser power, wavelength, spot size and laser density, etc.
2- Material specification such as distribution of particle size, flowability, type of material etc.
3- Environmental parameters including oxygen level, temperature, protective gas atmosphere etc.
4- Scan parameters such as scan speed, hatching distance, overlapping, layer thickness, part orientation etc. [77]

From these parameters, the powder particle size, layer thickness, laser power, scan speed and level of oxidation are the most significant variable factors which have an effect on the part property and surface quality. [78]

3.1.1 CAD Program

In most AM processes, the parts are first presented on a CAD system for designing as a 3D model. Also alternatively, data for special applications (e.g. medical) can be collected by using scanning or computer topography and imported into specialised software such as Materialise Mimics, for manipulation if required and generation of the 3D model. The CAD output has to be saved into data suitable for manufacture (a Stereolithography (STL) file or AMF file) and also be transferable to Computer Aided Manufacturing (CAM) systems for possible post-build machining. Autofab® or some other similar software is used to check for errors in the part and also generate supports on the part (for more details about Autofab software see experimental work section **6.1**). Autofab also helps to estimate the price of the part and time taken to build it, before manufacturing. High control of these steps will help to obtain parts with acceptable dimensional tolerance and surface finish. [3]

3.1.2 Layer thickness and orientation

SLM is an additive technique which is used to produce parts layer-by-layer, so it is possible to improve the surface finish of part by controlling the layer thickness. Commercial AM process systems use layers with a thickness range between 16 and 200µm. Thus, the layer will be visible on the surface of part, which also influences the surface quality. For instance, if the layer thickness is quite small then the laser energy will affect the layer itself through overheating, balling, waviness etc. On the other hand, if the layer thickness is very thick during the build process, it could result in incomplete melting which in turn leads to some defects such as internal porosity and surface roughness. [79] **Figure 3-1** shows the basic parameters.

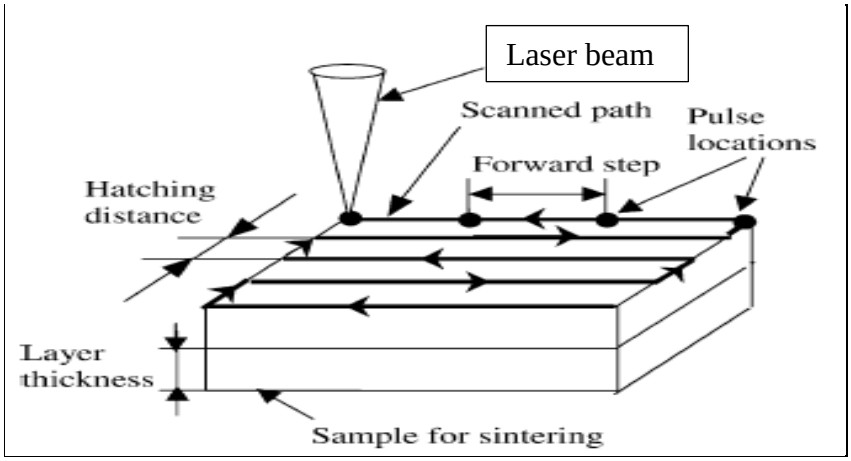

Figure 3-1: The basic parameters during additive manufacture. [80]

Laser assisted AM techniques offer an unlimited advantage, due to the possibility of manufacturing complex designs, providing important opportunities in many fields to construct according to customer needs, such as conformal cooling channels, dental implants, light-weight and other structures for specific purposes. Even though SLM provides so many advantages over other conventional manufacturing technologies, but it still has some major drawbacks, such as insufficient surface quality and the stair-case effect on the final part produced as shown in **Figure 3-2**. [81]

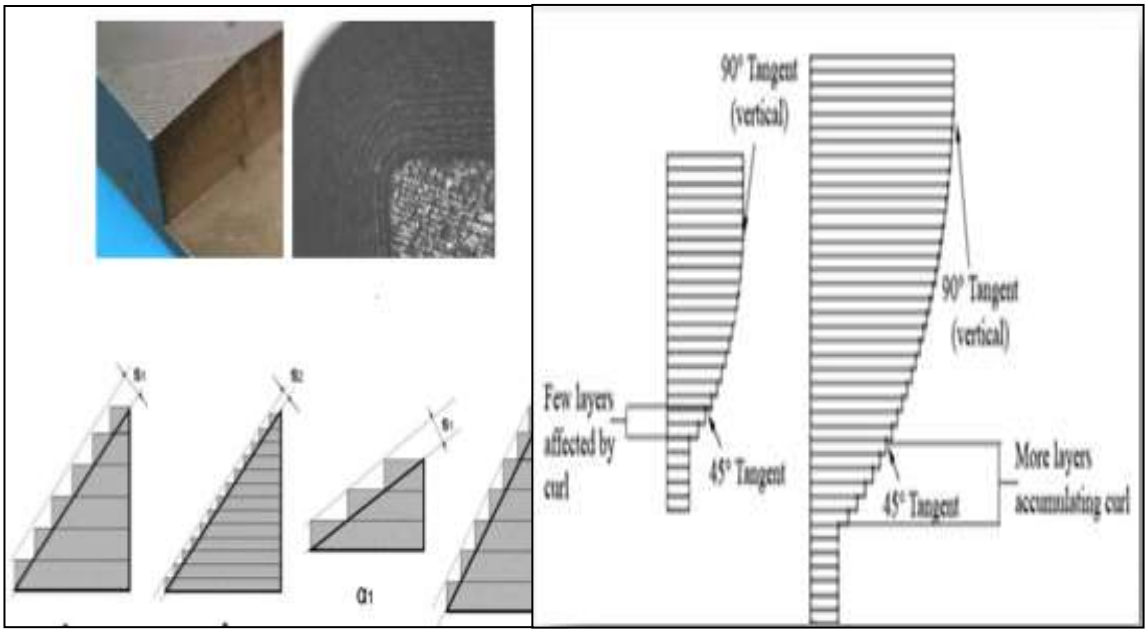

Figure 3-2: Layer thickness effects stepping and roughness. [61, 81]

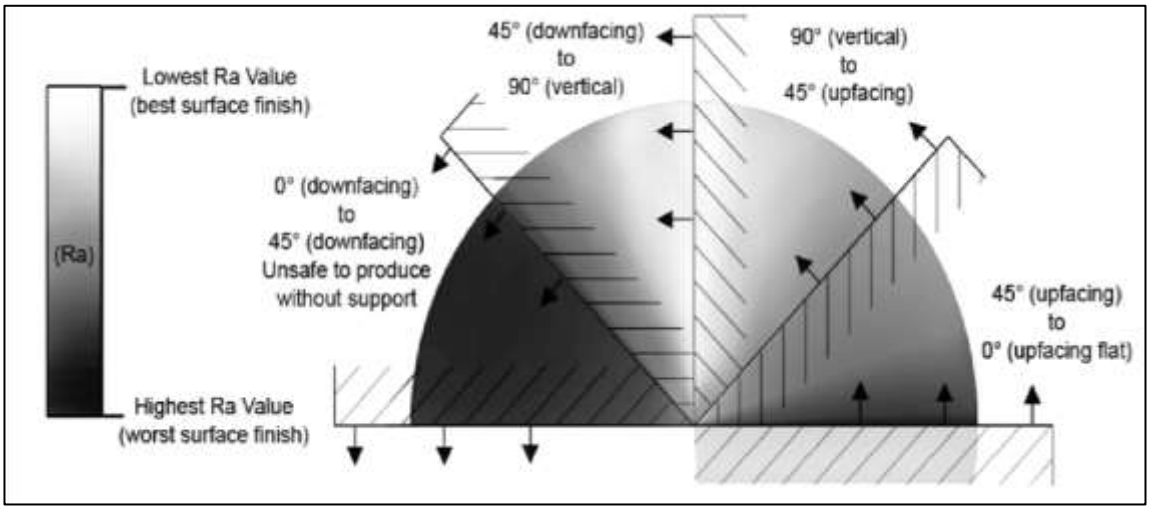

Figure 3-3: Surface roughness as a function of angle. [61]

The **Figure 3-2** and **Figure 3-3** show that the stepping effect is intrinsic to AM and it varies with the angle. Results show that a steeper surface slope and/or a smaller layer thickness will improve the surface finish, but at the same time the thinner layers will increase the build time and therefore the cost. [81]

The layer thickness, particle sizes and build orientation determine the surface roughness of the horizontal surfaces, whereas the vertical surfaces quality is affected by the special exposure, particle size and scanning strategy during the process. Thus, the particle size distribution has more influence on the surface roughness of the top and side wall. [82, 83] Also it is worth to mentions that, any inclined surfaces that have angles less than 45^{o} to the horizontal direction require supports to avoid any curling or fails during the process. [39, 61]

The unsatisfactory surface finish can only be improved by using a diversity of surface finishing methods which are readily available on the market. They include mechanical processes, such as machining or other abrasive blasting, thermal processes such as plasma spray or laser treating and chemical techniques like acid etching etc. [84]

3.1.3 Powder particle size and its components

Powder particle size has been widely thought of as a central factor influencing the surface roughness. The powder should be suitable for any AM system and spherical shape particles provide good flowability. Indeed, there is specific range which is recommended for each additive manufacturing technique. The powder particle size is preferable to be mixed and not fine or large, because it helps to establish full flow, high density, rapid solidification and homogeneity. The powder must have characteristics which make it suitable for the AM methods. Also, it is important to choose the most appropriate powder size for each application since it has a large influence on the quality of surface finish and the part properties.

Freeman has clarified some of these factors such as particle size distribution, shape, surface texture, flow rate, humidity, electrostatic charge, rapid solidification, homogeneity and chemical composition etc. The research concluded that the powder particle size distribution has the most influence in both surface finish and density as well. [85]

Another study by Badrosamay [35] and co-authors also stated that fine powder particles result in better surface qualities and densities than coarse powder. In all cases, fine powder is required in order to improve the part properties like surface quality, mechanical strength and density.

Joakim [86] and co-authors have investigated the effect of particle size on the bulk microstructures and final surface roughness through different setting parameters.

The results showed that the parts and surfaces built with small particle size are almost full dense and have lower surface roughness, whereas the coarse powder showed the opposite. [86]

Commercially there are ranges of material powder sizes depending on the type of material, chemical components and application required. **Figure 3-4** shows a range of titanium powder partial sizes for some different applications. [87, 88]

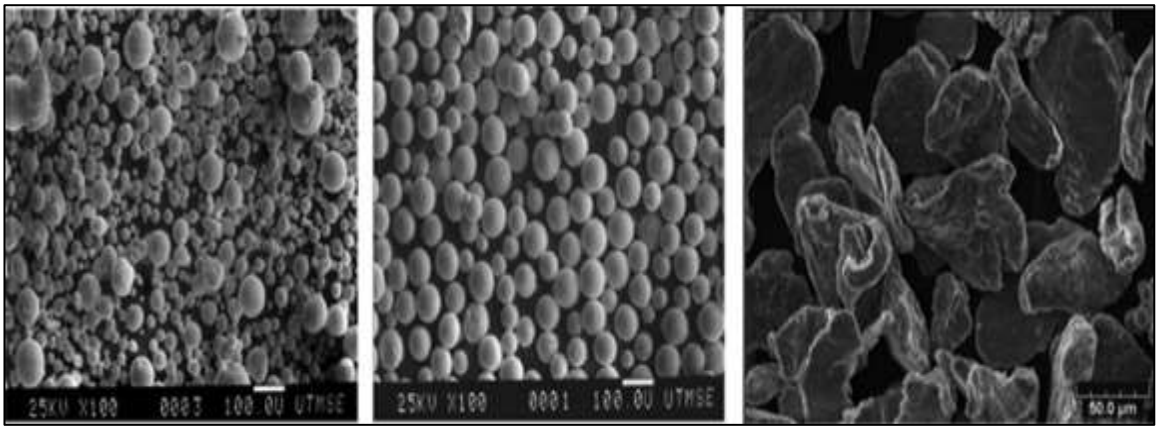

Figure 3-4: Ranges of powder size. [87, 88]

3.1.4 Laser power and scan velocity

In AM, laser power and scan speed are the most significant factors during the manufacturing process, because they directly affect the laser energy density absorbed by the constructed layers. Thus, surface roughness, density and mechanical properties of parts are influenced. In fact, a high scan speed can lead to underexposure of the laser resulting in partial melting of the powder. This incomplete melting leads to increased inner porosity and balling on the surface. On the other hand, if the scan velocity is too low it will result in overexposure of the laser intensity, leading to over-melting and non-homogenous layer construction. This will manifest itself as some defects on the part surface, such as balling, waviness, porosity and powder particle agglomeration as well. [89, 90]

The laser intensity is the laser power per unit area as given by following equation

$$\mathbf{I = \frac{P}{A} = \frac{P}{\pi r^2}} \quad \text{.... .....} \quad \textbf{Equation 3-1}$$

where, I is the laser intensity (irradiance in w/mm^2), P is laser power (W), A is the area of the spot (mm^2) and r is the radius of the spot (mm). [91]

On the other hand, laser energy density is a function of laser power, scan speed, and beam spot diameter and is given by the equation.

$$\mathbf{E = \frac{P}{V*D}\ \ (J/mm\hat{}2)} \quad \textbf{…….. Equation 3-2}$$

Where P is laser power (w), V is scan speed (mm/s), D is spot diameter (mm)

The combination of these parameters determines the energy density absorbed during the process, which in turn determines the melt pool size, heat effected zone and the penetration depth of the process. [92]

A study conducted by Steen [93] to discuss the principle of these parameters, showed that the spot size is the most significant factor and has two effects; first, reduction of beam diameter leads to increase laser energy density and second, reduction of exposure area leads to an increase in build time (cost effect).

3.1.5 Overlap factor and beam spot size

These are other factors which have a vital influence on the quality of the surface. For good surface finish, the overlap factor should be high to reduce scan spacing. The results showed that an increase of overlap factor has a considerable benefit on the process; it has the effect of preheating the workpiece ready for the next track. Thus, the reduction of overlap factor by more than 50% could lead to not enough adhesion between these tracks during the process, resulting in poor surface finish. [94]

Other researchers indicate that 30 to 35% overlapping could be enough to produce a good result during laser treatment of a surface. [95] The relation between them is as follows:

Scan spacing = (1 – overlap factor) * spot size …… .Equation 3-3

Where overlapping factor is dimensionless value of required overlapping percentage, and (1 – overlap factor) is the scan spacing factor. [94]

On the other hand, during successive scanning and where the hatch spacing is less than the beam diameter, some of powder is exposed to multiple scans. The numbers of effective exposures are given by this formula.

$$\textbf{The number of effective exposure} = \frac{D}{h} - 1 \quad \text{……..}\textbf{Equation 3-4}$$

D is the spot size diameter and **h** is the hatch spacing(Sc Spacing) between two centres of laser tracks [96]. The schematic in **Figure 3-5** illustrates this.

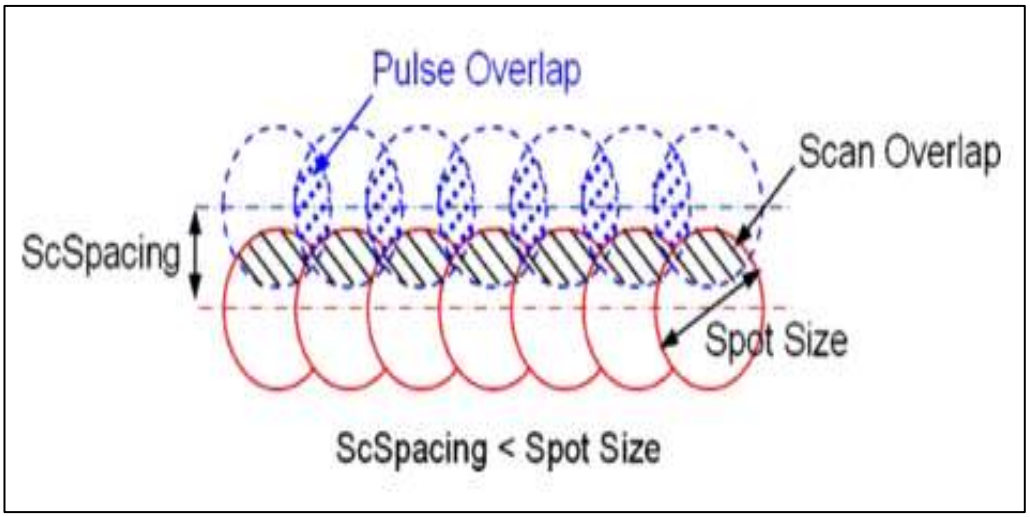

Figure 3-5: Schematic diagram presenting spot overlapping and track overlapping. [97]

.

3.1.6 Environmental control of oxygen ratio

The oxygen ratio has to be very carefully controlled as the oxidation is a chemical reaction, which involves addition of oxygen to an element of compound. For instance, the two commercial SLM machines (125 and 250) developed by MTT group (Renishaw) have to be operated at low oxygen level (fully shielded chamber). The oxygen has to be less than 100 parts per million for non-reactive metals. On the other hand, it has to be less than 50 parts per million for reactive materials like titanium and aluminium. [1, 10]

In addition, poor control of the oxygen ratio can cause insufficient consolidation of the layers during the process, because the tension of the liquid metal oxide on the melt pool surface will be less than the liquid metal without oxidation. For instance, iron liquid near its melting point has about 2n/m surface tension in fully shielded area, while increase of oxygen about 0.02 wt% (Percentage per weight) will reduce the tension towards 1 n/m. In such a case, the iron oxide could be a significant barrier to flattening of the top of the iron liquid on the construction surface, causing some defects such as pooling and porosity, even with an absence of contamination.

From this perspective, the reduction of oxygen level or high control of the environmental ratio will enhance the physical and mechanical properties of parts. [16]

4.0. Post-processing techniques (Surface modification methods)

Surface finish modification is vital for engineering materials because all fatigue failures, oxidation and wear are extend from the surface. Generally, surface finishing methods have been utilized as the prime technique for changing the part's appearance in order to enhance desirable properties such as wear resistance and abrasion, corrosion protection and development of aesthetic qualities etc on the surfaces lacking that property. [98] Many commercial methods are used in the market as post processing for different purposes such as **mechanical, thermal and chemical**. Some of the most commonly used as post-processing methods are following.

4.1 Mechanical methods

Due to the quick advance of technology especially in the last two decades there is increasing demand for different complex engineering parts, of unusual size, high accuracy and low manufacturing time and cost as well. All these factors have influenced the invention and development of several techniques, which are employed in the industry to produce or improve surface finish quality, mechanical properties and component brightness. These techniques range from the simple to the latest modern ones. [99] such as the following:

- Hand polishing
- Others methods such as vibratory method, abrasive tumbling, vapour blasting techniques, shot blasting techniques and shot peening techniques.
- Advanced machining including (ultrasonic machine, robotic finishing technique, CNC milling machines and hybrid SLM machine centres).
- Other methods related to one and two-way abrasive flow machines, for example the Extrude Hone process.

4.1.1 Hand polishing

Hand polishing is the oldest and simplest technique we know and is used to remove unnecessary materials attached to the surface from its natural state, in order to enhance its distinct properties and improve surface finish. Also the buffing process can be used to obtain the brightness required. However, this technique has some limitations such as its tendency to consume a lot of time that leads to an increased cost; it also requires good skills plus experience and training. On the other hand, the process is suitable to process any kind of material such as metal, polymer or ceramic as shown in **Figure 4-1** *Figure 4-1*in order to achieve acceptable surface quality and customer satisfaction. [100, 101] It is possible to use this process as a method to improve the surface finish of AM manufactured parts.

Figure 4-1: Shows part before and after polishing. [100]

4.1.1.1 Advantages and disadvantages of hand polishing

Advantage	Disadvantage
Improve surface finish, brighten	Time consuming
Suitable for different metals	Needs skill, experience
Improved mechanical properties	The accuracy is operator-dependant
Micro subtractive technique	Not suitable for complex shapes and internal surfaces

Table 4:1: Shows the advantage and disadvantage of hand polishing. [100]

4.1.2 Vibratory method

The vibratory finishing method is a simple technique used in the industrial sector as a method to enhance or improve part surface quality. The vibratory system is a very economical process. It is simple and available as an automatic or semiautomatic technique, with high volume and is a natural method giving the bonus of being environmentally friendly. All of these merits have encouraged use of this technique as a method of post processing for additive manufacture. However, the AM technique is used to produce parts with a degree of complication which may not be suited to vibratory methods. The samples need to be treated as shown in **Figure 4-2**. In simple terms, the parts are placed in a vibratory process tank with pellets and the machine starts vibrating them gently until bright surfaces are obtained. During this process, the amount of material removal is about 5 to 20 micron or more, based on the duration of application, amplitude and frequency. Through this process, parts are not in danger of major impairment. [102]

Figure 4-2: Big vibratory machine [102]

4.1.2.1 Advantages and disadvantages of the vibratory method

Advantage	Disadvantage
Economic process, natural process	Harms some small features on the part surface. Not suitable for complex parts and internal features.
Simple to use, high volume, surface finish and cleaning	
Automatic or semiautomatic technique	

Table 4:2 : Advantage and disadvantage of vibratory machine.

4.1.3 Abrasive tumbling method

The abrasive tumbling technique has been intensively used in industry as a method of improving the physical and mechanical properties of parts made by different techniques. Generally the method employs materials such as rubber, plastic, or small abrasive rocks with lubricants. Silicon carbide as small stones is often used with oil as a liquid lubricant, but water is used as a universal lubricant. The lubricant assists in suppressing the degradation of part surface from impact by the abrasive particles. Indeed, the process starts by loading them into the main barrel and starts by slowly rotating; later the speed is increased. This variation will generate a friction field to remove the majority of sharp edges, burrs and undesirable material on the part surface. The machine has a controller switch to control the speed, but the best possible rotating speed depends on many factors such as tumbling machine size, kind of metal part and the degree of accuracy required. Although this process has many advantages, it suffers from some limitations like tending to damage small fine features such as sharp edge and radii on the corners. Tumbling is used for polishing and smoothing, and is suitable for large batches of parts with minimal supervision for production. Many machines have been commercialized in different sizes to meet customer's needs as can be seen in **Figure 4-3.** [103]

Figure 4-3: Tumbling machine samples.

4.1.3.1 Advantages and disadvantages of tumbling machine

Advantage	Disadvantage
Simple, economic and different sizes available	It harms some small sharp edges and radii.
Suited for various materials	Some oxidation caused by lubricant on iron.
Improves surface finish, mechanical properties	

Table 4:3: Shows the advantage and disadvantage of tumbling machine. [103]

Spencer and co-authors described an experiment carried out and the models of each sample have been sent to Invicta Super Finishers Ltd, Gratham, UK. [104]

The process has been also conducted with the aim of investigation a number of automated finishing methods. Surface finish of the stereolithography parts were achieved by vibrating models in a 'u' shaped container at a constant speed with abrasive media. This process is less aggressive than the tumbling method. When the media is circulating in the container, the surfaces of the models improved. The samples were made using two different kinds of material; XB5143 and XB5081. Surface roughness (*Ra*) of parts was measured using Rank Taylor Hobson TalySurf 4. Vibratory bowl abrasion process of both parts made from material XB5143 and XB5081 were processed for 1¼ hours using Ø30mm and 10mm angle cut cylinders anØ13mm plastic green cones as media. On the vertical walls both bumps and steps were removed and the evident was shown on the figure below. All sharp edges and corners were removed, see **Figure 4-4.** [104]

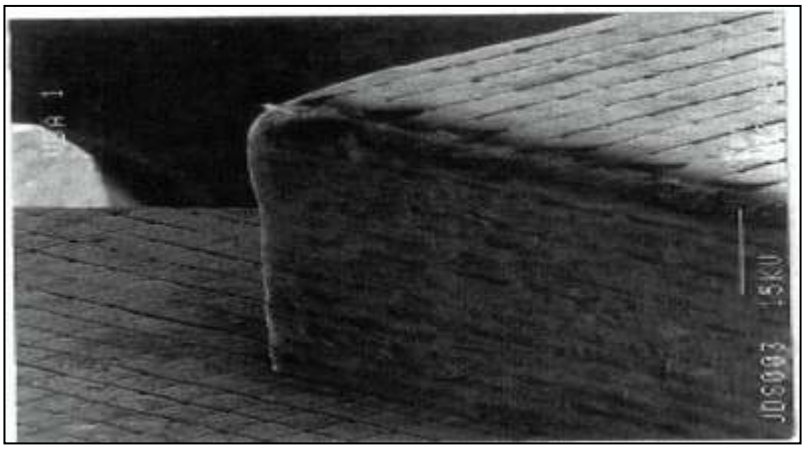

Figure 4-4: Steps around the corner removed. [104]

4.1.4 Vapour blasting technique

This process works using air or water with a fine abrasive powder. The stream of air or the water will be under specific pressure ranges 80 to 120 Psi. This process is widely used in industry for polishing parts which are made by different techniques. Vapour blasting is a highly economical process and it can be recommended as a technique of improvement of SLM parts surface finish and for its brightening ability. The vapour blasting process can cause some damage to fine features on the parts or remove some engineering textures such as embossing marks, casting marks etc. In addition it is not suitable for ferrous metals because a chemical reaction (oxidation) can be caused by the water during this process. **Figure 4-5** shows the process. [100, 105]

Figure 4-5: Vapour blasting machine process. [106]

4.1.4.1 Advantages and disadvantages of vapour blasting machine

Advantage	**Disadvantage**
Improves surface finish, brightens	May cause chemical reaction (oxidation) for ferrous material, and residual stress
Economic, easy to use	
Different material sizes available	Needs experience and training

Table 4:4: Advantage and disadvantage of vapour blasting machine. [100]

4.1.5 Shot blasting technique

Shot blasting is a simple subtractive technique which is suitable for machining many kinds of materials. The process works by accelerating water with controlled abrasive powder by pressure pump, to exit from a small nozzle. The directed water can be used to clean and improve surface appearance. Powder particle size range from fine to medium and are used to improve the efficiency of the process. The selection of media size depends on several factors such as surface finish required, degree of surface complexity, type of material and the degree of accuracy required. [105] Nowadays, micro-abrasive blasting is available. In this process a fine dry abrasive is accelerated under high pressure to come out through a small nozzle. Typically, nozzles range between 0.25 mm to 1.5 mm diameter, and are used to deliver a fine stream to a specific area and improve both physical and mechanical properties. The shot blasting process is extremely useful for many different purposes as mentioned but still has some limitations due to the fact that the process has side effects of destruction of small features or sharp edges. **Figure 4-6** demonstrates how this process works. [100]

Figure 4-6: Illustration of shot blasting technique [68]

A comparison study was completed by Mushambadope [68], at De Montfort University. Samples were manufactured using a SLM 125 machine at DMU. The samples have many features and the surface roughness was different according to the design complexity of the sample. The preliminary results showed that the surface roughness ranged between 10 and 25microns, which still need post-processing to enhance and improve, surface quality. Comparison results were carried out using the following post-processes methods:

- Sand blasting, Shot blasting, Electro polishing and Vapour blasting.

Surface characterisation was completed before and after improvement; using Surf test machines from Taylor Hobson and a 3D Keyence microscope at the MTC research centre. **Figure 4-7** and **Table 4:5** illustrate the method comparison results.

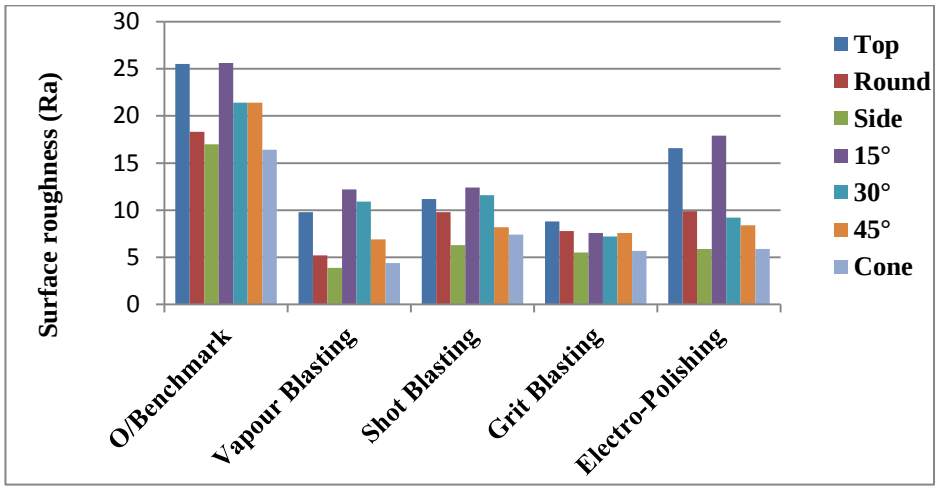

Figure 4-7: Comparison of post process methods. [68]

Comparison table of the post processing methods used				
Process	Ra	Accuracy	Defect	Time (minutes)
Shot blasting	Good	Poor	Yes	5-10
Grit blasting	Good	Poor	Yes	5-10
Vapour blasting	Better	Good	Yes	10-15
Electro polishing	Good	Good	No	10-20

Table 4:5: Comparison of post process methods. [68]

Through this investigation, the results showed that the manufactured samples surfaces were improved by the post processing techniques, but most of the methods destroyed the small features on the samples and three methods showed some side effects like oxidation, except the electro polishing method. [68]

4.1.6 Shot peening technique

Shot peening is a mechanical technique, which works on the metal surface by utilizing small spherical metal powder particles. The process works by shooting these small spherical balls onto the surface of the part, like peen hammers. Compressive stresses on the surface can be obtained, due to plastic deformation. These compressive stresses have merits such as increased hardness, fatigue resistance life up to 100% and wear resistance on the metal surfaces. As is well known, the degree of stress on the surface is higher than the stress in the part during mechanical loading. Based on this phenomenon, the shot peening technique is used to improve the mechanical properties of conventional surfaces. For AM metal parts, the results of reaming pores created during the process, can act as major problem for surface improvement. Thus, implementation of this technique could facilitate obtaining a good surface finish, but can lead to activation of the initial crack from internal pores due to the reverse of the compressive stress. **Figure 4-8** illustrates the basic principle of this technique. [107, 108]

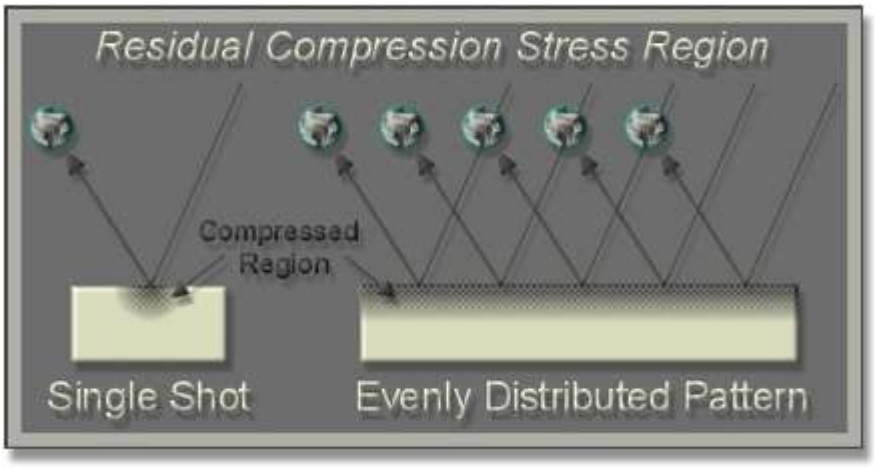

Figure 4-8: Shot peening process.

Yoshida [109] and co-authors have also defined the process as a cold working technique employed to produce a comprehensive residual stress layer, used to modify the mechanical properties of metal parts. On the other hand, this process also works similarly to sand blasting with the only difference being that it works by a mechanism of plasticity instead of abrasion. Shot peening process can also be used for cosmetic effects. The surface roughness from the overlapping dimples causes light to disperse upon reflection and due to the peening effects it results in larger surface features compared to sand-blasting. [109]

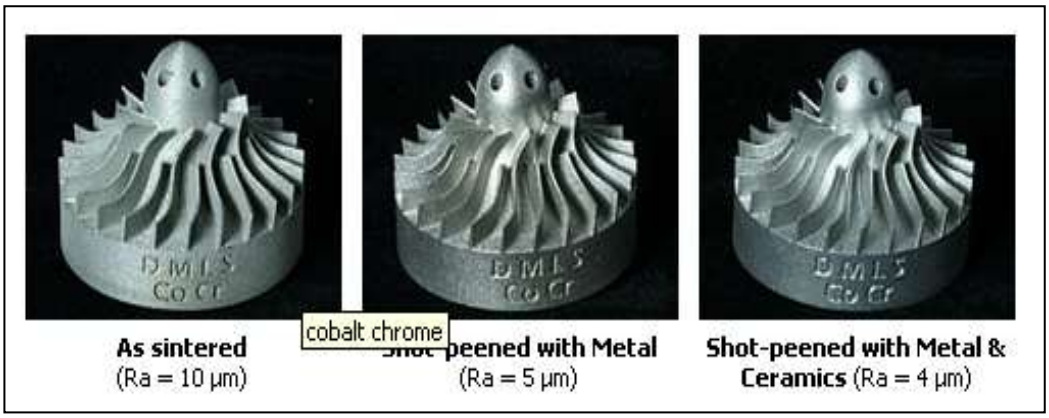

Figure 4-9: Parts before and after shot peening. [109]

4.1.6.1 Shot peening applications

Shot peening is a significant process in many applications of industry such as:

- Aircraft repairs - shot peening has been used in this scope to repair and relieve tensile stress after subtractive processes and replace it with compressive stress for the reasons noted previously.
- Spring making - many types of spring, including extension springs and compression springs which are widely are used for engine (valve springs), to increase cycle life for fatigue.
- Other applications such as gears parts, camshafts, coil springs, crankshafts, gearwheels, and turbine blades and to improve the surface finish of cast parts such as engine blocks. In addition, shot peening has emerged in cosmetic production because shot peening is capable of producing brighter surface features compared to other processes. [107 - 109]

4.1.6.2 Advantages and disadvantages of shot peening

Advantage	**Disadvantage**
Economic, suitable for many metals	Very harsh polishing
Improves surface finish, mechanical properties such as Fatigue, wear, friction and relieve residual stress caused during subtractive processes	It can destroy small features such as, sharp edges and small radii.
	Not recommended with porous materials Needs experience and training.

Table 4:6: shows the advantages and disadvantages of Shot Peening.

4.1.7 Ultrasonic machining

Ultrasonic machining (USM) utilizes high frequency vibrations with abrasive to remove material from the main work-piece. Micro erosion by impact of fine abrasives with the part surface can achieve accurate cavities, according to the forming shapes of the tool. However, the vibration energy comes from transfer of electrical energy into mechanical energy. Metallurgical changes on the parts physical properties can be obtained by this process. Consequently, it is possible to use this process to improve the surface finish of parts made by AM due to the reasons stated in the foregoing lines. **Figure 4-10** illustrates the basic principles of this technique. [110]

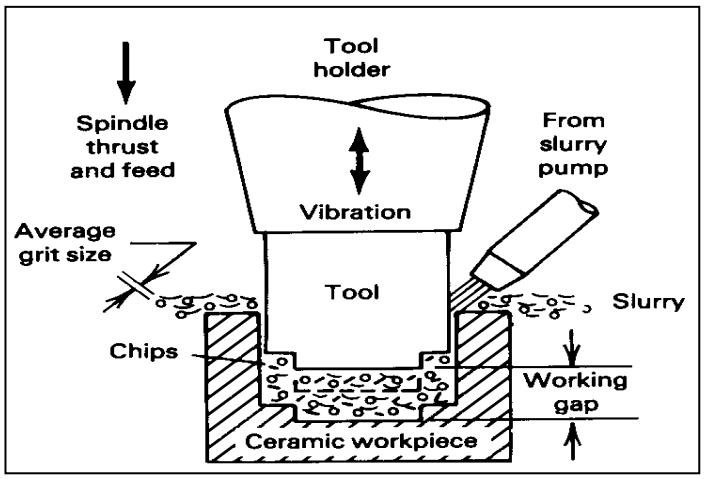

Figure 4-10: The basic principles of ultrasonic machine. [110]

A study conducted by Spencer and co-authors in the UK investigated how the USM process performs as a finishing technique. [104] Carborundum abrasive grit was used as the media and a ∅100mm container vessel was filled with 250µm size particles. The resin models were placed on the top of the grit and the ultrasonic horn was in contact with the model. 20 kHz frequency was used at amplitude of 80µm and material type 1 was XB5143.

Figure 4-11: The damage to the corners and little smoothing of steps.[104]

The main advantage of the process was identified on the horizontal surfaces where smoothing occurred on some localised areas. Some other areas were still rough as indicated in **Figure 4-11.** It appears that more erosion has occurred on the vertical edges. Material type 2 XB5081 was totally destroyed during the process and the model was not able to be improved. The process was more aggressive since it created excessive damage to the corners of the model.

From an experiment carried out using vibratory bowl abrasion and ultrasonic abrasion, it was found out that ultrasonic abrasion severely eroded the model manufactured from two kinds of polymer resin. Vibratory tumbling was able to smooth the surfaces with an improvement in *Ra* values of 74%. These processes can also be performed either using centrifugal tumbling or barrel tumbling. [104]

Process	**Media**	**Material type**	**Ra Value (Micron)**				**% improvement**
Reference Sample			X	Y	Z	Mean	
		XB5143	5.35	7.34	7.0	6.56	
		XB5081-1	6.46	7.68	3.0	5.71	
Vibratory Bowl Abrasion	(30x10)mm angle cut cylinders	XB5143	1.22	2.62	1.2	1.68	74
	ø13mm plastic cones	XB5143	1.32	2.3	1.9	1.84	72
Ultrasonic Abrasion	250µm Carborundum grit	XB5143	1.74	3.0	2.0	2.25	66
		XB5143	1.82	3.32	3.0	2.75	58

Table 4:7 : Surface finish texture readings (Ra values). [104]

4.1.7.1 Advantages and disadvantages of ultrasonic machining

Advantage	Disadvantage
1-Wide range of cutting options, high productivity	Requires calibration for each material
2- not destructive technique	Needs to be good contact with the surface
3- low stress levels, good accuracy	Accuracy depends on abrasive particle size
4-Accurate process, low operating cost	Initial cost quite high, needs a shaped tool

Table 4:8: Shows the advantages and disadvantages of ultrasonic machine. [104, 110]

4.1.8 Robotic finishing technique

This is a modern technique developed in the last two decades and the first fully automatic working robotic system was developed in 1997. It performed as an automatic technique which was used to improve the surface finish by polishing, grinding, buffing and flash removal. The robotic process is now more than a finishing process and it is presently used in a multi-system capable of adapting itself to a variety of processes. However, the spindle and tool selection for the process applications has to allow geometric freedom to move gently over the surface required. As a result of this development, there is the opportunity to use these technologies as post-process operations to improve the surface quality of simple or complex SLM parts. [111]

A robotic system is a very economical technique due to its ability to reduce labour costs and abrasive costs (up to 75%); it also offers safety and a high degree of accuracy. The overall surface finish quality of AM parts, when using robotic finishing systems is improved more than 80%, while the dimensional accuracy of the finished parts depends on the system accuracy. **Figure 4-12** shows the architecture of the robotic finishing system. [111,112]

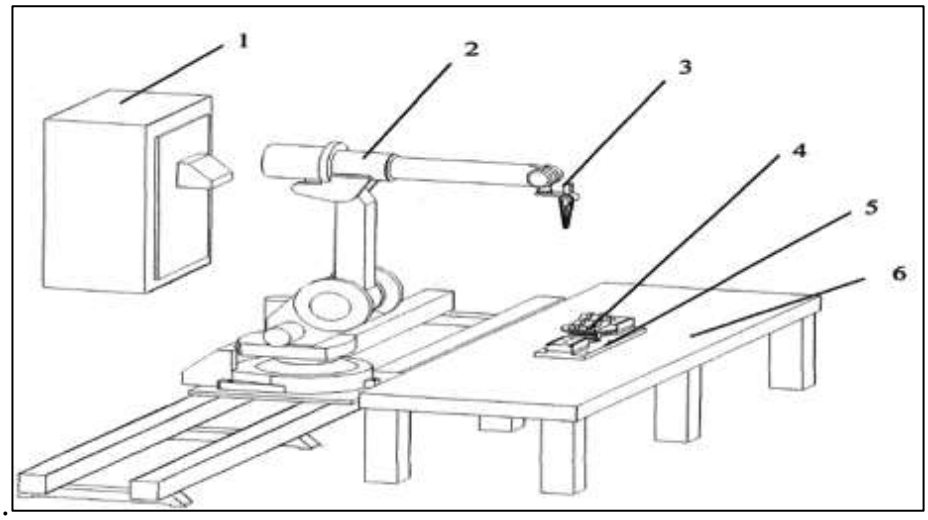

Figure 4-12: The architecture of the robotic finishing system: I-controller; 2-articulated manipulator; 3-finishing tool; 4-SLS part; 5-fixture; 6-platform.[111]

4.1.8.1 Advantages and disadvantages of robotic finishing systems

Advantage	**Disadvantage**
System software	Initial cost high
Excellent automatic polishing system	Not suited to some small features
High accuracy, 5D motion,	More cost for training
Suitable for different materials	Preventive maintenance high. High cost of breakdowns.

Table 4:9: Advantages and disadvantage of robotic finishing systems. [111,112]

4.1.9 CNC machining system

Computer numerical control (CNC) is a process of manufacturing parts by utilizing computer control systems to control motors which drive all machine axes. Recently CNC has been improved from 3 to 5 axes systems. This improvement has provided these machines with high flexibility to produce very complex parts with good surface finish. CNC machines can be used in many engineering processes like milling, drilling, cutting slots and cutting threads. The process efficiency to produce a good surface finish is highly controlled by factors such as feed rate, tool size, depth of cut and speed. **Figure 4-13** shows this machine and how its operation system is designed. [113, 69]

Figure 4-13: Shows a 5 axis CNC machines.

In the early days, additive manufacturing was applied as a single process. This provided a convenient and relatively effective approach for the production of prototype parts. However, parts were often subjected to hand finishing or simple machining operations to optimize the features required, such as milling and drilling, and the need for hybridization was not at this point recognized. In recent years a number of technologies have been introduced in industry that combine a CNC milling machine and an additive manufacturing method to providing a so-called 'Hybrid System'. [2]

4.1.10 Hybrid machining system

Hybrid machining system is an integrated system that combines two or more manufacturing technologies in order to expand the efficiency of production and minimize production costs. The combination of additive and subtractive processes is undertaken in series, with the complex features and cavities being fully constructed by the AM process and the subtractive technique being used to obtain the desired surface

finish and accuracy [2]. This technique is called Hybrid machining. After building the model, the near net shape is then finished by a machining process in the same station. For instance, the LUMEX Avance-25 combines a laser sintering machine with a high speed CNC milling machine in one operation as seen in (**Figure 4-14-A).**

A	B

Figure 4-14: A LUMEX Avance-25 metal laser sintering / high speed milling hybrid machine and B, sample from Matsuura.[114]

The integrated system of the LUMEX Avance 25 allows very complex molds to be manufactured for some specific applications such as aerospace, automotive and energy industries as well. Accuracy of about ±2.5µm on a complete component (internal and external features) can be obtained within one station by using hybrid machining systems. These components could not be created via traditional techniques. [115]

Figure 4-15: Additive manufactured part being machined.

Karunakaran [66] and co-authors, have reported that several hybrid machining centres have been developed today for specific purposes. The integrated systems all combine both the advantages of additive and subtractive manufacturing technologies. In these systems the near net shape of the model is built by additive manufacturing processes such as:

- Electron Beam Melting process
- Selective Laser Melting process
- Weld deposition process
- Laser engineered net shaping (LENS) etc.

while the final net shape is finished by machining processes. [66, 116, 117]

.

4.1.11 Extrude Hone Corporation

Extrude Hone is one of the most renowned companies offering different advanced technologies to improve surface finish, reliability, performance and with high quality as well. It utilizes many of the sophisticated techniques to achieve its targets. Some of these techniques are as follows:

4.1.11.1 Abrasive flow machining process

Abrasive flow machining (AFM) is a purely mechanical method and it uses a chemically inactive and non-corrosive media almost identical to soft clay. This process is mainly used to polish internal surfaces and radius edges. The media has an advantage because it can be used for different components without changing media. The process is capable of high quality of precision, and can be either used as one-way or two-way process. [118]

4.1.11.1.1 AFM One way system

In this system, the abrasive flows only in one direction through the component and then it goes to the hopper where it returns to the single functioning cylinder in order to improve and enhance the surface finish. Therefore, the most common advantages of this system are: high process performance and reliability, capable of handling large parts with facilities for cleaning, ease of changing parts, easy of changing tools and also the ability to control the temperature required with an easily adjustable mechanism. **Figure 4-16** given below illustrates the basics of this process. [119]

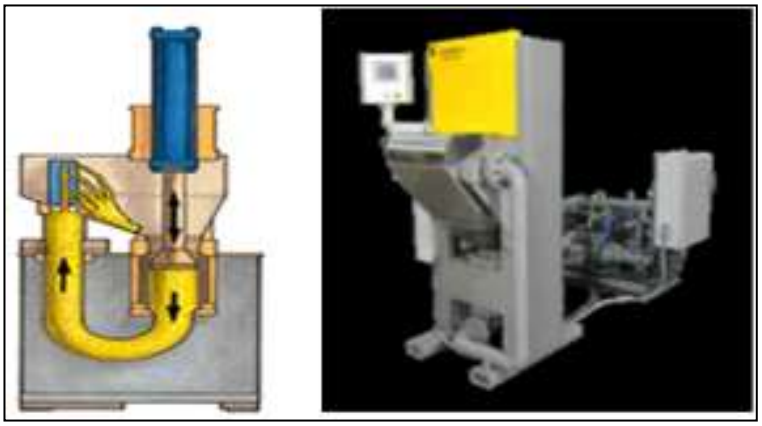

Figure 4-16: Illustrates one way AFM machine system[118]

4.1.11.1.2 AFM Two-way system

In this system the media is allowed to flow extremely gradually in directions throughout the work piece, in order to obtain the final finish. Two vertical cylinders are utilized to extrude a rough media through the part to improve its surface quality. In addition, advantages of this system are:

- A highly controlled process in which the system is fully automatic with facilities for fast setup, changeover of tooling and media as well.
- The extra advantage is that both internal and external surfaces can be processed simultaneously. **Figure 4-17** below illustrate this process. [119,118]

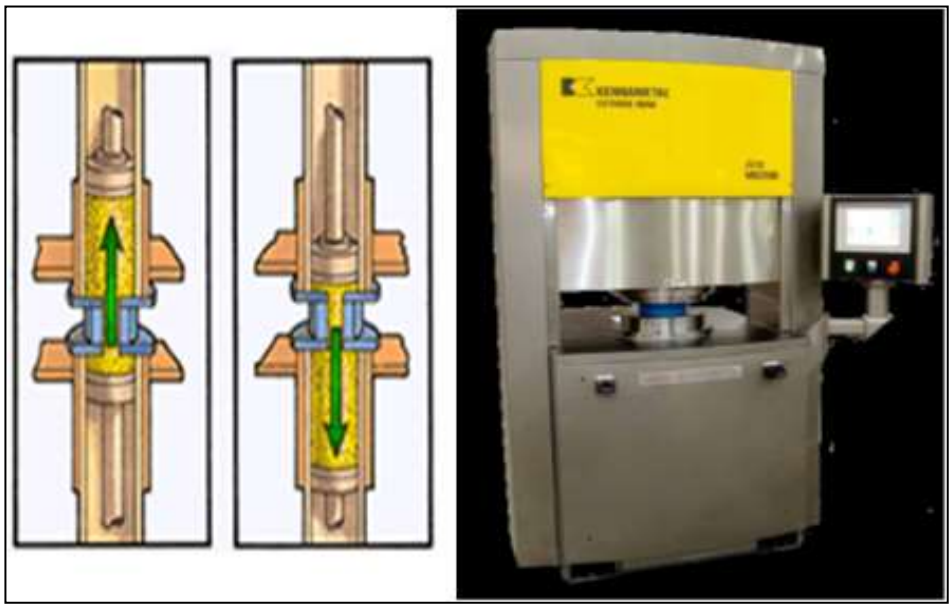

Figure 4-17: Illustrates two way FEM machine systems. [118]

4.1.11.2 Electrolytic machining (ECM)

Extrude Hone's method of Electrolytic machining is currently used in many industry sectors to provide surface treatment in areas such as aerospace, medical, and engineering projects. ECM is an electrolytic process, meaning it is an unconnected method. Thus, the fluid is pumped evenly over the surface of workpiece which is connected to a positive charge (anode) whereas the tool model is connected to a cathode. The amount of material removal depends on the quantity of the current flowing between the anode workpiece and the cathode tool, which is designed to be the reverse image of the workpiece. Although, this process is not directly connected and it does not leave any stress on the part's surface, the degree of surface finish quality still depends

on many factors such as tool surface quality, the complication of the part, part size, media particles size and current density. **Figure 4-18** illustrates this technique. [118]

Figure 4-18: Shows an ECM machine. [118]

4.1.12 BESTinCLASS

BESTinCLASS is a Swiss-based company working in the field of surface finishing. This company has invented a technique called micro machining process (MMP). This is a selective process which deals with specific wavelengths of surface roughness. According to the company, the process is innovative and produces significant practical solutions for surface treatment. This technique is able to obtain a good surface finish which it would be impossible to achieve by employing traditional techniques. It is also worth mentioning that the technique does not have side effects on the parts mechanical properties and tolerance accuracy.

The process is emergent, and has been available and in development since the beginning of this decade. MMP has been extensively used in many fields such as aerospace, medical and automotive engineering sectors, luxury goods, and other additive manufacturing applications. [120]

Table 4:10 illustrate some of the materials that can be treated and the degree of micro machining process.

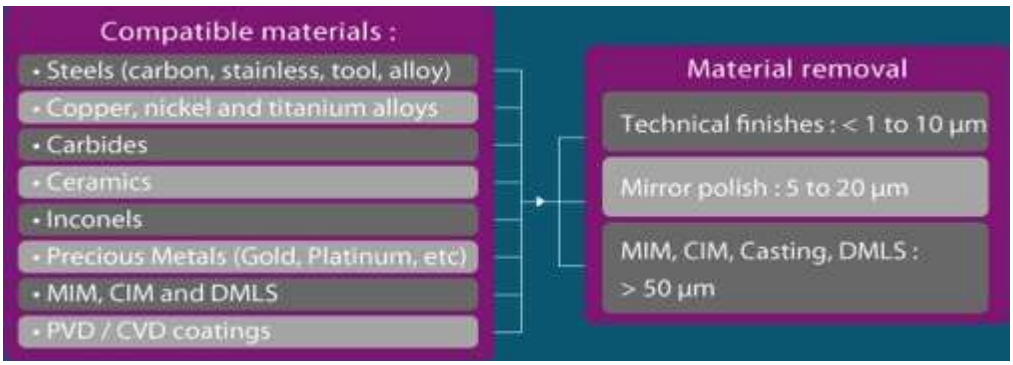

Table 4:10: Shows compatible material and its micro machining process. [120]

MMP is significantly effective on all kinds of alloys as was mentioned earlier. It is highly capable of treating parts produced by any manufacturing method such as subtractive, moulding/casting as well as additive manufactures techniques.

An investigation was completed by Jobin [121] on the surface topography of parts produced by direct laser sintering on an (M270) machine, EOS brand. This machine employs a 200 watt fibre laser, a 20 micron spot size and a build volume of 250x250x215 mm. A comparison between maraging steel (MS), Cobalt-Chromium alloy (CoCr) and Inconel 718 was carried out before and after exposure to different polishing techniques, in order to determine the influence of these techniques on surface topography. After creating the samples and following initial assessment, post processing was carried out using the following methods:

- Abrasive Flow Machining (Extrude Hone brand)
- Vibratory finishing (from Rosler)
- Micro Machining Process (MMP) from BESTinCLASS.

Surface characterisation was obtained before and after surface improvement; an Atomic Force Microscope (AFM) was used for qualitative images and a surface Stylus Profilometer (SP) was used for quantitative details. The main aim was to quantify which is the most significant technique for improving the surface roughness component. The authors found that each post-processing technique was able to completely remove the laser track structure from the raw materials, while keeping a dimensional tolerance about of 10 µm as shown in **Figure 4-19.** [121]

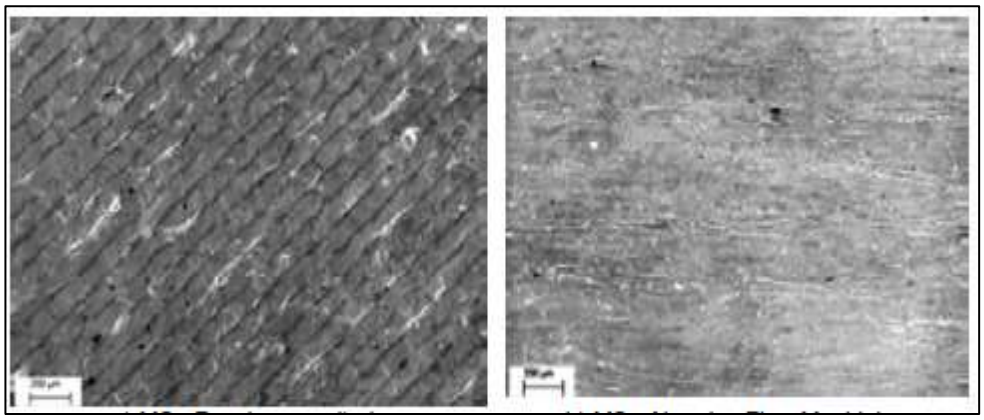

Figure 4-19: Sample before and after machining. [121]

Figure 4-19 shows, there was also good improvement of surface roughness after treatment, but the processes still presented some other drawbacks such as pores and dendrites spread over the surface. The results are summarised in **Figure 4-20.**

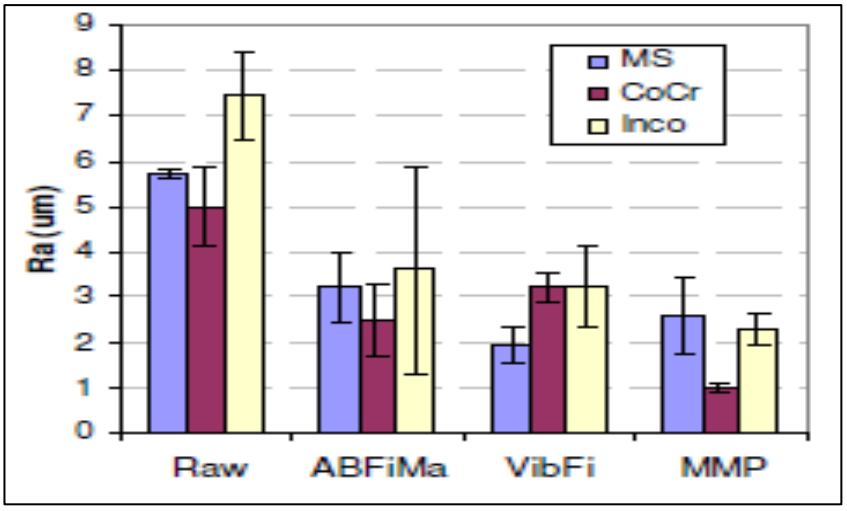

Figure 4-20: Roughness results comparison between the processes. [121]

4.2 Thermal methods

Thermal methods are another class of process used to improve the surface finish of AM parts and their mechanical properties; it includes several techniques, some of which are:

- Laser surface modifications such as laser re-melting, laser cladding, laser glazing, laser polishing and micro erosion.
- Plasma transferred arc cladding and re-melting.
- Other methods like infiltration.

This study focuses on laser surface modification.

4.2.1 Laser Surface Modification

Laser surface modification for material processing can be divided into three classes as shown in **Figure 4-21**, which are namely heat treatment, melting and vaporization. The classifications of these three classes are dependent on two factors, laser power density and time exposure during the process. Thus, significant results for a specific application can be achieved by careful selection of these factors. [122,123]

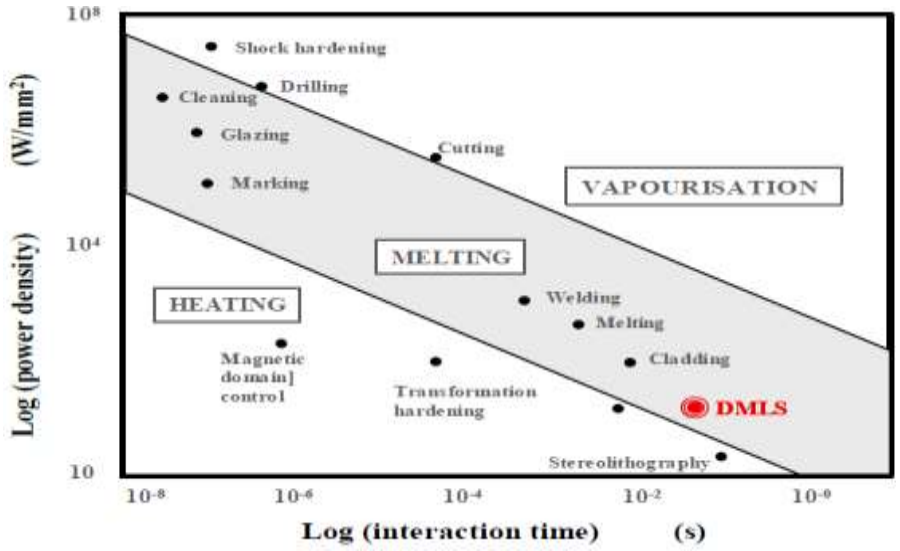

Figure 4-21: Classification of different laser processing techniques. [122]

The local temperature during the process is significantly controlled by the amount of laser energy absorbed by the material through the process. This energy is controlled by varying factors such as laser power P (w), scan speed V (mm/s) and spot size diameter D (mm). The energy absorbed is given by the equation. [92]

$$\mathbf{E = \frac{P}{V*D}} \quad \mathbf{(J/mm^2)} \ldots\ldots \qquad \ldots\ldots\ldots\mathbf{Equation\ 4\text{-}1}$$

4.2.1.1 Laser re-melting

Laser re-melting is a process that has been developed to assist several metal processes to improve quality both inside and outside of the parts. The best description of re-melting is that the metal surface is heated up to the melting temperature, but under the evaporation point. The melt pool has to be rapidly re-solidified without any element addition, in order to avoid modifying the surface chemical composition. The process actions are initiated by heating specific regions of the top surface to generate the melt pool, allowing to the interface elements to diffuse in the liquid phase; the laser then moves away leaving the surface to rapidly solidify. Internal and surface microstructures are refined through the melt region. In general, the depth of this process ranges between 10-1000microns, depending on the laser parameters and the purpose of the process. **Figure 4-22** showing the principle of process. [70,124]

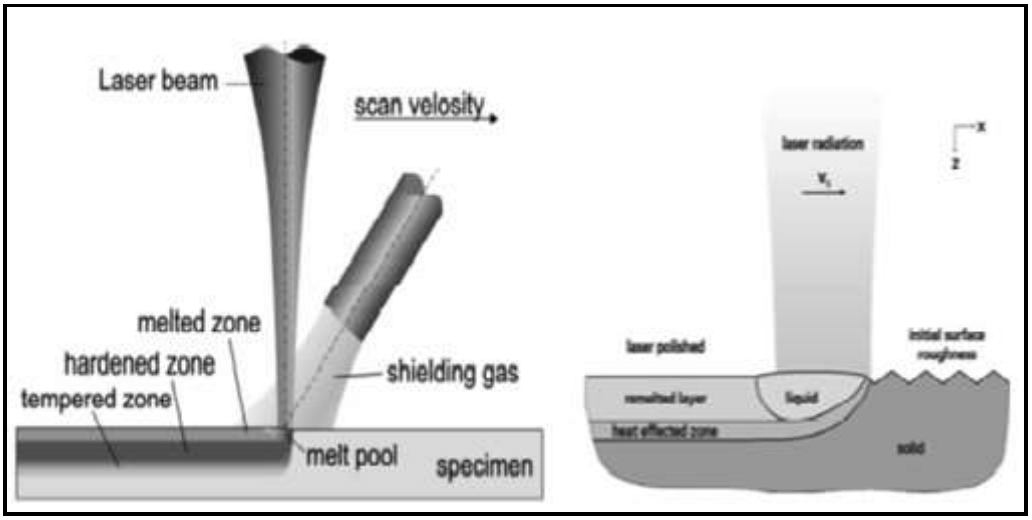

Figure 4-22: Laser re-melting Process. [71]

Generally, the laser re-melting process is applied after use of conventional machining techniques, to remove surface imperfections, improve mechanical properties (customise microstructural characteristics) and reduce residual stress on the outer layer. In additive manufacturing, applying the laser re-melting process during a build means that after scanning each layer and melting the powder, the same layer is re-scanned again before adding another new layer of powder on top of the surface [94, 4]. If this step is completed for every single layer, the manufactured parts will be almost 100% dense and have reduced residual stress by almost 10% [71, 7]. However, along with the increase in density, the manufacturing laser time will increase, leading to an increase in associated costs. Alternatively there is also a possibility of applying the technique on the last layer

that is built. This approach can be completed on the same machine (in-process) or as post-processing (out of machine). [94, 65]

There is a significant amount of research in the application of laser re-melting to AM. For instance, Kruth has indicated that surface roughness can be improved from 12 to 1.5 µm after this process, which means that laser re-melting has the ability to improve surface roughness up to 90% from the total value of the preliminary surface roughness. The best results were obtained when utilizing low scan spacing (20 µm) combined with a medium range of scan speed (200-400 mm/s) and a laser power of 85-95 w. [4]

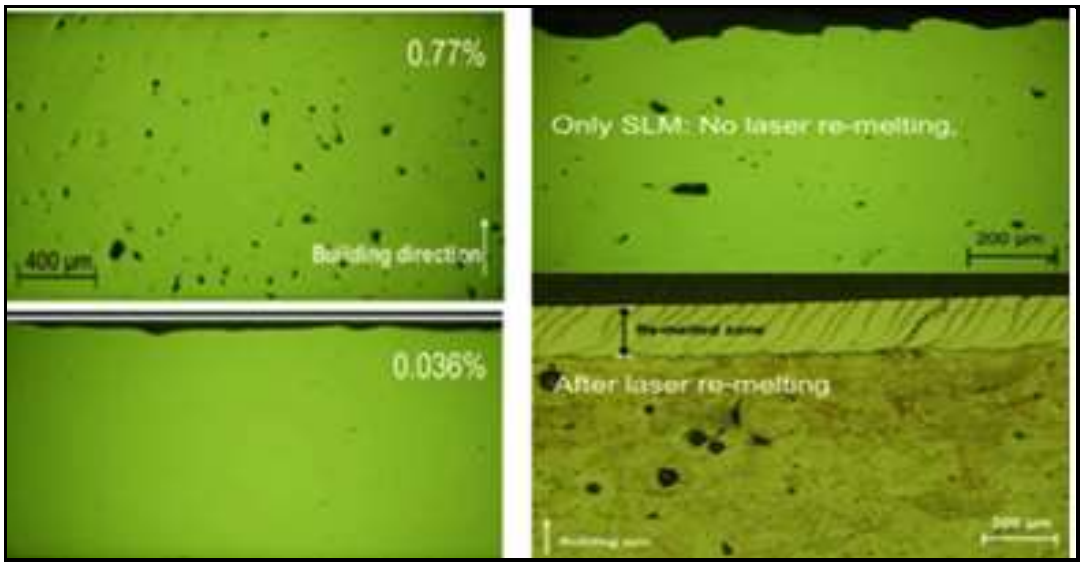

Figure 4-23: 2D micrograph to show the influence of laser re-melting on part characterization. [4]

Although SLM has the ability to produce parts up to 98% dense [23], the amount of residual pores may be a major problem for certain applications such as aerospace and automotive, where high strength and wear resistance are required. Thus, laser re-melting may not only be applied to the modification of surface roughness but may also be applied to improve other surface properties including surface accuracy, density and increased mechanical properties like strength, corrosion resistance, micro hardness, wear behaviour, fatigue and friction. [125, 4, 37]

Another study carried by Kruth [64] on stainless steel 316L improved surface roughness and other properties. Results showed that laser re-melting can reduce residual stress by almost 10%. It was also apparent that laser re-melting during the additive manufacturing process has not been studied in depth due to several issues such as powder remaining in the bed interfering with the process, access of the laser to the sides of the part etc. [64]

A further study by Kruth [72] and co-author was performed on stainless steel and titanium. The results of surface quality of parts produced by SLM, and also exposed to Selective Laser Re-melting (SLR) showed great improvement in *Ra*. A typical average roughness (*Ra*) of SLM parts is approximately 15µm with a standard deviation of 3µm. A good improvement after re-melting was obtained by around 90%, meaning that the *Ra* was reduced from 15µm down to 1.5µm.

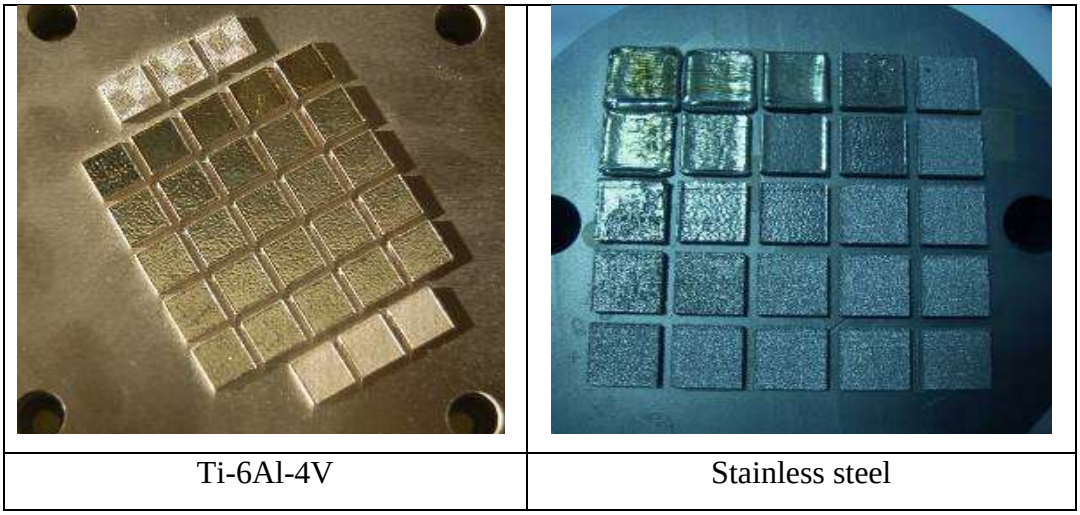

Ti-6Al-4V	Stainless steel

Figure 4-24: SLM parts prepared for SLR, Stainless Steel on right and Ti-6A1-4V on left. [72]

Through the investigation, laser re-melting was presented as a better method of improving the surface qualities of layer manufactured powder parts. Apart from this, the micro hardness and microstructure of the entire part were improved by this technique as well. [72, 7]

4.2.1.2 Selective laser erosion

This technique removes thin layer from the main part, by focusing small, highly controlled laser pulses. Thus, this technique (selective laser erosion) is considered a subtractive technique and is usually used for additive manufacturing for different the purpose. The process works by eroding small features (i.e. the surface texture) leading to enhanced surface topography, accuracy and mechanical properties on the part surface. [97]

Figure 4-25 shows parts built by the SLM process and later subjected to laser erosion followed by laser re-melting, to clarify how the surfaces have been improved. The fig also shows a 3D view roughness surface profile where the top half of the section has been improved by the laser erosion method.

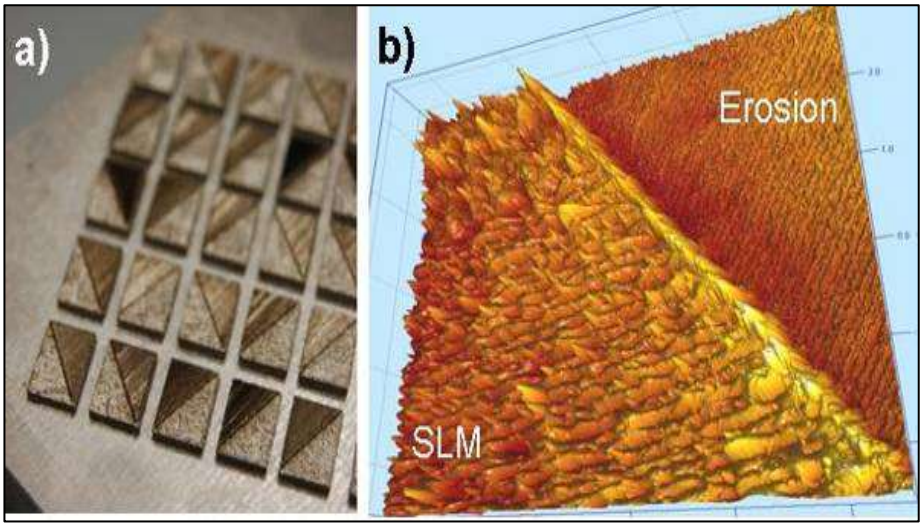

Figure 4-25: Selective Laser Erosion process. [72]

It can be clearly seen that the process specifically removes thin material features due to the laser power produced from the beam. High peak laser powers enable the material to evaporate. The results show that the average roughness (Ra) of selective laser melting parts can be improved to 6µm after SLE and can be reduced to 1.5µm after SLR. Therefore if both erosion and a re-melting process have been applied, the average roughness and total roughness will be reduced by almost 95%. They have pointed that it best to apply surface erosion first and then surface re-melting to produce a good surface finish. [6, 72]

Figure 4-26: Shows how the surfaces were improved. [72]

The SLE technique is also used for other reasons during the SLM process and some of them are as follows:

- To improve the quality of each layer deposited by removing recoating artefacts.
- Micro machining – to remove small features.
- To get better X and Y dimensional accuracy. [6, 72]

4.2.1.3 Selective laser polishing

Selective laser polishing is a technique used to re-melt the part surface to a small depth (< 5 micron), by utilizing pulses of laser beams moving in two directions (x,y),whereas the z direction used to position (focusing) the laser beam spot size vertically on the surface and controlled by specific parameters (CNC control). The laser polishing method can create a heat affected zone ranging from 100-150µm [73] . In this way, during the laser scanning process a thin surface layer is re-melted to create a smooth surface. Specifically, this surface smoothing is created by the surface tension of the melt pool. This process can be connected to an increase in surface accuracy and improved mechanical properties such as wear, fatigue and corrosion resistance of metal AM parts. This is because the fatigue phenomena is linked to surface roughness, but also because the microscopic structure of the surface is changed as a result of the laser polishing process, as is the heat affected zone. [71, 74] **Figure 4-27** shows a schematic of the laser polishing process.

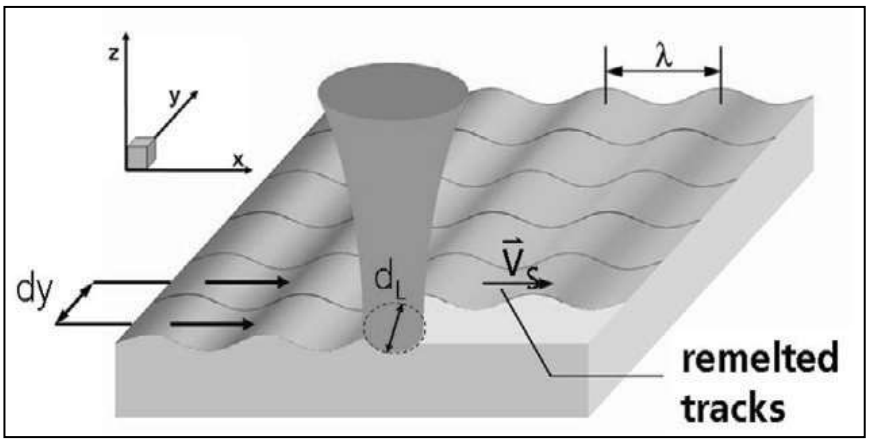

Figure 4-27: Shows Laser Polishing Process. [73]

The depth of tracks and material re-melting achieved with the process is variable and depends on factors such as scan speed, laser power and beam spot size.
The relation between these factors is

E = 6000*P/ (V*D) …… ……Equation 4-2

Where, E is energy density by J/cm^2, P is power (W), V is feed rate (mm/min) and D is spot diameter (mm).
Ukar [126] and co-authors have studied the influence of laser polishing on the surface roughness of tool steel by utilizing two different laser types, fibre laser and high power

diode laser in order to reduce the surface roughness. Results show that the best surface roughness values (*Ra*) were improved to lower than 0.9µm from 7.07µm initial roughness. These results were obtained from both type of laser and the optimal parameters implemented in this experiment were laser power ranges between 700 and 800 watts, while the feed rate and spot size were kept constant at 1920 mm/min and 2 mm respectively. Thus, the laser energy absorbed through this process is about 1100 ±10% J/cm,^{2} which is calculated with the above **equation 4-2**. [126]

Table 4:11 shows the optimal parameters and results.

Power (w)	**Feed rate (mm/min)**	**Spot width (mm)**	**Energy density J/cm^2**	**Initial values (µm)**			**Final values (µm)**					
				Ra	*Rz*	*Rt*	*Ra*	*Rz*	*Rt*	*Ra%*	*Rz%*	*Rt %*
700	1920	2	1093.8	7.07	30.78	31.60	1.37	9.19	10.59	80.62	70.23	66.49
750	1920	2	1171.9	7.07	30.78	31.60	086	4.69	7.68	87.84	84.81	75.70
800	1920	2	1250	7.07	30.78	31.60	1.39	1040	11.40	8034	66.31	6392

Table 4:11: The optimal parameters and results. [126]

In a study done by Lamikiz [75] and co-authors, the method was performed by scanning the top surface layer using CO2 and Nd-YAG laser beams at very high speed in a vacuum chamber. The chamber was set and maintained with argon flow. The laser beam power was carefully controlled to polish the microscopic top layer. The **Figure 4-28** shows a schematic diagram of laser surface polishing carried out [75]**.** It is worth mentioning that the laser process depends primarily on the energy density of the laser beam, the kind of metal surface and the initial surface texture of the original parts.

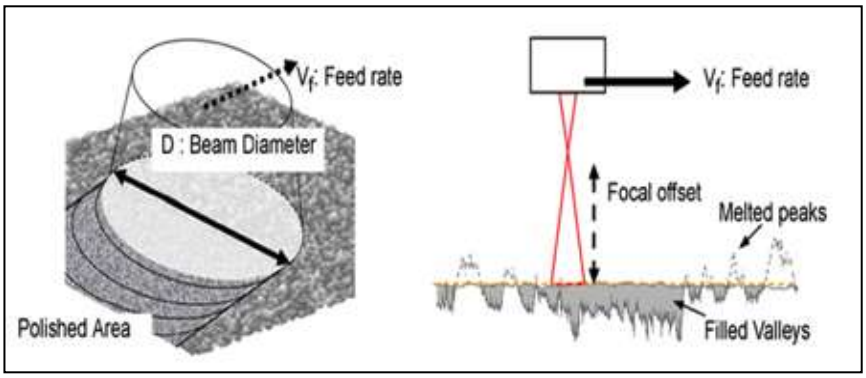

Figure 4-28: Schematic diagram of laser polishing process.

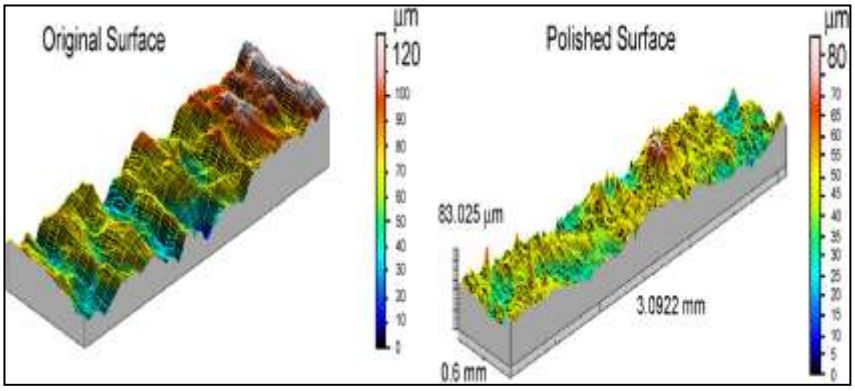

Figure 4-29: Shows an original and a polished surface. [75]

The experiments were carried out by constructing a physical 3D model using Selective Laser Sintering (SLS) in order to check the capabilities of laser polishing for surface texture improvement. **Figure 4-30,** shows a model test piece, with three different slope angles, namely 15^{o}, 30^{o} and 45^{o}. From the results, it was found that laser polishing is very effective on layer manufactured parts. The obtained average roughness (*Ra*) was between 1.2 and 1.5µm. [75]

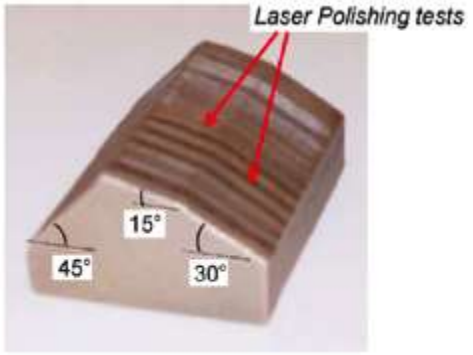

3D test piece built by SLS

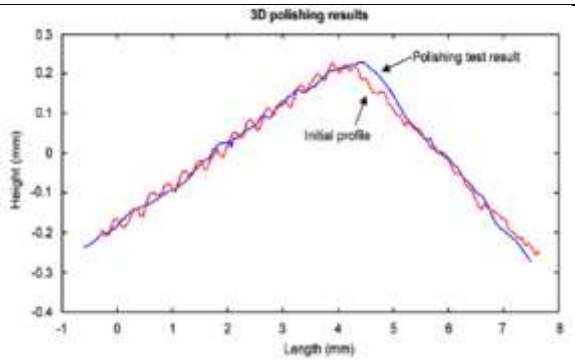

3D laser polishing profile

Figure 4-30 : Shows test piece and laser polished profile. [75]

The results showed that the laser-polishing process is a very effective method, due to its capability to eliminate the surface texture of layer-manufactured parts by almost 80% and with no signs of profile deviations.

A study by Ramos and co-authors on silica rods and a stainless steel part acknowledged that the laser is an excellent tool for surface modification and this primarily depends on laser density and period of interaction. Laser polishing of silica rods improved surface

texture from 2.0µm to 0.5µm *Ra* when conducted with a 25W CO_2 laser to give an energy density of 1000 J/cm.^{2} [76]

The aforementioned parameters were used to polish SLS stainless steel (grade 420 SS 40 wt. % bronze) parts. **Figure 4-31** Shows optical micrograph polished using Nd: YAG laser 420 SS 40 wt % bronze SLS and resolution was 100x, surface roughness was reduced from 9.0 – 2.40µm. [76]

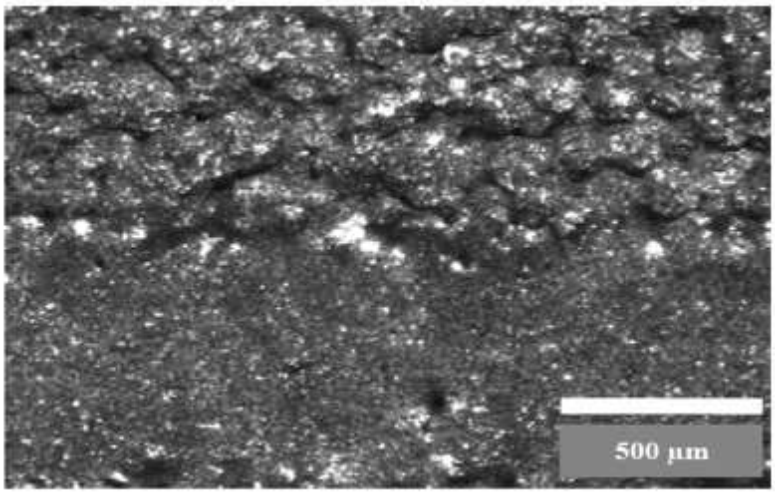

Figure 4-31: Optical micrograph of Nd: YAG laser polished tracks on top surface, resolution was 100x. [76]

4.2.1.4 Surface glazing using electron beam

Surface glazing is another method of improving the surface finish of layer manufacturing parts. This method occurs simply by remove the loose powder particles and glazing the surface by electron beam. Most of the parts produced through the SLM process have a surface texture which resembles sand cast parts. The loose powder is always in contact with the area that is being fully solidified by the laser beam during the construction and partially melted particles adhere to the edge of the melt pool. Surface glazing can be used to improve the surface roughness of AM manufactured parts based on removal of these powder particles by blowing them using air and finally glazing the surface of the part by electron beam.

This post-processing method was investigated by Cormier [127] and co-authors, when they were optimizing the electron beam melting (EBM) process. The technique was performed by utilizing a rectangular box of 100*100*150 mm dimension, which was placed inside the EBM machine as shown in **Figure 4-32**. The surface roughness

measurements by a profilometer indicated that the initial surface roughness measured on this box was 19.78µm *Ra*. This box had been exposed to EBM for optimisation and this was evidenced by the loose powder which was in contact with the area that was completely solidified by the electron beam. [127]

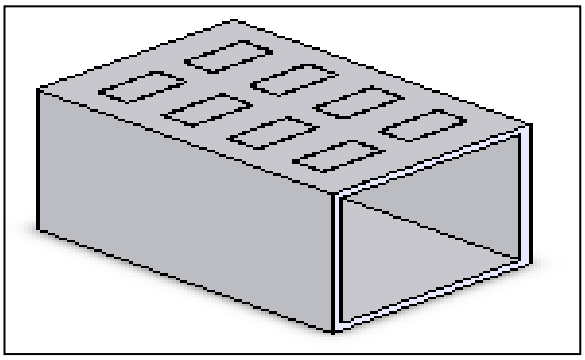

Figure 4-32: Surface finishing testing box. [127]

Glazing was applied to the upwards facing rectangular patches using a combination of different parameters of electron beam power and scan speed, to see their effects on surface roughness. The beam current used was varied from 5mA to 20mA and beam velocity from 100mm/s to 500mm/s.

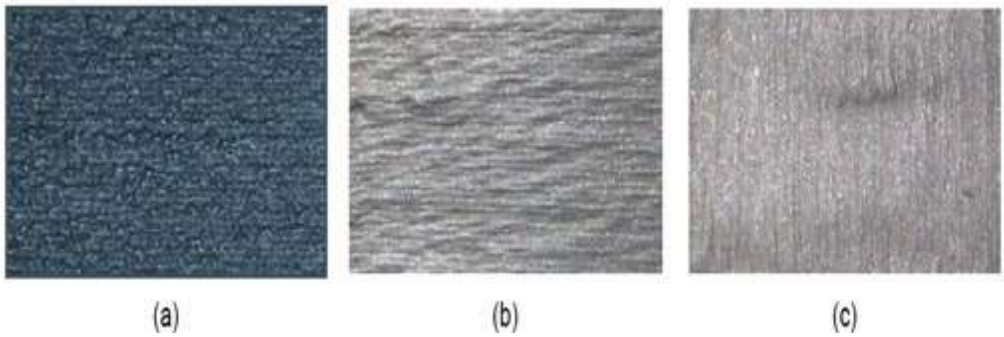

Figure 4-33: Micrographs showing the original A, and the glazed B and C. [127]

The difference between A, B and C, **Figure 4-33**, was that the beam power on B was scanned parallel to the layers deposited, and on C was perpendicular to the layers. The surface roughness (*Ra*) on B was 1.78µm and C was 0.65µm. Thus, the results reported suggest that scanning perpendicular to the layers deposited gives the optimal surface texture improvement. [127]

4.3 Electro chemical techniques

This section describes the definition of this process, the mechanism and the effects of an electropolishing process on the surface roughness of metal parts. The technique can be divided in two different techniques: electropolishing and electrodepositing; this section concentrates on electropolishing as a technique implemented for surface improvement.

4.3.1 Electropolishing process

Electropolishing is an electrochemical technique of controlled dissolution useful for improving the surface topography of several metals/ alloys. Generally, the electro chemical process (ECP) is a post-processing method that is used for surface property improvement. The normal amounts of surface dissolution are between approximately 0.05 to 50 µm depending on the process duration. These results can improve surface characteristics such as corrosion resistance, wear and friction by reduction of the amplitude of surface roughness parameters; this subsequently increases its optical brightness and reflectivity.

Several materials can be polished such as copper, nickel and titanium etc. The majority of research has been conducted on stainless steel alloys. [128, 129]

Generally the process mechanism involves the immersing of a metal part in a chemical solution and bringing it in contact with the anode in a direct current circuit. The ECP technique depends mostly on the ability of the solution to consistently polish the surface of the metal/alloy (the substrate) without leaving any corrosion marks on the surface. The main factors that influence the effectiveness of this process are:

- The period spent by the component in the solution.
- Uniformity of the material microstructure.
- The consistency of the surface finishing over the required area.
- Cell parameters (current, voltage and temperature).
- Concave surfaces.
- Internal features.

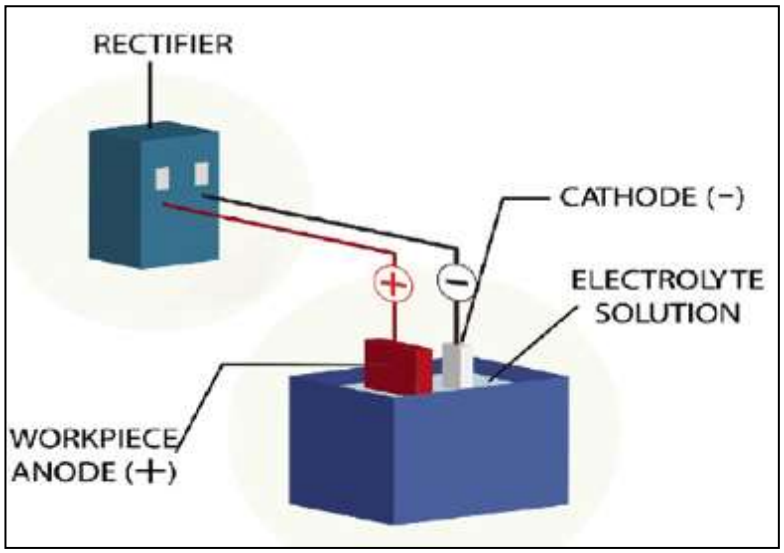

Figure 4-34 : Schematic of Electro Chemical Process. [128]

The process works by anodising and dissolving the substrate in an electrolyte using electricity as an external source. It is worth mentioning that in electropolishing generally two surface phenomena happen, namely anodic levelling and anodic brightening.

Anodic levelling

This results from the different dissolution rates of the peaks and valleys of the surface texture of the substrate that occur due to the primary current distribution in the cell [128]. In such cases, the amount of the primary current distribution has a significant effect on the material dissolution (mass transfer), which leads to a reduction of the surface roughness by a number of micrometres. [129, 130]

Anodic brightening

This phenomenon is due to control of the dissolution rate for the metal microstructure. It takes place when the dissolution rate of the metal is in a mass transport controlled system, leading to deposition of a salt layer which is formed on the electrode (metal/alloy) surface [131]. During the dissolution, a salt layer causes suppression of the crystallographic orientation and surface defect dissolution in the liquid, leading to a nanocryestalline structure can be obtained [132, 133]. Thus, Anodic brightening improves the surface roughness on the submicron scale and brighter reflectivity of the substrate can be achieved.

4.3.2 Major advantages and disadvantages of Electropolishing and challenges

Since being patented in 1930, mixtures of concentrated sulphuric and phosphoric acids have been used for electropolishing of stainless steel and other metal alloys on different commercial scales worldwide.

The primary benefits of this process are:

- Improvement of corrosion resistance and surface roughness.
- Improvement of surface reflectivity.
- Removal of machining burrs.
- Improvement of surface clean ability compared to mechanically finished surfaces.
- Lower bacterial growth rates.
- Lower machined compound surface stress.
- Improved part durability. [128, 129]

Although, the polishing quality of this process is very good, the major disadvantages of it are:

- The solution usually used is extremely corrosive
- The process is hazardous for both the environment and the workers involved in this technique.
- Extensive gas formation is associated and low current efficiency. [134]

In recent years much research has been concentrated on the use of green processes to minimise the environmental effect from the current technologies, by minimising the waste, pollution and high toxicity with the use of stable room temperature ionic liquids (RTILs) for the process.

Various investigations have been completed on utilising ionic liquid reactions such as catalysis, nanomaterials, electrodeposition and striping which are a greener alternative to the current toxic and polluting volatile organic solvents. [135]

From an electrochemical perspective, RTILs have significant properties such as high thermal stability, non-volatility, high polarity, large viscosity, natural conductivity and wide electrochemical windows. [136, 137]

These properties of RTILs commend their use for electrochemical processes. Abbott *et al* introduced a new alternative for electropolishing based on a mixture of choline chloride and ethylene glycol, a type III deep eutectic solvent called Ethaline 200, which was used for electropolishing of stainless steel because the raw materials used were

cheap and available. This process showed considerable advantages over the commercial process, among those being high current efficiency, negligible gas evolution at the anode/solution interface and a benign liquid compared to the acid mixture solution normally used. [138, 133]

4.3.3 Ionic Liquids

Ionic liquids are salts that exist in liquid state at room temperature and below 100 C°. Cations and anions are both contained in the liquid, usually in large scale organic compounds. By carefully selecting the anions, ionic liquids with a melting point around and below room temperature can be prepared. [133]

In an ionic liquid the cation has great effect on the physical properties of the salt, while the anions demonstrate more effects on chemical stability and reactivity.

The ionic liquids can be modified to meet the criteria for a specific application by selecting suitable cations and anions or can be fine-tuned by modifying a single cation class by changing the nature of one or more substituent alkyl chains. [139]

Nowadays, applications of ionic liquids range from fuel desulfurization to organic synthesis to catalysis to electrochemistry to precious metal processing. This leads to the use of ionic liquids having many advantages over conventional organic solvents but very few have come to practical use although several are at the pilot stage. [139, 140]

4.3.4 Ionic Liquids as Electrochemical Solvents

By far the largest academic activities have been concerned with chemical synthesis and metal deposition and the lack of commercialized processes naturally has some economic reasons.

Ionic liquids have a wide range of applications in electrochemistry, including electro deposition, electropolishing for ferrous and non-ferrous material, and in electrochemical devices like lithium batteries, photo-electrochemical cells, fuel cells and capacitors. The key advantages of ionic liquids being used in electrochemistry are:

- Low vapour pressure
- Wide variety of potential uses.
- High solubility of metal salts.
- Avoidance of water and oxidation.
- High conductivity, compared with acid mixture solvents. [137, 133]

4.3.5 Deep Eutectic solvents

Deep eutectic solvents (DES) are a sub-category of ionic liquids. Recently, the Abbott group introduced the concept of Deep Eutectic Solvents. A DES is a fluid coming from materialisation of the eutectic point as a result of the mixing of two or three components which are capable of combining with each other, frequently through hydrogen bond interactions.

In such cases the eutectic mixture formed can be characterized by the lowest melting point, compared with the melting points of each individual component. [141, 142]

Figure 4-35 shows eutectic point of the mixture components resulting in the lowest temperature point.

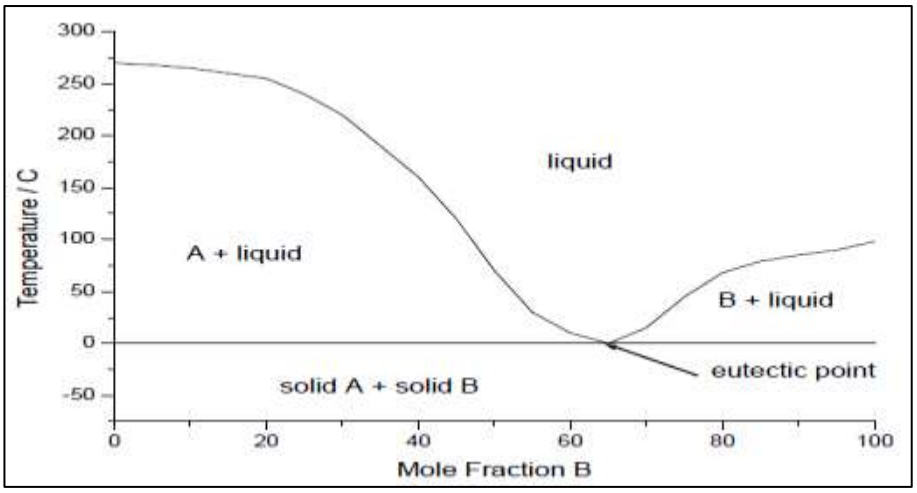

Figure 4-35 : Schematic eutectic point on a two component phase diagram

Since DES has been used, reductions of several hundred C^o in freezing temperature have been observed. [143]

In general there are four types of deep eutectic solvent, shown in **Table 4:12.**

Type I, II and IV all utilise some form of metal salt mixture with organic salts or a hydrogen bond donor, whereas type III utilises a hydrogen bond donor with organic salt.

Type I	Metal salt + Organic salt
Type II	Metal salt hydrate + Organic salt
Type III	Organic salt + Hydrogen- bond donor
Type IV	Metal salt hydrate +Hydrogen-bond donor

Table 4:12: Shows four types of deep eutectic solvent. [144]

Type I DESs are systems consisting of a mixture of metal halide salts such as AlCl2, ZnCl2 etc. with choline chloride (ChCl) in a1:2 ratio. The physical properties of the liquid are highly dependent on the interaction between components. Empirical results have shown that the type I eutectics are mostly suitable for Ga, Al and Ge deposition.

Type II DESs are systems used to mixed metal salt hydrates such as CoCl12.6H2O, CrCl3.6H2O etc. with choline chloride (ChCl) to create the DESs. In such cases the metal hydrate is the anionic component and it is difficult to make DESs with anhydrous CoCl12, even if the equivalent of 6 moles of 6H2O is added to the liquid. It is worth mentioning that the type II DESs are easier to make rather than type I, demonstrating less sensitively to the air and water due to the metal salt hydrate. Also, studies have shown that it is most suitable for Cr deposition. [145]

Type III DESs are made by mixing an organic salt (choline chloride) with hydrogen bond donors. Many types of hydrogen bond donor have been used in this system. The first system was studied by Abbott et al; it involved choline chloride mixed with urea in a 1:2 ratio (Reline) in order to generate DESs with a lower freezing point. Also, other systems can be made such as Ethaline and Oxaline. The Ethaline is a mixture of ChCl with ethylene glycol (EG) as hydrogen bond donor in a 1:2 ratio, whereas Oxaline is made by mixing ChCl with Oxalic acid dihydrate in a 1:1 ratio. The type III eutectics are suitable for many applications such as deposition of Ag, Cu, Zn etc. and electropolishing. [146]

Type IV DESs are the newest class of DESs, which use a metal salt hydrate such as $CoCl_{12}.6H_2O$ or $CrCl_3.6H_2O$ instead to organic salt (choline chloride) to mix with hydrogen bond donors (Urea). The eutectic result from this class is commonly used for metal deposition. [145]

It can be seen that the most common quaternary ammonium used in this field (DESs) is choline chloride with different metal halides (hydrogen bond donor).

4.3.6 Electropolishing using ionic liquids

Electropolishing is an electrochemically controlled technique mostly used for improving surface properties such as a reduction of surface roughness, brightening corrosion and wear resistance. Most current electropolishing of stainless steel is performed on a commercial scale using a mixture of phosphoric acid and sulphuric acid. The practical aspect of the process is extremely successfully conducted although with some

drawbacks e.g. the liquids are highly corrosive and extensive gas creation occurs during the process, leading to poor current efficiency. [147]

In recent years, studies have established that a type III DES (choline chloride mixtures with ethylene glycol as hydrogen bond donor) can be used for metal electropolishing. The process has significant advantages such as high current efficiency with limited gas creation at the anode interface surface. The results also showed that the liquid is non-corrosive, in contrast to the current aqueous solution. It is worth mentioning that the mechanism that occurs during electropolishing in an ionic liquid can be controlled by the amount of the chloride ion at the anode surface. [137, 146]

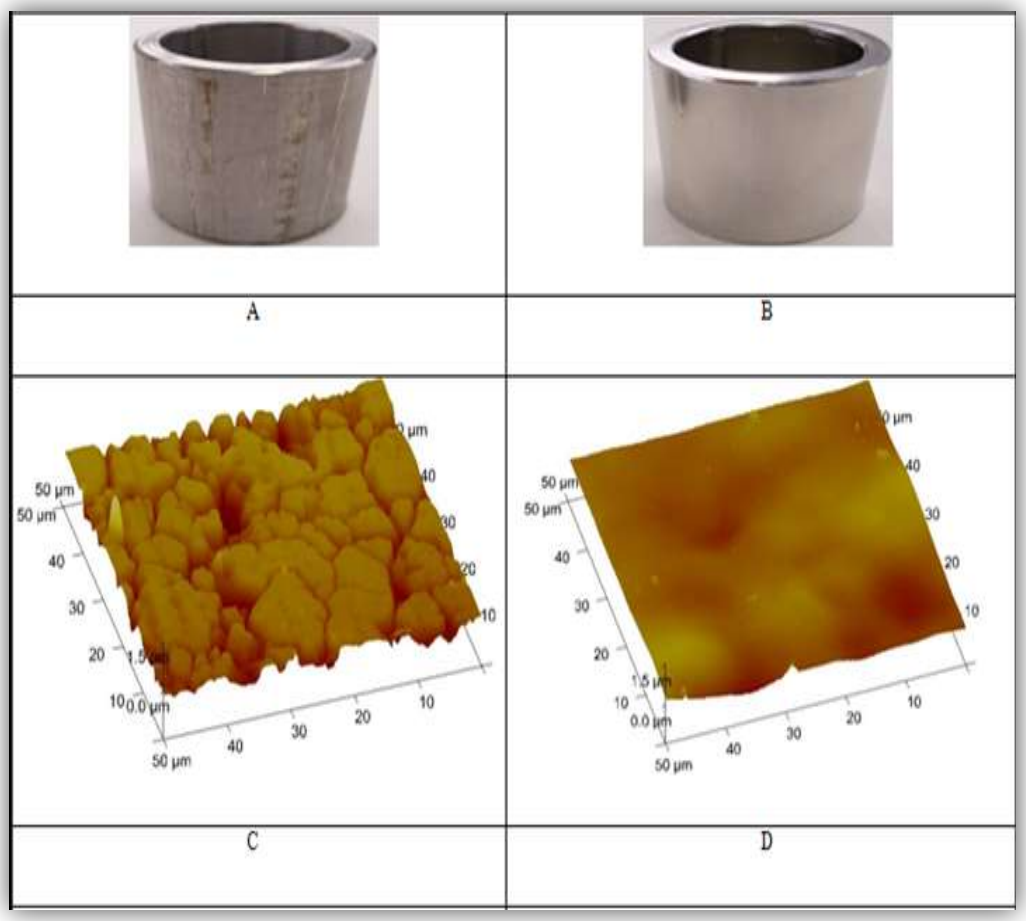

Figure 4-36: Comparison of unpolished and electropolished stainless steel (AISI 316L) in deep eutectic solvent (ChCl: EG).

Figure 4-36 shows photographs of a stainless steel part before and after electropolishing (photographs A and B respectively) with graphs C and D showing the respective AFM images of the part's topography. [138]

Figure 4-37: Parts polished using ionic liquids. [148]

Figure 4-37 shows typical stainless steel type 316 parts that that have been successfully electropolished in a ChCl: EG. In this process the oxide film was removed at a lower current than typically used with aqueous acidic solutions and also micro-roughness was reduced to less than 100nm. Also the results showed that electropolishing based on an ionic liquid is non-corrosive and moisture stable compared to aqueous acid solutions [137, 149]. The process is safe due to the naturally occurring components which are non-toxic. Choline chloride, known as pro-vitamin, has been used for many years in chicken feed. Regarding the cost affect, the technology was scaled up to pilot plant scale (50 litres) and then to commercial scale (1300 litres). Empirical results have shown that the cost of electropolishing by using DESs is the same as using a scale mixture of phosphoric acid or sulphuric acid, due to the improved current efficiency which was shown to be about 4 times better than an equivalent aqueous system. [150]

Reviews of electropolishing based on DESs for conventionally made parts have been published, whereas for AM components none were found by the author.

4.4 Chapter summary

Various techniques have been used over last decade to improve the surface properties of AM engineering materials, to increase their mechanical and physical properties. In conventional applications, several techniques prove to be very effective in achieving good improvement of surface finish, but some of them suffer from some limitations associated with the complexity of the engineering parts' features, or the need to be tailored for specific purposes. Furthermore, they can damage small features, or leave residual stresses in the part. In addition, for AM parts, the residual porosity associated with AM technology can be a major limitation to achieving a good surface finish; which can be appearing on the surface.

Thus, the selection of a method to improve the surface finish of a part will depend on the part feature (geometry), mechanical properties required, type of material and degree of accuracy required. **Table 4:13** shows a technical comparison between the three classes of finishing process.

Characterization	Mechanical	Thermal	Electrochemical
Cost	**Low/ high**	**Low / high**	**Low**
Carbon footprint	**Low /high**	**Low/high**	**Low**
Improve surface finish	**Yes**	**Yes/no**	**Yes**
Reduce porosity	**On the surface**	**On & in surface**	**On surface**
Typical cycle time	**Low / high**	**Low / high**	**Low /high**
Part volume	**Good**	**Good**	**Extra**
Cost effective for Low value parts	**Low / high**	**Low / high**	**Low**
Material	**Metal & non metal**	**Metal & ceramic**	**Metal**
Material removal(rate)	**Low /high**	**Low/ medium**	**Very low**
Residual Stress	**Low /high**	**Low**	**No**
Side effect	**Yes**	**Yes**	**No**
Maintenance	**Low/high**	**Low/high**	**Low**
Adapts to automation	**Yes**	**Yes**	**Yes**

Table 4:13: Technical comparison between Mechanical, Thermal, Electrical methods.

Table 4:13 shows how the techniques interrelate with the parts properties. Also the comparison between these methods has shown that the electrochemical technique could be the best for micro roughness treatment.

On the other hand, thermal techniques show significant advantages as alternative surface treatment methods to the conventional ones, due to the process' capacity to suppress surface texture and porosity issues.

Other methods such as Hot Isostatic Processing (HIP) and Impregnation may facilitate in some cases. HIP is a method which is used to reduce or eliminate porosity in ceramics and metal castings. This method can also be used on SLM parts and the residual porosity will be not fully eliminated due to a number of the porosity defects being connected with the surface of the part. Another method is impregnation of the base material with another metal that has a low a melting point, which can be used for certain purposes. However it can be not generally recommended due to fatigue failure implications. [49, 50]

As an example, interesting work has been carried out by Kruth et al, in which all the re-melting was done in the same SLM machine. The results obtained show that the surface finish on the top surface of the parts was improved by approximately 90%, whereas inclined surfaces with different angles (10°, 30°, 50° and70°) showed less improvement (ranging between 60 and 70%) compared with the initial roughness. This was attributed to the absence of flexibility of the laser to move perpendicularly to the surface during the re-melting process. However, the results did show that there was an improvement of surface finish compared to the initial results. The best average roughness (*Ra*) result recorded in this field was 1.25µm obtained by combining laser erosion and laser re-melting in the same station. [6, 7]

The work in this project will be focused on work that has been done by Kruth to re-melt stainless steel parts, but will use other surface improvement technologies, firstly laser re-melting as a post-processing technique, for flat surfaces inclined at angles of (0, 15°, 30°, 45°, 60°,75 and 90° from the horizontal). The main aim of this is to optimize the parameters and to find out the capacity of laser re-melting to eliminate the primary surface roughness and improve other properties such as porosity and reduce residual stress as well. Analysis of surface characterization results will be performed, to compare with the initial manufactured results, to see how surface has been improved.

In the next stage (the stage after re-melting), electropolishing using ionic liquid will be implemented to reduce the secondary surface roughness obtained from the previous stage (re-melting). Again, the surface characterization results will be assessed and compared with the initial results.

In addition, fatigue tests will take-place after the second stage to check the performance of SLM parts subjected to two stages of surface improvement (fatigue life with varying amounts of surface roughness improvement).

According to my research, the above proposed work has not been done by anyone before and it will help to contribute to the efficiency of these techniques for improving the surface finish of parts made by SLM.

5.0. Methodology

5.1 Scope of research

The scope of the study is to improve the surface finish of SS316L parts produced by SLM. The unique aspect of the proposed methods is to provide a high quality of surface finish while maintaining the geometric accuracy of the parts. The proposed method is a combination of two different post-processing techniques laser re-melting and electropolishing to address the limitations of the current methods used (**see chapter four for surface finishing methods**). This work is divided into three phases (chapters) and each chapter involves several stages as shown in **Figure 5-1**. Preliminarily experimental work will take place to assess the machine repeatability and obtain part characterizations.

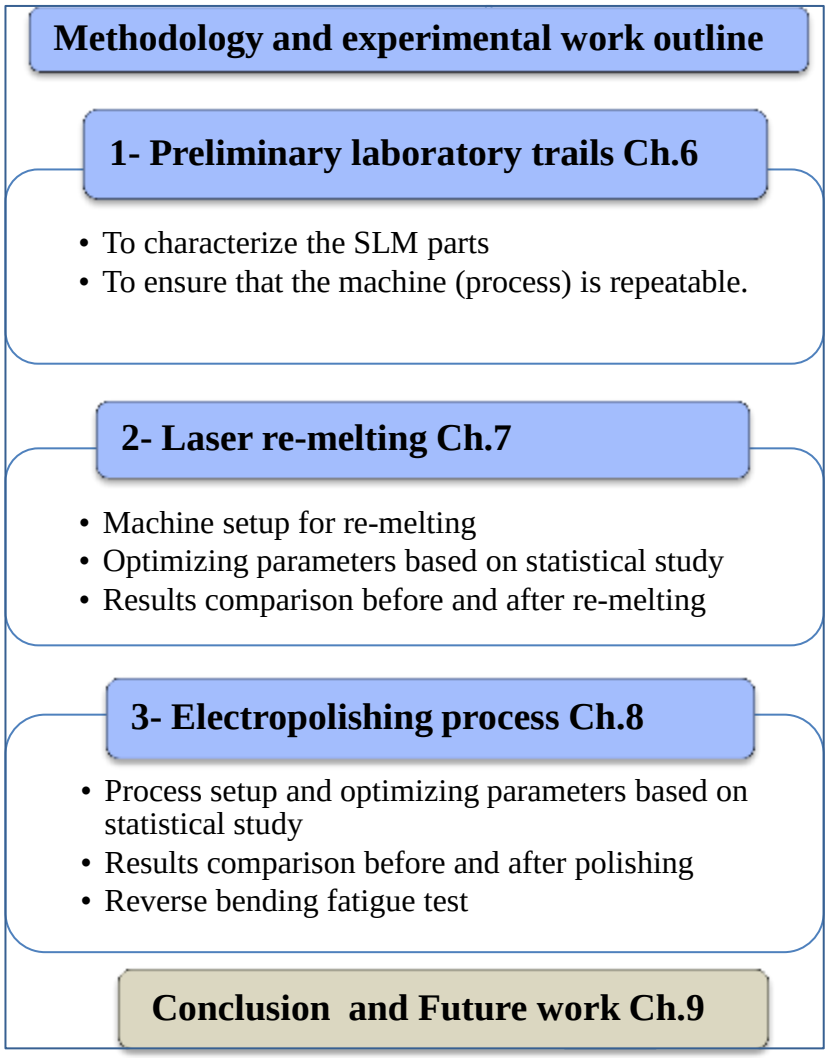

Figure 5-1 : The three phases of experimental work.

5.1.1 Preliminary laboratory contact trial

The main aim is to devise and explore the effect of the machine parameters on part geometry and quality (part characterization). The assessment of surface roughness (*Ra*), topography and density are significant factors to evaluate the machine repeatability. This work will be carried out through three stages as shown on **Figure 5-2.**

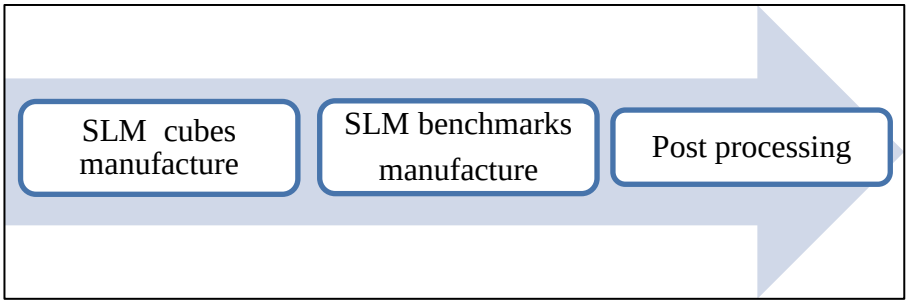

Figure 5-2: The three stages of phase one.

5.1.1.1 Stage one (cubes manufacture)

Experiments will be carried out by producing cubes, and after individual inspection a stylus profilometer will be used to assess the surface roughness.
Surface topography and density determination will be obtained to ensure that the cubes were produced properly and the machine process is repeatable.

5.1.1.2 Stage two (SLM benchmarks manufacture)

Small benchmarks will be made of flat surfaces with different slope angles and horizontal surfaces at different heights. At this stage surface roughness, topography and density are also important, in order to realize the effect of part geometry design on the surface roughness, topography and density as well.

5.1.1.3 Third stage (implement two different post-processing approaches)

The previous benchmarks of stage two will be exposed to two different steps of post-process: sand blasting and electropolishing. The surface character will be investigated after each step and assessed for roughness and topography in order to quantify the improvement after each step and also to determine the surface defects after post-processing.

5.1.2 Laser re-melting

In this chapter laser re-melting will be employed to improve the surface roughness of SLM components. Also to consider the reliability of the technique by comparing results before and after have been re-melted. This chapter is divided into two stages as follows:

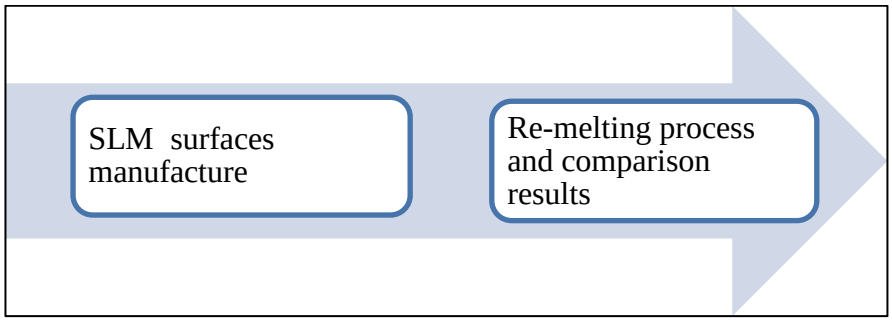

Figure 5-3: The outline of re-melting phase

5.1.2.1 Stage one (surfaces manufacture)

- Use SLM 125 machine at DMU to create samples.
- Remove supports and visually inspect parts to ensure that the parts can be made reliably.
- Determine surface roughness and surface topography.
- Determine density of parts.

5.1.2.2 Stage two (re-melting process)

- Machine setup for re-melting.
- Optimizing parameters based on statistical study
- Implement the optimum parameters to re-melting different inclined surface.
- Determine the surfaces roughness and surface topography to ensure that the processes are being performed appropriately.
- Compare the results before and after re-melting.

5.1.3 Electropolishing

In this chapter, the study will focus on implementing the final finishing method by electropolishing using a green process (ionic liquid) to refine the secondary surface roughness obtained from the previous phase (re-melting) and improve surface roughness and brighten of the parts. The process will be carried out with different parameters in order to optimize the parameters for polishing.

- The test samples obtained from this processes (electropolishing) will be assessed for surface finish and surface topography and compared to the results with the previous two phases (as fabricated and re-melted).
- Finally, reverse bending fatigue tests will be implemented to investigate the effects of the surface roughness component of SLM parts subjected to different stage of surface roughness improvement and to compare the results.

5.2 Materials and manufacture equipment

5.2.1 Materials used (Stainless steel 316L)

Stainless steels are very important category of alloys due to their plenitude of applications, which range from highly sophisticated ones like aerospace, medical and automotive applications, to very low end use like cooking utensils and furniture. Furthermore, stainless steel has become the most popular metal used for SLM applications due to its ability to produce fully dense parts direct from CAD. Stability and corrosion resistance are major concerns in the engineering sector. These are NiCrFe alloys in which iron creates the bulk material and contains at least 16.5% chromium and up to 13.5% nickel and smaller amounts of other components as shown **Table 5:1**. An adherent chromium oxide layer is formed on the surface which confers its corrosion resistance. Nickel is used to obtain an austenite microstructure hence improving its ductility, toughness and weldability. Molybdenum is added to enhance resistance to pitting and crevice corrosion in more hostile environments.

By properly adjusting steel chemistry there are three types of microstructures which can be obtained namely ferritic, austenitic and martensitic. [151, 152] Thus, on the basis of these categories, stainless steel can be classified into several classes. "These are (1) ferritic stainless steels, (2) austenitic stainless steels, (3) martensitic stainless steels, (4) duplex stainless steels, (5) precipitation hardening stainless steels and (6) Mn-N substituted austenitic stainless steels." [153]

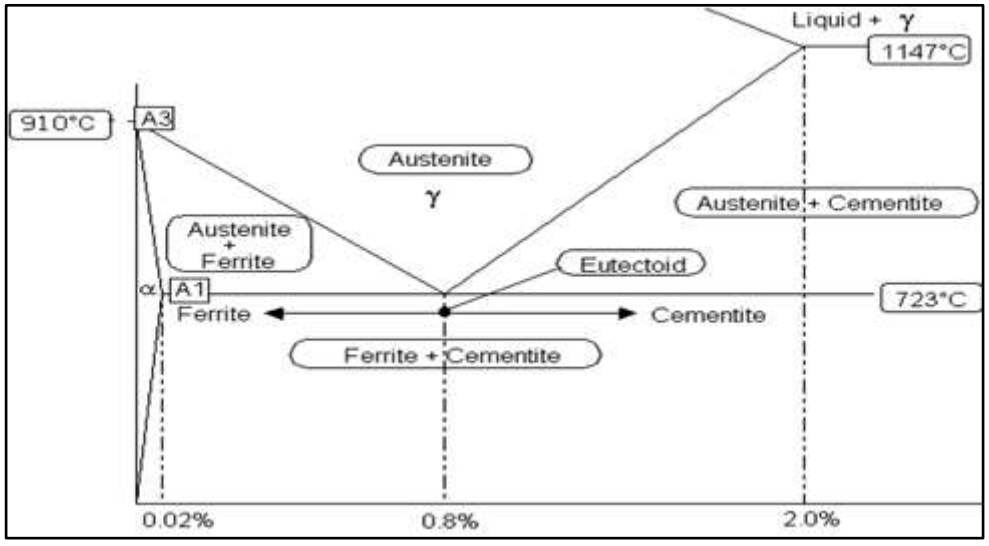

Figure 5-4: The iron carbon diagram showing cooling transformation of different carbon steels. [151]

Several types of metal have been commercialized in the additive manufacture field for more information see **Table 2:2**, but the most common one is iron based powder due to its stability for applications (it is less reactive during processing), price and low toxicity compared to other powders such as Ti, Co-Cr, Al etc. [154, 155]

In this study, stainless steel 316L will be used as the material for all experimental work, and will be in the form of powder with particle size ranges from (15 - 45) micron as it is approved from its supplier (Renishaw).

5.2.1.1 Stainless steel (316L) chemical components

Chemical components	**Percentage**	
	Minimum Wt%	Maximum Wt%
Iron (Fe)	Balance	Balance
Chromium (Cr)	17.50	18.00
Nickel (Ni)	12.50	13.00
Molybdenum (Mo)	2.25	2.50
Manganese (Mn)		2.00
Silicon (Si)		0.75
Copper (Cu)		0.50
Nitrogen (N)		0.10
Oxygen (O)		0.10
Carbon (C)		0.03
Phosphor (P)		0.025
Sulphur (S)		0.010

Table 5:1: Stainless steel (316L) chemical components. [152]

The following **Table 5:2** shows the mechanical properties of steel 316L parts made by SLM, according to the machine provider (Renishaw).

Mechanical properties	
Tensile strength	625 (±30) MPa
Yield stress	525(±30) MPa
Impact value	75(±4) J
Thermal conductivity	15 W/m.K
Powder particle size	15 – 45 µm

Table 5:2 Stainless steel (316L) Mechanical data sheet.

5.2.2 Selective laser melting (SLM125) details

The experiments in this work were conducted on parts made with a Renishaw SLM 125 (Renishaw PLC, Gloucestershire UK). The machine employs an ytterbium fibre laser beam source to create solid geometry parts associated with specific parameters.

Renishaw is UK based company that specializes in the manufacture of machines which are available in different platform size configurations and laser powers, as mentioned in **Table 2:1.** The Machine works by laser to melt fine metal powders together, layer after layer straight from the CAD data to create metal parts. Immediately after each layer was constructed, a powder recoat system is employed to add another layer of powders on the previous one. Whereas the laser is move to specify the model profile. This process is repeated until the final model obtained.

The machine utilises vacuum evacuation that is fuelled by pure argon gas. This is used to create a non-reactive environment which is necessary when processing reactive materials. The machine is built in a way that has fully shield chambers, properly welded, strength and the low consumption of gas. Also it is designed for factories, with a simplified touch screen user interface as shown in **Figure 5-6**.

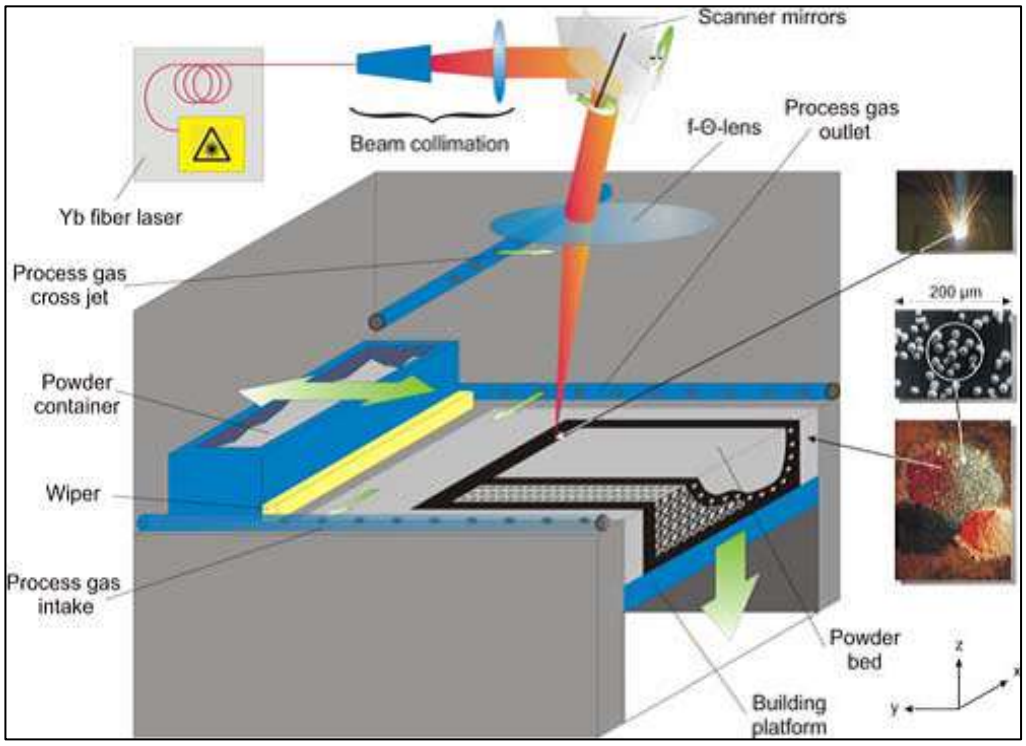

Figure 5-5: Cross section through SLM process chamber.[156]

Figure 5-6: The key components of the Renishaw SLM 125 machine, and control system; laser gun source (A), control system (B), chiller system(C), laser lens(D), monitor control(E), powder hopper(F), wiper(G), overflow chamber (H), building base plate(I)

The Renishaw machines give the users more control over all the process parameters than other typical commercial AM machines. It allows people to experiment with any materials of interest to them. However this experimentation poses some safety risks especially if the powders are explosive or flammable in the presence of oxygen. To counter this risk, the machine has been made with additional safety features to minimize the risks. [157]

5.2.2.1 Renishaw Selective Laser Melting (SLM) Machines Technical Data

SLM technical date	**SLM 125**
Max building area	125 x125 x 125 mm^3
Building rate	5cm^3 - 20 cm^3 per hour
Scan speed	Up to 2000 mm/s
Position speed (max)	7000 mm/s
Layer thickness	20 - 100µm
Laser beam diameter	35 µm diameter at powder surface
Laser option	100 or 200 W
External dimensions	1350L x 800W x 1900 H mm
Weight	1125 kg gross, 900 kg net
Power supply	230 V , 1HP , 16 A

Table 5:3 : showing Laser Melting (SLM) Machines Technical Data. [157]

5.2.3 Cladding machine

The laser re-melting trials were done on the RECLAIM machine (REmanufacturing of high value products using Combined LAser cladding, Inspection and Machining system) at the Manufacturing Technology Centre (MTC) Coventry, to re-melt specific part surfaces made by SLM. The machine has an integrated system of laser cladding and machining in one unit cell. The aim of RECLAIM is to remanufacture by laser cladding, inspection and machining. The worn or damaged components will be placed in the cell and inspected using a high speed contact scanning head to identify the damaged surfaces. The data is used to select the repair strategy and the damaged areas will be laser clad, machined and finally inspected to ensure that the parts comply with the quality standard set for new parts. [158]

The integrated system components to makeup the cladding system are listed below.

- Laser power source (SPI -200 W)
- Chiller system (DMU)
- Argon bottle (BOC)
- Control system
- Laser cladding head (MTC)
- 3-axis machining (DMU)
- Automated inspection (Renishaw)
- Workstation (MTC)

Figure 5-7:The key components integration of RECLAM machine and control system; laser source(A), chilling system (B), argon source(C), control system(D), cladding head(E), argon gage(F), CNC machine(G).

The machines employ an ytterbium fibre laser beam as a source to repair the worn surfaces by making up solid geometry layer by layer to obtain the final product. Also this integrated system can be used to re-melts surfaces associated with sequence of default parameters fixed by the operator.

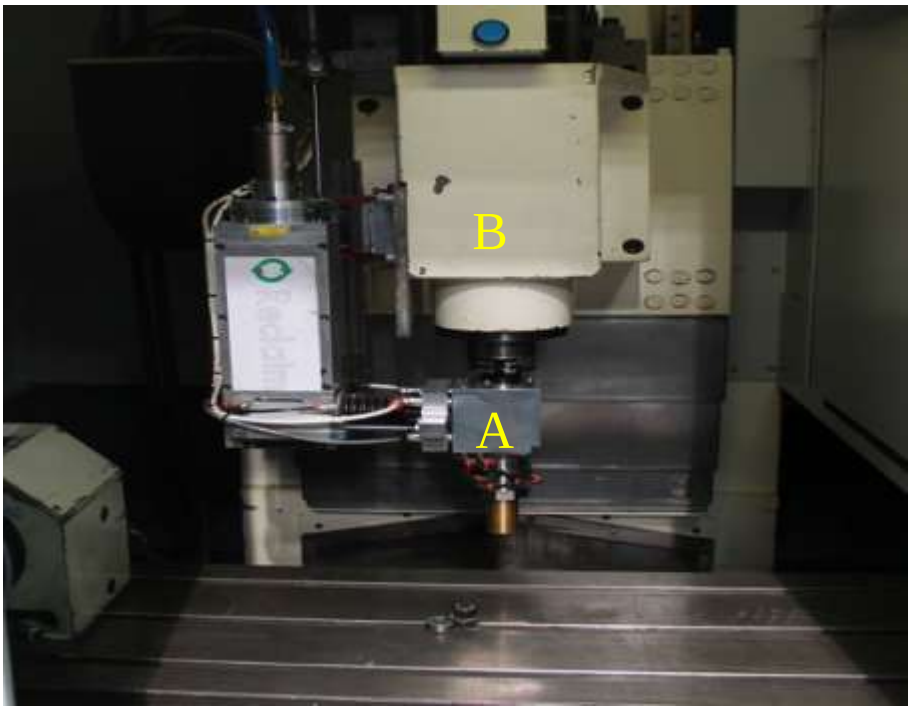

Figure 5-8 : Showing the laser cladding head (A) loaded in CNC chunk (B).

The system was developing an automated cell which combines laser cladding (using the latest fibre laser technology), 3-axis machining and automated inspection. Also it is very economic, rapid and reliable re-manufacturing of high value engineering parts. It can be fitted onto existing machine tools, and allows seamless transition between cladding, machining and inspection operations. It is worth to mention that the laser remanufacturing system is a growing sector which, in addition to cost savings, provides significant benefits for the environment with a reduction in CO2 output. [158]

As a further development of the integrated laser cladding and machining cell the new RECLAIM machine comes with high laser power 2KW, 6-axis machining and high automated inspection, in order to make a great contribution to the efficiency, by re-manufacturing high value components that would otherwise have gone for scrap. [159, 160]

5.3 Surface characterization techniques and equipment

5.3.1 Common surface parameters

Nowadays, a wide range of surface textures are generated by different engineering manufacturing techniques. Thus, these surfaces need to be carefully measured and provide us the opportunity for deep understanding of surface characterization and constructed causes. [161] **Table 5:4** shows the most common parameters used in profiling.

Commonly used surface parameters	
Ra	Arithmetic of average roughness
Rq	It is the root mean square of average roughness
Rp	Maximum profile peak height
Rv	Maximum profile valley depth
Rt	Maximum distance of peak to valley on the Profile
Rz	Average maximum of Height to valley of the Profile
Rsk	Skewness measuring of the symmetry of the profile around the mean line

Table 5:4: Commonly used surface parameters. [162, 41]

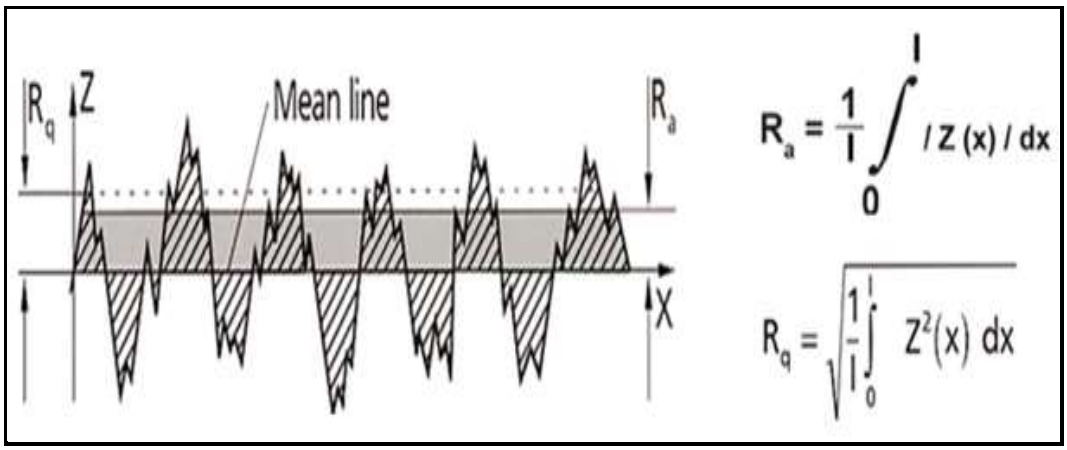

Figure 5-9: Surface profile to illustrate Ra and Rq. [123]

In general, there are two types of technique used to measure the characteristic of a surface's texture, which are respectively called:

- Connected techniques (stylus profiling)
- Non- connected techniques (optical techniques). [163]

5.3.2 Contact methods (Stylus Profiling)

The first Stylus profilometer was a German basic instrument which was made by Gustav Schmatiz and it has been developed by different companies to be used in a wide range of industrial sectors, as a technique for measuring surfaces, to provide quantitative details on the surface characterization. [164]

All contact profilometers work by utilizing a stylus. There are two methods which are used to measure the surface finish according to the stylus technique which are respectively called skid and skidless techniques.

In the skid technique the stylus continuously measures the surface roughness while the skid is positioned behind the stylus. On the other hand, the skidless technique measures the roughness and waviness in term of accuracy because it uses the internal surface as reference, as shown in **Figure 5-10.**

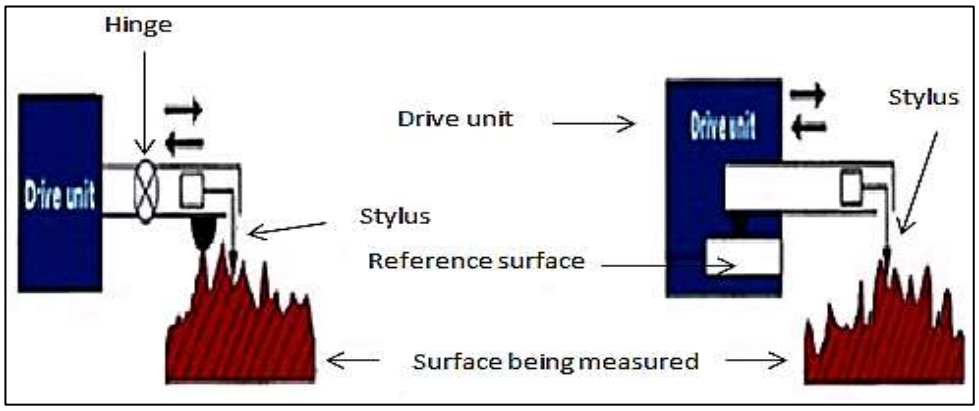

Figure 5-10: Illustration of skidded & skidless techniques. [162]

In this study a (Sj400) Taylor Surf tester profilometer, version 3.00 (see **Figure 5-11)** from (Mitutoyo) was used for surface characterisation as a contact technique. A diamond tipped stylus with a 20 nanometre tip diameter was used to determine surface roughness parameters such as *Ra*, *Rq* and *Rz*. The measured data was recorded by computer software for storage and analysis.

After individual inspection of SLM test samples and to achieve reliable results, all profiling measurements were carried out by making five runs along each key surface, with a measurement length of 8mm, and then the average roughness value for recorded data was obtained.

Figure 5-11 : Sj400 Taylor Surf tester profilometer.

5.3.3 Non-Contact technique (Surface imaging techniques)

Generally three-dimensional measurement surface methods provide more detailed information about surface characteristics. The optical techniques, unlike stylus techniques, utilize a laser beam or light for scanning the surface being measured. The techniques involve the use of digital microscopes and detection sensors, hence offering final image data to illustrate surface characteristics such as roughness, waviness and porosity, which are results of the manufacturing process. Many people prefer this technique because it does not damage the parts as well as being faster and the image covers the whole area of the surface instead of a single line. [165]

5.3.3.1 2D Digital microscope

The optical microscope (B – 350) provided by Brunel Micro-Scope Ltd (at DMU) was used as a full integrity 2D optical profilometer utilized to provide large two dimensional images for surface characterisation. This instrument is able to quickly analyse the surface topography for different kinds of materials, and provide different magnification ranges from 40 to 400 times.

In this experiment, all the samples were inspected at low and medium magnification in order to assess any small features or defects which could not be seen by the naked eye. A digital camera was attached to capture the images formed by the microscope and specific software (ScopeTek ScopePhoto, Version 3.0.12.867) was utilized to process the images.

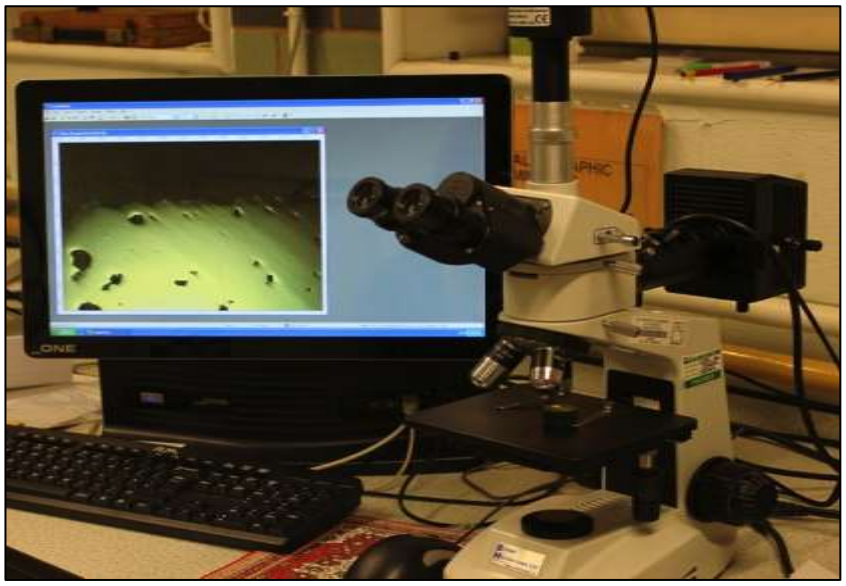

Figure 5-12:2D optical microscope used for surface morphology examination.

5.3.3.2 3D Digital microscope (Zeta)

Most optical profilometers are used to measure the characteristics of surface topography. They use a laser beam or light or electron beam as a rule to obtain surface measurement. Optical profilometer works as a nature technique and can be applied on transparent layer. [166] In case of (Zeta -20), the optical light source is fully integrated into the system to enable capture 3D colour imaging on specific surfaces with high resolution. The Zeta-20 has a large working range (i e, magnification) in order to provide precise details of any small features and measure surface curvature. [167]

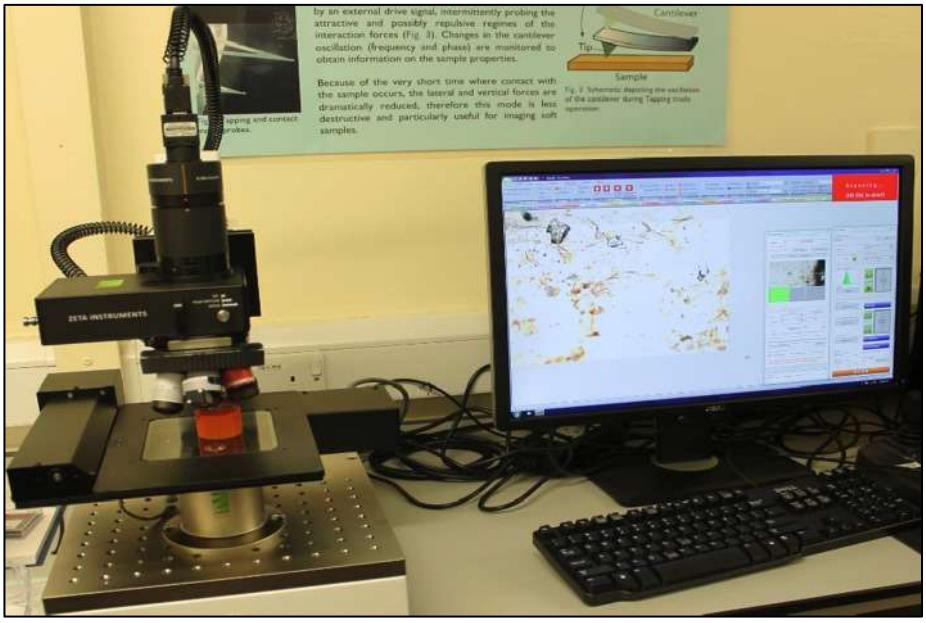

Figure 5-13: Zeta-20, 3D digital microscope.

In general terms, the optical light profilometer works by comparing two optical paths. The beam of light is split into two paths; the first one is reflected by the material which is on the microscope plane, the other beam is reflected by a reference surface (mirror). The beams then combine again. This combination of beam is focused into high a resolution camera, which shows the constructive space as a lighter and the destructive area as a darker feature which clearly appears on the screen. Nowadays most of the sophisticated digital cameras are used to measure 2D and 3D samples from pixel to pixels. Also 3D measurement is done through image stacking. [168]

5.3.3.3 Scanning Electron Microscope

The scanning electron microscope (SEM) utilizes the high energy of an electron beam to produce different signals on solid specimens. This electron beam signal received from interaction with the sample shows data of the specimen such as; surface morphology, chemical composition, and structure of the crystals. The information or data can be collected on a specific surface area of the sample, and two dimensional pictures can be produced to show different characteristics of the sample. [169] The sample preparation for testing is quite simple; the sample must also be solid, conductive and fit into the microscope chamber. In addition, the surface area which can be scanned by SEM ranges from5μm^2 to 250mm^2. The ease of sample inspection and assessment makes the SEM a significant tool for surface imaging. In this work the SEM images for the test samples were taken by a Zeiss EVO HD15 SEM at De Montfort University as shown in **Figure 5-14.** The electron hits the specimen with a voltage acceleration range between 0.2 kV to 30 kV. It is worth mentioning that a special analysis on selected areas can be performed using this technique, typically when looking for qualitative or semi quantitative data such as; chemical composition, crystalline structure and its orientation etc. [170]

Figure 5-14: Shows a Scanning Electron Microscope.

Today SEMs produce detailed data of selected points on the specimen and they are one of the mostly used tools for surface characterization in industry. **Figure 5-15** below shows the basic operation of an SEM. SEM is considered non-destructive since the X-rays produced do not destroy the sample. [169]

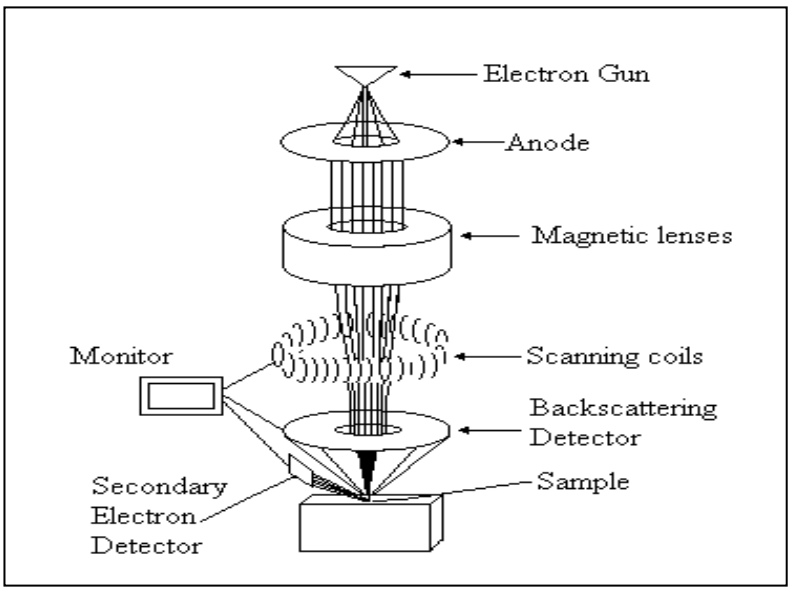

Figure 5-15: Shows operating principles of SEM. [169]

5.4 Fatigue test equipment

The measurement of fatigue failure on SLM stainless steel (316L) parts subjected to two different stages of surface finish improvement was achieved using the fatigue tester HSM20 shown in **Figure 5-16**. The machine employs an induction squirrel cage motor, with a specific speed of 3000rpm and uses a 220V single phase power supply. A counter mechanism is equipped at one side of the motor, which has the ability to record **7 figure** numbers. A fixture is connected by its end to the shaft. A spherical ball bearing is positioned in the loading device with a micro switch. When fracture occurs, the motor is automatically switched off by the micro switch. The process is set with the help of a fatigue tester, which is designed to be positioned on the bench. A standard design of specimen with dimensions of (1x 10 x100) mm is provided for the apparatus use according the material data sheet. [171]

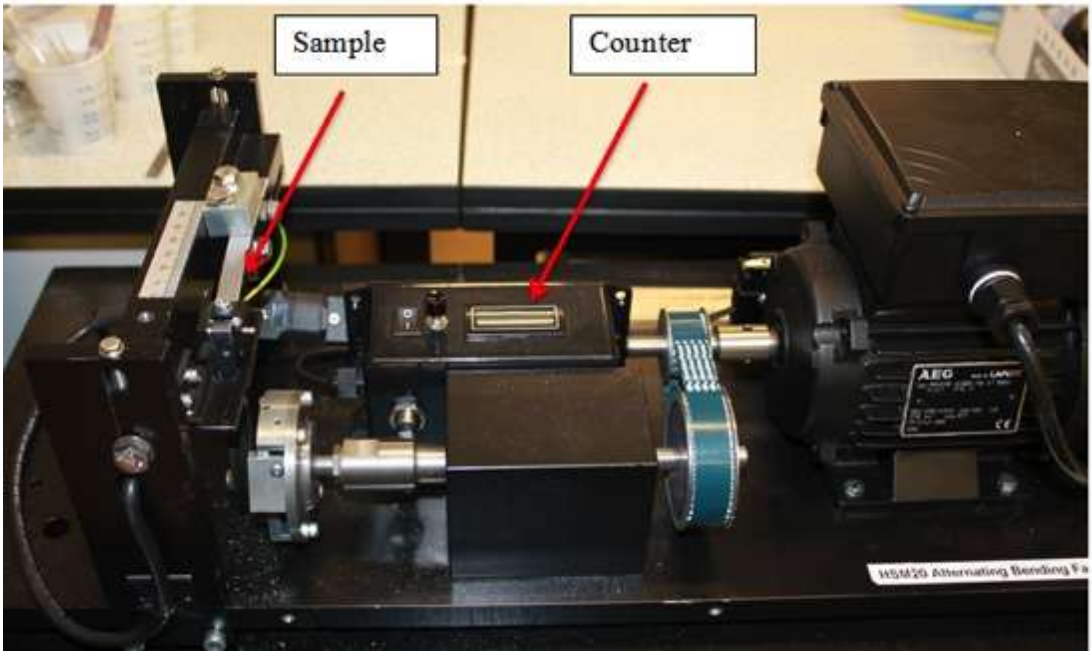

Figure 5-16: Fatigue tester HSM20.

Experimental work

This work is divided into three chapters (phases); the first one (**Chapter. 6**) is conducting trials to assess the machine performance repeatability and the parts' surface characteristics. The second chapter (**Chapter.7**) focuses on the manufacture of different inclined surfaces, as detailed in the methodology chapter, in order to assess the characteristics of SLM parts before and after exposure to laser re-melting as a post-processing method. The third chapter (**Chapter. 8**) focuses on electropolishing after re-melting, to obtain the final goal (a good surface finish).

6.0. Preliminarily laboratory conduct trial

The experimental aims were to investigate the characteristics such as surface roughness (*Ra*), topography, density of SLM 125 parts and also to determine if the machine is repeatable for production. The work in this phase (chapter) was carried out through three specific stages as shown in **Figure 6-1.**

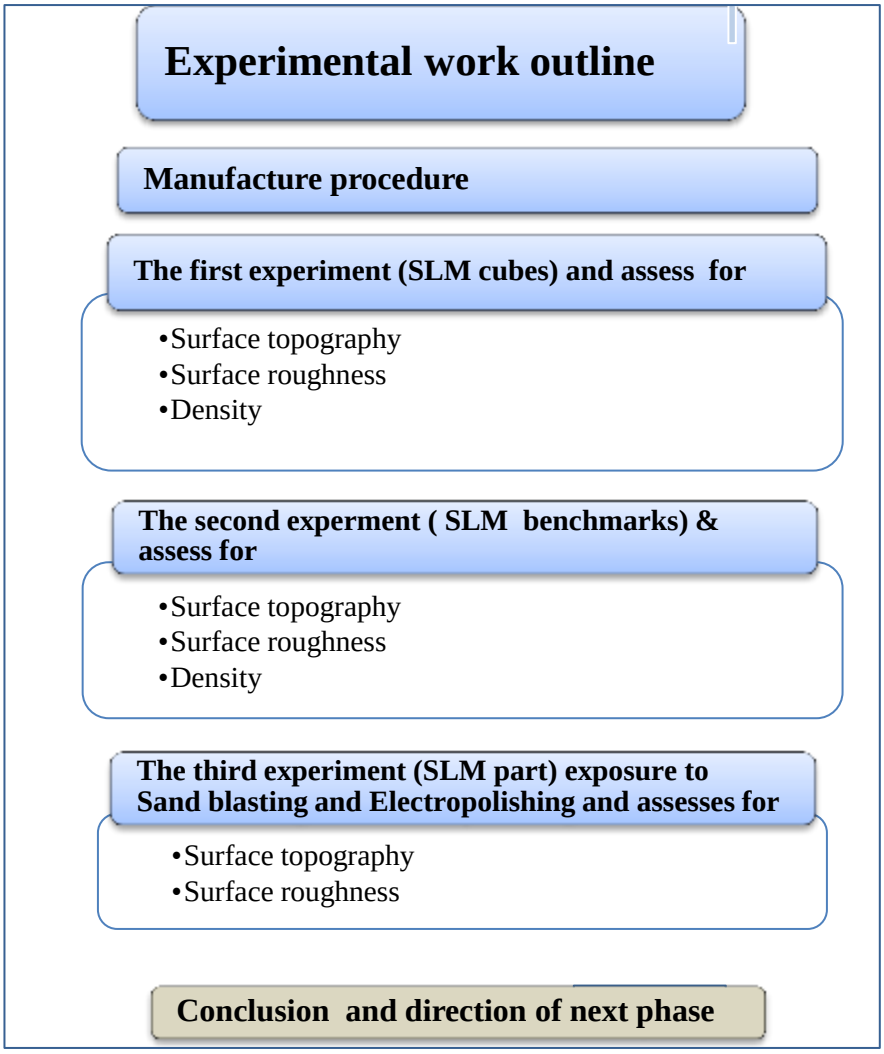

Figure 6-1: Shows the outline of experimental procedure employed in the first phase.

6.1 Manufacture procedure

The chart above has shown the sequence of experiments and their objectives. It is worth mentioning that all experimental parts were built by the same build parameters, which had already been developed on the De Montfort University SLM 125, utilizing stainless steel powder with a specific ranging of particle size 15 to 45 µm. The parameters are shown on **Table 6:1**.

Laser power	**200 watt**
Scan speed	480 mm/s
Focus offset	0 mm
Point distance	60 µm
Layer thickens	50 µm
Exposure time	100 µs
Powder dosage	90%

Table 6:1: Laser setup parameters.

6.1.1 Process of 3D printing part on SLM machine from CAD Packages

This section shows the data transection steps from CAD to AM as follows:

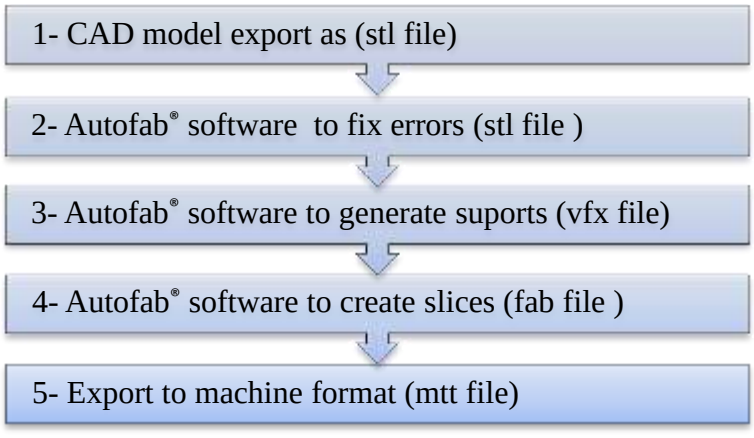

Figure 6-2: The data translation steps from CAD to AM.

- Initially the part to be printed by SLM is designed using CAD packages like Auto CAD, Solid Works, Pro-E, etc.

- Once the part is designed by using CAD packages, then the designed file is converted into .STL format (Triangular representation of a 3D object).
- Autofab software is well known for accurate slicing of parts to use on additive manufacturing machines. It is worth mentioning that the autofab software has 3 stages of processing the file.
- The .STL file is loaded in Autofab software to fix the basic errors in the part.
- Once all the errors in the file are fixed then the operator must add supports to the part. There are different types of supports like line, point, transverse angle, and longitudinal angle.

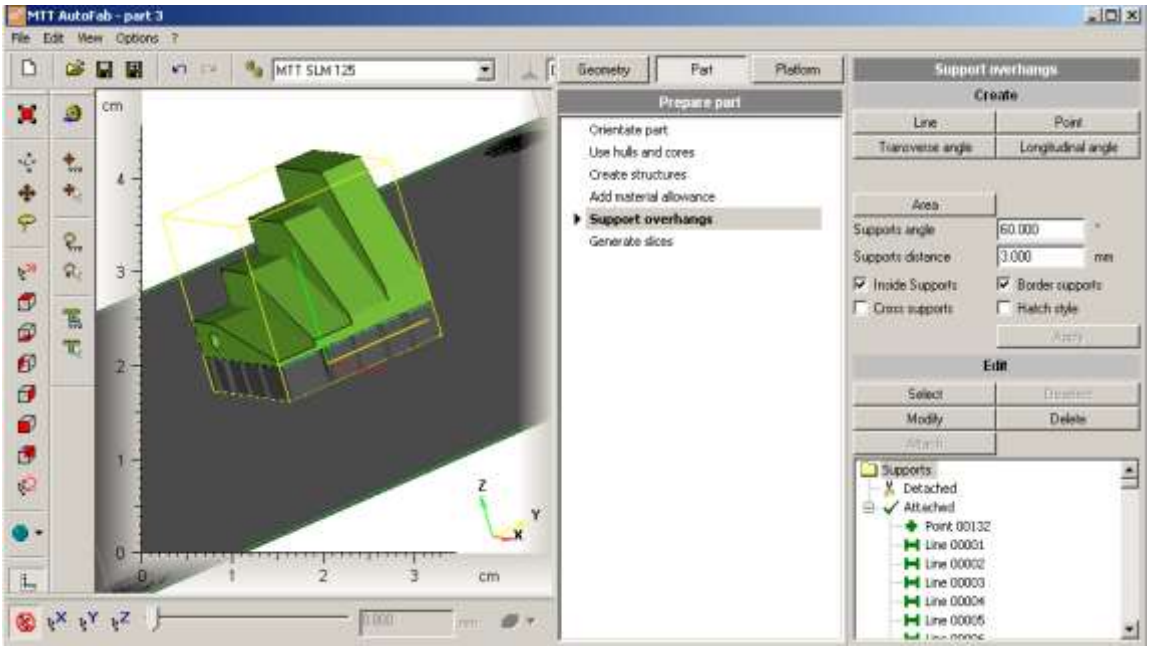

Figure 6-3:3D model with supports generated in Autofab software.

- The supports are selected according to factors such as; kind of material, part shape and orientation. **Figure 6-3** shows the supports attached to the part.
- After creating supports the file is converted automatically into .VFX format (This format saves triangle data).
- After the part is saved in .VFX format the operator generates slices by using the software in the hatch style of "Meander". Once the slices are generated then the part is automatically converted into .FAB format and saved.
- Finally the part positioned in the build chamber is set by the operator. It is very important to locate the part in the best way to utilise the area allowance of the build substrate, and reduce build time.

- It is also used to build multiple test samples in very less time and in accurate area allocation on substrate.
- Once the part is arranged in the right way, the file is exported to the (MTT) format for (SLM) Renishaw Machine and loaded onto the machine's computer by file transfer.
- The process parameters, material cost and time taken will be calculated by the machine.

6.1.2 Machine process

All the samples were built using the parameters defined in **Table 6:1.** The specific steps taken to begin the build are as follows:

- Load the 3D samples i.e. (mtt) file into the machine.
- Turn on the machine; laser chillier and argon gas for about two hours as pre-heating recommended by Renishaw.
- Fill the powder hopper with material and fit it into the machine
- Fix the substrate on the build platform area.
- Adjust the wiper height on the substrate and set the datum of the substrate to zero
- Check the dosage, use the wiper to spread the first layer on the substrate
- Set the powder dosage (90%).
- Select the build file and start the build.

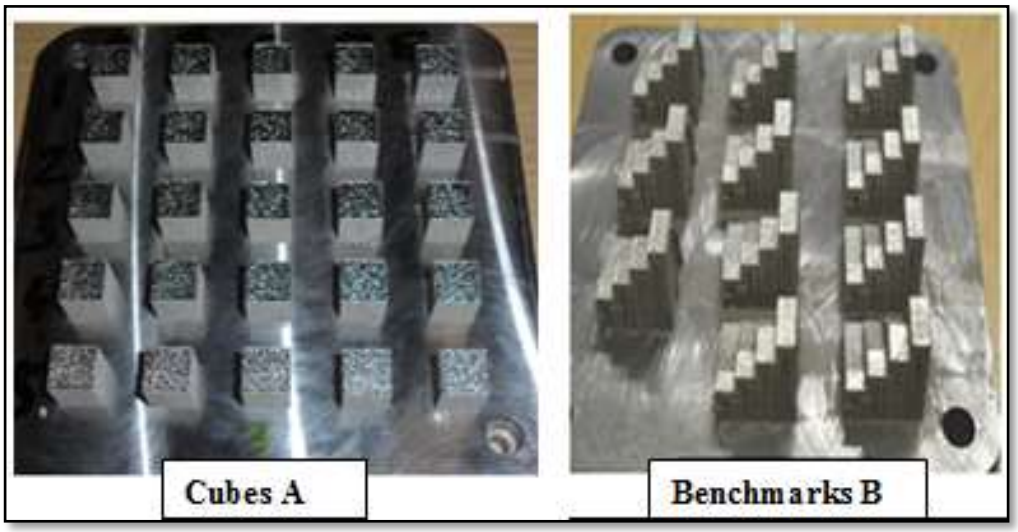

Figure 6-4 : Cubes & benchmarks were made by use SLM 125.

6.1.3 Post-processing and inspection

In this stage and after the samples had been completely manufactured, the extraction of the parts from the machine build chamber was also carefully done. Subsequent post-processing involved support remove and individual inspection. A manual saw was used to take off the samples from the substrate, whereas hand pliers were used to remove the supports from the samples. Individual inspection was also carried out to ensure that the samples had been made reliably, as can be seen in **Figure 6-5**. These steps of manufacture and inspection were done consistently during the whole project.

Figure 6-5: Benchmarks after support removed and inspected.

6.2 The initial manufacturing trial

This experiment was carried out by producing five plates each of which had twenty five cubes with specific dimensions of (10 x10 x 10) mm as shown in **Figure 6-6**, with specific parameters, set as in **Table 6:1**. The aim was to obtain preliminary characterization of the SLM parts, such as surface roughness, surface topography, and density and ensure that the machine was building consistently.

Figure 6-6: Shows cubes made by SLM 125.

The investigations of the effect of process parameters on the density and surface quality of SLM parts were conducted with a digital microscope, SEM and stylus profilometer (SJ400) at DMU.

6.2.1 Results and discussion

6.2.1.1 Surface topography

Generally, due to the interaction between the laser and the powder during the process and solidification, recognizing features in SLM surface micrographs is quite complicated. Thus, pictures were taken by digital microscope and subsequently by SEM as shown in **Figure 6-7, Figure 6-8 and Figure 6-9**.

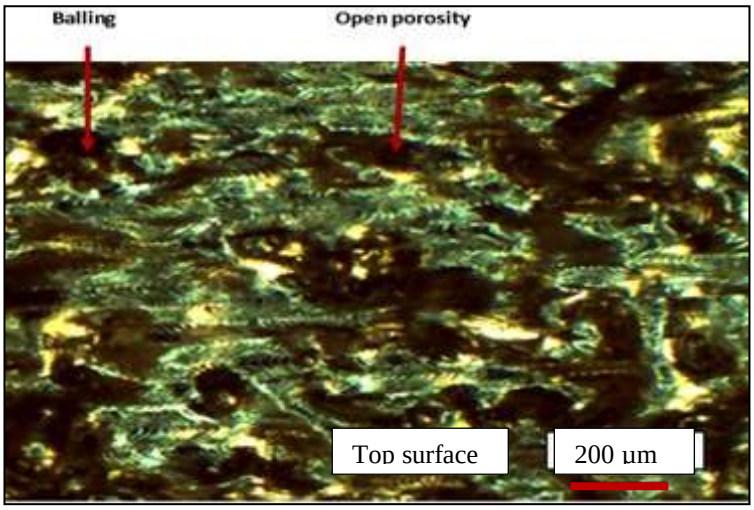

Figure 6-7: 2D micrographs of cube.

The above picture was taken to show some of the errors on the top surface of the cubes such as balling, porosity, fully molten areas and partially molten areas, which occur during the interaction of material with the laser radiation, and its behaviour during shrinkage. [14] It is noted that the defects on the surface, such as roughness and pores have a significant influence on the mechanical and physical properties of the part because during mechanical loading, the surfaces are the first area to cause failure. [172]

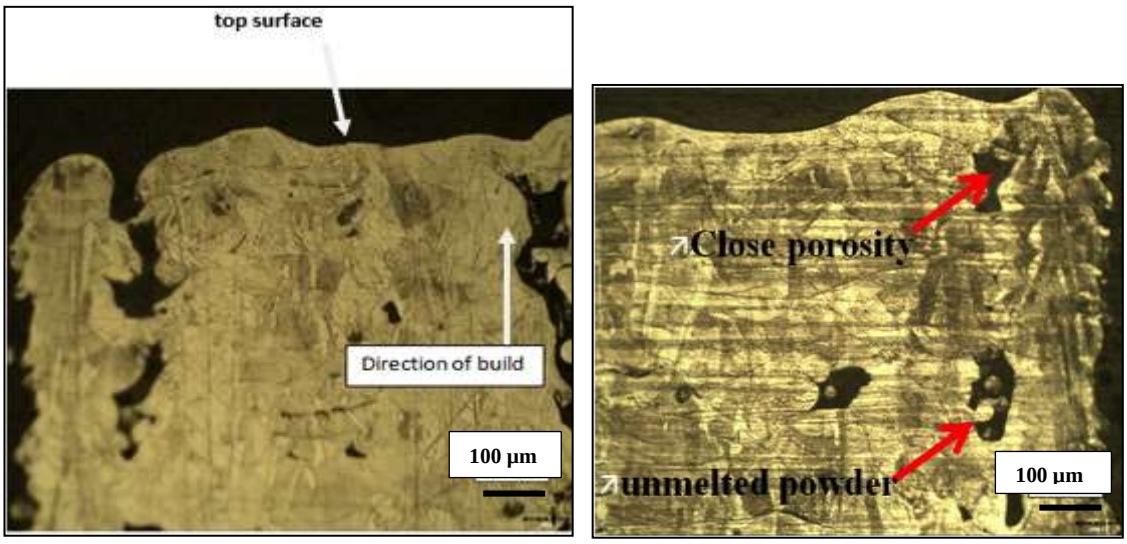

Figure 6-8: Shows 2D micrograph cube cross section (C1)

Figure 6-8 shows 2D digital micrographs taken to assess the presence of porosity. The majority of the porosity is located under the skin of the side wall; these defects are attributed to insufficient cohesion of the contour track and fill tracks during the build process.

The micrographs are clearly show defects such as irregular pores ranging from small to large plus closed and open pores, which are mostly concentrated close to the side wall surface. In particular these defects are the main obstacle for surface improvement, because the post-processing techniques are subtractive. For instance, machining the surface will improve the surface roughness, but at the same time deep pores will appear on the surface as defects. In such cases, mechanical properties such as fatigue, stress, strain, fracture, wear and surface quality etc., are influenced as well. [173]

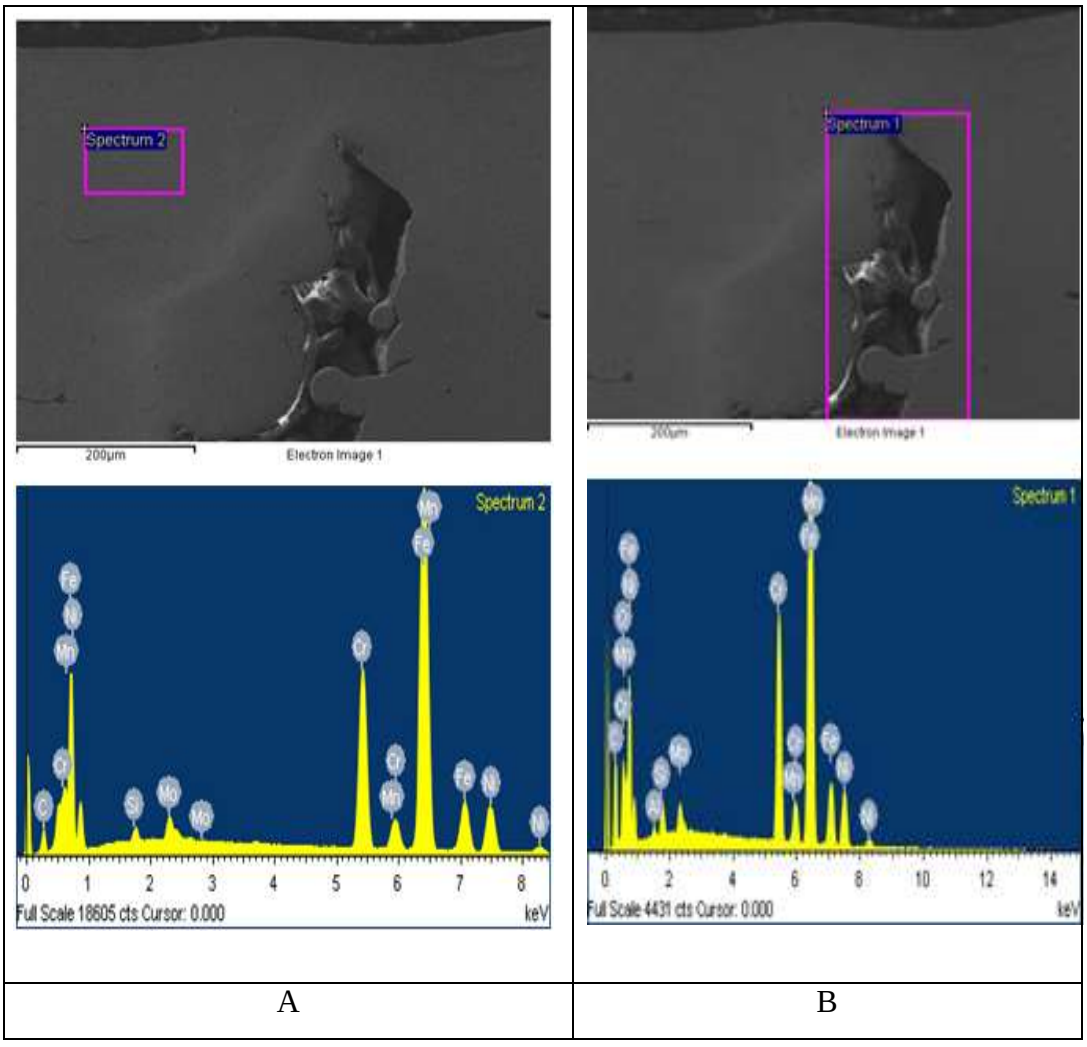

Figure 6-9: 2D micrograph tracked by SEM & elements tracked by EDX at DMU.

The micrographs in **Figure 6-9** were taken by SEM to verify these defects. Surface characterization was performed to identify the reason for the defects and Electron Dispersive X-ray (EDX) identified the chemical components of the sample in different areas, solid material (A) and pores (B). The results show that there is a contamination located in the porous areas involving metals oxide and mostly iron oxide, whereas the solid area showed the unique chemical composition of stainless steel 316L.

6.2.1.2 Surface roughness measurement

Surface roughness could be defined as a number of texture on the surface and affects as major limitation on parts. Surface quality of SLM is not only a main concern to the user, but also plays as a foremost concern during the process manufacture and post-processing (finishing) as well. The surface roughness of the SLM components demonstrated various poor quality on the top surface of the cubes, see **Figure 6-12**. So these parts need further treatment.

Figure 6-10: Surface measurement by using stylus profilometer (Sj400).

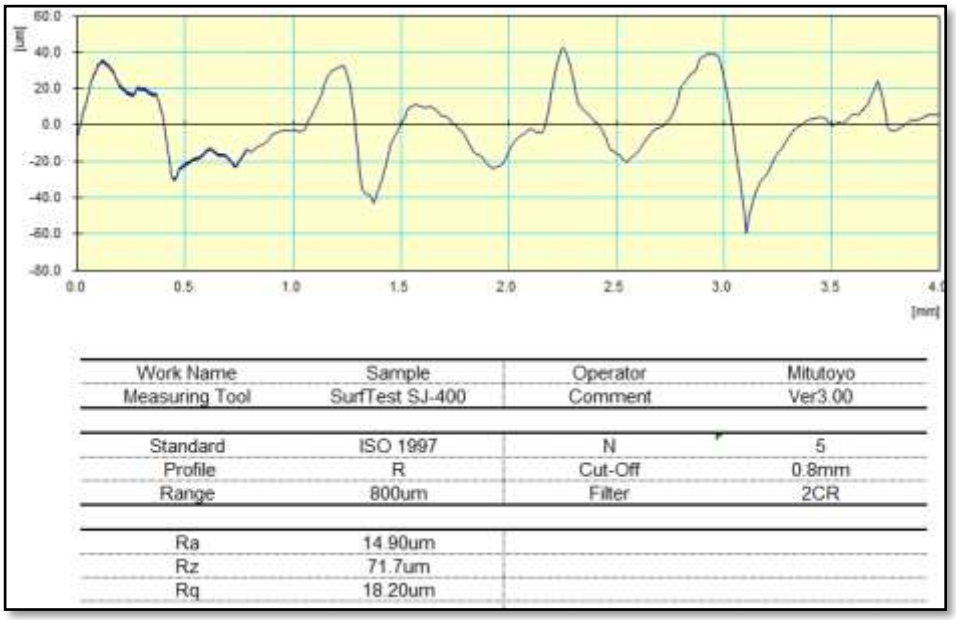

Figure 6-11: Amplitudes parameters of surface roughness obtained on sample (C1).

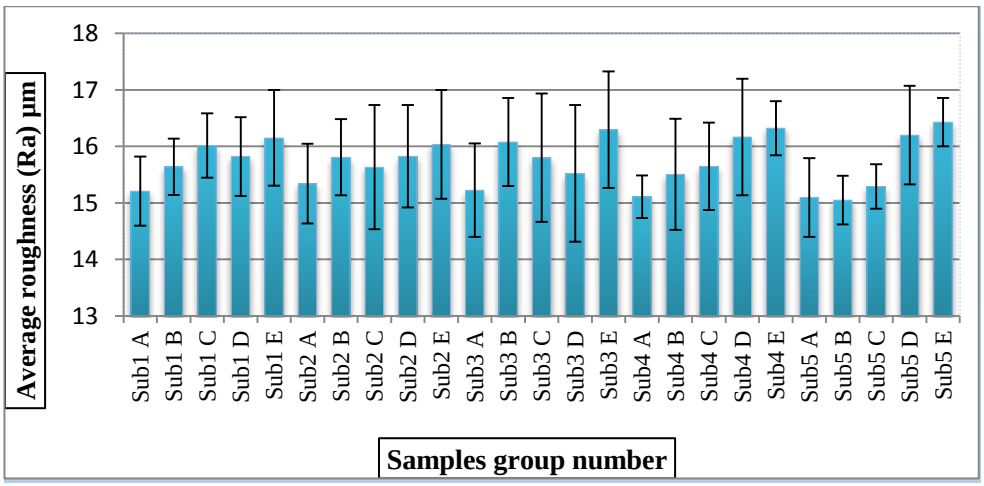

Figure 6-12: Comparison of surface roughness measurements performed by stylus profilometer (Sj400) on all groups.

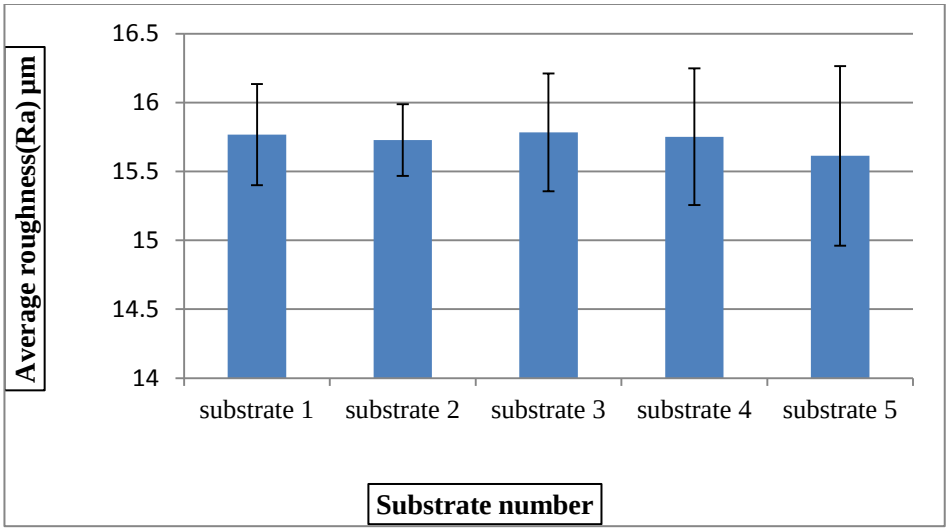

Figure 6-13: Comparison of surface roughness on all substrates.

Five successful readings were obtained on the top surface of each sample to calculate average roughness (*Ra*). The results show that (*Ra*) ranges from 14 to 17µm obtained as average results of five surfaces built at different positions on the substrate. The results show in **Figure 6-12** and **Figure 6-13** show that the machine performance is repeatable and also that surface roughness slightly increases at the right side of the substrate. This could be due to the effect of the argon flow from right to left across the substrate during the build process. These results have been performed employing, ISO 1997 as shown on **Figure 6-11**.

6.2.1.3 Density

The main aim of SLM is to produce fully functional complex parts with. Thus, the measurement of density is one of the most important results, and directly reflects the production condition and how the interaction of laser parameters occurs during the build process. Density can be defined as mass divided by volume.

Density = Mas/ Volume (gm/cm^3) …… Equation 6-1

The analysis of density was verified on two substrates (Sub1, Sub3), by carefully removing the cubes from each substrate to determine their mass and volume. Data collection and analysis were performed. **Figure 6-14** illustrates the results.

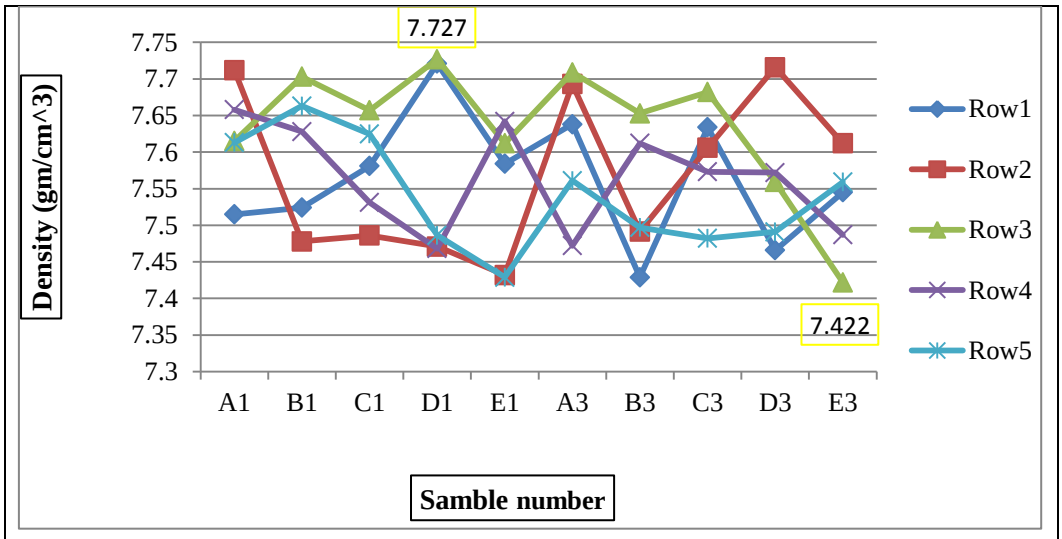

Density of all cubes from substrates 1 and 3.

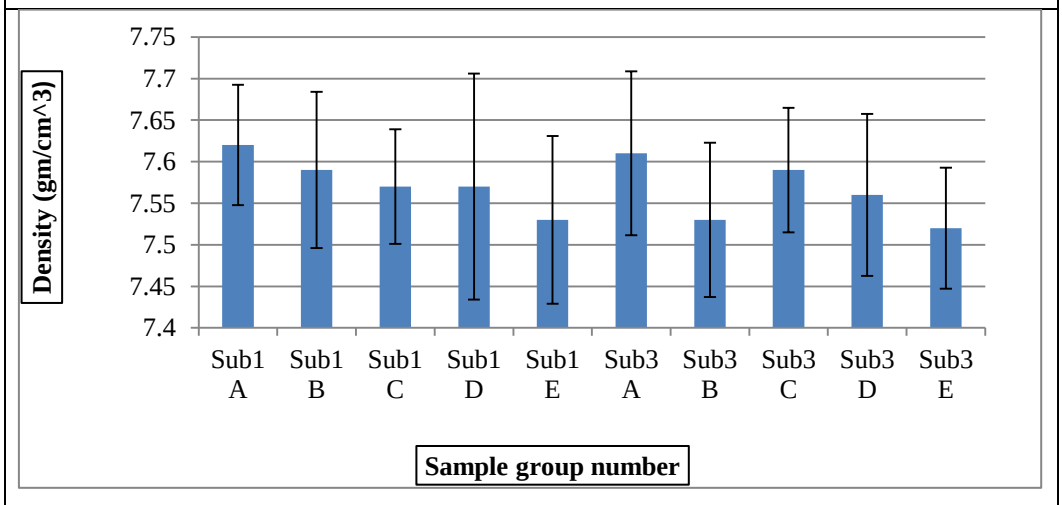

Average density with error bars.

Figure 6-14: Density measurement of cubes realized on sub (1&3).

Although, the main priority of SLM technique is to create full function parts with fully density, but it could be quite difficult to obtain that due to missing mechanical pressure during the interaction fabrication.[4] The measured density ranged between 7.422 to 7.727 gm/cm^3 compared to 7.9 gm/cm^3 for fully dense parts produced by conventional methods. Also it is possible to say that there is a coherent relationship between density and surface roughness. The results obtained from **Figure 6-12** and **Figure 6-14** indicate that a reduction of density corresponds to an increase of surface roughness, demonstrated on group E.

6.3 The second scope trial (benchmark development)

This experiment was designed to investigate the effect of build process parameters on part characterization, for instance, the influence of laser parameters on the top surface for different build heights and angles, in order to obtain the stair effects (angle inclination) and machine repeatability as well.

6.3.1 Experimental procedure

The experiment was carried out by setting up the machine and using the same parameters as the previous experiment as per **Table 6:1.** The benchmark model designed for this work contains top surfaces with different heights (4, 8, 12 and 16) mm and inclined surfaces at 15°, 30°, 45°, and 60° as shown in **Figure 6-15.**

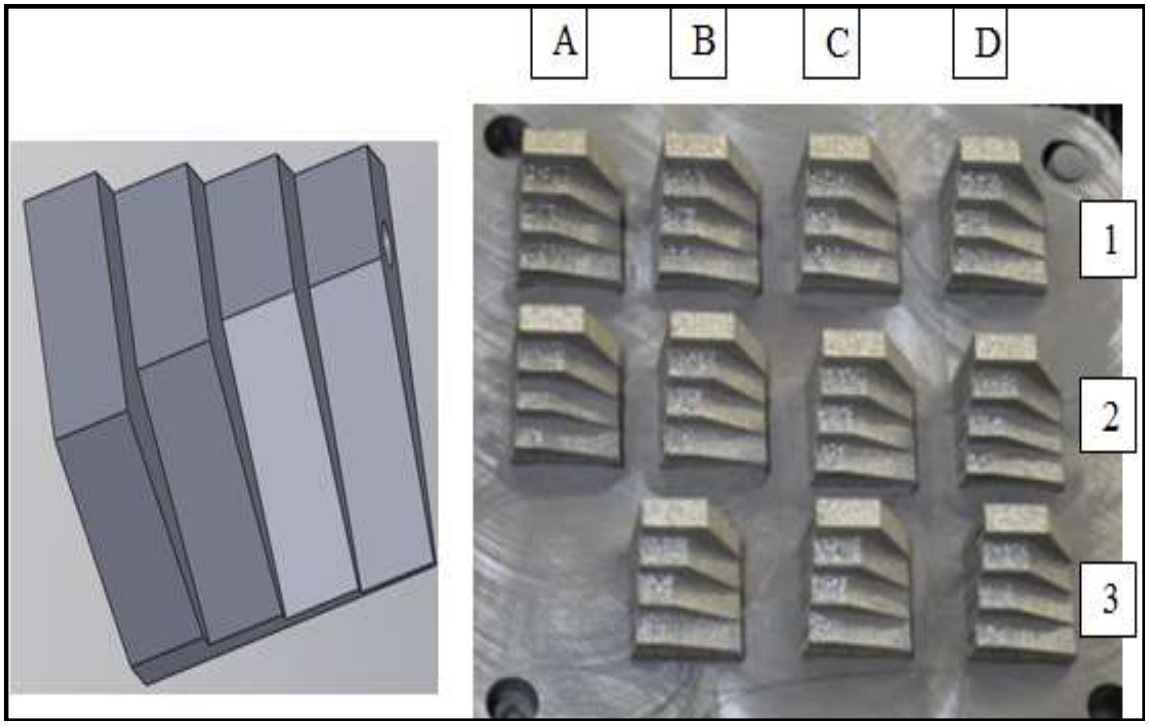

Figure 6-15*: Benchmark 3D model (left) and built samples (right*)

Eleven samples were produced on one substrate. The manufacturing steps were kept constant as specified in section **6.1.1**. Measurements of the surface roughness, topography, and density were carried out and the results are demonstrated below.

6.3.2 Results and discussion

6.3.2.1 Surface topography

All benchmarks were investigated by taking pictures on the top of surface using a digital microscope. The results demonstrated that the same defects which were obtained on the cubes, such as balling, porosity, waviness, were also present on the benchmarks. These defects provide confirmation that the process interactions have significant influence on the surface quality as shown in **Figure 6-16.**

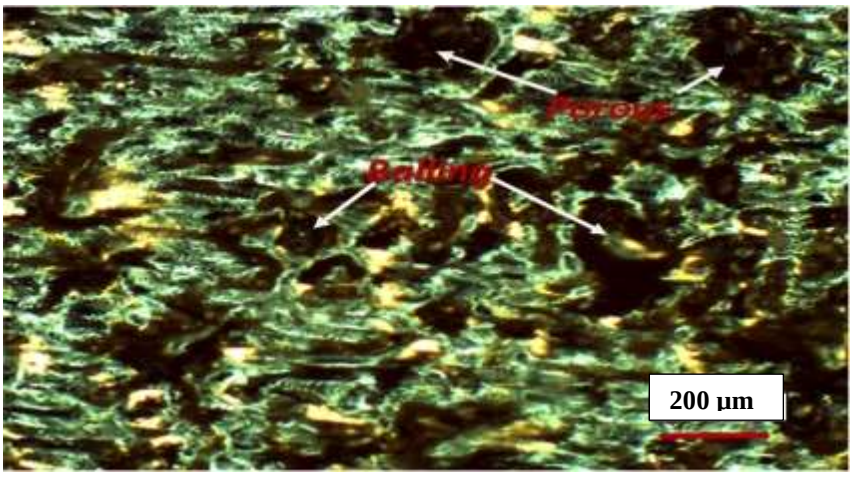

Figure 6-16: 2D micrographs of the top surface of benchmark (C2).

6.3.2.2 Surface roughness

In SLM component, surface accuracy or quality is the first concern from customer; because it is the key of integration of the process parameters during the manufacture and reflecting a good image of part quality. Thus, the ability to produce significant surface quality is still considered as one of the drawbacks of this process. [37]

In this stage surface roughness was measured on both the top and inclined surfaces, utilizing the same profilometer (SJ400) at DMU) as indicated in the first trial, see **Figure 6-10**. The results show that the top surface roughness has ranges between 13.7 to 17.0µm as shown in **Figure 6-17** below.

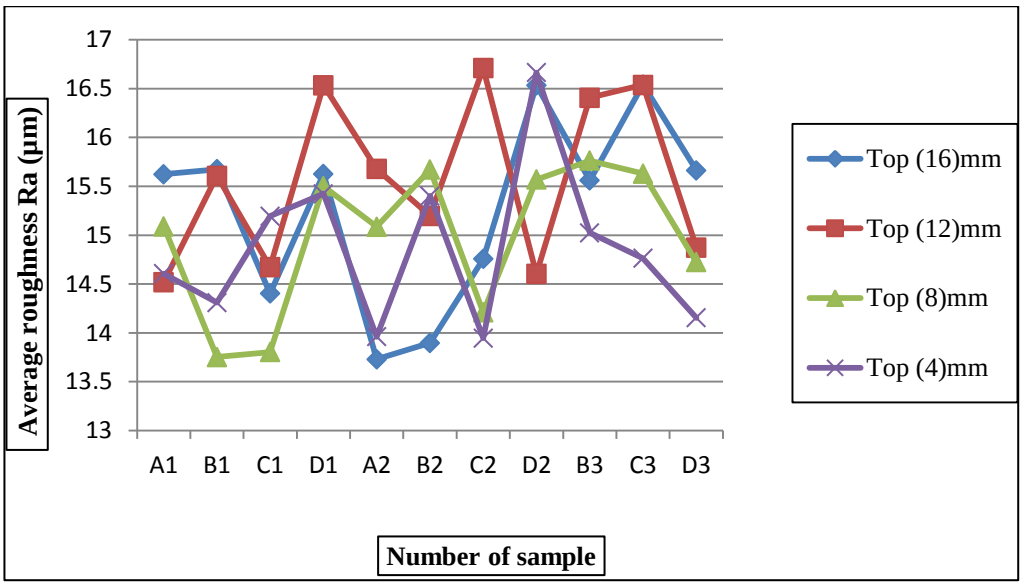

Figure 6-17: Surface roughness Ra obtained on the top different heights surfaces.

It is clear that the surface roughness increases with inclined surface angle decrease due to stair effects (more information see **3.1.2**). The best results were obtained on inclined surfaces that have inclined angle of 60°. Overall, the average surfaces roughness of the inclined surfaces ranged from 10 to 17µm as shown in **Figure 6-18**.

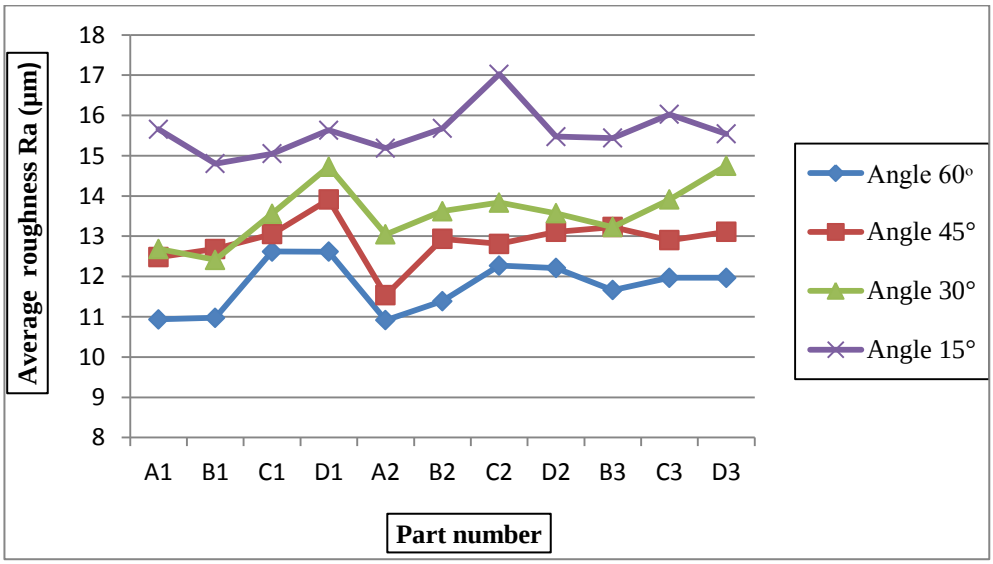

Figure 6-18: Surface roughness Ra obtained on different inclined surfaces.

According to the literature review, research carried out by Kruth and co-authors found the surface roughness of SLM parts ranged from 10-30 microns *Ra* depending on the orientation of parts, machine parameters and powder characterization. The above results are comparable to the literature review. [6, 7, 174]

6.3.2.3 Density

Due to the complexity of the benchmarks, the density was obtained using (MPIF standard 42) to determine both dry and wet density. The steps given by this standard were followed. The procedure starts by weighing the test specimen before and after impregnated in oil, and then weighing the impregnated specimen in water. For more information about the experimental procedure see appendix (1). The density determination was based on following formulas.

$$\textbf{Dry density} = \frac{\mathbf{A\,\rho w}}{\mathbf{B-(C-E)}} \quad \frac{\mathbf{gm}}{\mathbf{cm^3}} \ \textbf{.....Equation 6-2}$$

$$\textbf{Wet density} = \frac{\mathbf{B\rho w}}{\mathbf{B-(C-E)}} \quad \frac{\mathbf{gm}}{\mathbf{cm^3}} \ \textbf{.....Equation 6-3}$$

where A is the weight of specimen before impregnated, B is the weight of specimen after impregnated, C is the weight of specimen in the water, E is the basket weight in water, ρw is the water density.

sample no,	Mass A	Mass B	Mass C	E = constant	ρ w= constant	Dry ρ	Wet ρ	Dry ρ%	wet ρ%
A1	9.899	9.921	9.853	1.281	0.999	7.303	7.346	92.79	92.99
A2	10.112	10.116	10.04	1.281	0.999	7.344	7.357	94.23	94.26
B1	10.088	10.12	9.985	1.281	0.999	7.117	7.139	90.09	90.37
B2	10.148	10.159	10.07	1.281	0.999	7.359	7.397	93.66	93.77
B3	10.135	10.162	10.045	1.281	0.999	7.242	7.261	91.67	91.92
C1	9.907	9.915	9.85	1.281	0.999	7.352	7.358	93.07	93.15
C2	10.14	10.145	10.033	1.281	0.999	7.271	7.275	92.05	92.09
C3	10.134	10.152	10.015	1.281	0.999	7.139	7.152	90.37	90.53
D1	9.789	9.884	9.812	1.281	0.999	7.227	7.297	91.491	92.379
D2	10.045	10.12	9.998	1.281	0.999	7.152	7.205	90.53	91.21
D3	10.017	10.102	10.011	1.281	0.999	7.293	7.355	92.32	93.109
					Average	7.270	7.295	92.02	92.34

Table 6:2: Density measurement of benchmarks.

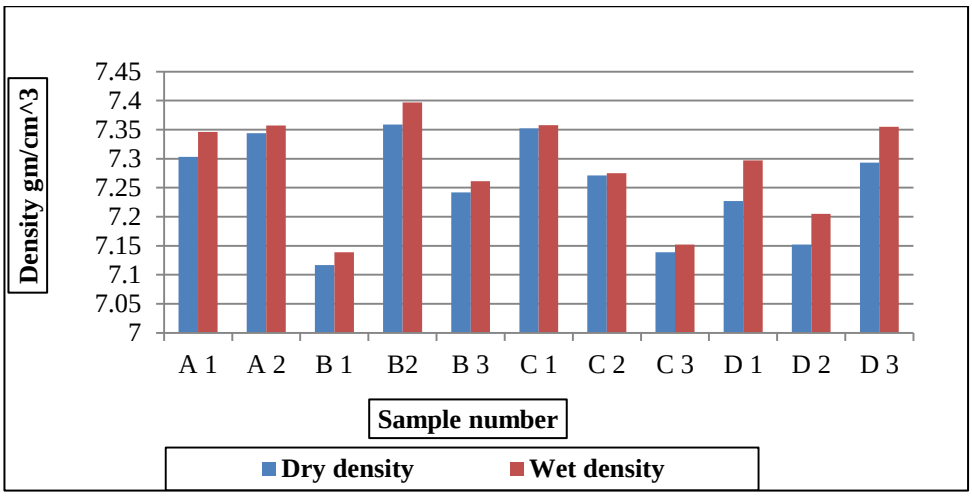

Figure 6-19: Density of benchmarks.

The data in table illustrates the density results of all benchmarks. The table shows that the average results of dry and wet density are 7.270 gm/cm^3 and 7.295gm/cm^3 respectively with total percent 91%, compared to 7.9gm/cm^3 for a fully dense part. Also the results showed less density than that of the first experiment (cubes). This is considered to be due to the increase of the area of the side walls for these benchmarks. Some cross sections were taken which demonstrate how the porosity is intense under the side wall and to illustrate the reason for the decrease in density, as shown in **Figure 6-20**. All the porosity was concentrated close to and under the surface, probably due to the scanning strategies used. The scan strategy starts by first scanning a line (the first contour) to melt powder around the profile vectors, and afterwards the fill vector continues scanning to melt the powder area inside the contour line.

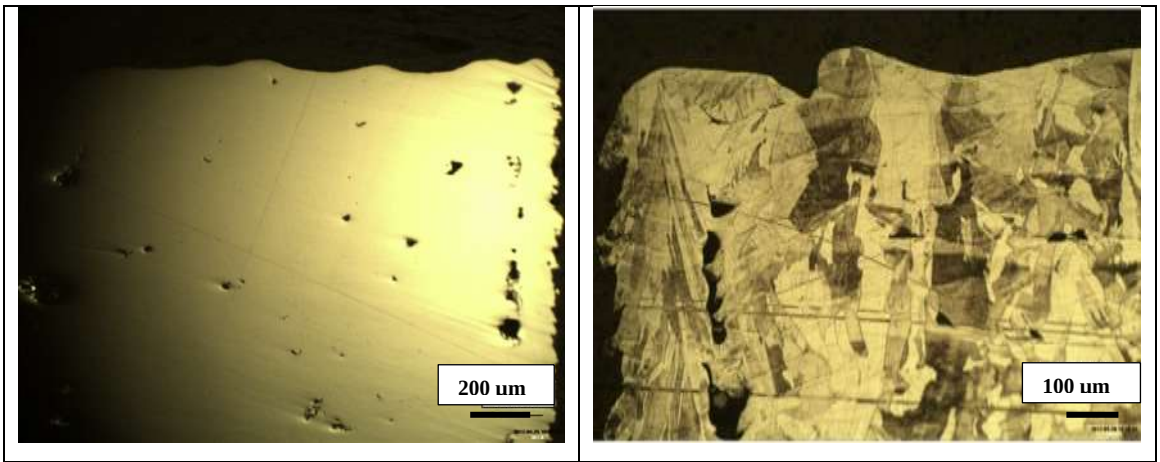

Figure 6-20: 2D cross section obtained from benchmark (C2).

6.4 The third trial combining Sand blasting and Electropolishing

6.4.1 Experimental procedure

This section describes the method of combining sand blasting followed by electropolishing. In this investigation the parts were treated by combining two different post-processing techniques in order to assess the efficiency of these techniques to improve or reduce the surface roughness of SLM manufactured parts. This was done by measuring the surface topography before and after treatment of the selected benchmarks. Sand blasting was used as the first stage. The experiment was carried out using 100 Psi pressure with an aluminium oxide abrasive material (grit 60 – 80 microns) in order to reduce roughness features such as waviness or any dendrites located on the surfaces of benchmarks. Afterwards, electropolishing was applied to obtain the final surface roughness. The electropolishing was carried out implementing an ionic liquid solution in the electrical cell with a source potential of 6 volts for 1 hour at 30C° temperature.

6.4.2 Results and discussion

6.4.2.1 Surface topography

Pictures were taken using digital microscope and SEM as shown in **Figure 6-21**. These pictures show significant improvement on the surfaces. The results demonstrated the efficiency of these techniques. On the other hand, some remaining defects are clearly present on the surface profile such as open deep pores. The remaining porosities were came to present and clarify the reason for re-melting process as second stage of experimental (see methodology section.

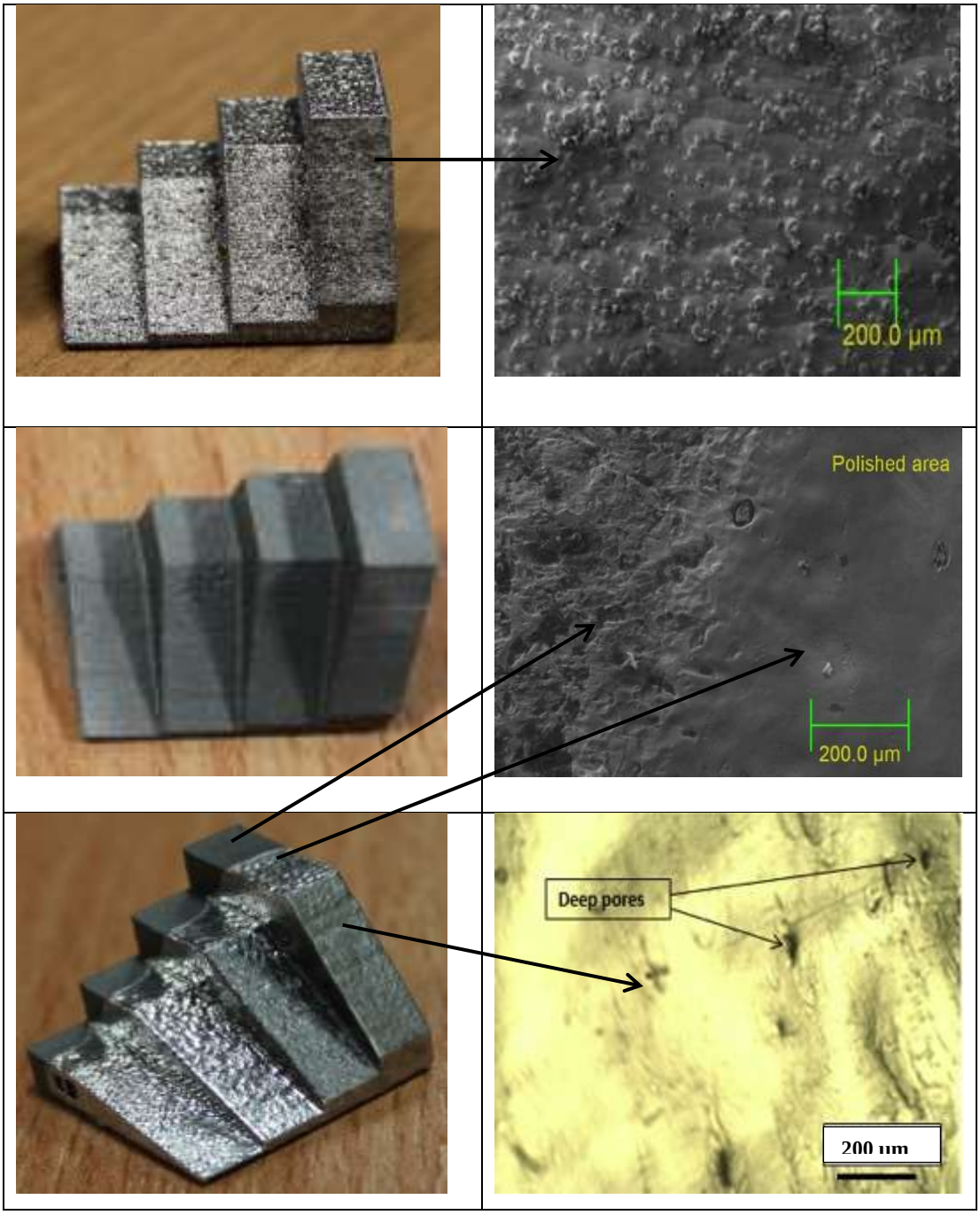

Figure 6-21: 3D models on the left and 2D micrograph to verify the number of defects on the treated areas on the right.

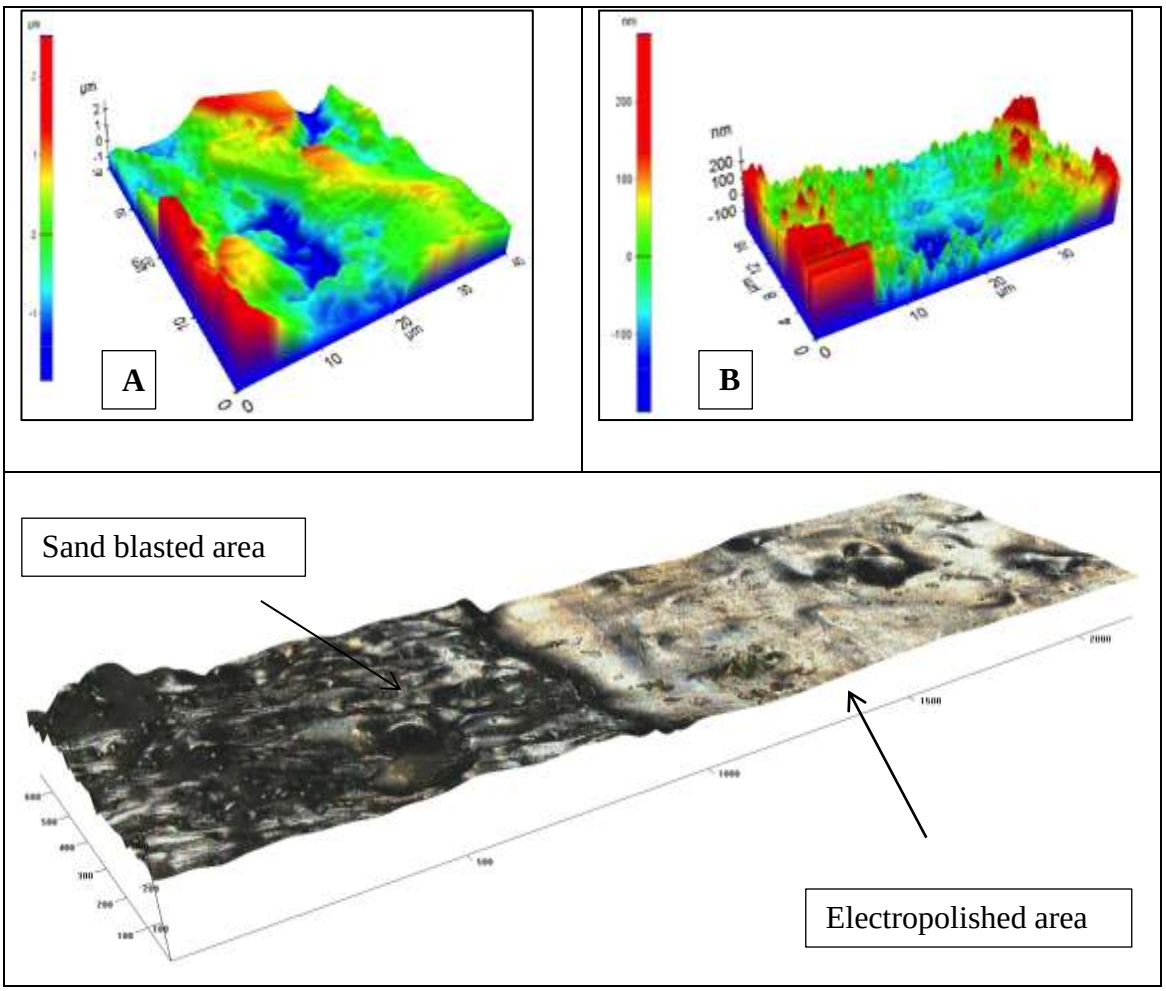

Figure 6-22: 3D micrograph to verify the difference between sand blasted (A) and electropolished (B) areas.

Figure 6-22 shows micrograph roughness obtained by 3D Zeta Microscope on two different regions of the top surface of the part. The dark blue colour indicates the maximum valley and the red one indicates the highest peak, also showing the amount of surface dendrite reduction.

6.4.2.2 Surface roughness

A stylus profilometer was used to obtain the results. The results show that the amplitude of the surface roughness parameter *Ra* has significantly reduced after employing the processes. The total amount of improvement was recorded at approximately 80 to 86%. Also, the best results were linked to slope angle increase, because the initial roughness of the surfaces was lower due to the angle increase, although, the percentage reduction of surface roughness is approximately the same, as shown in **Figure 6-23 and Table 6:3**.

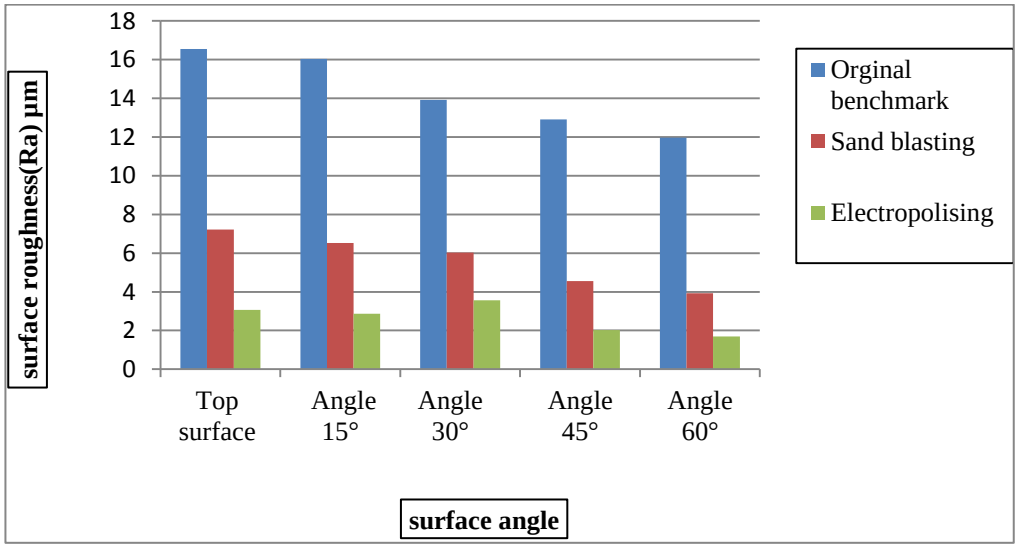

Figure 6-23 : Surface roughness comparison results.

	Top surface	Angle 15°	Angle 30°	Angle 45°	Angle 60°
Original benchmark	16.54	16.026	13.91	12.9	11.97
Sand blasting	7.21	6.53	6.03	4.56	3.93
Electropolishing	3.06	2.87	3.56	2.03	1.69
Improvement %	81.49	82.1	74.4	84.2	85.88

Table 6:3: Comparison amplitudes parametric of surface roughness (Ra), before and after processing& also showing the percentage of improvement.

6.5 Chapter summary and direction of next Phase

The characterization of SLM component surfaces and surface improvement has been briefly covered in this chapter. The results showed that the machine is fully functional for manufacture and the overall conclusion can be summarized as followed.

- Surface topography of the SLM cubes and benchmarks showed the same surface topography involves balling, porosity, peak, valley, agglomeration, fully melted area and partially melted areas. The variations of these features depend on the process parameters and the surfaces' build orientation.
- The surface roughness ranges between 10 to 20 µm Ra on the top surface.
- The cubes built in the first trial at the right side of build area demonstrated a small increase of the top surface roughness, possibly due to the flow of argon being from right to left in the build chamber.
- Surface roughness reduced as surface angle increased to 90°.
- Some pores were clearly apparent under the top and mostly under the side wall surface due to the machine scan strategy.
- Density decreased as the area of side wall surfaces increased, due to the porosity issue.

Unfortunately, open pores and subsurface porosity presented a major obstacle in reaching the final objective of surface finish. Thus, mechanical methods cannot be recommended with SLM parts, because they work by eroding a specific amount of the surface, leading to subsurface porosity appearing on the surface as roughness, also leave some residual stress and destroy small features such as radii, fillets, sharp corners and small holes, which effects on the parts physical and mechanical properties.[173, 68,175] On the other hand, thermal technique (laser surface modification) has been used in different areas such as laser marking, cladding, micro machining, engraving and currently being used in latest technologies such as laser ablation, laser polishing and re-melting of AM metal powder parts to enhance the surface defects. Therefore, thermal techniques such as laser re-melting and laser polishing may be a better solution, due to their own advantages such as improved surface topography, mechanical properties, reduced porosity and residual stress.

The results obtained from this investigation strongly support the methodology and demonstrate the reason for laser re-melting as an approach for SLM parts surface improvement.

7.0. Laser re-melting

The AM process has been developed to fabricate fully functional parts with good surface texture, but the parts still suffer from some drawbacks such as inadequate surface finish, as already mentioned in the previous chapter. In this phase of the experimental work, the samples were made at different build angles in order to provide a range of surface roughness to test the re-melting process. Optimization parameters for laser re-melting were developed in this chapter. Also, a comparison of as-fabricated with re-melted inclined surfaces is demonstrated in this chapter. The work was divided into two stages, as shown in **Figure 7-1**.

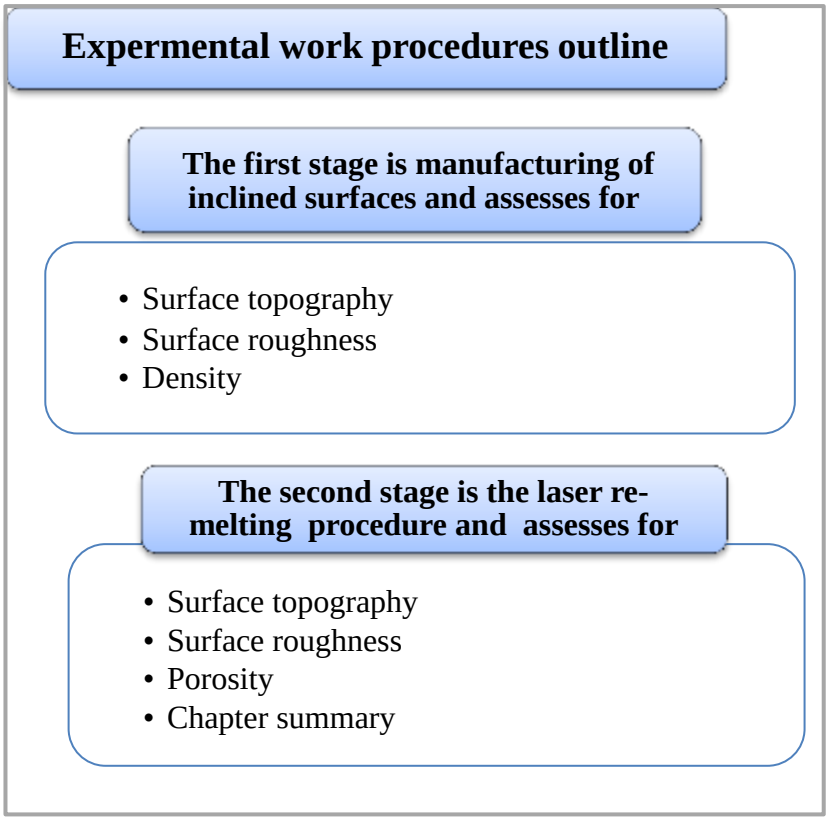

Figure 7-1: shows the outline of experimental procedure employed in the second phase.

The experiment in this phase starts by re-designing the benchmarks and inclined surfaces were made instead to the previous benchmarks as shown in **Figure 7-2.**

7.1 Inclined surface manufacture

7.1.1 Manufacture procedure

The manufacture was completed by producing inclined samples instead of the previous benchmarks **Figure 7-2.**

The aim was to adapt the surfaces for the re-melting process, by making them separate parts which could be re-melted without obstructing the laser. The samples were again made on the Renishaw SLM125 at De Montfort University. The experiment was carried out by setting up the machine and implementing the same parameters as in the previous experiment, as per **Table 6:1**. The same stainless steel powder was used to build the inclined surfaces, with dimensions 30 x10 x 4mm, at angles of 0°, 15°, 30°, 45°, 60°, 75° and 90° from the horizontal as shown in **Figure 7-2**. Five samples were made for each angle to complete this investigation; the total number of samples was 35.

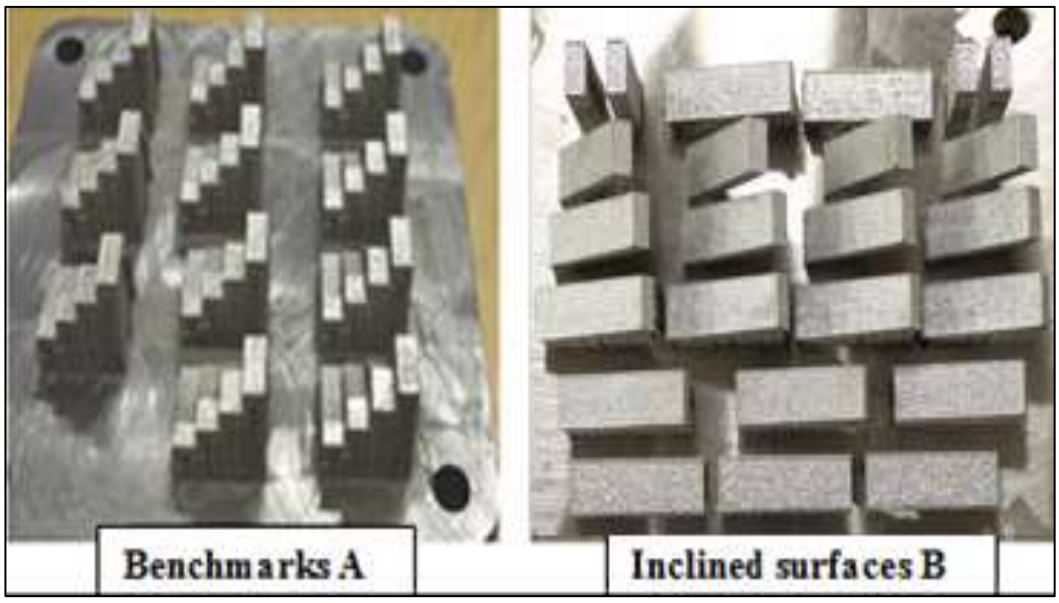

Figure 7-2: Re-designed inclined surfaces for the re-melting experiments.

The samples were removed from the substrate and cleaned according to the same method as section **6.1.3**. After completion of supports removal and inspection, the samples were checked to assess for surface roughness, topography and density, as shown in **Figure 7-3**.

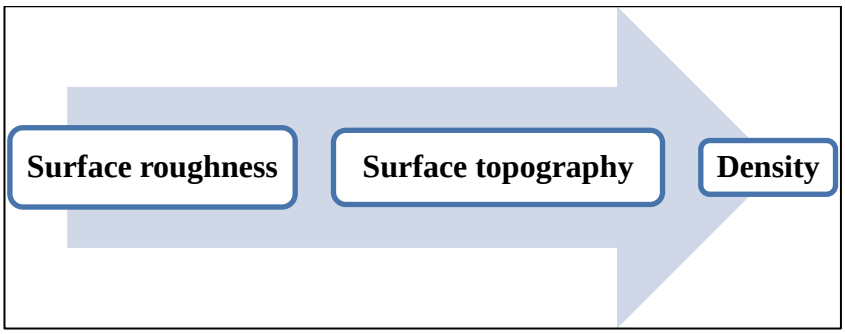

Figure 7-3: Stages of surface assessment.

Surface characterisations such as surface roughness measurement and imaging were done at De Montfort University, implementing the same techniques as in the first phase of the experimental work, i.e. stylus profilometer (SJ400), SEM, 2D microscope and 3D microscope. For more information about this equipment see the methodology chapter, **section 5**.

7.1.2 Results and discussion

7.1.2.1 Surface roughness

The surface roughness (*Ra*) component of the SLM parts (inclined surfaces) showed various ranges of value due to the gradient of sample orientation, the lowest results observed on samples with specific angle trends to 90° degree, although the scanning strategy, powder specification and laser parameters were fixed.

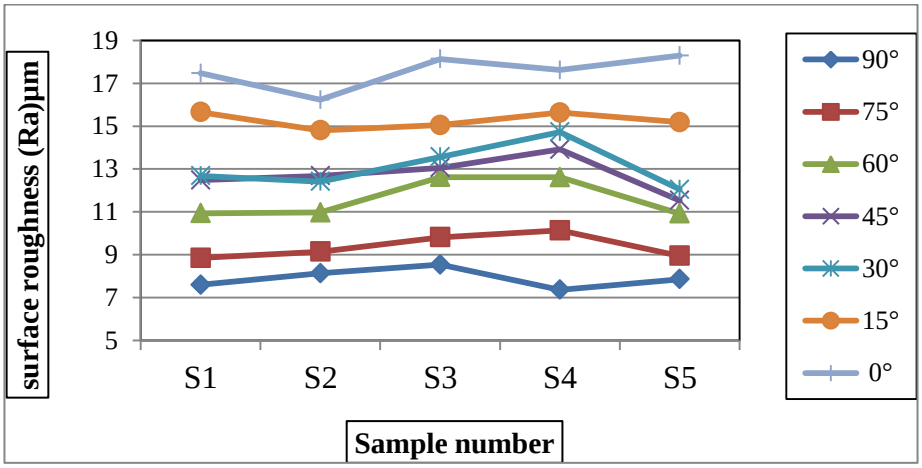

Figure 7-4 : Stylus profilometer results for average roughness (Ra).

Figure 7-4 shows the surface roughness (*Ra*) obtained from all samples, whereas **Figure 7-5, Figure 7-6 and Figure 7-7** below show the amplitude parameters with errors margins of parameters *Ra, Rq* and *Rz* measured on the top surface of all samples. It can be seen that the response of surface roughness is negatively proportional to surface angle.

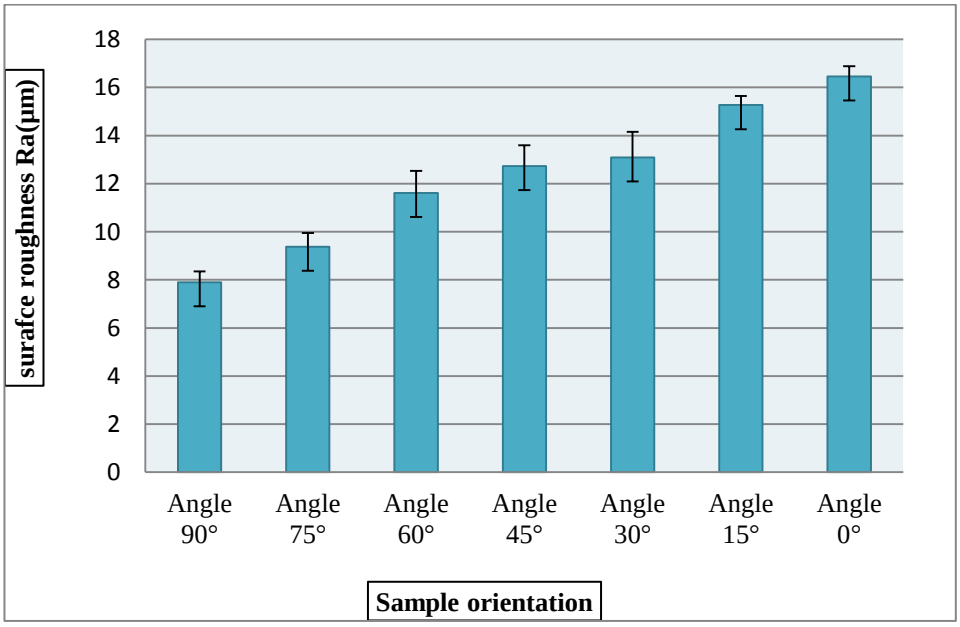

Figure 7-5: Average roughness (Ra) with error realized on all inclined samples.

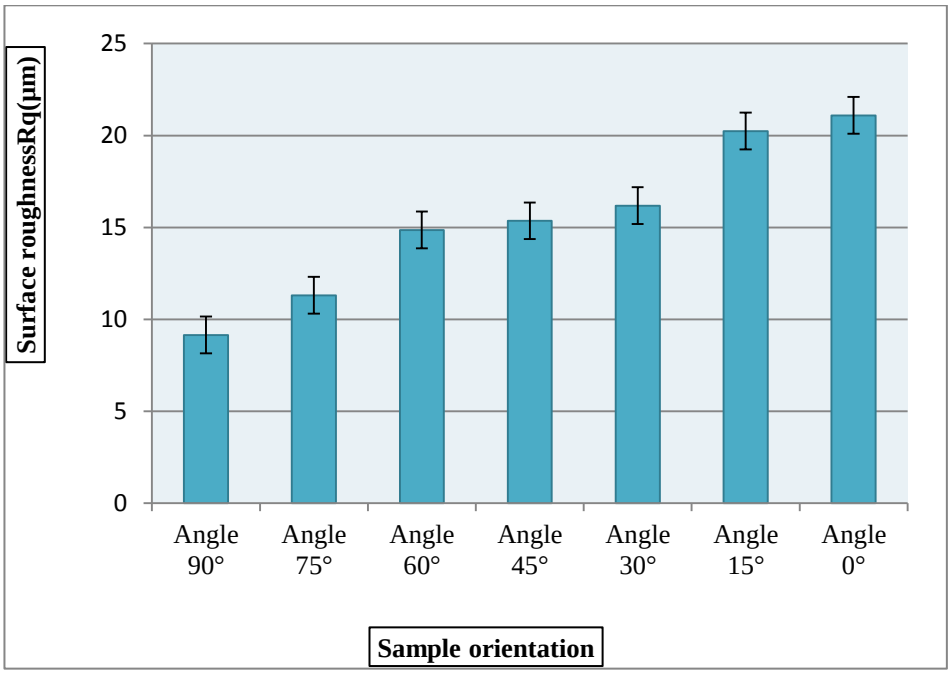

Figure 7-6: Mean square of average roughness (Rq) with error.

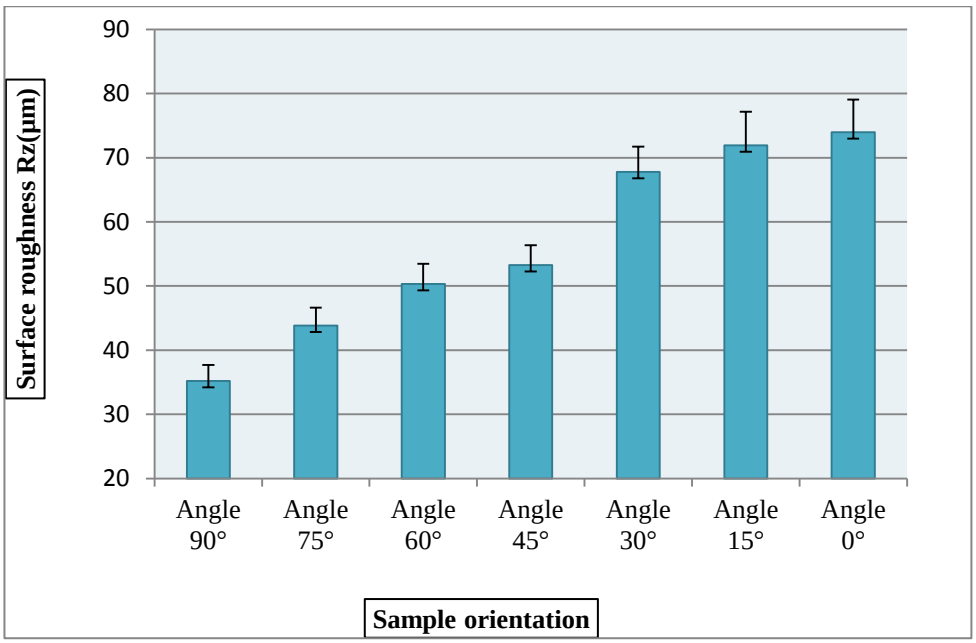

Figure 7-7 : Average maximum of height to valley (Rz) of the Profile with the error.

As demonstrated in the figures above, the surface roughness of SLM components are highly influenced by the surface orientation and showed considerable improvement in terms of data measured and the best results obtained by 90º. This is because of the stair effect factor. The presented results in the above graphs are in agreement with results from other researchers regarding the stair effect. [81] Other factors such as no-homogeneous powder spreading during the deposition process can affect surface roughness, creating high peaks and valleys adherent on the outer surface profile. These peaks and valleys will also prevent a homogeneous deposition of the powder on each subsequent layer and leading to an imbalance of the layer thickness. Moreover, an imbalance of layer thickness causes insufficient melting of the powder during the laser process, demonstrated by a considerable number of pores and associated surface texture.

7.1.2.2 Surface topography

Different optical microscopes were used to reveal the surface topography of the results obtained from the experiment. The results showed some defects on the top of the samples such as irregular ridges, peaks, valleys, deep pores, over melted areas and balling. It is worth mentioning that the sizes of these defects increases with the increase in surface angles from the horizontal. **Figure 7-8** shows the increase of surfaces degradation during the manufacture process with reducing build angle. The dendrites are clearly present the foremost difficulty for some engineering applications, where surface roughness is considered a main concern.

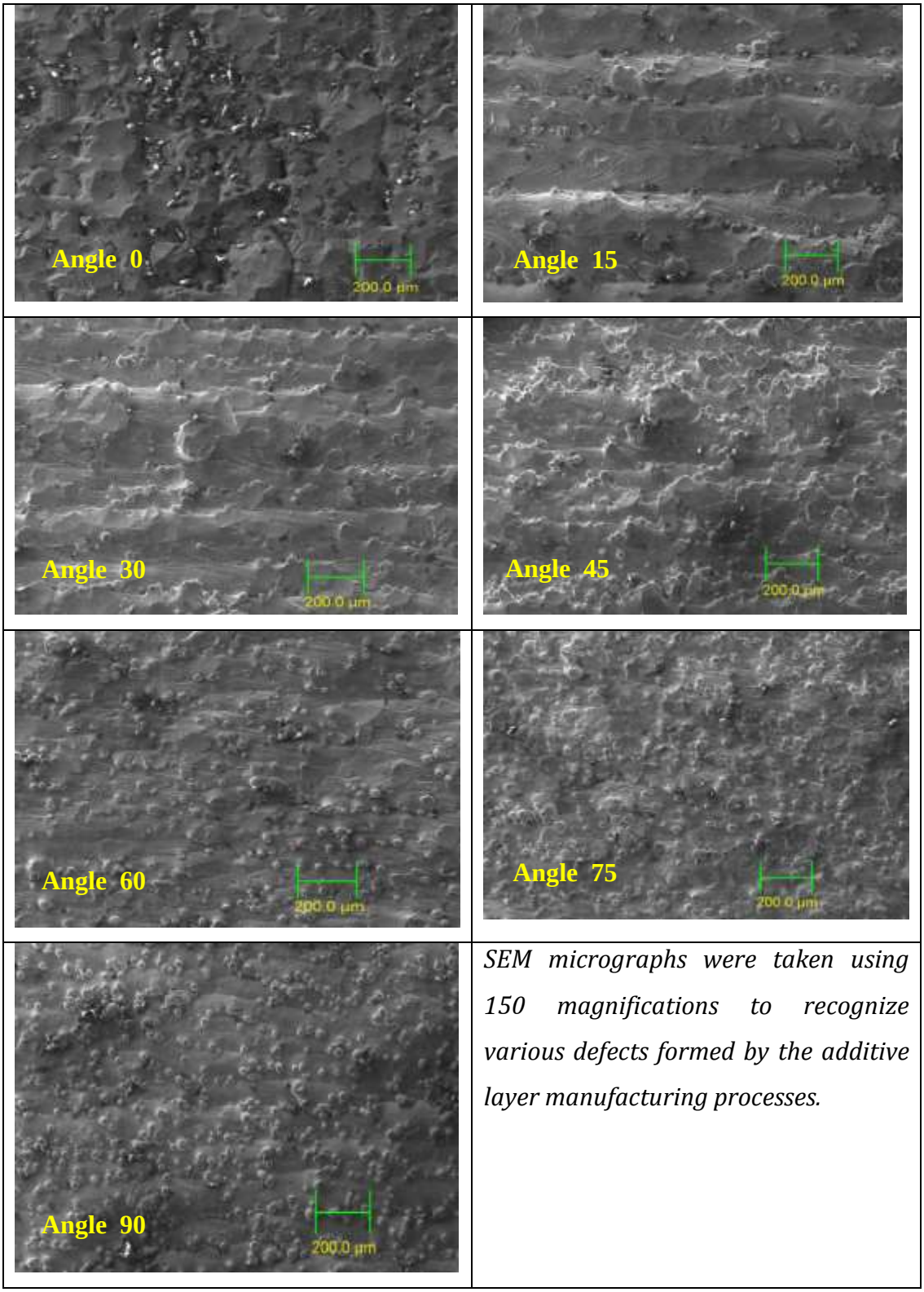

SEM micrographs were taken using 150 magnifications to recognize various defects formed by the additive layer manufacturing processes.

Figure 7-8: SEM results performed on all inclined samples.

3D images were taken (as can be seen in **Figure 7-9**, **Figure 7-10** and **Figure 7-11**) to see how the surfaces are after the layer manufacturing process. The figures demonstrated several different areas which are deformed due to the high laser power

and interaction parameters during SLM manufacture. These deformations are formed due to high laser energy leading to different response of shrinkage when the part was being built. The figures show defects such as balling, agglomerations, peaks and valleys. They also show areas with a lack of melting, sufficient melting and extreme melting. Thus, all these defects have significant effect on the surface topography and roughness results.

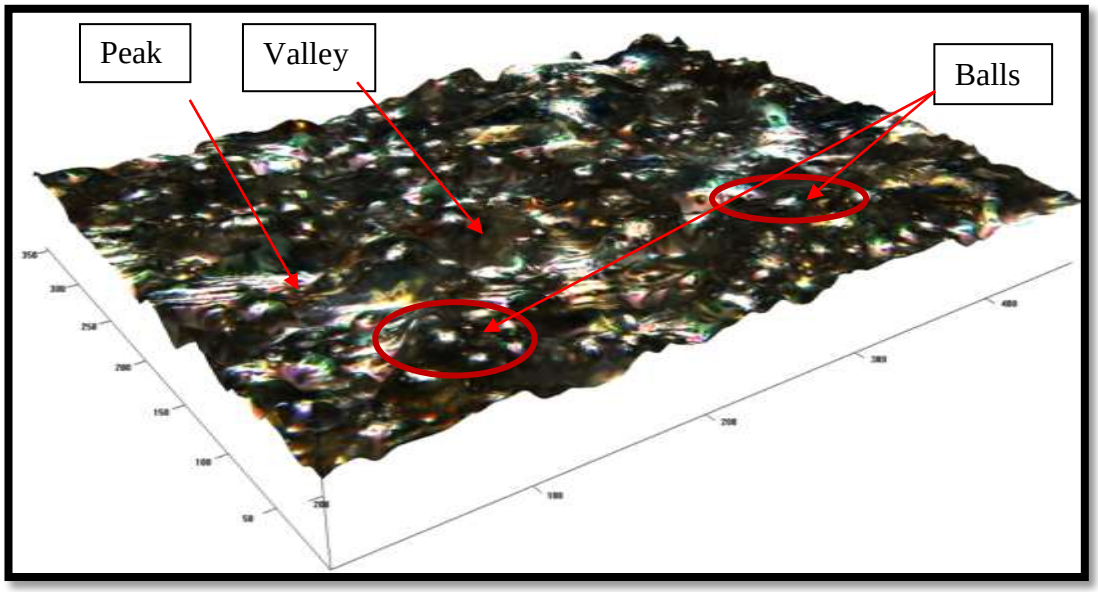

Figure 7-9: 3D image obtained on surface 90°.

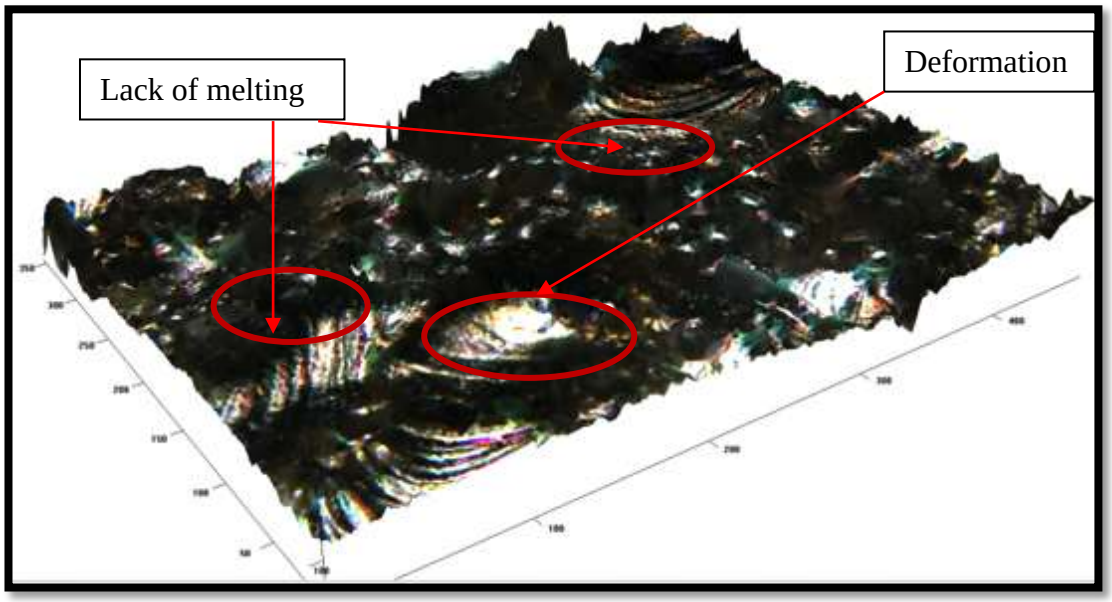

Figure 7-10: 3D image obtained on surface 45°.

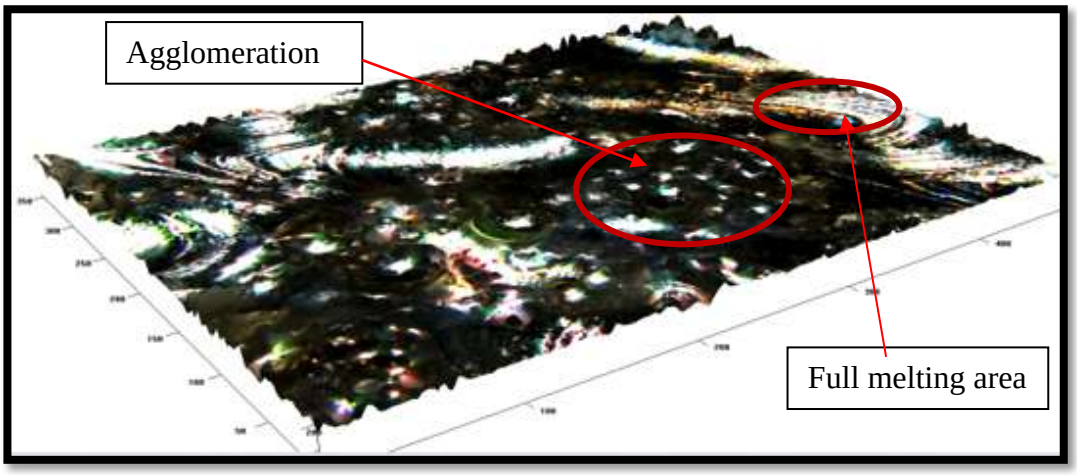

Figure 7-11: 3D image obtained on surface angle (0°).

As can been seen on the surfaces, the phenomena of spheroidization or balling is a problem which happens during deposition process. It causes severe weakening of the interconnection between layers. Balling is creation of isolated areas that have an equal diameter with the focus of the laser beam and it affects the deposition process, causing a reduction of the density of the created part. It happens when the molten material is not capable of fully wetting on the substrate. Also, it can happen due to differing high surface tension, resulting from varying thermal properties across the melted pool. [176]

The impacts of these previous defects after each layer has been constructed are reduced material density and increased surface roughness. Laser re-melting after each layer has been constructed may the best solution to solve this problem for improving the density and surface roughness of AM, despite the fact that the production cost and time will increase.

In addition to this, a comparison between Kruth and Hauser [176,177], shows that they contradict each other; the results of Kruth indicated that balling defects can be reduced by increasing the scan speed, while Hauser suggested the opposite. Thus, it could be both right toward this phenomenon, because the results of an excessive amount of energy density that gives the melted powder viscosity has specific range. This range of energy density is proportion of scan speed, indicated by **equation 3-2.**

7.1.2.3 Density and porosity

In additive manufacture techniques, the porosity is considered as a crucial factor for many applications such as medical ones, when complexity and weight are coming in the first concern. The characteristics of SLM parts such as microstructure and densification are completely reliant on the temperature of the processing system, which consequently mainly depends on the laser parameters used during the process. [77, 78, 178]

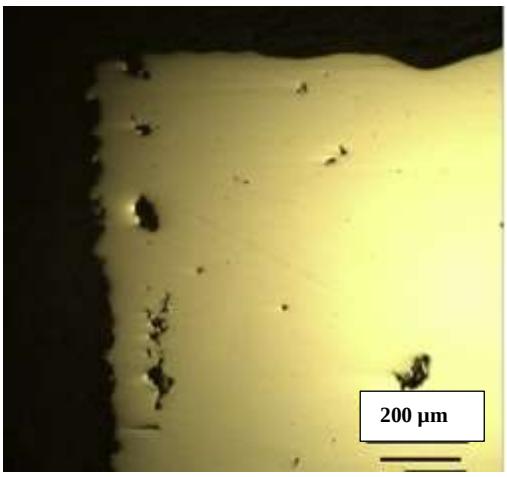

A obtained from angle 90°

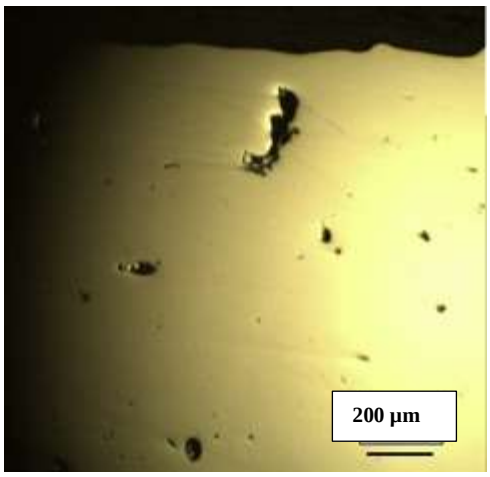

B obtained from angle 0°

Figure 7-12: 2D Micrographs of cross sections were obtained from different inclined surfaces (90°& 0°).

Figure 7-12 shows micrographs of two different inclined surfaces produced by using same parameters. There are large pores found on the cross-section areas. These pores contribute to decrease the density associated with angle increase as shown **Figure 7-13**. The black spots are pores and the yellow area is the fully melted material.

Due to the homogeneous nature of the samples, the density can be determined by mass divided by volume as with the previous parts (cubes and benchmarks). The determination of density was carried out by evaluating the mass by a normal balance, whereas the volume was determined directly from the dimension geometry of the samples. The density was measured according to **Equation 6-1.**

.

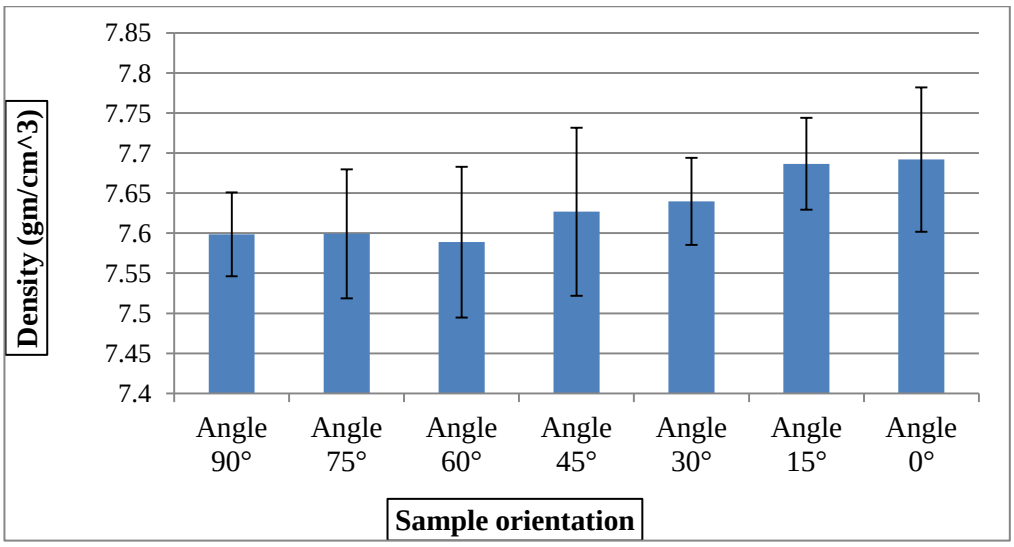

Figure 7-13 : Density results of inclined surfaces.

Figure 7-13 shows that the densities of the parts are linked to the number of pores, which is also connected with the angle increase. It also can be suggested that the process parameters have a high influence on the part density linked with elevated angle due to the scan strategy. These black points are pores, and play as major obstacles to obtain good surface finish as it can be seen in **Figure 7-12** and **Figure 6-8.**

It can be summarised that the quality of components manufactured by SLM machine is significantly influenced by the machine parameters and design orientation were showed very rough surfaces. Surface roughness and porosity associated with this technology are depending on the laser parameters and scanning strategy. Also the major influences have been associated with the part orientation during the building process. Thus, the samples produced had balling effects and the surface was uneven due to balling, peaks, valley, agglomeration, full melting and insufficient melting areas which caused by unwell distribution of powder particles during layer deposition and the interaction of laser parameters during the process as we noted above.

These defects (internal and external) are needed an additional treatment. Thus, to eliminate these defectives, laser re-melting could be an alternative solution rather than any techniques (see surface finish chapter).

*The samples were mounted horizontally in a substrate frame to fit the re-melting machine, and kept to be used in section **7.2.2**, in order to see the ability of the optimal parameters to reduce any surface defects connected with SLM components.*

7.2 Laser re-melting procedure

Laser re-melting (LR) has been promoted as a process for AM metal components due to its ability to supress some drawbacks of the parts. This approach (LR) can be used after each layer that has been built on the main substrate or later on as post-processing on the outer layer of the part surface. [4]

Methodologically, this trial follows work done by Kruth, where the author did all his experiments in a Concept Laser M3 linear machine (re-melting in-process). [4] However, these trials evaluated re-melting as a post-process. They were carried out on the RECLAIM machine, as described in section **5.2.3** through two specific steps as shown in **Figure 7-14**.

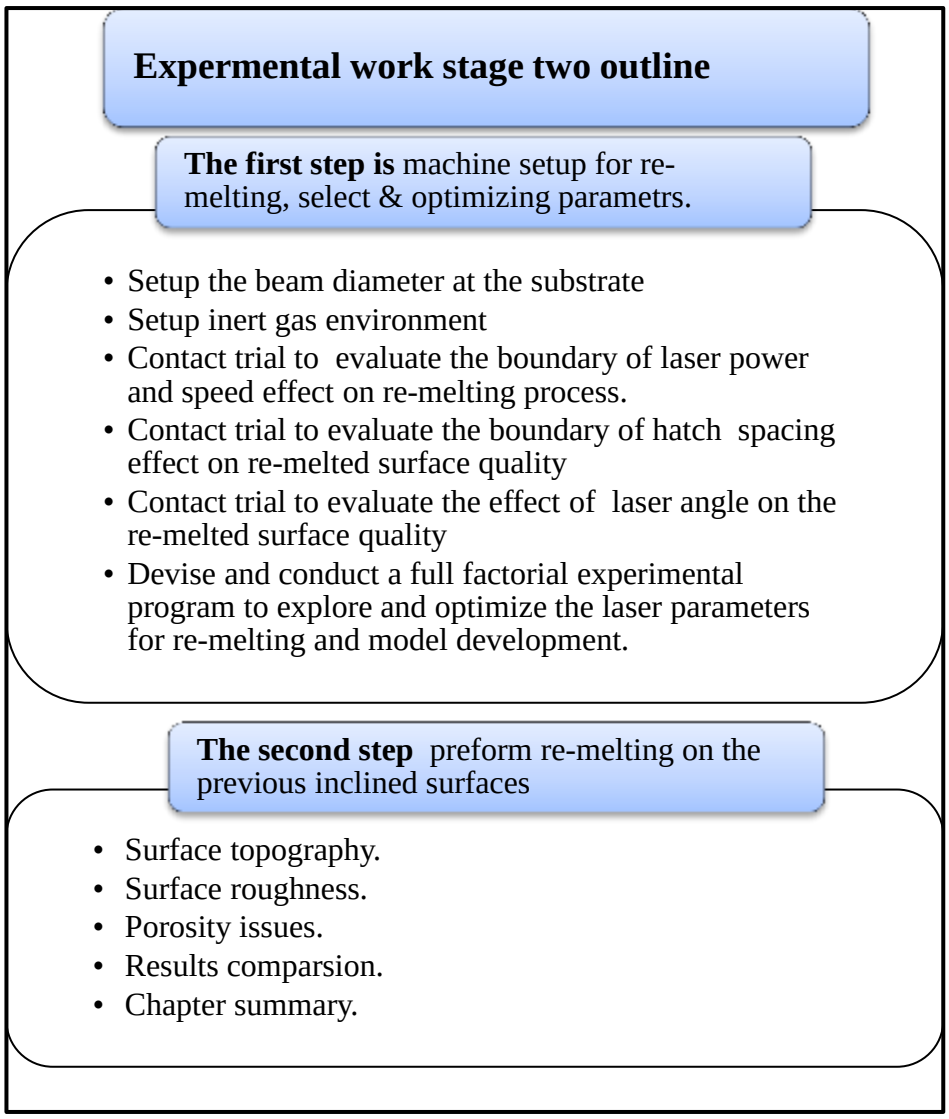

Figure 7-14: Outline of re-melting procedure.

7.2.1 Machine setup for re-melting

Machine setup is very important as it subsequently affects the quality of the results. Many attempts have been made in this field, and the results show that the surface finish quality and part density after re-melting process are dependent on the amount of energy input into the surface. Energy density is directly influenced by factors such as type of laser, power, speed, hatching spacing, focus distance and beam diameter. Also, the environmental condition (oxygen level) is significant factor and has a high influence on the surface results. [4, 94] It is possible to say the above factors are the key points for controlling the re-melting process. To obtain a usable re-melting process, several experiments were planned to optimise these parameters for the re-melting process as shown in **Figure 7-14**.

7.2.1.1 Setup of the beam diameter at the substrate

7.2.1.1.1 Aim and experimental procedure

The laser beam spot size is a vital factor which affects the amount of energy observed by the work piece. Thus, it affects the re-melting results according to the following formula.

$$\textbf{Energy density} = \frac{\textbf{laser power}}{\textbf{speed} * \textbf{spot diameter}} \quad \left(\frac{\boldsymbol{J}}{\boldsymbol{mm^2}}\right) \qquad \textbf{Equation 7-1}$$

The main purpose of this trial was to adjust the distance of the stand-off between the lens and the work piece to give the maximum and minimum of the response factors (track width and depth of re-melting). The best results should be obtained with a depth of more than 100µm. This is because the amplitude of the surface roughness (*Rz*) of the SLM component can vary as shown in **Figure 7-7**.

For this trial a small square flat sheet from stainless steel was made for this purpose with a stand of dimension 12 x 8 cm^2, instead of using SLM sheet, to reduce costs.
The experiment was carried out using the RECLAIM machine at MTC Coventry, described in section **5.2.3**.

The process was started by setting the power and stand-off in different sets and carried out as shown in the following steps.

- Pass the laser beam over the sheet at a stand-off distance of 130mm, melting with various power settings: 50, 60, 70, 80 and 90 % of the available 200watts.
- Repeat the above process with various distances between the lens and the substrate (standoffs of 129, 128, 127, 126, 125 and124 mm.

Whereas, other parameters were kept constant as shown below:

- The focal length of the lens: 120 mm
- Beam diameter at lens: 16 mm
- Scan speed: 400±5% mm/min

The measurement of the laser re-melting tracks' width and the depth were obtained using a 2D microscope, to measure the marked details on the sheet.

7.2.1.1.2 Result and discussion

Figure 7-15 and **Figure 7-16** show the results of laser single track pass on the flat sheet of stainless steel, in order to determine the width and the depth of the track at different setups through the process.

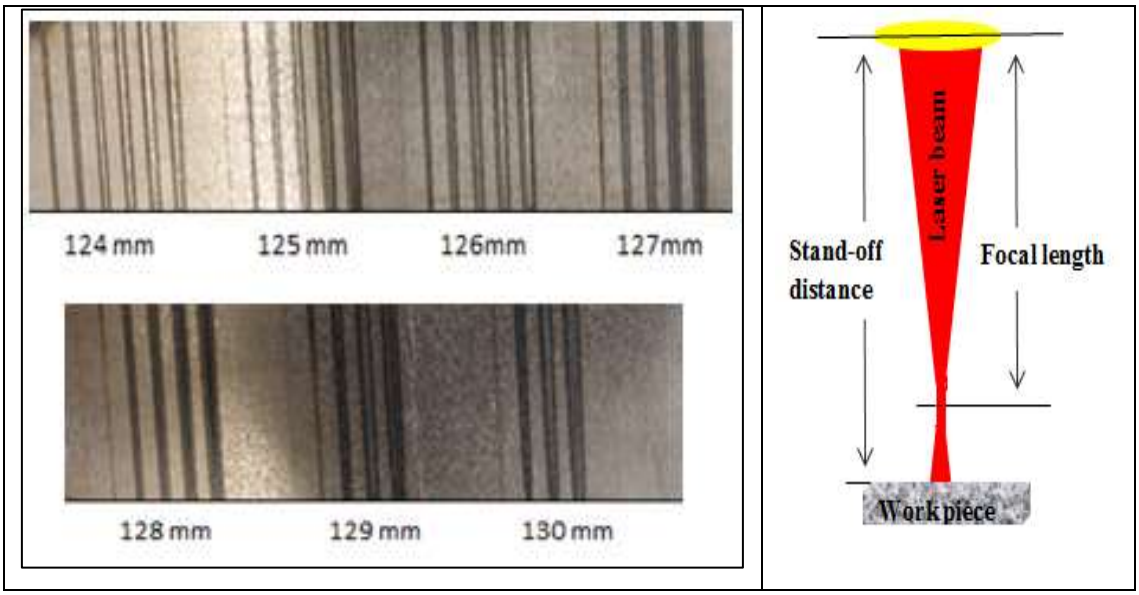

Figure 7-15: Re-melted tracks width dimension (µm) at varies power and stand-off distance.

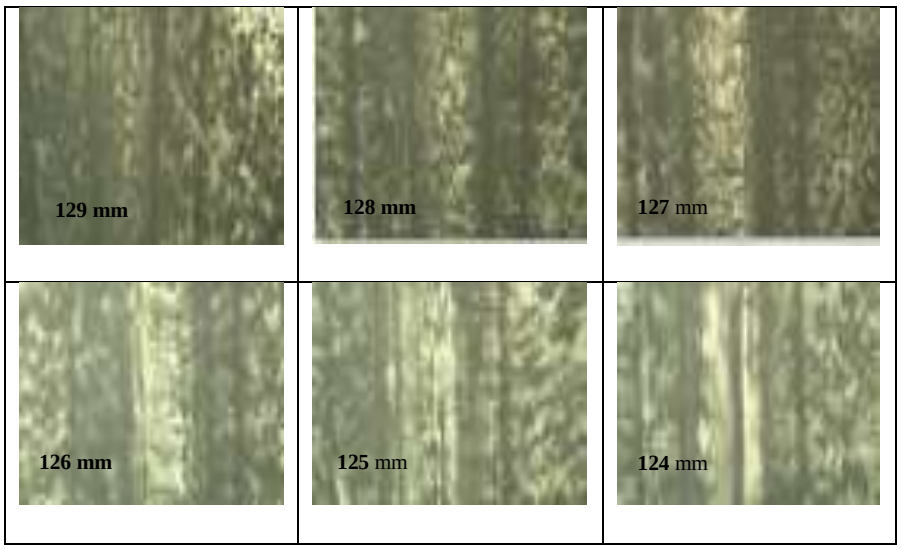

Figure 7-16: Width of re-melting track at fixed requested power (90%) and various stand-off distances (129, 128, 127, 126, 125 and 124) mm.

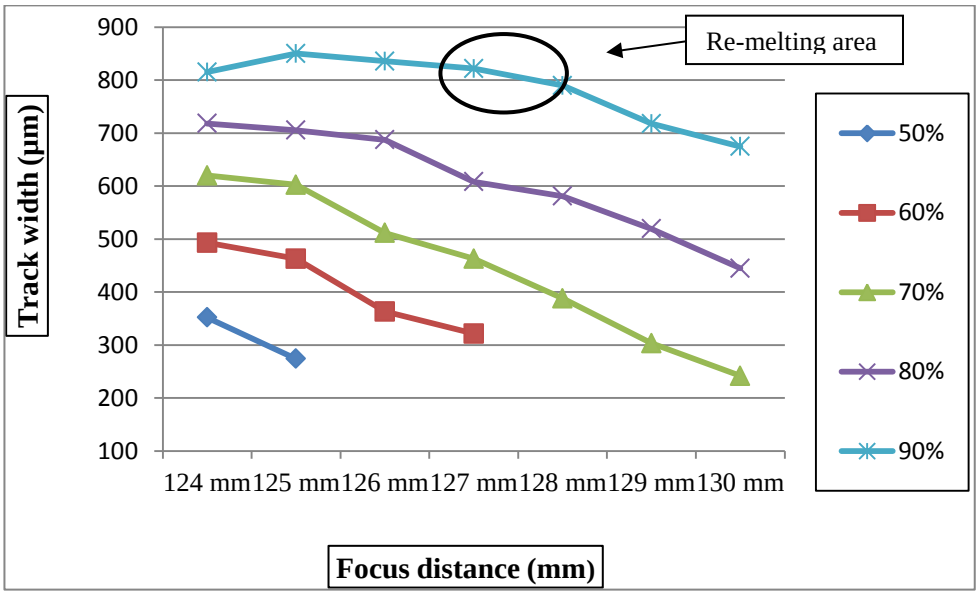

Figure 7-17: Re-melted tracks width dimension (µm), Laser power against focus distance.

Figure 7-17 shows the width profile of the re-melted tracks, which varied with laser energy and stand-off distance. The results demonstrated that the re-melted track width became bigger with increased laser power and with decreasing nozzle stand-off distance. On the other hand, the results also suggest that the decline of track width can be connected with high power 90% and 124mm as stand-off distance. This is likely due to the beam intensity profile which is normally concentrated in the centre as it can be seen in

Figure 7-18. Figure (3D) shows the laser beam profile energy distribution and the top view shows the entire power density of laser beam profile in contours indicated by colours. Also the results from **Figure 7-16** connected with a 124mm stand-off distance and 90% of laser power, showed a 'slot' (visible in the 124mm image) along the length of the re-melted track. This can be attributed to the elevated energy on the surface leading to cutting of a small track instead of re-melting the surface.

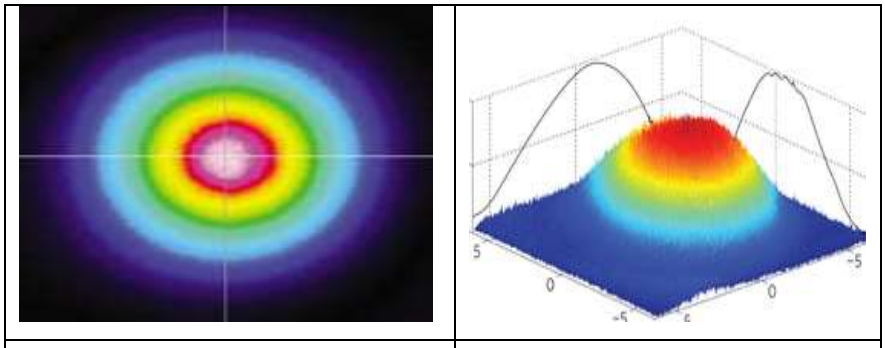

Top view	3D

Figure 7-18: Beam intensity concentration. [179]

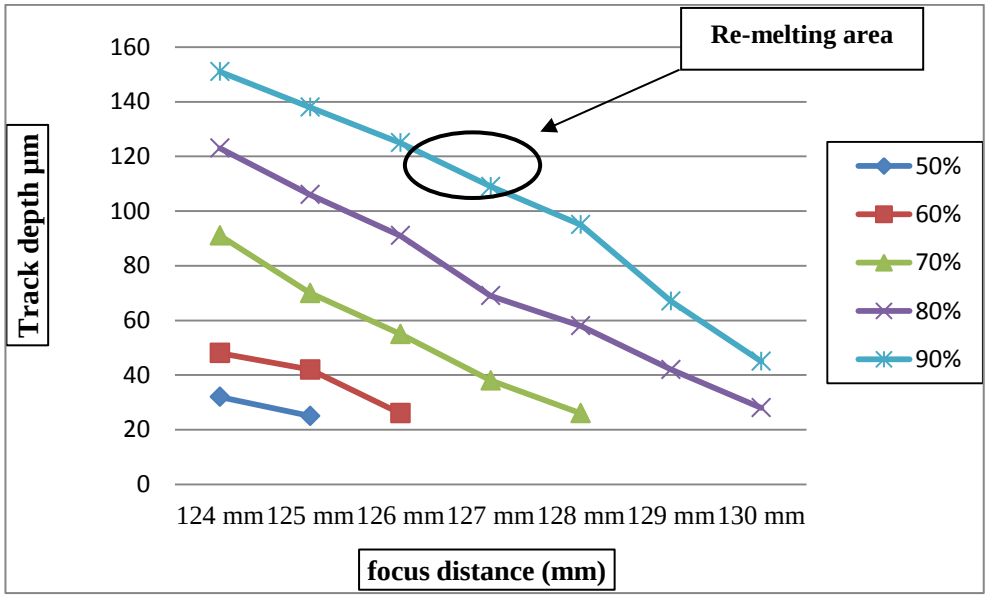

Figure 7-19: Depth of re-melting track.

Figure 7-19 shows that the depth of the re-melting track is proportional to laser power and inversely proportional to the focal distance between the re-melting head and substrate. The graphs in **Figure 7-17** and **Figure 7-19** both demonstrate that several stand-off distances can be selected for re-melting process which is depending to the depth of re-melting associated with energy density. However, to enable proper re-

melting for SLM components, the depth of re-melting should be more than the range of the amplitude roughness *Rz*, which ranges between 35 to 80µm, see **Figure 7-7**.

According to the results obtained in **Figure 7-17** and **Figure 7-19** there is a specific range of stand-off values (127-128)mm, linked with 80% or 90% of laser power that give both a track depth of more than 100µm and a track width of approximately 0.8mm. The area of optimal parameter interactions are shown by the black circle in each of the two graphs.

The next steps focused on 128mm as a fixed stand-off distance for completion of the setup and re-melting process.

7.2.1.2 Setup inert gas environment

7.2.1.2.1 Manufacture procedure

For this trail of the process (setup and optimizing parameters for re-melting), stainless steel 316L SLM samples with dimensions 30 x10 x 4mm were made, with a fixed build angle (75°) in order to provide models with the same range of roughness. They were made on the SLM 125 machine at De Montfort University using powder with particle size ranging between 15 to 45µm, with the parameters indicated in **Table 6:1**. The initial surface roughness of these samples was (*Ra*) = 10µm ± 10%.

The steps of manufacture and inspection were kept constant as described in **section 6.1** and after individual checking, the samples were placed horizontally onto a substrate, shown in **Figure 7-20-A**.

7.2.1.2.2 Aim and experimental procedure

The main aim of this trial was to check if the samples could be successfully re-melted without oxidation and to select the best boundary of argon flow level to maintain the part from oxidation. The trials used the flow of argon from the cladding head fitted to the RECLAIM machine, as shown in **Figure 7-20-B**. If oxidation could not be prevented, then an additional gas shield would be used as extra gas for shielding the melt pool.

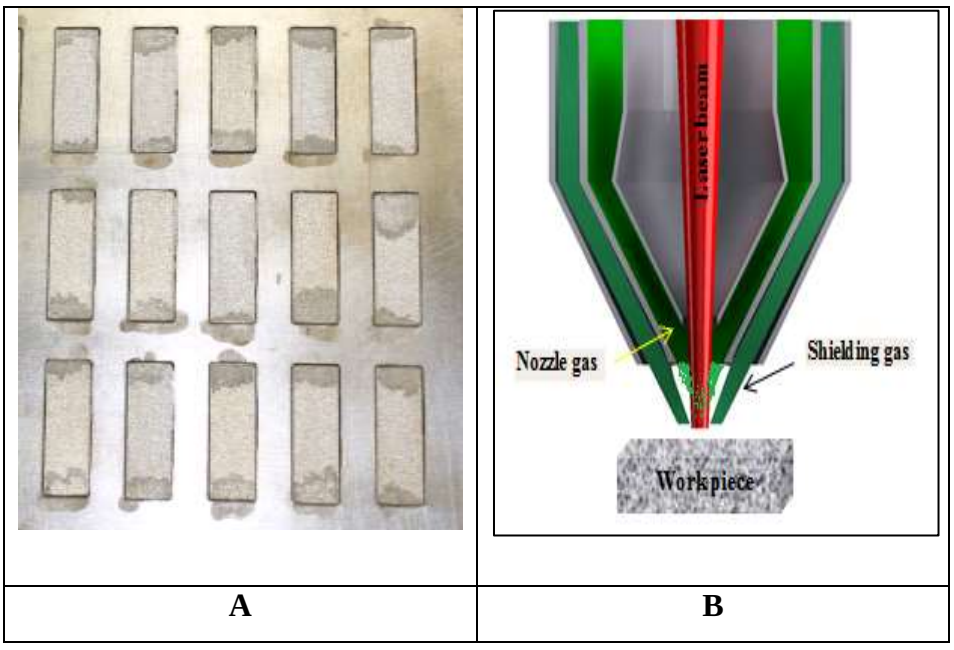

A	B

Figure 7-20: Inclined surfaces on the substrate.

In order to investigate the effect of the three alternative gas flow methods (nozzle, shielding and both) on the surface finish and oxidation level during re-melting process, the gas flows were set at different values in the range 2, 3, 4, 5 and 6 L/min, whereas the other parameters were fixed as follows:

- The requested laser power: 200 watt
- Scan speed: 1000 mm/min.
- Focal length of lens: 120mm
- Distance between the lens and the substrate: 128mm.
- Beam diameter: 16 mm at the lens and approximately 1mm at the substrate.
- Hatch spacing: 0.5 mm.

7.2.1.2.3 Results and discussion

Oxidation is a chemical reaction that involves addition of oxygen to an element of a compound. Oxidation in a real sense occurs when the oxidation numbers of atoms changes in what is commonly known as a redox reaction. The chemical process may be the best solution to remove undesirable oxide layer. [16]

In the re-melting process, it is very important to control oxidation, because it can cause irregular consolidation of the re-melted layer. An increase of oxygen level causes an increase of metal oxides. In the case of stainless steel 316L, the iron oxide can be a significant barrier to flattening of the liquid iron of the melt pool top surface during the process, causing some defects such as pooling and porosity, although with an absence of contamination. This phenomenon occurs due to the tension of the liquid metal oxide on the main surface being less than the metal liquid without oxidation. [16]

Figure 7-21 indicated that the occurrence of oxidation during the re-melting process was inversely proportional to the argon flow rate, although the energy density was the same throughout the experiment. In other words the result showed that the samples exposed to a higher rate of argon flow had less oxidation.

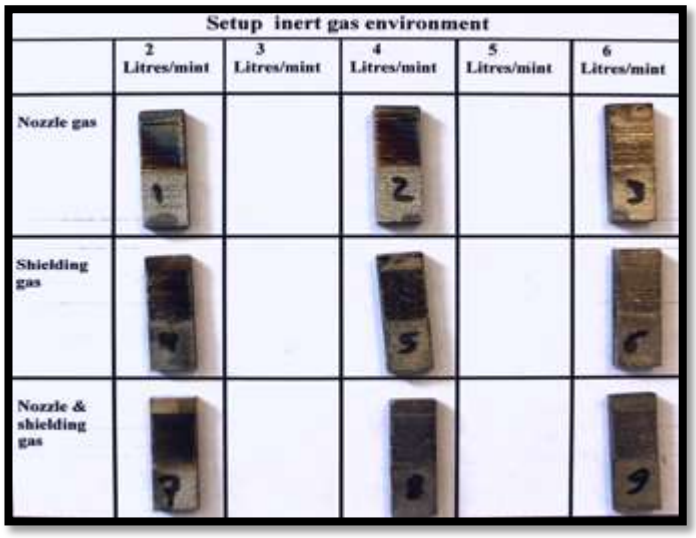

Figure 7-21: The amount of oxidation during re-melting process.

An EDX instrument was implemented to check the amount of oxygen on the top layer of the re-melted surfaces. The observation involved the samples that were exposed to 2, 4 and 6 litre/min of argon gas flow as shown in **Figure 7-22**.

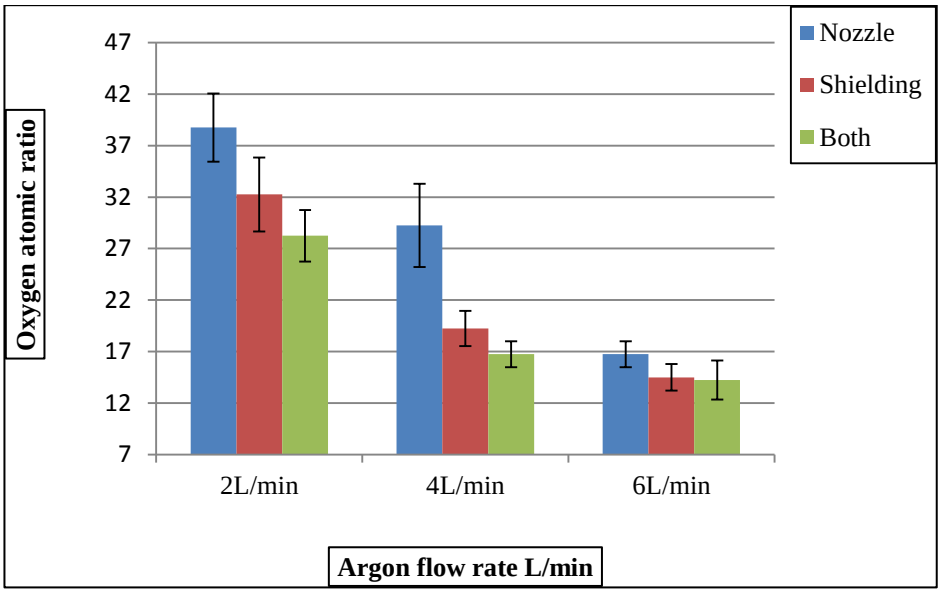

Figure 7-22 : The amount of oxygen atomic ratio obtained through three different setups of argon flow methods.

Figure 7-22 shows the results of the oxidation measurements obtained through different methods of argon flow. The level of oxidation increases with a decrease of argon flow rate. In a comparison between the three methods of gas flow, the samples demonstrate less oxidation, conducted with flow rates between 4 and 6 litre/mins. These results were observed in the 'both' and the 'shielding' methods.

Although surface roughness for this experiment was not very important, the samples demonstrated a noteworthy improvement of surface roughness in comparison with the initial values. These significant results were driven by the level of laser energy density of about 1200J/cm^2 during the process. The laser energy density was calculated according to **equation 7-1** above.

Images were observed by SEM to identify how the surfaces had improved; some are shown in **Figure 7-23**.

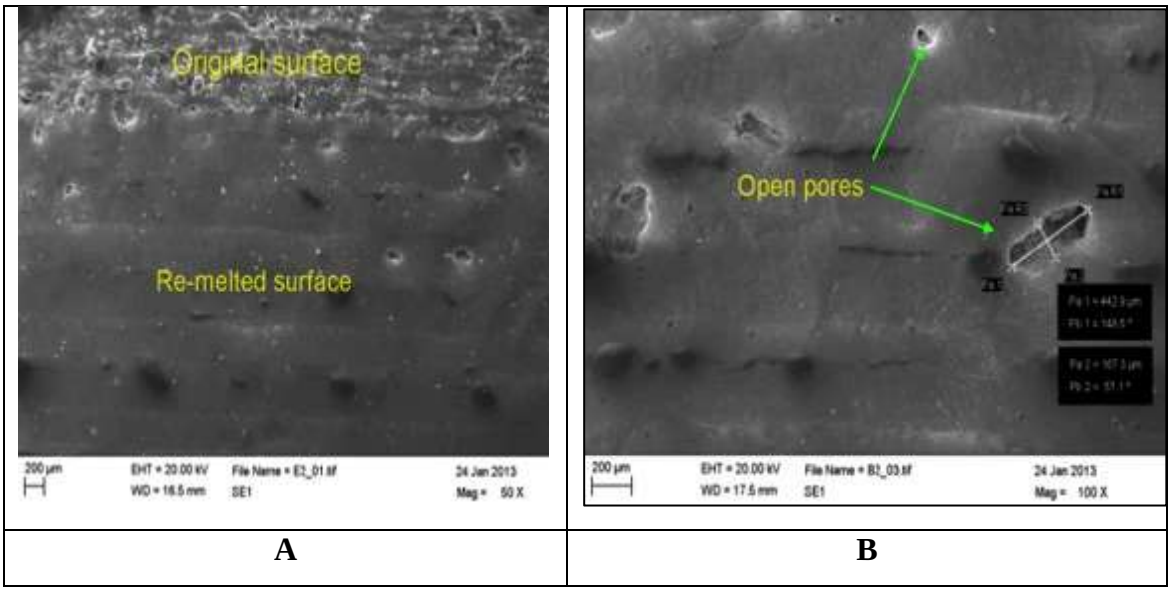

A **B**

Figure 7-23 : 2D micrograph obtained to demonstrate the surface before and after re-melting.

The results also demonstrated more information about the level of energy density required for re-melting as noted in the above paragraph. To obtain successful re-melting results, the level of laser energy density has to be more than 1200J/cm^2 in order to overcome the porosity issue, as shown in **Figure 7-23-B.** Also the parts have to be fully shielded with argon gas flow. The selection of gas flow rate needs to protect the melt pool against oxidation. A reduction of gas flow will increase the presence of the oxide layer, whereas increasing the gas flow rate too much can affect the solidification of the melt pool. The next experiment focused on employing the 'shielding' method, with a level of argon flow 4L/min. This level of gas flow was expected to be good enough to protect the surface against oxidation and cost effect.

7.2.1.3 Effect of laser power and scan speed on surface finish

7.2.1.3.1 Experimental aim and procedure

The aims of this trial were to set the optimum boundary of re-melting parameters such as laser power and scan speed and also to understand the influence of these parameters on establishing good surface quality, by reduction of the primary surface roughness. The depth of re-melting and the energy absorbed during the process are important, due to their impact on the final surface profile during the solidification time.
For this trial, 25 flat samples were carefully made employing the SLM 125 at De Montfort University; for more information see section **7.2.1.2.1**. The selected samples were mounted horizontally for the re-melting process.

The re-melting procedure was again carried out on the RECLAIM laser cladding machine at MTC**.** The factors related to this process such as spot size diameter and environmental factors were kept constant throughout this experiment. The spot size diameter was set at 0.8 to 1mm by adjustment of the stand-off distance between the lens and the substrate which was approximately 128mm (**see Figure 7-17**). The 'full shielding' gas flow method was used at 4 l/min in order to protect the samples against oxidation. The overlapping factor is recommended to be 50% for good results[94] and this value was used. The determination of hatch spacing and laser density was based on the following formulae:

- Scanning factor = (1 – overlapping factor). Equation 7-2
- Hatching spacing = scanning factor * spot size. Equation 7-3
- Laser density = laser power / scan speed * spot size. Equation 7-4

According to the above formulas, the resulting of hatching spacing ranges from 400 to 500 micron, from the selection of 50% overlapping factor and a beam diameter spot size of approximately 0.8 to 1mm on the samples' surface.

The process was carried out based on the following steps:

- The laser power starts by set up the laser power at 50% and elevated to 90%.
- The speed was started by 200 mm/min and increased to 600 mm/min.

Other factors such as distance between the lens and substrate, focal length of lens and beam diameter at lens were kept constant at the values shown:

- Distance between the laser lens and substrate: (128) mm
- The focal length of lens: 120 mm
- Beam diameter at lens: 16 mm

7.2.1.3.2 Scanning strategy

The scanning strategy is another factor that has an important effect on the results of the process. Thus, a grid scanning method was used for this experiment to re-melt the top of the built surfaces after placing them horizontally on the substrate.

Figure 7-24 below shows the strategy, which features bi-directional scan tracks performed first in Y-direction (i.e., perpendicular to the part build direction) and then turned by 90 degrees to do the same process in the X- direction.

In this study the scanning strategy method was kept constant.

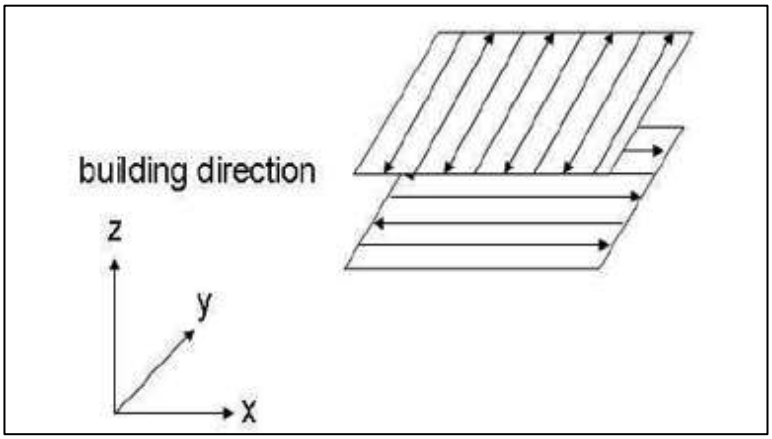

Figure 7-24: Grid scanning method.

The results obtained from this experiment will present the percentage improvement of surface roughness as interaction results associated with both laser power and scan speed. They will also demonstrate that the process window for re-melting in the next steps.

7.2.1.3.3 Experimental results and discussion

7.2.1.3.3.1 Surface topography

Generally, recognizing the visual effects of physical properties of the metal surface during laser re-melting is quite complicated and variable due to variation of laser parameters and the environmental conditions. [180] In practice, the results of **Figure 7-25** demonstrated different melting of a metal texture caused by different energy of the laser, tends to produce a series of mark tracks on the melted areas. The laser track end up reacting with oxygen found readily in the environment to form a dark marks on the top of surfaces which are clear on all samples. It is possible to say that, the degree of visual quality of the created surface is simply improved through the effect of laser energy to generate melting area, which is subsequently back solid in order to yield a mew surface texture (more smooth).

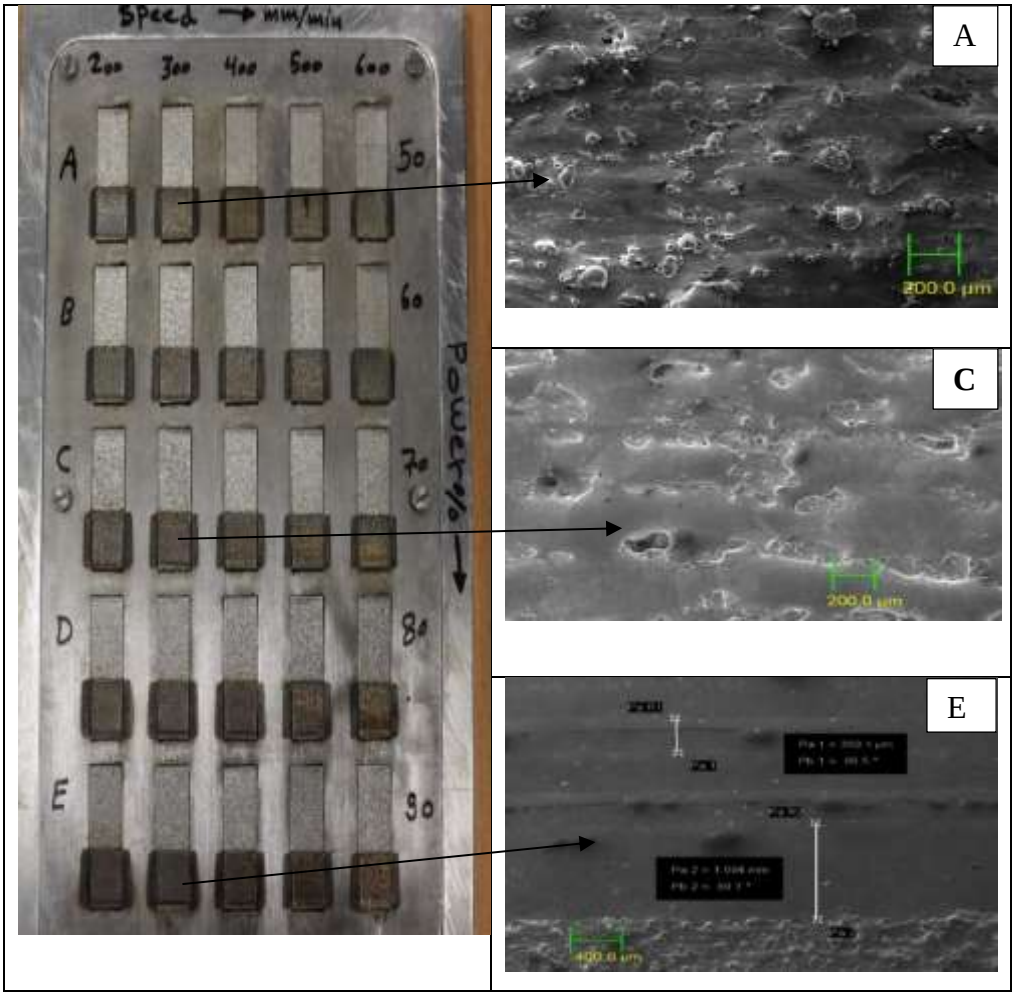

Figure 7-25: Results of laser parameter adjustment for re-melting, at different powers and speeds.

The results illustrated in **Figure 7-25** show some dark points and a centre line formed due to the high energy density absorbed during the process. It is worth mentioning that the parts showed a significant improvement of surface roughness results at high power (90%) and speeds from medium to high, but some areas demonstrated small balls and centre lines, see group (E), because of the non-uniform cooling of the melted zones caused by the non-uniform laser beam profile, which is concentrated in the middle of the re-melted track, see **Figure 7-18**.

On the other hand, partial re-melting is encountered with insufficient of energy density, due to the reduction of laser power leading to areas of partially re-melted and inhomogeneous surface texture. These areas present some defects such as open pores and balls see **Figure 7-25**C.

7.2.1.3.3.2 Surface roughness

The results of using lower laser power and time (high speed) which causes lower energy density, leads to a completely different effect, whereby the metal fails to melt and black marks are present on the surface. These marks, commonly referred to as black metal oxide, are spread over the surface. The black film is formed in heat affected zone, when the laser passes over the samples, but it does not affect the surface roughness of the material as shown in **Figure 7-25,** group A and partially in the right of group B at a different speed. Thus, it is possible to say that when the laser power is relatively low, no major effect on roughness may be achieved. This is because there will be no interaction as no melting occurs at low energy density. In most cases, the roughness values under low laser power are normally comparable to values of the untreated surface which has not yet undergone melting.

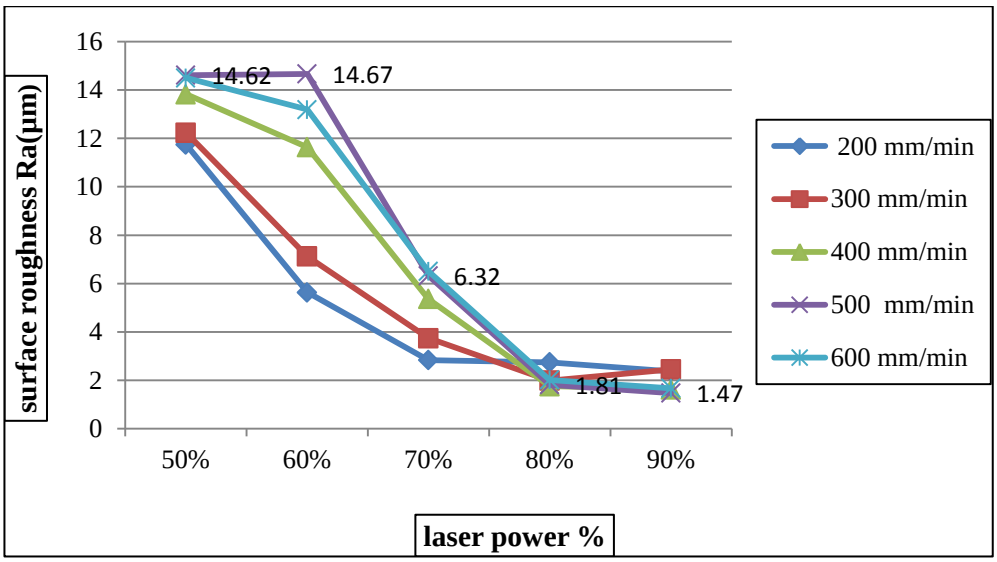

Figure 7-26: Surface roughness results with different speed and laser power.

Conversely, according to investigations and research performed recently, the roughness of a material can increase with an increase in irradiance. Irradiance simply refers to laser power per unit area. Most experiments that tried to increase the exposure time of the laser beam caused elevated temperatures on the surface of the materials, but with reduced cooling rates. [181] In such situations, the roughness of material surfaces can be increased as a result of ablation on the material surface. Regardless of exposure time, most researchers, after undertaking several experiments were able to establish a strong correlation between energy and roughness. It has been suggested that a linear increase in roughness is realized in cases of higher energy, due to metal vaporization. [180, 181] With this in mind, it is possible to explain the existence of a strong correlation between roughness increase/reduction and energy.

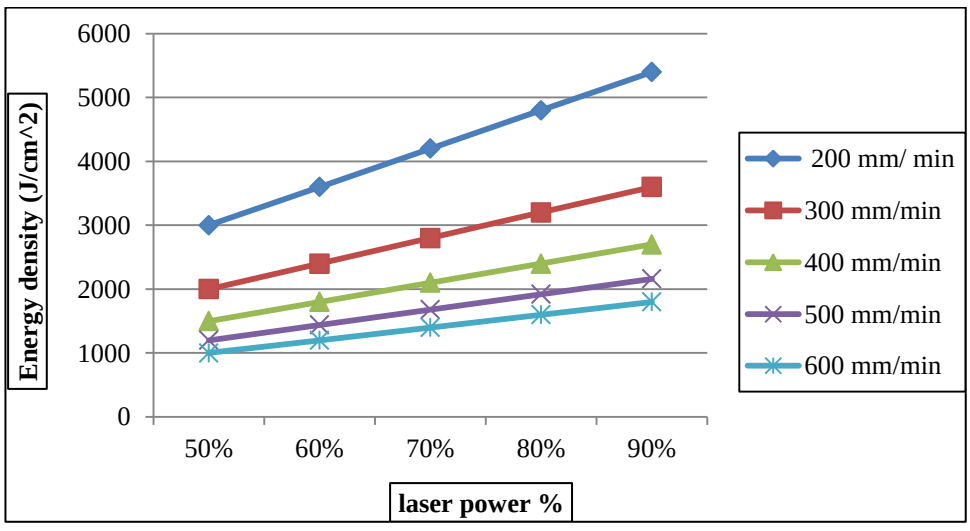

Figure 7-27: Energy density as a result of laser power and scan speed.

As results obtained in **Figure 7-26** show, low energy density has no melting effect on the surfaces. With the mid-level energy densities, a uniform melting on the metal surface can be achieved, but combining high energy and high residence time (low speed) has been showed as not the best method for improving roughness of surface due to the high thermal gradients.

Also the results shown in the above **Figure 7-26** indicate a coherence of the expected results; the reductions of surface roughness values are associated with the amount of absorbed energy. The sufficient values of energy density can be significant for re-melting process. This is relevant to mass transferee phase ("the thermal gradient in the melt pool") leading to change the peaks and valleys and generate new texture. [126] The best surface roughness (*Ra*) that was been obtained ~1.50μm, was between two different amounts of laser density, from 1800 to 2800 J/cm^2 as a result of laser power ranges from 160 to180Watt and scan speed ranges 400 to 500mm/min. Thus, in the next trial, the level of power was set at 90%, in order to detect the effect of hatch spacing on the quality of the surface at various scan speeds. The test focused on changing the laser density by controlling the feed rate at different hatch spacing, whereas other parameters such as focus distance, argon flow and beam diameter at the substrate were kept constant as noted in the previous experiment.

.

7.2.1.4 The effect of hatch spacing on the quality of the surface

7.2.1.4.1 Experimental aim and procedure

During the re-melting trials, the results showed surface quality is proportional to laser energy density whereas, the main aim of this trial was to check the effect of hatch spacing on the quality of the re-melted surface in order to find out the boundary level of hatch spacing for a good surface finish.

To determine the effect of hatch spacing, twelve samples were made using the same method as the previous samples and mounted horizontally for the re-melting process as described in section **7.1.1**.

The laser power was set at 90% of the total power of 200Watt. The other parameters were set as follows;

- Scan speed: varies (400,500,600,700)mm/min
- Hatch spacing: varies from (500,600,700) micron
- Distance from laser lens to the work piece: 128mm
- Shielding argon gas: approximately 4 L/ min
- The focal length of lens: 120 mm

7.2.1.4.2 Experiment results and discussion

The top surfaces of parts manufactured by SLM and without further exposure to any surface treatment (e.g. re-melting) are quite rough as compared with those obtained after re-melting as can be seen in **Figure 7-28**. The amounts of improvement were highly dependent on hatch spacing.

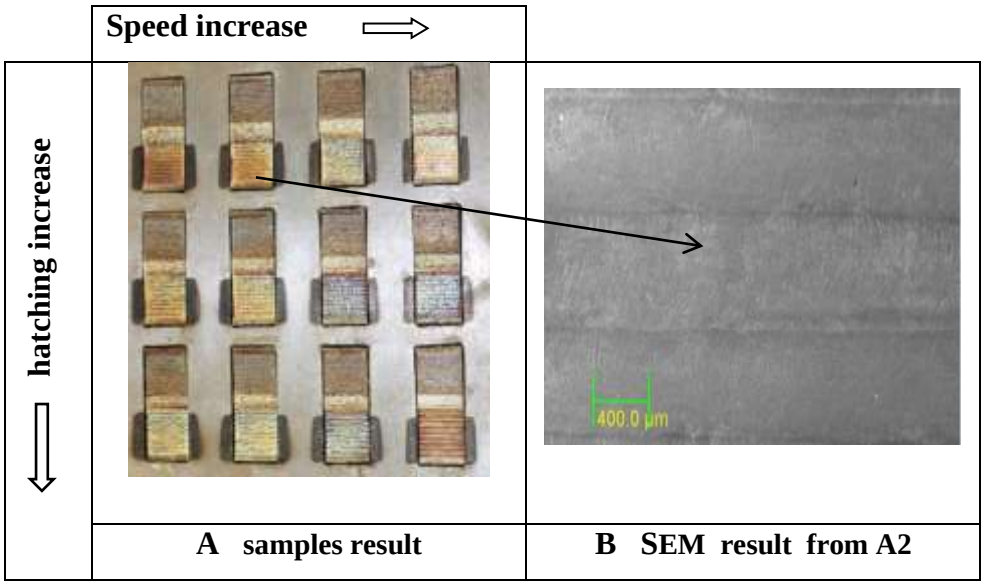

Figure 7-28 : Micrograph results realized after re-melting.

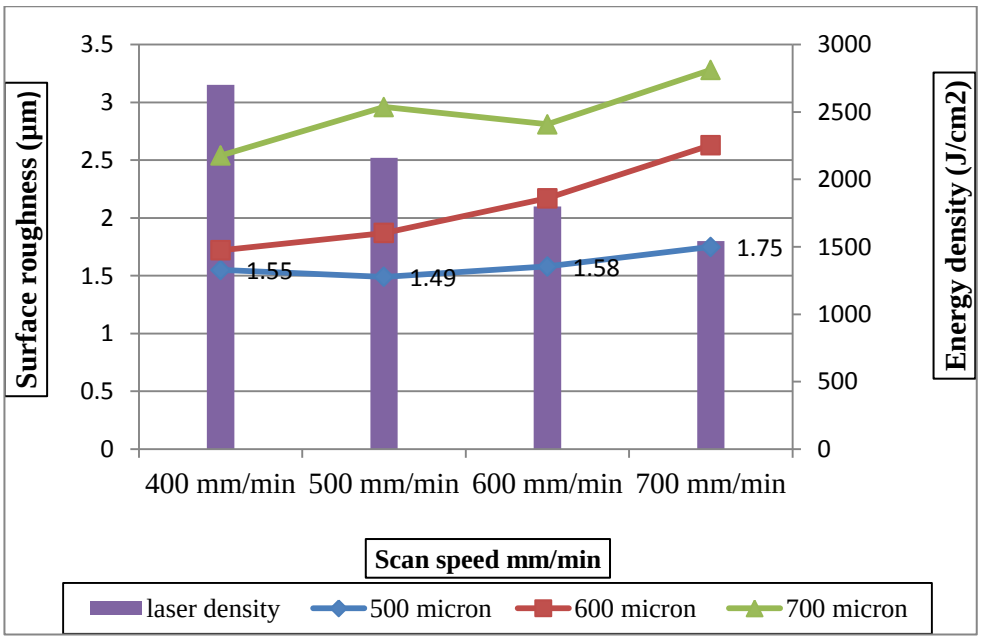

Figure 7-29: Surface roughness as a result of hatch spacing and energy density.

Figure 7-29 demonstrates that the reduction of surface roughness was highly influenced by hatch spacing, and also by laser energy density, due to the variation scan speed. However, the significant improvement of surface roughness, to a *Ra* of approximately 1.50µm, was achieved with 50% overlapping combined with a medium scan speed during the re-melting process. However, the material surface flatness might be declined. This might be caused by an elevated point of melted material and rapid solidified after laser beam moving. Overall, the best surface roughness achieved in this experiment was with greater than 50% overlapping, together with a laser density ranging between 1800 and 2160 j/cm.^{2} as a result of 90% power and 500 to 600mm/min scan speed.

Also, the results demonstrated some waviness being created, which tends to worsen the texture of the re-melted surface, specifically with those samples that had been re-melted with insufficient percentage of overlapping (high hatch spacing). The waviness is initiated in the middle of the re-melting track and appears as balls or a dark Gray centre line. These results were caused by the difference in surface temperature between the solidifying zones of the laser track beam and the main surface body, due to the laser beam concentration. For more information see **Figure 7-18**.

Thus, to overcome these problems (centre line and waviness) and generate surface textures of re-melted surfaces that are free from defects, the design of the process parameters has to counteract the external shear force during the solidification time. This can only be achieved by reducing the thermal gradients of the laser beam centre by

inclining the laser beam angle with respect to the surface being re-melted, allowing a more regular melting zone to be generated.

In this case, the laser power during the post treatment process has to be higher because of the angle effect.

This method (re-melting with angle) can facilitate achieving a flatter, smoother and more regular surface of the re-melted area of the metal parts as shown in the next experiment.

7.2.1.5 The effect of re-melting angle on the quality of the re-melted surface

7.2.1.5.1 Aim and procedure

The aim of this trial was to assess the effect of re-melting angle on the quality of the re-melted surface by reducing the effect of the higher laser density in the centre of the re-melting track. A secondary aim was to determine the best values of re-melting angle to provide sufficient energy density for surface treatment as can be seen in **Figure 7-30**.

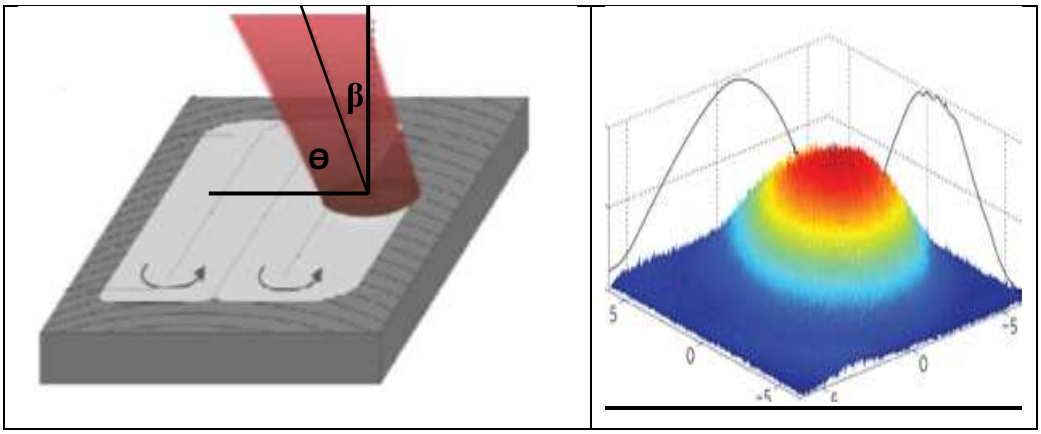

Figure 7-30 : Angle of re-melted track of on the left and the beam profile on the right.

The parameters of this experiment were chosen according to the best results obtained in the previous trials see (**sections 7.2.1.3** and **7.2.1.4**). The parameters used were as shown in the following points.

- Laser power: varies between (90% and 100%)
- Re-melting angle (ϴ): varied between (60, 70, 80) degree.
- scan speed: 500 mm/min
- Hatch spacing: 500 micron
- Distance from laser lens to the work piece: 128mm

- Shield argon gas: approximately 4 litres per min
- The focal length of lens: 120 mm
- Beam diameter at lens: 16 mm
- Beam diameter at substrate: approximately 1 mm

This experiment was pending, due to several aspects related to (RECLAIM machine) as followed

- The laser head is limited to move in the Z direction only
- The movement of the platform is limited to the X and Y directions
- The distance between the cladding head and the substrate is not large enough for the process (5mm). Thus, it was not possible to incline the substrate and generate the process.
- The maximum laser power of machine (200 watt) is not enough to compensate for the angle effect.

However, to run this trial a proper machine is required, which it could be not available recently.

Finally the previous two trial sections (**7.2.1.3& 7.2.1.4**) were used to determine the boundary of the optimum parameters for laser re-melting as well as to establish the effect of these parameters on the surface topography change.

The next experiment (Re-melting trials) focused on finding the best parameters boundary by conducting a full factorial experimental program to devise and explore the effect of the parameters on the response value *Ra* of the parts and optimize the parameters based on a statistical study.

7.2.1.6 Optimizing laser parameters for re-melting

The experiment was carried out with a set of parameters that were defined based on the previous experimental results sections (**7.2.1.3** and **7.2.1.4**) The three important parameters were selected that have a major effect on improving surface quality as shown on **Table 7:1**.

7.2.1.6.1 Experimental Aim and procedure

The aim of this experiment was to optimise the parameters of speed, power and hatch spacing as they have an important effect on improvement of smoothness (*Ra* value) in SLM components during re-melting process, as shown in the preceding trials. The process was carried out by designing a classical approach of a full 3 against 3 factorial experimental set up as shown in the following table

(A) Power (watt)	**(B) Scan speed (Mm/min)**	**(C) Hatch spacing (micron)**		
		400 (0)	500 (1)	600 (2)
160 (0)	400 (0)	000	001	002
160 (0)	500 (1)	010	011	012
160 (0)	600 (2)	020	021	022
180 (1)	400 (0)	100	101	102
180 (1)	500 (1)	110	111	112
180 (1)	600 (2)	120	121	122
200 (2)	400 (0)	220	201	202
200 (2)	500 (1)	210	211	212
200 (2)	600 (2)	220	221	222

Table 7:1: The three levels of the full factorial design.

The samples prepared for this experiment were made as noted in section (**6.1**). Also the samples came with an initial surface roughness of 10 ±15% microns due to the build angle affects, which was constant in this experiment and equalled 75º. The experiment was carried out by using the RECLAIM machine at MTC Coventry as noted in the previous trials. The experiment was completed with different Power, Speed and Hatch Spacing as showed in **Table 7:1**. Each setup was replicated 5 times to find out the results for the response value (*Ra*).

Other factors were kept constant as follows

- Focus distance from laser lens to the work piece: 128mm
- Shielding argon gas: approximately 4 litres per min
- The focal length of lens: 120 mm
- Beam diameter at lens: 16 mm
- Beam diameter at the substrate: approximately 1mm
- Scanning method as noted in section (**7.2.1.3.2**)

7.2.1.6.2 Result and discussion

The figure below shows the re-melting results obtained by different amounts of laser energy. The newly created surfaces demonstrated significant improvement of surface finish (response value (*Ra*)) as showed in **Table 7:2**, compared with the initial surfaces. Also, different visual qualities were apparent on all samples due to the effect of laser energy density and the variation of hatch spacing to generate new textures during the re-melting process.

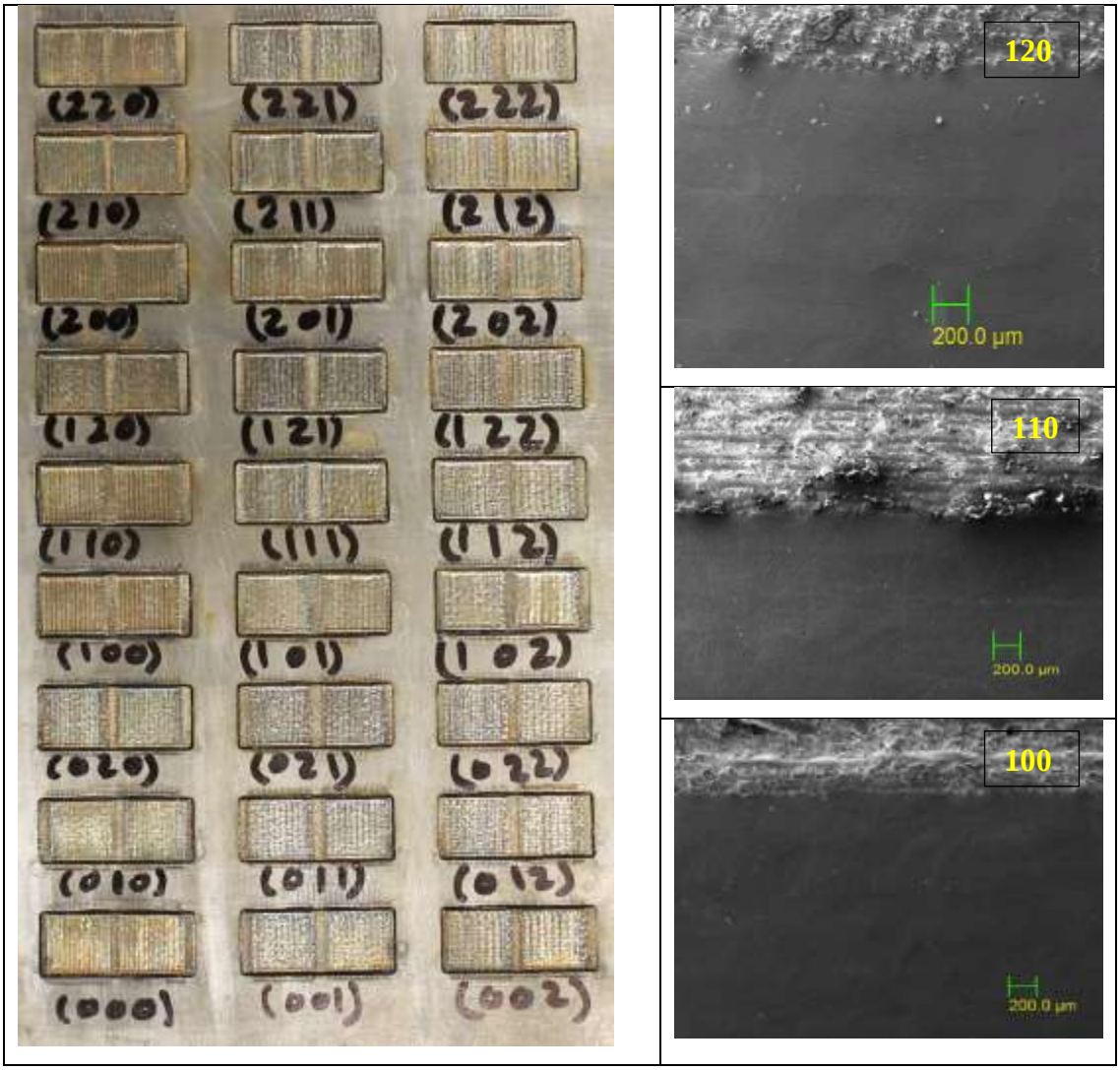

Figure 7-31: Micrograph results realized after re-melting for a full factorial experiment.

The following table shows the data for the experiment, the results for variation of Speed, Power and Hatch Spacing and the effect of these variations on the response value (*Ra*). Calculations were made to find the average result for the improvement

of roughness. Furthermore, the errors were determined and tabulated as shown in **Table 7:2**.

(A) Power (watt)	(B) Scan speed (Mm/min)	(C) Hatch spacing (micron)					
		400 (0)		500 (1)		600 (2)	
		Ra (µm)	Error	Ra (µm)	Error	Ra (µm)	Error
160 (0)	400 (0)	1.54	0.093	1.79	0.084	2.11	0.148
160 (0)	500 (1)	1.68	0.083	1.94	0.112	2.21	0.161
160 (0)	600 (2)	1.71	0.156	2.01	0.119	2.21	0.118
180 (1)	400 (0)	1.41	0.062	1.61	0.089	1.97	.0164
180 (1)	500 (1)	1.44	0.048	1.51	0.088	1.98	0.179
180 (1)	600 (2)	1.56	0.086	1.70	0.097	2.190	0.103
200 (2)	400 (0)	1.61	0.076	2.06	0.127	2.54	0.149
200 (2)	500 (1)	1.67	0.113	2.11	0.153	2.36	0.151
200 (2)	600 (2)	1.65	0.083	1.92	0.131	2.25	0.129

Table 7:2: The three levels of full factorial design with the average results of response factor results (Ra) and error.

As **Table 7:2** shows, the hatch spacing has more effect on the surface roughness. The roughness values for 5 trials were calculated to give an average of 1.414µm, which is the lowest response value (*Ra*) from all the results. This indicates that the above mentioned setting gives the maximum optimised smoothness for SLM components. The validity of this result is further proved by a very minor error of just 0.06% which supports the results strongly. The significant surface roughness results were achieved by a laser power of 180W, speed between 400 to 500 mm/min and hatch spacing of 400 microns (i.e. more than 50% overlapping) to give an energy density between 2160 to 2700 J/cm^2.

7.2.1.6.2.1 Statistical analysis and Model development (DOE)

Analysis was carried out on results of **Table 7:2** employing DOE software, in order to find out the multiple response regression of the experiment. The impact parameters are shown in **Table 7:3** below which was employed to write a model later on.

Factor	Name	Coefficients	P level
	Constant	1.681	1.4E-87
A	Laser power	0.059	0.0565
B	Scan speed	0.0763	0.0141
C	Hatch spacing	0.2744	5.7E-15
AB	Laser power*Scan speed	-0.0718	3.8E-05
AC	Laser power*Hatch spacing	0.0516	0.0026
BC	Scan speed*Hatch spacing	-0.0275	0.1039
ABC	Laser power*Hatch spacing*Scan speed	-0.0307	0.13729
AA	Laser power*Laser power	0.2546	3.6E-19
BB	Scan speed*Scan speed	0.0017	0.94419
CC	Hatch spacing*Hatch spacing	0.045	0.06039
AAB	Laser power*Laser power*Scan speed	-0.0715	0.01539
ABB	Laser power*Scan speed*Scan Speed	0.0035	0.90439
AAC	Laser power* Laser power* Hatch spacing	0.0283	0.33159
ACC	Laser power* Hatch spacing*Hatch spacing	-0.009	0.75739
BBC	Scan speed*Scan speed* Hatch spacing	0.0218	0.45399
BCC	Can Speed*Hatch spacing*Hatch spacing	0.0045	0.877
Standard Error = 0.130			
R^2 = 0.853			

Table 7:3: Results of multiple response regression based on full factorial design.

It is clear that the impact of parameters scan speed and hatch spacing indicate good confidence levels p=0.014 and $p=5.75*10^{-15}$ for linear impact, while laser power indicates significance at confidence level p=0.0565 with a positive coefficient of 0.059. Also, a Pareto diagram was plotted to demonstrate the impact of the factors' interactions.

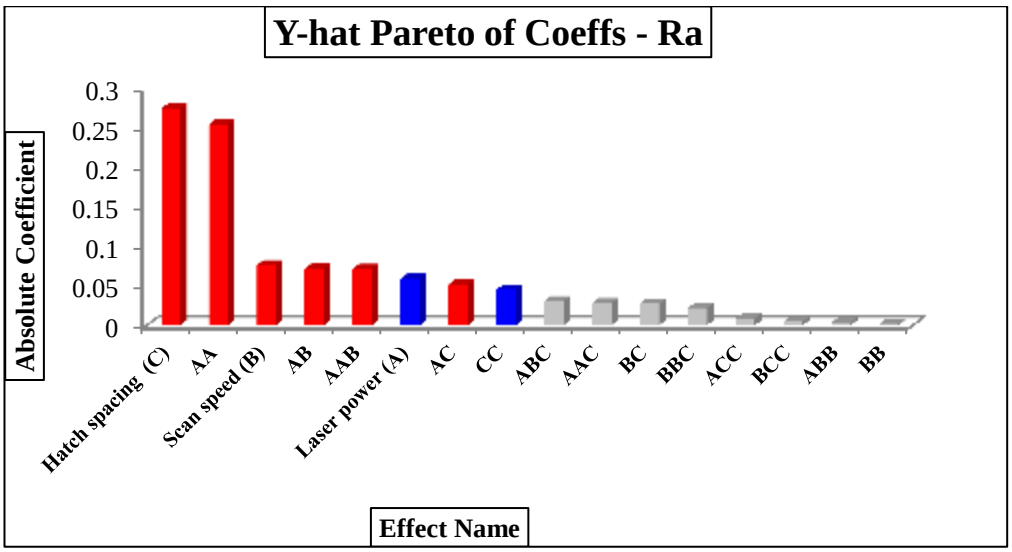

Figure 7-32: Y-hat Pareto diagram for Average Roughness- response variable.

The Pareto diagram, **Figure 7-32** compares graphically the individual impact of the factors and their interactions, indicating that the hatch spacing (C) and quadratic term of laser power*laser power (AA) have the highest impact on the average roughness *Ra*, with coefficients 0.274 and 0.255 accordingly. The next three factors, scanning speed (B), laser power*scan speed (AB), and the cubic term laser power*laser power*scan speed (AAB) on the diagram, have comparable impact in the range 0.071 to 0.076. Also the Pareto diagram shows that the impact of 3 next terns decreases: linear terms of laser power (A), laser power*hatch spacing (AC) and quadratic hatch spacing*hatch spacing (CC). All other terms have not acceptable coefficients as well as low confidence levels (p), see also **Table 7:3**.

The overall model can therefore be written based on the results obtained in **Table 7:3** which takes into account only factors with a good confidence level as shown below

$$\hat{Ra} = 1.682 + 0.059A + 0.076B + 0.274C - 0.072AB + 0.052AC - 0.255AA - 0.072AAB \quad \textbf{Equation 7-5}$$

Where A is Laser Power (watt), B is scanning speed (mm/min), C is hatch spacing (mm), Ra-hat is the predicted average roughness (μm) and the coefficients are various related to the factors as shown in **Table 7:4**.

factors	Coefficients	Dimensional units
Ra-hat		µm
constant	1.682	µm
A	0.059	µm/W
B	0.076	µm./(mm/min) $=10^{-3}$ min
C	0.274	µm/mm = ratio $x10^{-3}$
AB	0.072	µm/(W x mm/min) = 10^{-3} min/ W
AC	0.052	µm/(W x mm) = 10^{-3} / W
AA	0.255	µm/W^2
AAB	0.072	10^{-3} min/ W^2

Table 7:4 the dimensionality of coefficients in the equation 7-5.

The result of R-square is 0.853, which means that there are other factors that have an impact factor of approximately 15%, which still need to be overcome. The remaining factors could be the environment conditions or solidification time after re-melting. The validity of this model as shown in **Equation 7-5** and its limitations are illustrated in **Figure 7-33-A** which indicates good linear dependence between actual and predicted values *Ra*. On the other hand, **Figure 7-33-B** indicates that there is a non-random distribution of residuals in the range of high *Ra* values, where some other factors need to be included. However, the overall validity of model is R^2= 0.85, which is satisfactory for 3 factors.

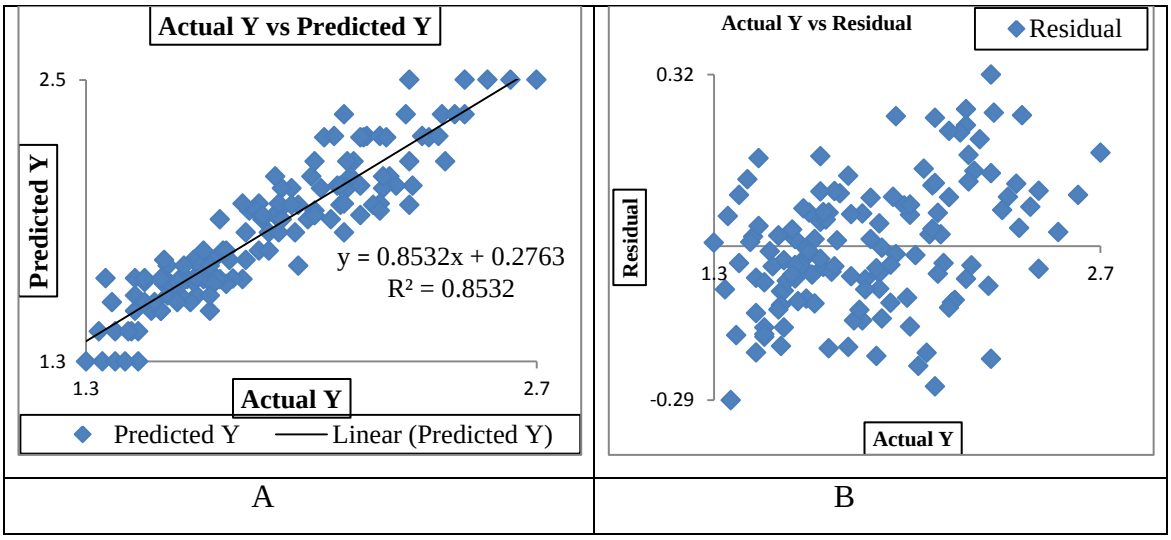

Figure 7-33: Shows the actual roughness against predicted roughness (A) and against residual (B).

7.2.1.6.2.2 Interacting parameters and surface roughness results

It has been made clear that there are interactions between the factors illustrated in the Pareto diagram of **Figure 7-32**. Also, the effect of these factors on the response factor (*Ra*) can be clarified in the followed graphs.

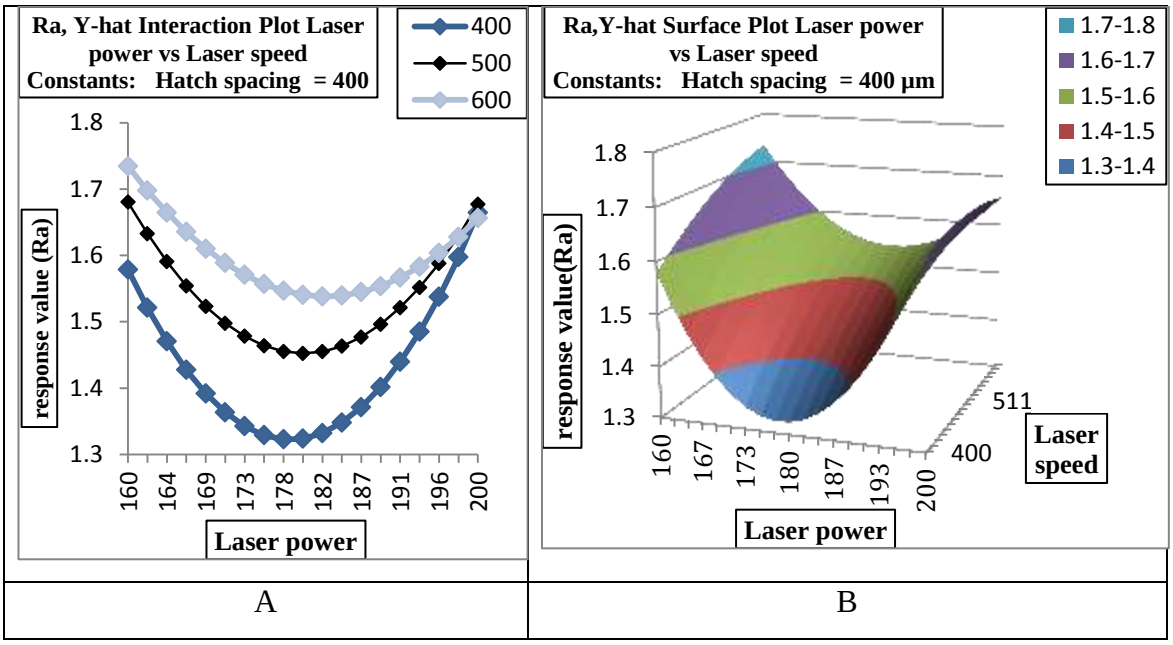

Figure 7-34: Response values of Ra. Y-hat Interaction plot (A)and Y-hat surface plot (B)of laser power varies scan speed at constant: Hatch spacing =0.4mm.

The above two predictive (Y- hat) graphs (**Figure 7-34**) show the variation of response value (*Ra*) with a constant hatch spacing of 400 microns and for varying speeds and power. The general trends shows that there is a drop in response value for all three speeds with an increase in power up to about 180W and then the response value increases in different patterns for the three different speeds.

In **Figure 7-34-A**, for 600 mm/min the initial response value is 1.73 µm at 160W and then it decreases constantly up to a value of 1.54 µm at about the power of 182W. Then there is a very slight increase of response value from 180W to 200W recorded at approximately 1.65 µm.

For 500 mm/min, the initial response value is 1.68 µm and then it decreases to 1.45 µm at a power of 178W. Followed by that is an increase in the response value with the increase in power, due to the elevated temperature.

For 400mm/min the initial response value is 1.58µm which was the lowest Initial response value for the three speeds used in the experiment. The response value

decreases with power to a very low value of 1.32µm at the power of 178W and this is by far the lowest response value determined from the whole experiment. The response value increases after this point with increase in power and was recorded at approximately 1.65µm as the Response value at 200W.

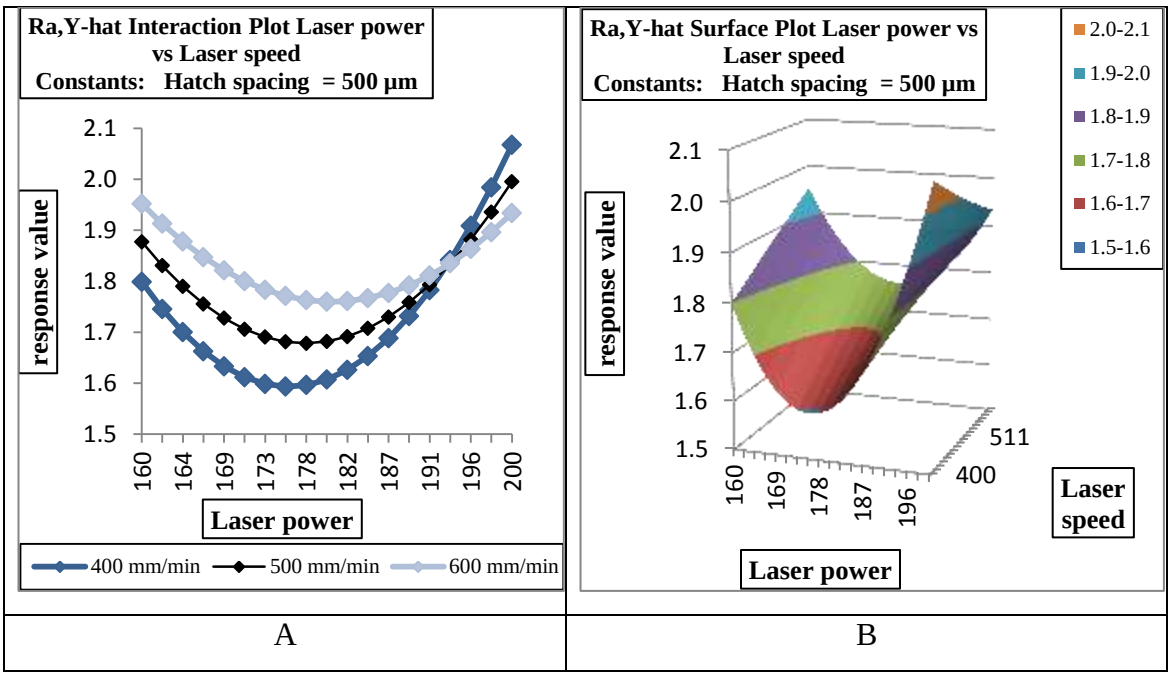

Figure 7-35: Response values of Ra. Y-hat Interaction plot(A)and Y-hat surface plot (B)of laser power varies scan speed at constant: Hatch spacing = 0.5mm.

The above two predictive (Y- hat) graphs **Figure 7-35** are drawn for a constant Hatch Spacing of 500 microns. The variation is between speed and power. The Y axis shows the response value from the results. The general information shows that the response factor (*Ra*) value is reduced for the three different speeds, connected with an increase in power input up to 175 W. Then the roughness values increase with power in the three different patterns.

In **Figure 7-35**-A, for the speed of 600 mm/min at an initial power of 160W the response value is 1.95µm. The general trend is that the response value (*Ra*) decreases with power until about 180W. And then it increases until 200W to a value of 1.93µm.

For the speed of 500mm/min the trend is the same although the response values were lower than that for the results of 600 mm/min speed. The initial response value was about 1.87µm at a power of 160 W and then it decreased until about 180W. Then it tends to increase after that power.

For the speed of 400 mm/min the roughness values were the lowest and the best result for this hatch spacing of 500 microns is shown in the graph above. The general trend was the same. The lowest *Ra* value was 1.59µm at about 175W.

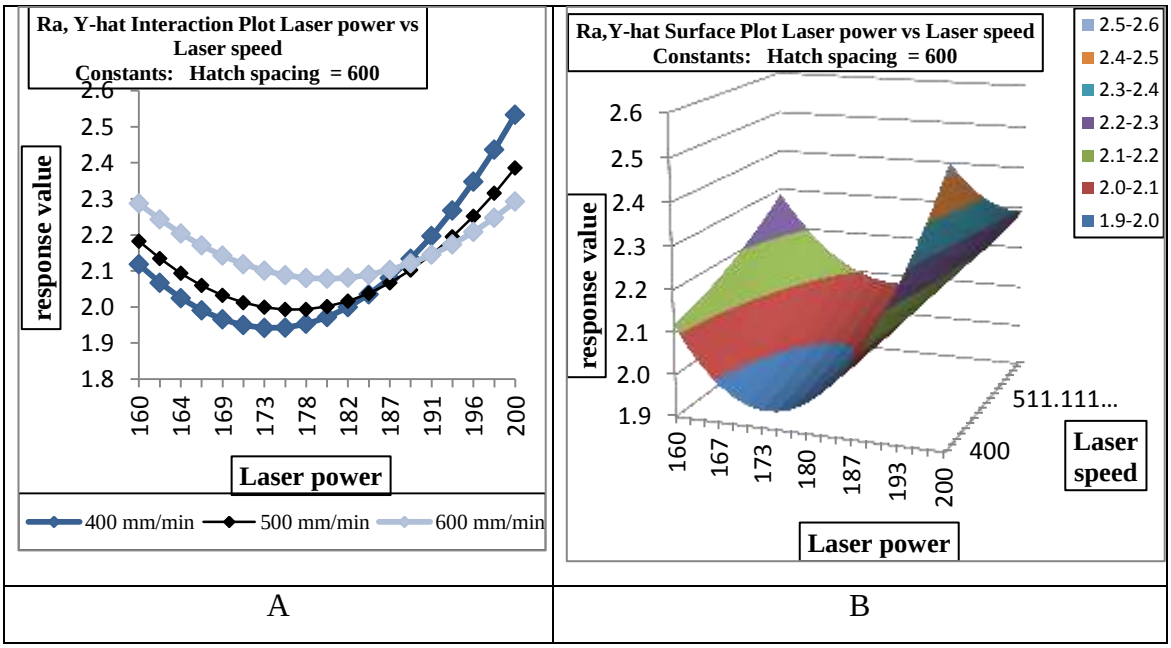

Figure 7-36: Response values of Ra. Y-hat Interaction plot(A) and Y-hat surface plot(B) of laser power varies scan speed at constant: Hatch spacing = 0.6mm.

The above two predictive (Y- hat) graphs **Figure 7-36** show the results for the hatch spacing of 600 microns for the variations of power and speed. The general trends show similar patterns as shown in the previous figures (hatch spacing 0.4 and 0.5mm) for the three speeds 400,500 and 600mm/min. The response value (*Ra*) decreases proportionally with the increase in laser power until 173W. After that the roughness rises with different response for the three patterns of speed, due to the elevated energy during the process.

In **Figure 7-36-A,** for 600mm/min the response value is about 2.3µm for the power of 160W. The response value decreases to 2.07µm for a power of about 180W. Then it increases again with the increase in power and for the power of 200W the response value is 2.29µm.

Looking at the speed of 500mm/min the initial response value is about 2.12µm for a power of 160W. The lowest response value is 1.992µm for a power of 176W. Then the response value increases with the power up to about 2.38µm where the power was 200W.

For 400 mm/min at a hatch spacing of 600 microns, the response value is 2.11 μm which is the lowest initial response value for all the speeds used in this experiment for the power of 160W. The response value decreases as the power increases up to 173W. After this point the response value increases again and at about 200W the response value is 2.53 μm

Furthermore, for all the samples, an increase of power decreases the surface roughness (*Ra*) with range between 170 to 185W and then it increases after that range. This is due to the amount of energy absorbed by the surface. The heat required for re-melting is of a certain value and up to this point the surface roughness improves but when the heat provided with extreme power (high energy density) is more than the required amount, the surface roughness increases.

7.2.1.6.2.3 Overall statistical results

Overall analysis of the experimental data shows that the hatch spacing has a major effect on the surface roughness in the linear region. The best results were obtained using laser power of 180W, hatch spacing 0.4mm and scan speed ranging between 400 to 500 mm/min. In each case, laser energy density was calculated according to **Equation7-1**, to give a range between 2160 to 2700 J/cm^2. The best average roughness of the response value is about Ra =1.4μm, obtained as the optimal smoothness and the validity of results comes with an error margin of 0.06 thereby strongly supporting the results, as shown in **Table 7:2**. The current study was limited to the effect of three factors (laser power, scan speed, hatch spacing), which gave about 90% of total variation. Further work will examine other factors that may have an impact on the results of the re-melting.

The next stage (**section 7.2.2**) of experiment focuses on implementing the best laser re-melting parameters in order to re-melt top surfaces, with different ranges of roughness (see **section 7.1**). Finally the efficiency of this technique (re-melting) to supress any dendrites connected with SLM components will be concluded.

7.2.2 Re-melting of inclined surfaces

7.2.2.1 Aim and procedure

The aim was to validate the optimal parameters of laser re-melting (see section**7.2.1.6.2.3**) and to realize the capacity of these parameters to eliminate any dendrite structures formed during SLM manufacture of parts and to overcome the porosity issue which is considered a major obstacle to achieving an acceptable surface finish.

The experiment was carried out using RECLAIM machine as with the previous described. The process parameters were determined and chosen according the optimized previous setup; see results of (section **7.2.1.6.2.3**). The parts' surface roughness was compared with the initial (as fabricated) surfaces.

In this experiment, laser re-melting was applied after the SLM process was completed, on the top surface of inclined samples. The samples had different surface roughness, see section **7.1.1**. The samples were held horizontally on the substrate and the parameters used for re-melting were as follows:

- Laser power: 90% from total power of 200 watt
- Scan speed: 500mm/min
- Distance between the lens of laser source and the substrate: 128mm
- Shielding argon gas: 4 L/ min
- The focal length of lens: 120 mm
- Beam diameter at lens: 16 mm
- Hatch spacing: 400 micron.
- Beam spot size: approximately 1mm

After completion of the process (re-melting) and inspection, the samples were assessed for surface roughness, topography and porosity.

7.2.2.2 Results and discussion

7.2.2.2.1 Surface roughness

Quality of the material surface has been one area of concentration by most studies as it has always been a problematical issue when it comes to completing fabrication of components. The metal surfaces of the parts obtained from SLM or other AM techniques without any post-processing are quite rough. The most available solutions to this drawback involve removing the part having the problem from the platform and

exposures to normal mechanical post-processing such as hand polishing, shot blasting, grate blasting or any other modern machining like CNC and hybrid machine centre etc. In these trials, laser re-melting was shown to be able to eliminate dendrites that can arise during construction of SLM parts and to make the surfaces more flat and defect free as shown in **Figure 7-37**

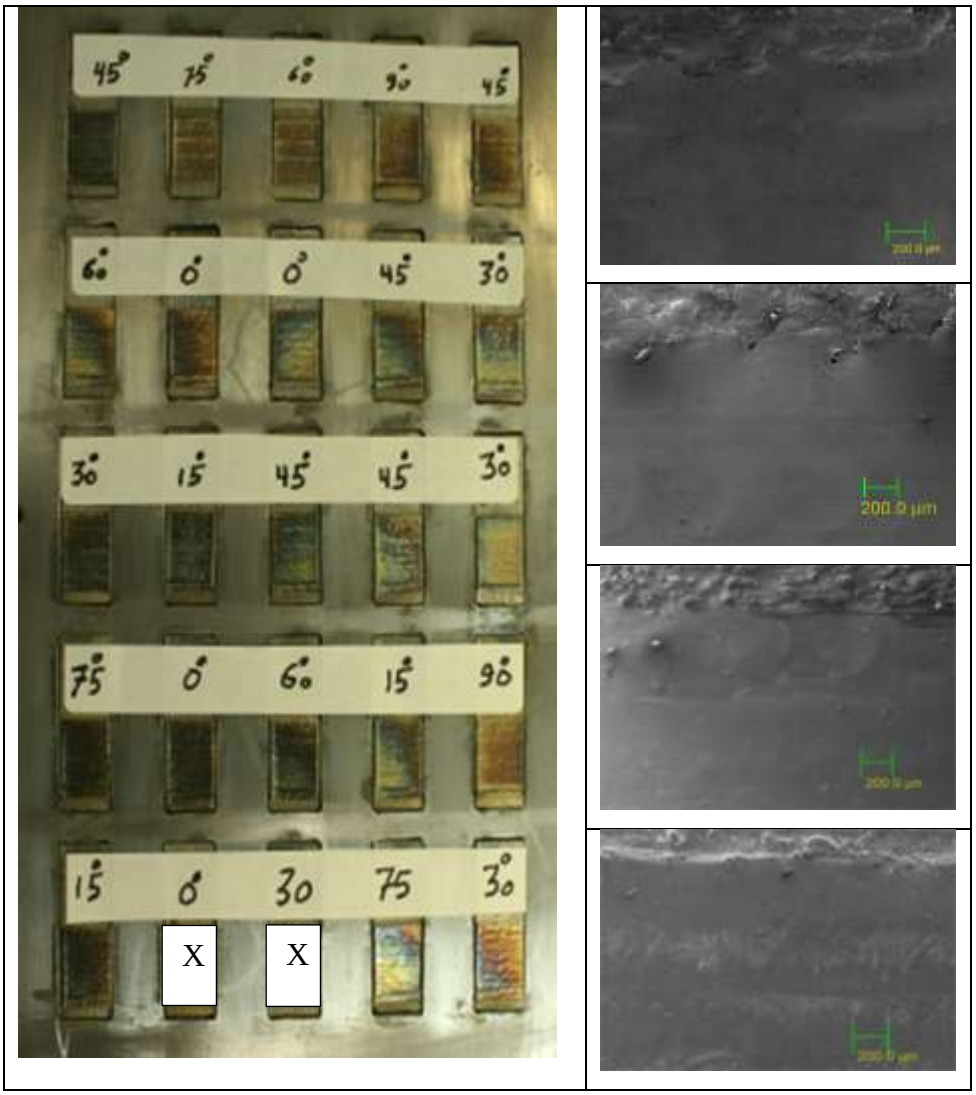

Figure 7-37: Micrograph results of re-melted samples built at different angles.

In this experiment, after the top surfaces of the SLM parts were exposed to laser re-melting, a comparison of surface roughness were measured using a roughness tester instrument (stylus profilometer Sj400 at DMU) to obtain quantitative results by determining the amplitude of the following parameters: the average roughness (*Ra*), the mean square of the average roughness (*Rq*) and the average maximum of peak to valley of the profile (*Rz*). Surface roughness results after SLM (as fabricated) were determined

and demonstrated in **Figure 7-5, Figure 7-6** and **Figure 7-7**. Also the results after LR were measured and are shown in **Figure 7-38, Figure 7-39** and **Figure 7-40**.

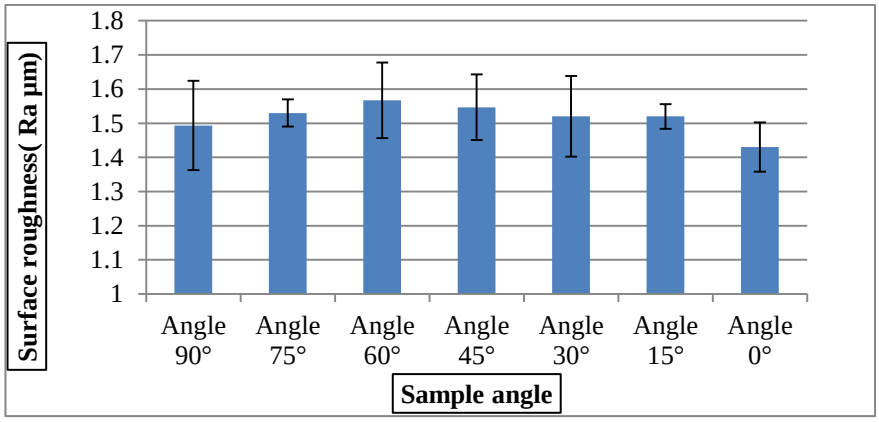

Figure 7-38: Average roughness (Ra) with error realized on all samples after LR.

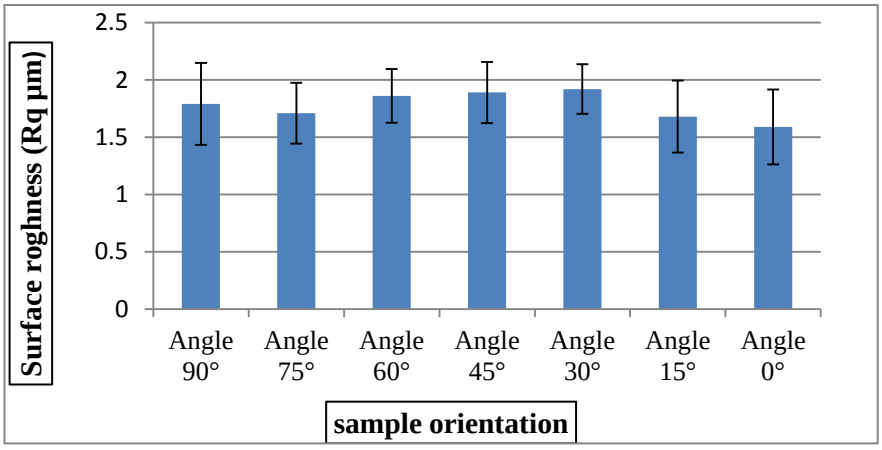

Figure 7-39: Mean square of average roughness (Rq) with error realized on all samples after LR.

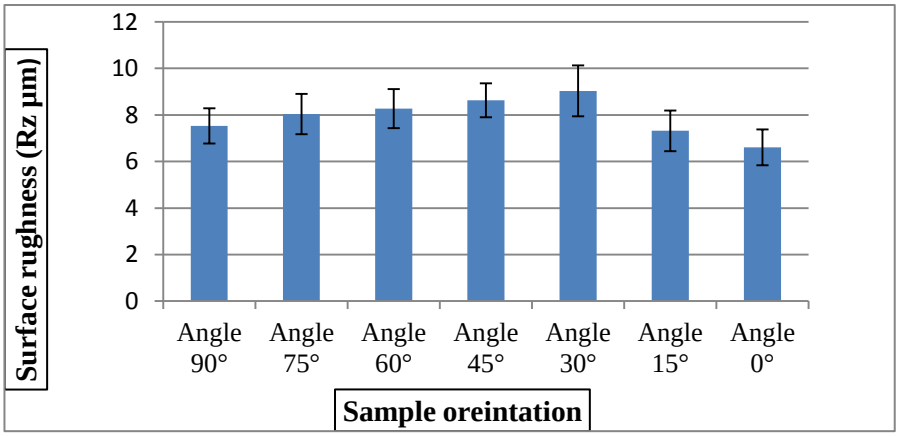

Figure 7-40: Average maximum of peak to valley (Rz) with error realized on all samples after LR.

The texture of the metal surface produced after (SLM), and therefore exposed to laser re-melting showed good improvement. Thus, it is possible to say that re-melting provides a unique ability to supress any degradation in surface texture on SLM layer manufactured parts, by re-melting a specific thin layer on the top surface and loop back to solidify and create a new surface structure. It is worth mentioning that the characteristics of the new microstructure depend on the energy density absorbed, overlapping factor and the environmental conditions during the process. The comparison results in **Figure 7-41**and **Table 7:5** show the amount of improvement.

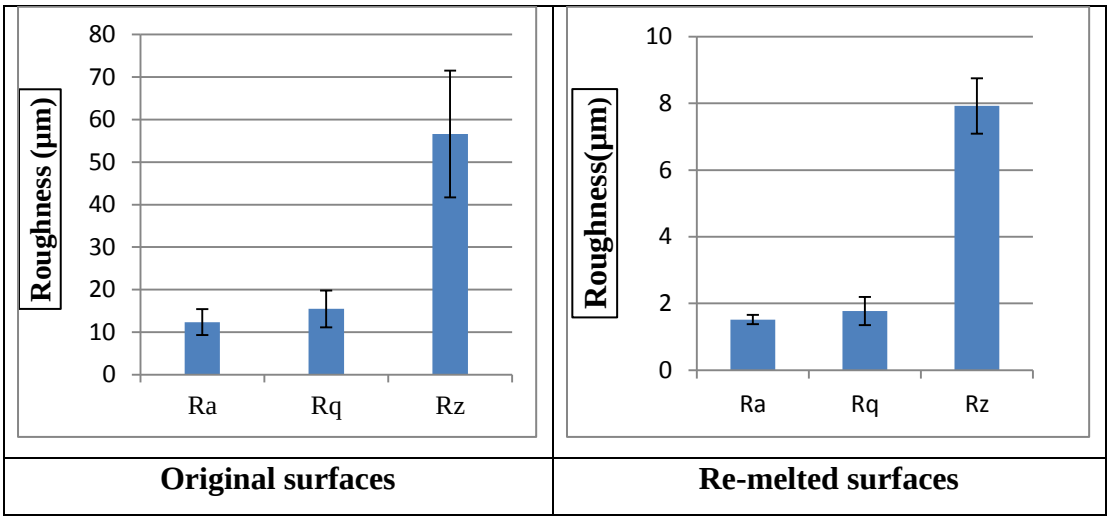

Figure 7-41: Comparison results of the amplitude of surface parameters.

Unit	Original surface	Re-melted surface	Improvement (%)
Ra (µm)	12.347	1.507	87.7
Rq (µm)	15.456	1.777	88.5
Rz (µm)	56.621	7.919	86.0

Table 7:5: Comparison results of the amplitude of surface parameters with percent improvement.

Figure 7-42 below illustrates the comparison of dependence of re-melted Ra and the initial (*Ra*) on angle of build.

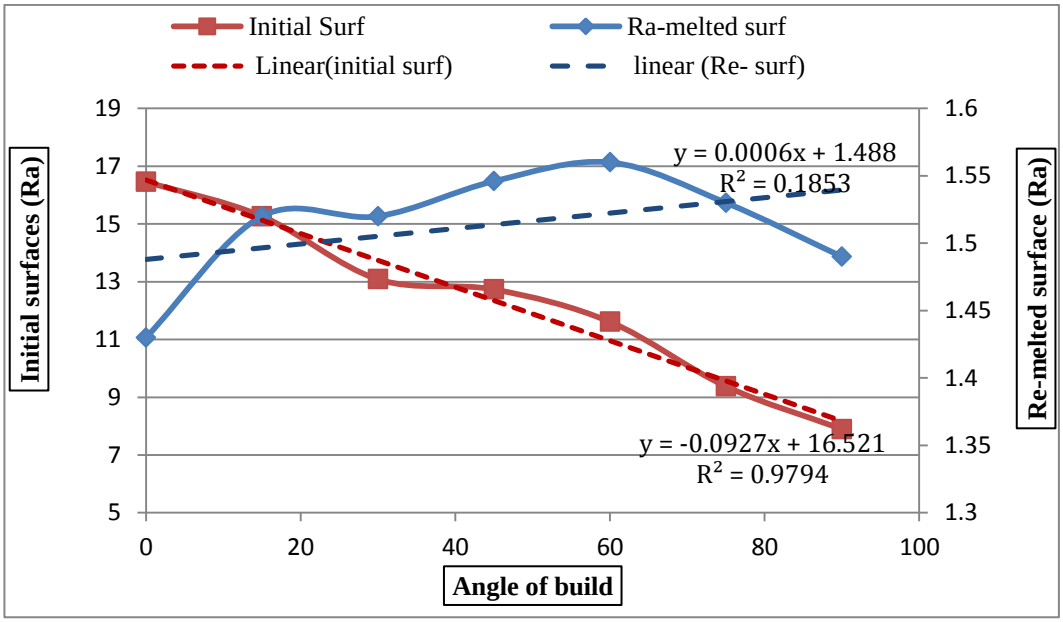

Figure 7-42: Dependence of re-melted Ra and initial Ra on angle of build.

It can clearly be seen that the initial roughness (*Ra*, red) decreases with the increase of angle of build (A), while the average roughness after re-melting Ra has a tendency to increase with the increase of angle of build (A), blue colour and trend. This can be due to the number of pores located near to the wall side surface of the parts, which increase with an increase of build angle; for more information see **Figure 7-12**. The major pores are located just under the external surface of the built parts.

In the general, the top surface of the material obtained from SLM but not passed through laser re-melting was rougher as compared with those obtained after being re-melted. The average roughness (*Ra*) of SLM inclined surfaces as built was approximately 12.4µm with a standard deviation of 3µm, whereas the recorded average roughness after re-melting was approximately 1.5µm with a standard deviation of 0.12µm. This means that laser re-melting has a capacity to reduce surface roughness (*Ra*) values from 12.4 to 1.5µm with a total improvement of approximately 88%. In addition, *Rq* and *Rz* values also have significant improvement as shown in **Table 7:5.** Some sectioned samples were observed by 3D Zeta microscope to verify that, as shown in **Figure 7-43, Figure 7-44 and Figure 7-45**.

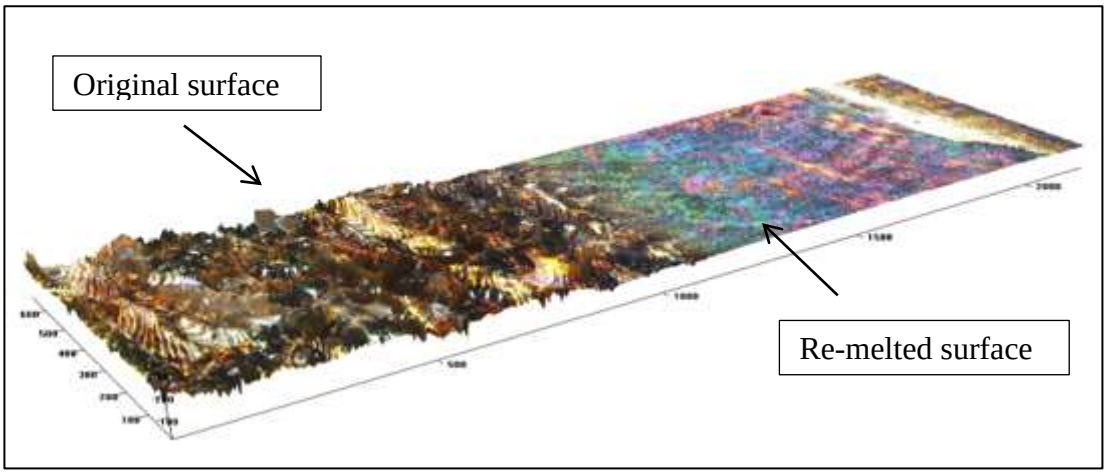

Figure 7-43 : Micrograph of 3D Zeta microscope was used to view how the surface becomes after re-melting obtained on a surface built at 45º.

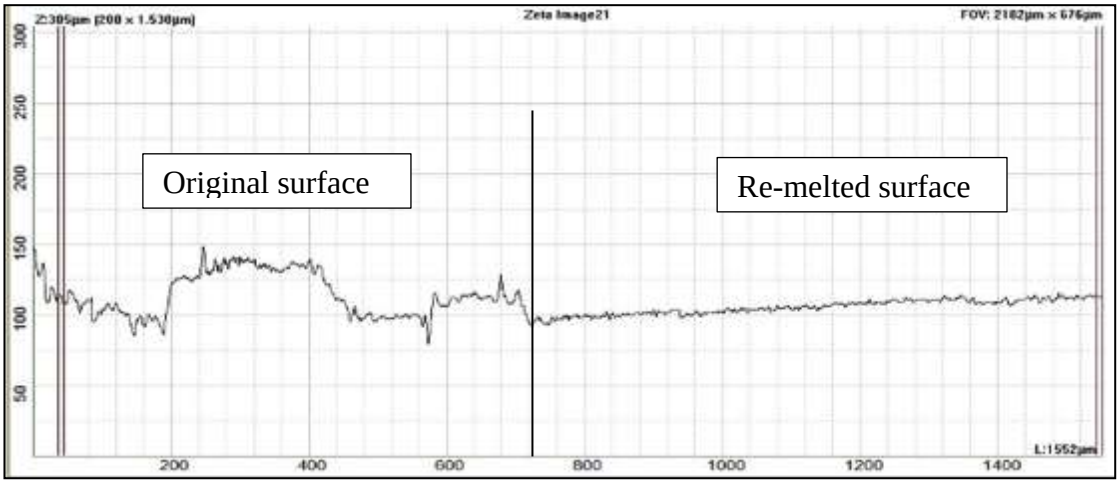

Figure 7-44: Roughness profile before and after re-melting realized on surface 45.º

Unit	***Ra***	***Rq***	***Rp***	***Rz***
Original surfaces	13.40	16.0	31.09	55.69
Re-melted surface	1.289	1.549	3.423	6.687

Table 7:6 : Amplitude parameters realized on a surface built at 45°by Zeta (3D) microscope.

As a result a very good improvement has been observed and recorded, realized on all inclined surfaces by implementing the optimum laser parameters obtained in the preceding trials.

7.2.2.2.2 Surface topography

The surface topography associated with the re-melting process embodies the reliability of technique to achieve the desired surface quality. After the process was performed the majority of defects could not be seen with the naked eye. Thus, a 3D microscope and SEM instrument were used to observe the images of the cross-section of the SLM parts before and after re-melting, to verify the qualitative results and to assess the amount of improvement of dendrite structures which are formed due to the rapid cooling rates encountered during the SLM process. The methods have also shown how beneficial the technique (re-melting) is for suppressing defects on AM component surfaces as seen in the **Figure 7-45**.

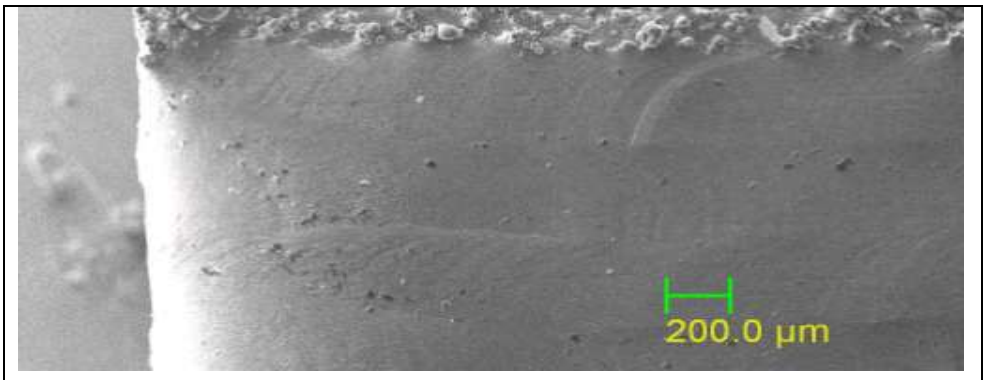

SEM micrograph realized on a surface built at 30°

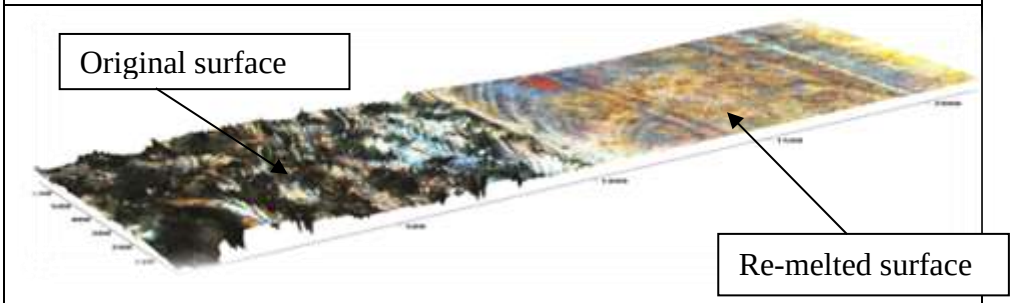

3D image obtained on surface built at 30°

3D image obtained on surface built at 0°

Figure 7-45: SEM micrograph & 3D zeta result to show how the surfaces appear before and after re-melting.

Figure 7-45 demonstrates that laser re-melting has the capacity to change the micro texture of the thin surface layer of a material and make it highly smoothed and normally free of defects such as porosity, balls, deformation, peaks, valleys and agglomerations which are normally associated with metal AM processes. This is observed especially when high heating and cooling rates are induced.

During RL a fully molten pool having a depth higher than *Rz* (80µm). When this occurs, it turns out clearly that the laser energy density is enough during laser re-melting process. The results also proved that good results are associated with specific interaction times, i.e. scan speeds of (400 and 500 mm/min), and a hatch overlap of 50%. Thus, it is possible to say that employing laser re-melting with proper parameters has the ability to create sufficiently deep molten pool free defects, which has capacity to yield a stable and strong connection with the solid material found underneath as can be seen in **Figure 7-46**.

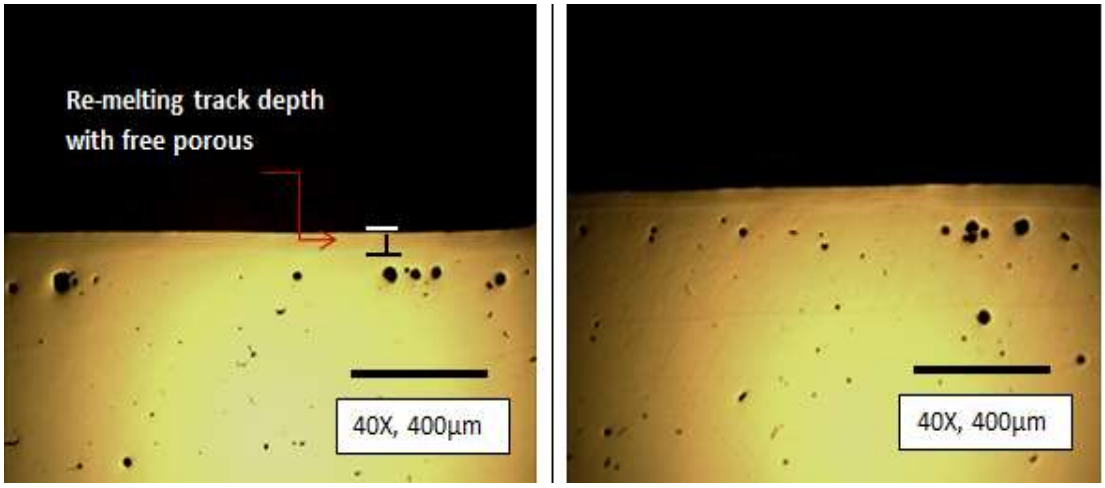

Figure 7-46: 2D micrograph demonstrating a re-melting track free of pores.

Figure 7-46 shows the uniform distribution of a re-melted surface, free of dendrites and pores, which have been formed via formation of crystalline and create a fine structure surface. In such a case, the microstructure and mechanical properties are improved; it is only for completely re-melted layers. This may limit application of laser re-melting, if used as a post-treatment method. [180, 182]

Different sets of parameters could generate a various thickness of the re-molten zone which can achieve different microstructures texture on the re-melted surfaces.

7.3 Chapter summary

SLM is a layered manufacturing process that produces fully dense and functional metallic parts which have high geometrical complexity. The poor surface quality of parts produced limits the process, but this limitation can be overcome by several techniques available on the market today based on machining, thermal and electrochemical processes.

In the current work, surface modification was done by using a thermal technique (laser re-melting) as a post-process and, according to the results found in this investigation; laser re-melting is a promising technique to substantially improve the surface roughness of SLM parts. The most important points can be summarized as follows:

- Combining selective laser melting with laser re-melting has great potential to make the surface quality better. The amplitude of surface roughness parameters were reduced by approximately 80% when compared with the initial surfaces, which are very encourage results.
- Microstructure dendrites such as balling, waviness and agglomeration can be substantially reduced in the re-melting process. Also, the microstructures of shrinkage cavities on the surface are eliminated as well.
- Laser re-melting has the potential to improve the inner density of parts and the surface porosity will be completely eliminated; the result will be a fully dense microstructure. Hence, the re-melted zone does not show any pores and the density reaches almost 100%.
- The process showed minor damage to the sharp corner of the part due to the large beam spot size, see **Figure 7-45**. Also the amount of improvement was limited to the thin layer (100um)
- This makes the process (LR) highly recommended for the production of 316L stainless steel since stainless steel has the capacity to be re-melted with less oxidation, due to it being a non-reactive material.

8.0. Electropolishing and fatigue test experiments

This chapter has been divided into two sections. The first section is electropolishing based on an ionic liquid, and the second section focuses on the cyclic cantilever bending test (fatigue test) to assess the performance of the test samples (SS 316L) through different stages of surface roughness improvement.

8.1 Electropolishing Experiment

Electropolishing is an electrochemical process and employs controlled dissolution of the metal's/alloy's atoms from the surface which is submerged in an electrolyte. The current will be controlled by the amount of fresh reactant reaching the interface surface from the solution. Movement of reactant in and out of the interface surface is important in predicting the current flow. One of the fundamental laws of electrochemistry is Faraday's Law.

$$Q = FN$$

Where (Q) is total charge passed, (N) it relates the number of liquid moles, (F) is faradays constant. The differential form of this law is:

$$\frac{dQ}{dt} = i = F\frac{dN}{dt}$$

According to this Faraday's Law may be stated as follows

The amount of material removal from the work piece at an electrode is directly proportional to the quantity of electricity (electric charge) passing through the cell solution. This also demonstrates that the current is straight proportional to the ratio of liquid concentration. [140, 183]

The aim of this study was to perform electropolishing by use of a green process - for the environmental benefits - to reduce the surface roughness of an SLM made, SS316L component that has already been re-melted, and to improve surface quality with minimal material removal by optimising the parameters used.

The experiments were divided into three stages as follows.

- Liquid preparation
- Liquid physical properties
- Electropolishing of SS316L samples obtained after re-melting stage.

8.1.1 Liquid preparation

This experiment was carried out by using Choline chloride (ChCl) (Aldrich, 99%) and Ethylene glycol (EG) (Aldrich, >99%) in a 1:2 ratio. The Choline chloride was first recrystallized, filtered and dried from the ethanol, whereas the Ethylene glycol was used as received. 5% and 10% oxalic acid was added to improve properties of liquid; the components were mixed first and then stirred at 80C°, until a homogeneous liquid colour was obtained. [184]

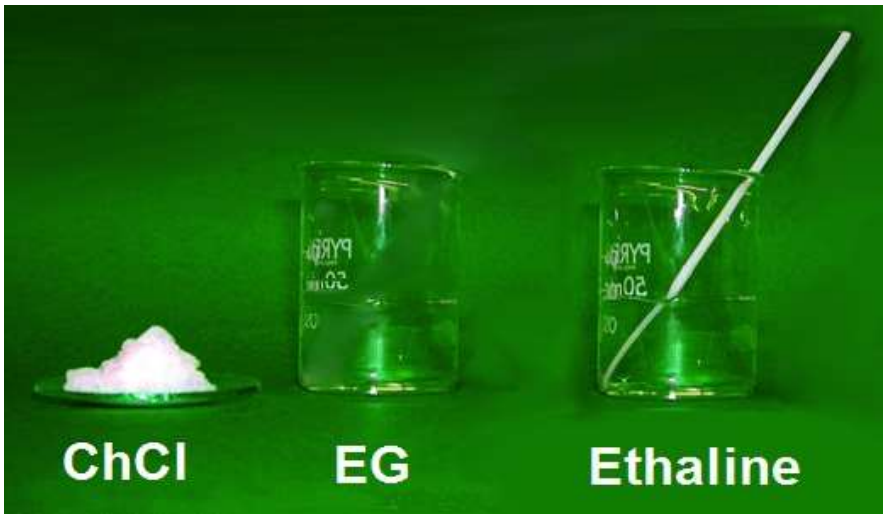

Figure 8-1: Shows the chemical component of the liquid (Ethaline).

8.1.2 Physical properties

8.1.2.1 Viscosity Measurements

The viscosity measurement of the liquid was obtained as a function of temperature. The temperature range used was 20-75 C°. A Brookfield DV-E Viscometer (Brookfield Instruments, USA) fitted with a temperature probe was used. The liquid was first heated up to 80 C° and then measurements of viscosity were taken from that temperature, down to 20 C°. The liquid was allowed to cool naturally (i e, at room temperature) without use of any cooling systems. The viscosity measurement was obtained using a spindle attachment, which measures the ease at which the spindle can move at a set amount of revolutions per minute. The measurements were taken with the temperature maintained constant within ±1 C°. An average of three readings of viscosity was used for the analysis.

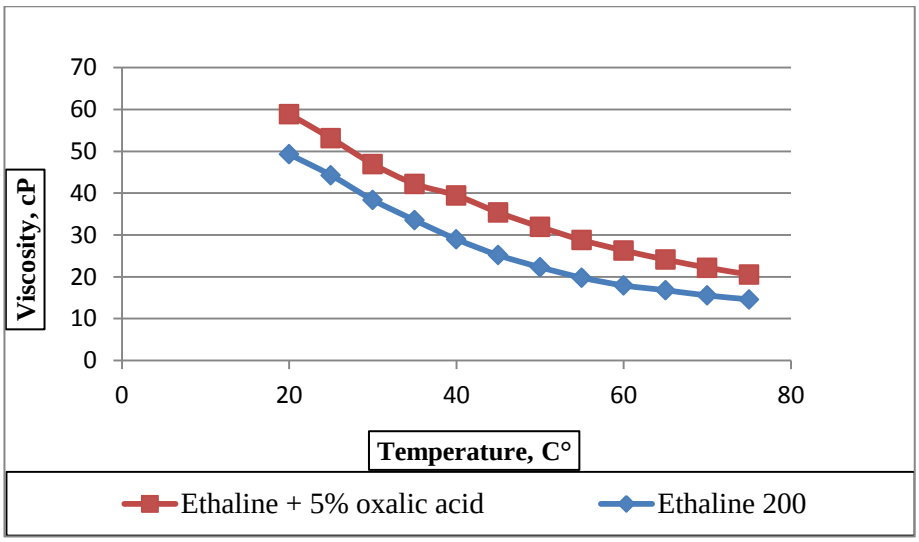

Figure 8-2: Dependence of viscosity on temperature for Ethaline200 and Ethaline 200 with 5% oxalic acid.

8.1.2.2 Conductivity Measurements

The conductivity of the liquid was measured as a function of temperature. The temperature range used was 20-75C°. The instrument used was a Jenway 4510 conductivity meter fitted with an inherent temperature probe (cell constant = 1.01 cm-1). Each mixture was heated up to 80C° and measurements were taken from 20 C° up to 75 C°. All conductivity measurements were recorded at exactly the same temperatures as the viscosity experiment and were for the same eutectic composition. To confirm good correspondence between the results, the samples used for conductivity were made from the same batch as that used in the viscosity experiments.

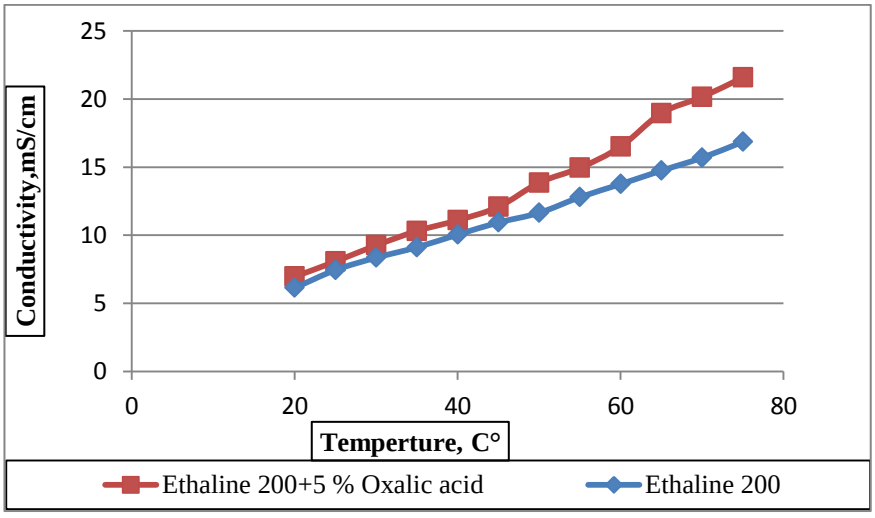

Figure 8-3: Dependence of conductivity on temperature for Ethaline200 and Ethaline 200 with 5% oxalic acid.

8.1.2.3 Cyclic Voltammetry

Cyclic voltammetry is a popular method that is used to obtain physical information of electrochemical systems, which is obtained firstly by controlling the potential of scanning rate of the surface reaction mechanism. Much information can be obtained by knowing the peak current. In this case the information involved in the redox transformation of electro active species, due to different concentration liquids can be obtained.

A cyclic voltammetry investigation was carried out using an (Autolab PGSTAT12) potentiostat controlled with GPES2 software. A three-electrode system was used, consisting of the SS 316L test piece as the working electrode, a platinum counter-electrode and a silver reference-electrode. All cyclic voltammograms were taken at 30 C° and at a scan rate of 20 mV s-1, in order to see the effect of increasing the Oxalic acid content and to observe the height and peak position of the redox interaction which are all important during the electropolishing and deposition process. The samples of liquids for this test were taking from the same batch as used in the previous testes.

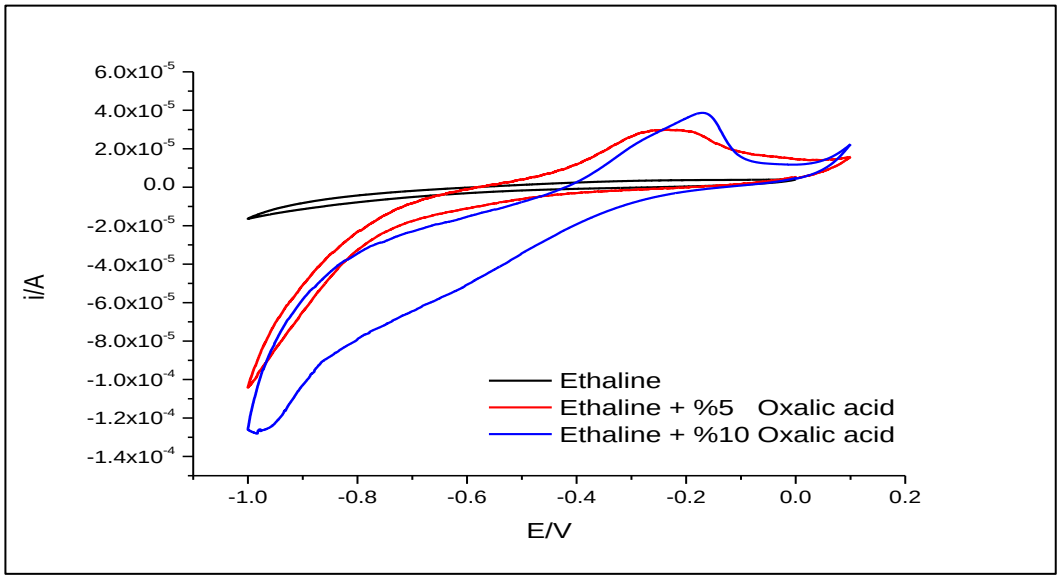

Figure 8-4: Comparison of the cyclic voltammetry of Ethaline200 and Ethaline 200 with 5% oxalic acid.

The results showed that the solutions become more reactive proportionally with the oxalic acid rise, as shown in **Figure 8-4.** It was also noted that this trend tends to be diminished in liquids that have less oxalic acid. This could be due to the fact that oxalic acid is a strong acid and is a reducing agent and its conjugate base.

8.1.3 Electropolishing procedure

Experiments were performed on a number of samples from (SS 316L) made by SLM as per the previous experiments, with the specific parameters of section **7.1.** The sample dimensions were (4, 10, and 30) mm, and they had an initial surface roughness (*Ra*) measured at between 10 and 17.5µm, due to the stair effect indicated previously. The samples were re-melted using the specific parameters used in section**7.2.2** (optimal parameters), in order to eliminate the initial surface roughness and porosity issues and to be ready for electropolishing. At this stage, the surface roughness of the samples was measured at approximately (1.4 ±15% µm). Specific areas were selected to be polished and Acrylic resin was used to mask undesired polishing area.

The effect of the electropolishing process on the surface quality of SLM components can be affected by many factors. The main factors are potential source, polishing duration, temperature, cell component (concentration), current density and the method of agitation (stirring rate). [185, 186]

The set of parameters used was selected according to the most important factors, established in preliminary trials, as follows:

- Source potential: start from 4 volt and vary (6 and 8) volt respectively.
- Duration time: start with 30 min and vary (45 and 60) min respectively.
- Temperature: start at 20C° and vary (40 and 60) C° respectively.

The other factors were kept constant as follows:

- Type of liquid and liquid concentration: (Ethaline 5% oxalic acid)
- Method of agitation (stirring rate): approximately 300 rpm (revolution per minute), as recommended in [186, 187]

The effect of the above selected parameters on the response values (1) surface roughness and (2) loss in weight (depth of polishing area) were investigated through a design approach of a classical full factorial experimental set up, with a 3 against 3 as shown in **Table 8:1**

(A) Source potential (Volts)	(B) Time (mins)	(C) Temperature (C°)		
		20 (0)	40 (1)	60 (2)
4 (0)	30 (0)	000	001	002
4(0)	45 (1)	010	011	012
4 (0)	60 (2)	020	021	022
6 (1)	30 (0)	100	101	102
6 (1)	45 (1)	110	111	112
6 (1)	60 (2)	120	121	122
8 (2)	30 (0)	220	201	202
8 (2)	45 (1)	210	211	212
8 (2)	60 (2)	220	221	222

Table 8:1 the three levels of the full factorial design.

At the beginning of the experiments the work piece was attached to the finishing region (anode), whereas the negative terminal of the cell was connected with the cathode, which in this case was made of titanium radium mesh, due to its stability. The two poles (cathode, anode) were immersed in the liquid (Ethaline 5% Oxalic acid) as shown in the photograph of **Figure 8-5**.

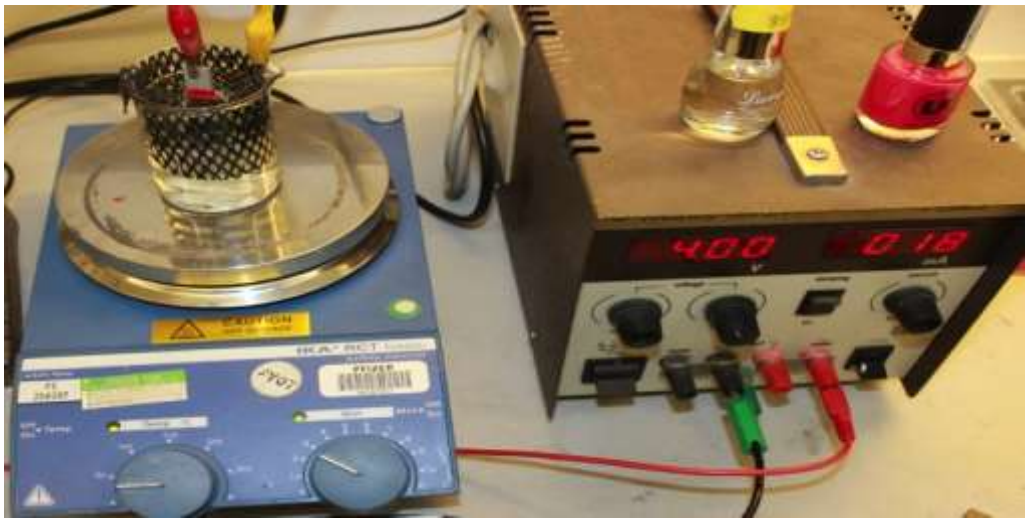

Figure 8-5: Shows a photograph of the Electrolytic Finishing set up.

In this experiment, the response values surface roughness (*Ra*), and loss in weight (from which depth of polishing area can be deduced) were obtained by passing current through the cell using specific parameters. The anodic dissolution of the specimens was completed at different potentials, times and temperatures, as shown in **Table 8:1**. Each setup was replicated **3** times to find the average results for the response values.

8.1.3.1 Experimental results and discussion

The surface quality of the polished parts is a result of optimum conditions of current density, which is related to the cell parameters.

Thus, the overall surface quality of the anodic surface can be characterized through three response factors, which are (1) surface roughness, (2) surface defects (pitting) and (3) surface brightness. The surface roughness was quantified by using a stylus profilometer as well as the depth of polished area was calculated. DOE software was used to calculate the interaction of the average results of the response values surface roughness (*Ra*) and depth of polishing area; the errors were also determined and tabulated as shown in **Table 8:2**. The other response factors (pitting & brightness) were qualitative and were surveyed (characterized) using optical techniques.

Factors			Response			
Volt	Time mins	Temperature C°	Polishing depth (microns)		Surface roughness (microns)	
			Average	Error	Average	Error
8	60	60	79.951	4.351	0.836	0.12
8	60	40	59.087	2.336	0.686	0.04
8	60	20	13.438	2.214	0.436	0.07
8	45	60	67.712	2.402	0.84	0.07
8	45	40	33.127	2.405	0.743	0.061
8	45	20	12.437	0.811	0.426	0.056
8	30	60	51.136	3.238	0.826	0.07
8	30	40	17.368	0.759	0.59	0.062
8	30	20	10.328	1.03	0.543	0.08
6	60	60	43.145	2.393	0.413	0.047
6	60	40	19.943	1.588	0.336	0.051
6	60	20	8.409	1.088	0.376	0.037
6	45	60	28.244	2.552	0.383	0.035
6	45	40	13.124	1.682	0.383	0.041
6	45	20	7.009	1.174	0.4	0.026
6	30	60	20.873	3.498	0.41	0.04
6	30	40	10.81	0.426	0.343	0.041
6	30	20	8.545	2.558	0.386	0.035
4	60	60	16.175	1.947	0.346	0.035
4	60	40	10.27	1.761	0.34	0.04
4	60	20	5.088	1.061	0.4	0.036
4	45	60	13.64	2.032	0.36	0.036
4	45	40	6.494	0.507	0.37	0.052
4	45	20	4.451	0.512	0.386	0.03
4	30	60	10.834	0.771	0.363	0.032
4	30	40	5.719	1.388	0.353	0.015
4	30	20	4.032	0.945	0.433	0.045

Table 8:2: Results data for the response factors obtained Ra and depth of polished area.

Table 8:2 shows the variation of surface roughness and polishing depth with the variation in voltage, process duration and liquid temperature. For all the cases, three trials were completed and averaged to improve the accuracy. Errors were calculated for further analysis and comparison.

After re-melting, the surface roughness *Ra* was approximately 1.4 ± 15% µm and *Rz* was approximately 7 ± 15% µm. For good polishing the response value for the depth should be in a range of *Rz* of re-melted results. Although, from the results the majority of surfaces display acceptable surface roughness, in some samples the required

polishing depth was exceeded. This in turn, affects the accuracy of the part's dimensional tolerance.

Profilometer results (**Table 8:2**) showed that the best results for average surface roughness were achieved at a temperature of 40Cº, a time interval of 60 minutes and a voltage of 6V. The surface roughness obtained at these conditions was 0.34µm, but the polished depth was 19.9µm, which exceeds the required polishing depth. In such cases, reduction of the process duration may facilitate a reduction in polishing depth.

Reducing the time of polishing from 60 to 30 minutes and keeping the temperature at 40Cº and the voltage at 6V, the polishing depth changed to 10.81µm and the surface roughness at these conditions was 0.35µm which is a good result.

Furthermore, when the time was kept at 60 minutes and the voltage was reduced from 6V to 4V at the same temperature of 40Cº the polished depth was 10.27µm and the surface roughness was 0.34µm. According to the obtained results, the best response factors can be achieved with a range of cell parameters between 4V to 6V, at a temperature of 40Cº and process duration between 30 and 60 minutes.

8.1.3.1.1 Current density

The following three graphs show the recorded current density variation with time and temperature during the experiments. The current density is in mA/cm^2 and is a results of 3 different voltages - 4, 6 and 8 Volts - measured for 3 different time intervals (30, 45 and 60) minutes.

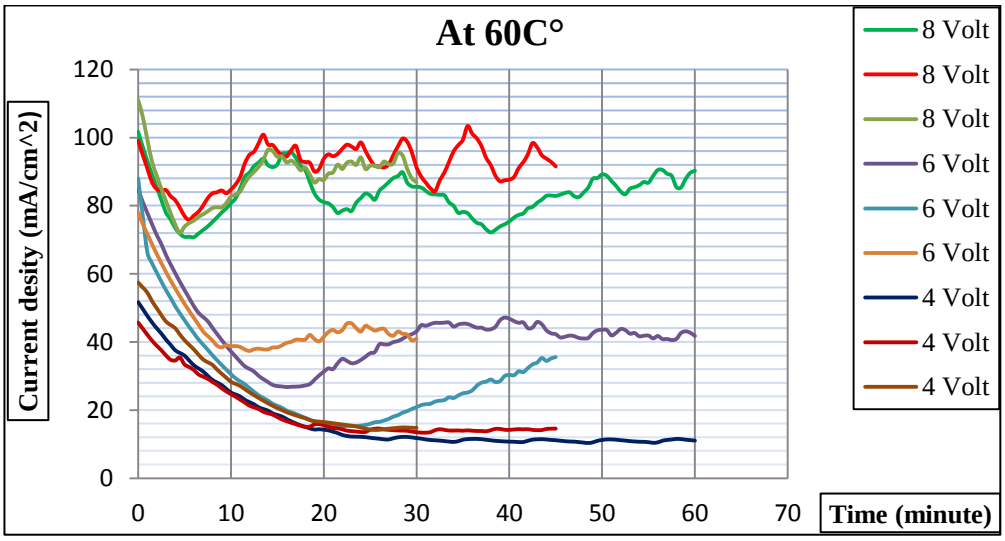

Figure 8-6: Shows the current density against time for the temperature 60 Cº.

Throughout **Figure 8-6,** it can be seen that similar patterns were observed in variations for all the time intervals used in this experiment.

At 8 Volts, the current density keeps fluctuating with time. Unstable variations showing peak and valley behaviours were observed. The average of current density was within the range of 91 mA/cm^2 and 83 mA/cm.^{2}

At 6 Volts, the fluctuations of current density are much less than that for 8 Volts. It can also be seen that the pattern of peak fluctuations is similar regardless of time. The average current density varied between 45 mA/cm^2 and 30mA/cm.^{2}

At 4 Volts, the current density fluctuates less than with the other two voltages and shows a similar pattern of fluctuations as well for the three different time intervals. The average of current density was within the range of 26 mA/cm^2 to 16 mA/cm.^{2}

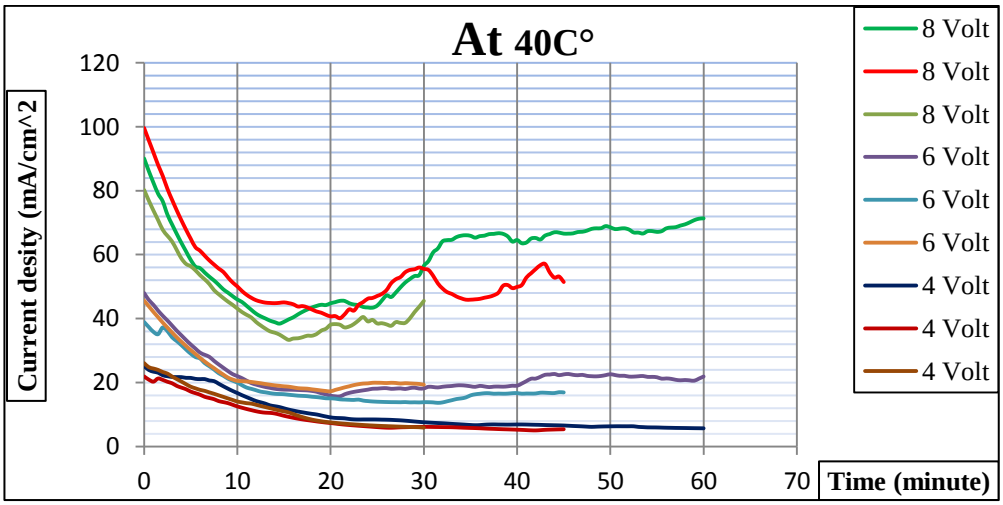

Figure 8-7: Shows the variations of current density against time for the temperature 40 Cº and 3 different voltages, 8, 6 and 4 Volts.

Figure 8-7 it can be observed that the fluctuations of peaks are less than that for the previous graph of 60Cº. Regardless of the duration of the experiment the variations in the pattern remained similar for all 3 voltages used in this experiment.

The highest current density was observed at 8 Volts where it was in the range of 44 mA/cm^2 to 58 mA/cm^2. Minor fluctuations and peaks were observed in current density against time.

At 6 Volts, the current density in this level more stable manner, with very minor fluctuation observed in the time intervals used in the experiment, and it was in the range of 18 mA/cm^2 to 24 mA/cm^2.

At 4 volts, the current density is in the range of 8 mA/cm^2 to 13 mA/cm^2 and shows almost no fluctuations.

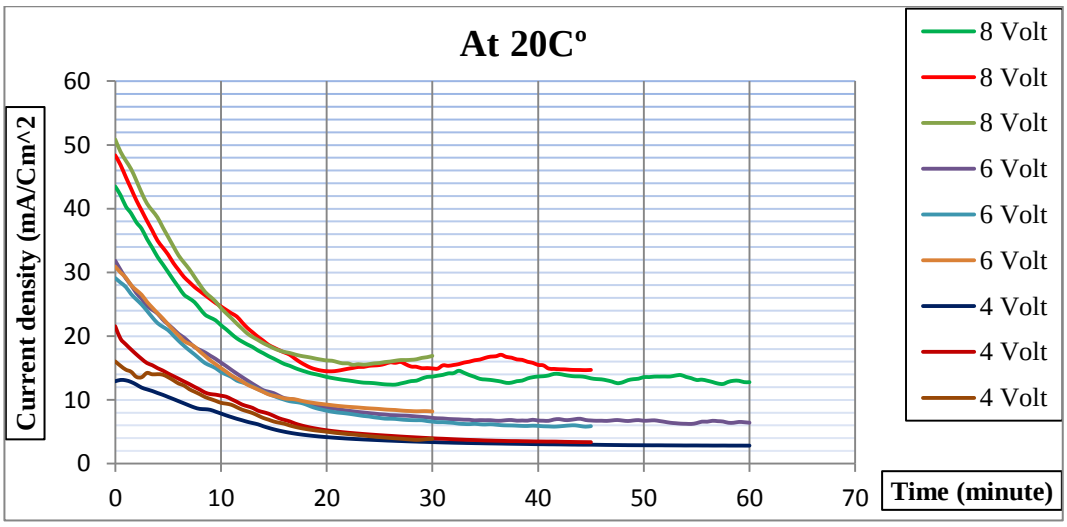

Figure 8-8 : Shows the variations of current density against time for the temperature 20 Cº and 3 different voltages, 8, 6 and 4 Volts.

Figure 8-8 above (20C° temperature) shows fewer fluctuations in the variation of current density against time for the three different voltages used in this experiment.

At 8 Volts, the pattern of fluctuations is minimal compared to the pattern observed in the previous two graphs and they are in the range of 16 mA/cm^2 to 23 mA/cm^2.

At 6 Volts, the variations and peaks are minimal as well and it can be stated that the variation of current density against time is stable, varying from 10mA/cm^2 to 14 mA/cm^2.

A similar kind of pattern is observed with lower current density for the 4 volts Voltage in a smooth pattern of variations of current density, within a range of 4 mA/cm2 to 8 mA/cm2.

The comparable results of the three previous graphs with the results Table 8:2, it can be clear that the variation of the response values (surface roughness and depth of polishing) are highly depending to the amount of dissolved material (current density). Also, these results may explain the reason for the high surface roughness at high current density may leading to non-homogeneous dissolving material (see Table 8:2). Thus, the process parameters should be set to control the amount of metal removed within a range of current density between 10 mA/cm2 to 20 mA/cm2, at a constant temperature of 40C°. This can be obtained with a range of voltages between 4 to 6 volts and process duration between 30 and 60mins. These results may be good enough to maintain the dimensional tolerances of the parts and obtain a good surface roughness of about 0.35µm Ra. The next section discusses the analysis of Table 8:2 results by use of DOE software.

8.1.3.1.2 Statistical analysis and models (DOE analysis)

DOE software was used to analyse the results of the response factors demonstrated in **Table 8:2**, in order to calculate the multiple response regression connected with the experiment. The table below shows the impact parameters of the selected factors.

		Surface roughness (micron)		Polishing depth (micron)	
Factor	**Name**	**Coefficients**	**P Level**	**Coefficients**	**P level**
Constant		0.377284	3.45E-32	14.96585	1.36E-21
A	**Potential**	0.165185	6.24E-14	14.41604	4.33E-20
B	**Time**	0.014815	0.394858	8.008581	3.83E-10
C	**Temperature**	0.013889	0.424907	11.33442	1.74E-15
AB		0.005278	0.579365	5.224602	1.25E-12
AC		0.103889	2.45E-16	11.29299	4.87E-28
BC		0.012222	0.201605	4.366542	4.39E-10
ABC		0.0125	0.285333	2.677664	0.000475
AA		0.134259	9.67E-15	5.615731	6.48E-09
BB		-0.00907	0.500626	1.259794	0.138307
CC		0.01537	0.25551	2.975924	0.000739
AAB		-0.00306	0.852852	1.837655	0.078581
ABB		-0.00861	0.601511	0.150729	0.883893
AAC		0.071667	4.69E-05	4.422824	5.9E-05
ACC		-0.02444	0.141174	0.548834	0.595278
BBC		-0.01	0.54436	0.073042	0.943579
BCC		-0.02556	0.124265	-4.19571	0.000127
Standard Error		**0.057**		**3.56**	
R^2		**0.91**		**0.97**	

Table 8:3: Results of multiple response regression based on a full factorial design.

The interaction parameters of the factors in **Table 8:3** are also shown in graphical form in **Figure 8-9**. The figure illustrates results for *Ra* as the response variable. As can be seen, the potential (variable A), its square (AA), its interaction with temperature (term AC) and the interaction of its square (AA) with temperature C (term AAC) - the red colour in the Pareto diagram, showed good confidence (P) level of see **Table 8:3**. The impact of other factors, including the linear impact of time (B) and temperature (C) is small and do not indicate good confidence level. Quantitatively, the individual impact

of these factors is a decimal order less than the first four (A, AA, AC and AAC). R-square for this model is 0.91 These means that all other factors not taken into account in this 3-factorial model give almost 10% of the total impact, which in fact means that potential (A), temperature (C) and time (B) play the most significant role in forming the surface roughness *Ra*.

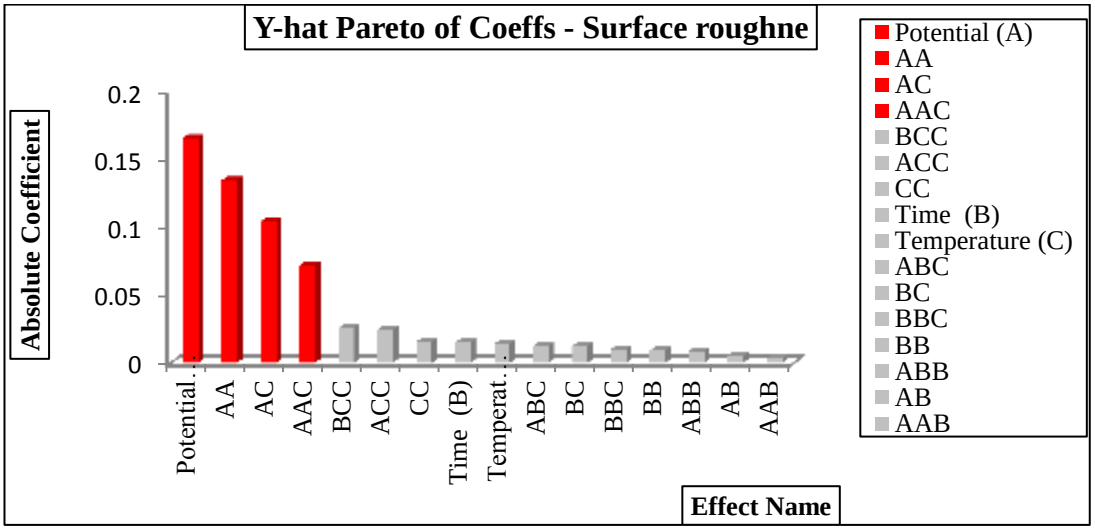

Figure 8-9: Y-hat Pareto diagram for average roughness response variable.

On the basis of the data in **Table 8:3,** the model for predicted average surface roughness *Ra*-hat can be determined as:

$$\hat{Ra} = 0.377 + 0.165A + 0.134AA + 0.104AC + 0.772AAC$$

Equation 8-1

Where *A* is the potential (Volt), *C* is the temperature (Degrees Celsius), Ra-hat is the predicted average roughness (microns) and the coefficients are variable related to the factors as shown in **Table 8:4**.

factors	Coefficients	Dimensional units
Ra-hat		µm
Constant	0.377	µm
A	0.165	µm/ volt
AA	0.134	µm/ volt^2
AC	0.104	µm/ volt x C^o
AAC	0.772	µm/ volt^2 x C^o

Table 8:4 the dimensionality of coefficients in the equation 8-1.

The correctness of this model and its limitation are illustrated in **Figure 8-10** which shows a good linear relationship between actual and predicted values of *Ra*. **Figure 8-10- B** indicates that there is non-uniform distribution of residuals in the range of large actual *Ra* and therefore some other factors need to be included. However the overall correctness of the model is R^2=0.91, which is good for 3 factors.

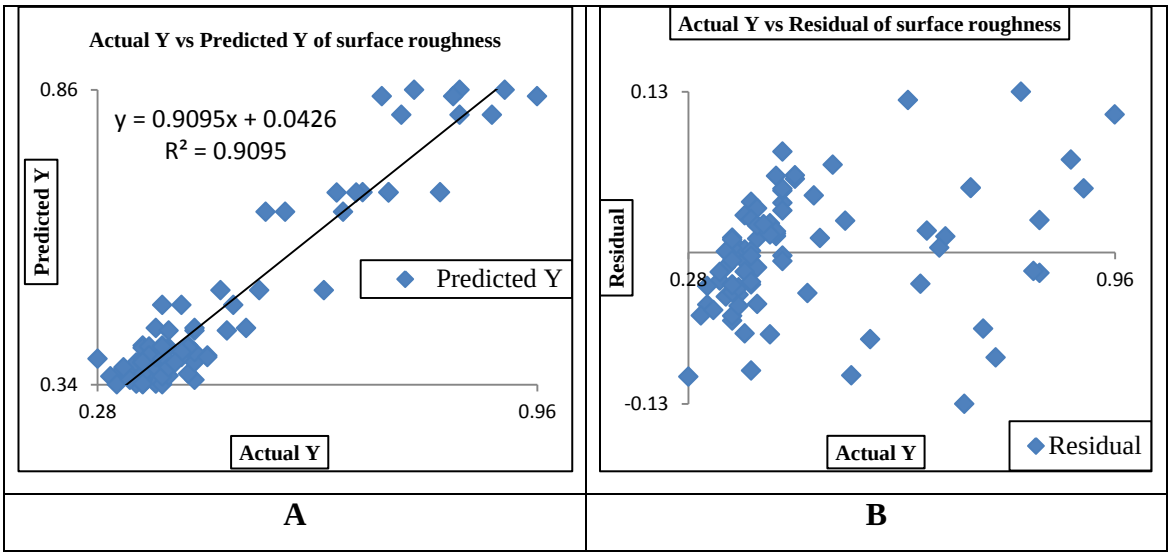

Figure 8-10: Shows the actual roughness against predicted roughness (A) and against residual (B).

On the other hand, the effect of these parameters on the calculated polishing depth - in the sense of overall effect indicated by R-square in **Table 8:3.** R-square is 0.97 and more convincing, which can be interpreted statistically as very good. However the impact of the variables differs significantly from the impact on the average roughness (*Ra)*. As is shown in **Figure 8-11**, potential (A) still has the greatest impact, however the linear impacts of temperature (C) and time (B) take second and fourth place in diagram and both have good significance. Quadratic effects for AC, AA, AB, BC, and CC are observed together with cubic effects of AAC, BCC and ABC. AAB impact is confident at a level of 0.08. The overall good fit of this model is also indicated in **Figure 8-12**, where the residual analysis is illustrated.

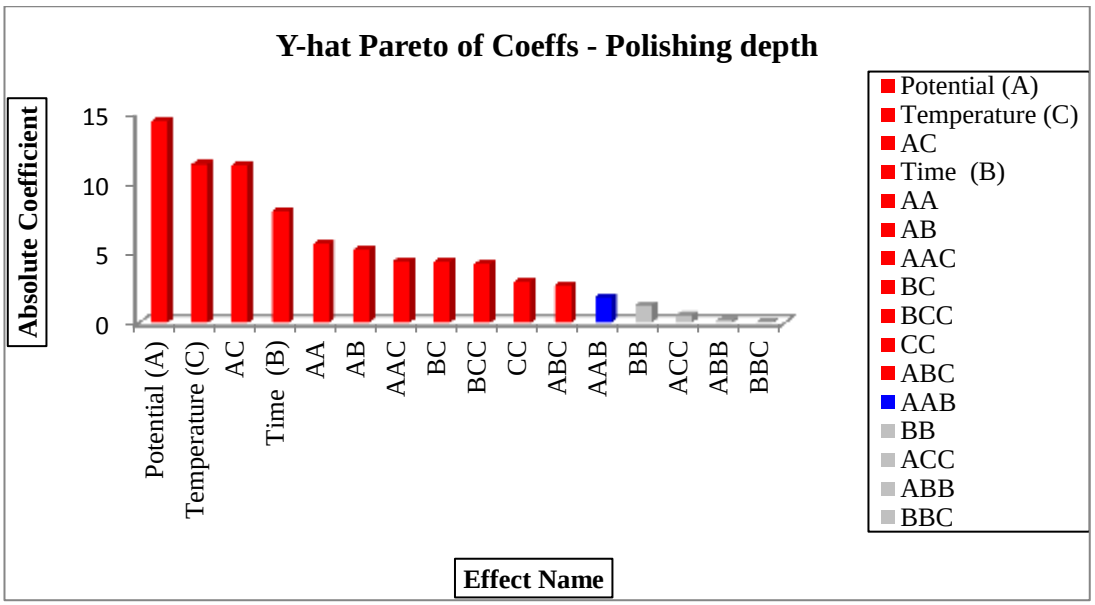

Figure 8-11: Y-hat Pareto diagram for the polishing depth response variable.

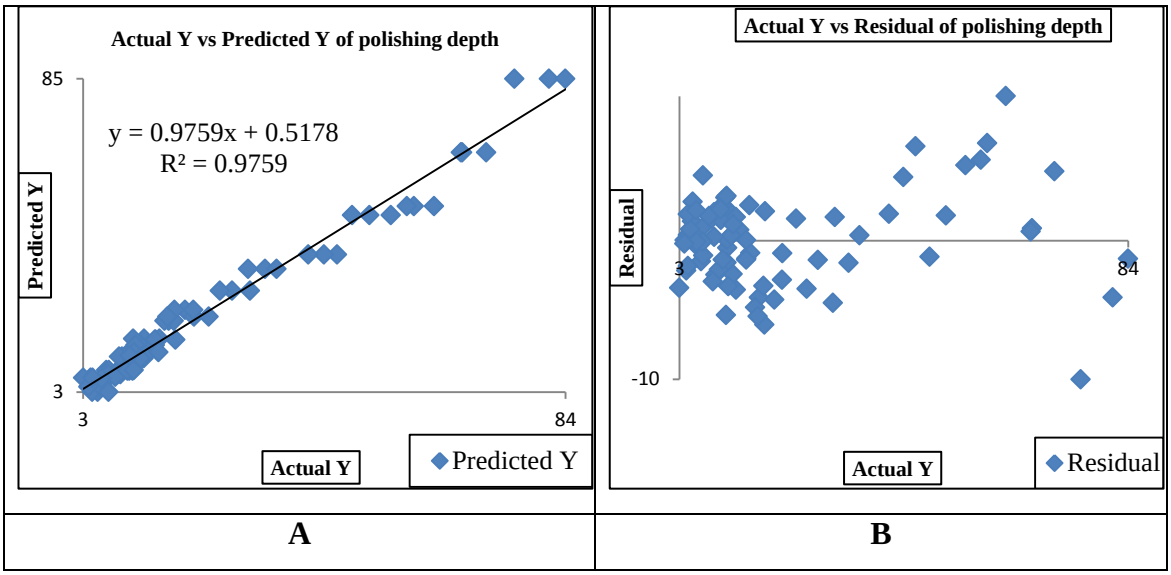

Figure 8-12 : Shows the actual depth against predicted depth (A) and against residual. (B).

8.1.3.1.3 Surface roughness (DOE analysis)

Surface roughness measurements after the electropolishing process describe how well the area has been polished. The stylus profilometer results showed the surface roughness of the polished areas was improved, but with different grades, depending on the current density to make an overall planar surfaces as shown in the following figures.

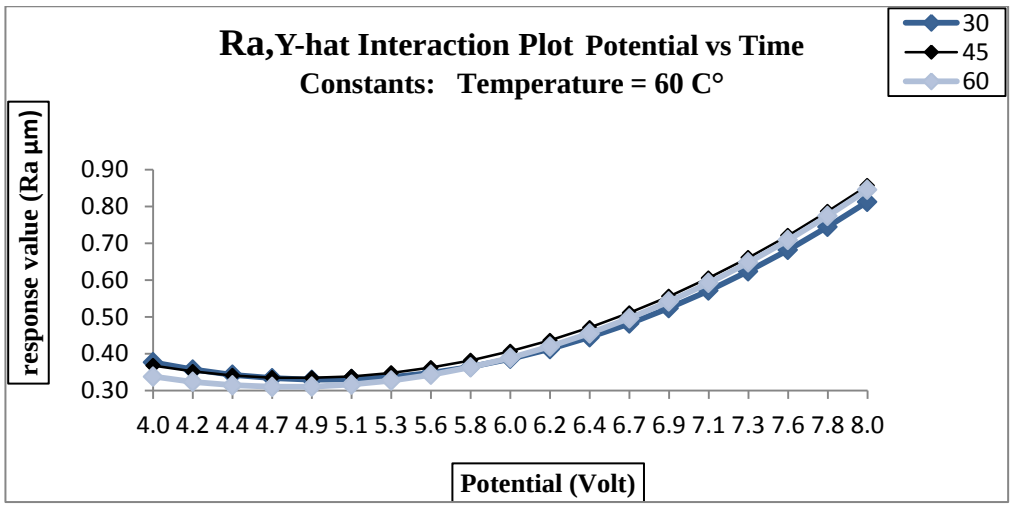

Figure 8-13: Response values of Ra, Y-hat Interaction at a constant temperature of 60 C.°

Figure 8-13 above shows the variation of response value (*Ra*) against voltage (potential) for the three different process durations used in this experiment, at a constant temperature of 60 C°.

At a potential of 4V the response value was 0.38µm for 30 minutes, 0.37 µm for 45 minutes and 0.34µm for 60 minutes. It is clear that in the three patterns, the potential increases lead to reduced response values *Ra*, recorded at approximately 0.3µm, at 4.7 volt and 60 minutes duration. After that, the response values *Ra* rise with the potential increase and record a highest response value of approximately 0 .85µm. These results are due to the elevated current density, leading to non-homogenous metal removal during the process. For the three patterns, at a constant 60C°, the best results can be obtained with predicted potential ranges between 4.7 and 4.9 volt.

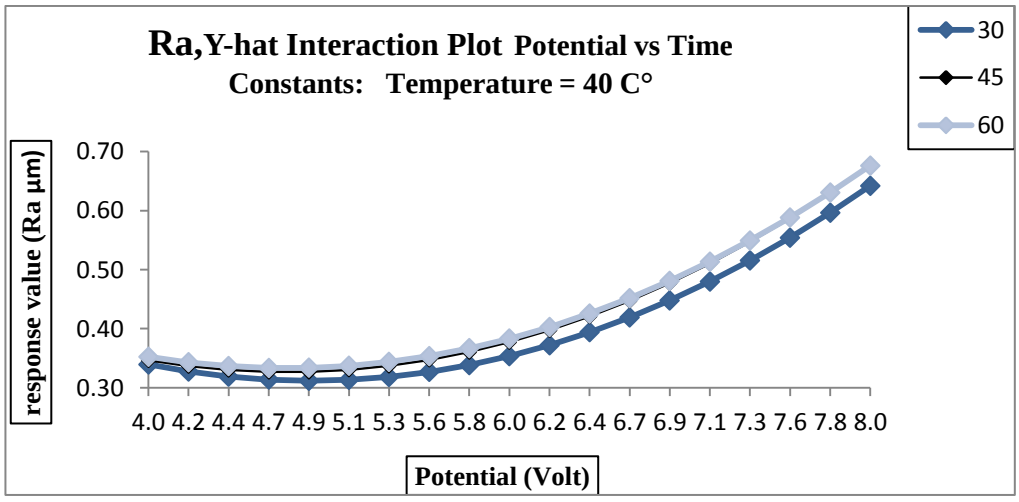

Figure 8-14: Response values of Ra. Y-hat Interaction at a constant temperature of 40 C.°

The above **Figure 8-14** shows the variation of response value (*Ra*) against potential, for the three different times used, at a constant temperature of 40C°. The general pattern shows that the response values keep decreasing slightly with an increase of potential from 4 to approximately 5 volts and then the response values increase from the potential of 5 volts and further up to 8 volts. In this case, the lowest response value (Predicted *Ra*) observed is 0.32µm for the 30 minutes process duration, at a predicted potential of 4.9 volts

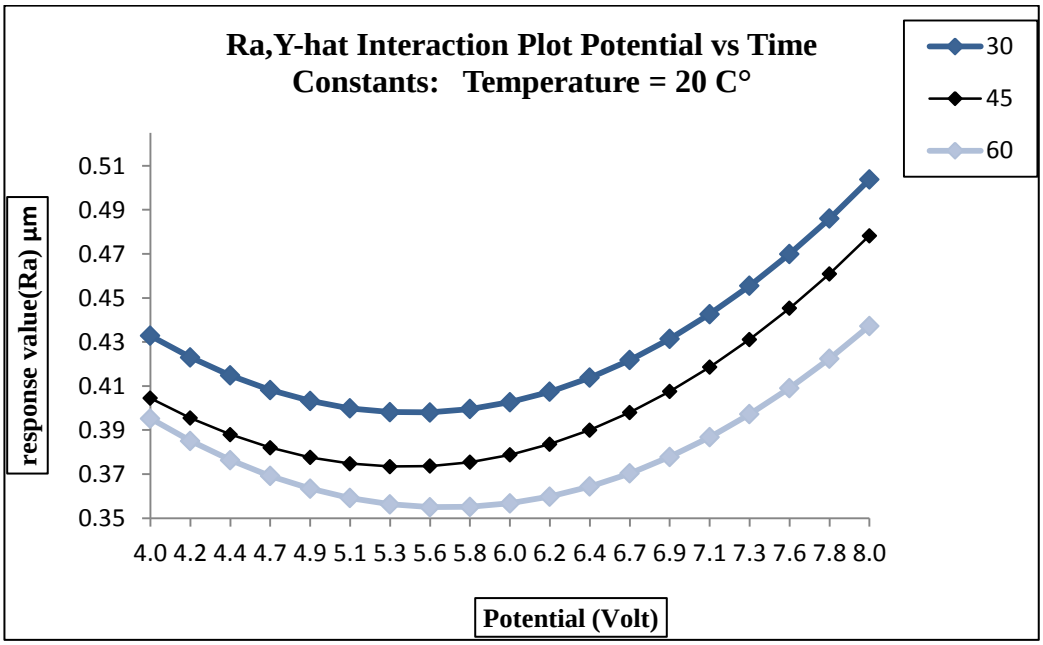

Figure 8-15: Response values of Ra, Y-hat Interaction at constant temperature 20 C.°

The above **Figure 8-15** shows the variations of surface roughness response value against potential for a constant temperature of 20 C°. The lowest response (*Ra*) value is 0.35µm, obtained between 5.6 and 5.8 volts for the 60 minutes process duration. It is clear that in all of the patterns the results response values (*Ra*) are reduced between 4 and approximately 5.6 volts and later increase from a potential of 5.8 volts up to 8 volts. The results also demonstrate that a reduction of the temperature needs more potential to obtain a satisfactory surface finish.

8.1.3.1.4 Polishing depth (DOE analysis)

The polishing depth of the polished area (due to loss in weight of the anode) is a crucial factor, due to its effect on the dimensional accuracy of the part. Calculations of polishing depth were made and the results are tabulated in **Table 8:2**. It was found that loss of weight is linearly related to the applied current density and processing duration; the following figures show the predicted results of polishing depth as a result of cell parameter interaction.

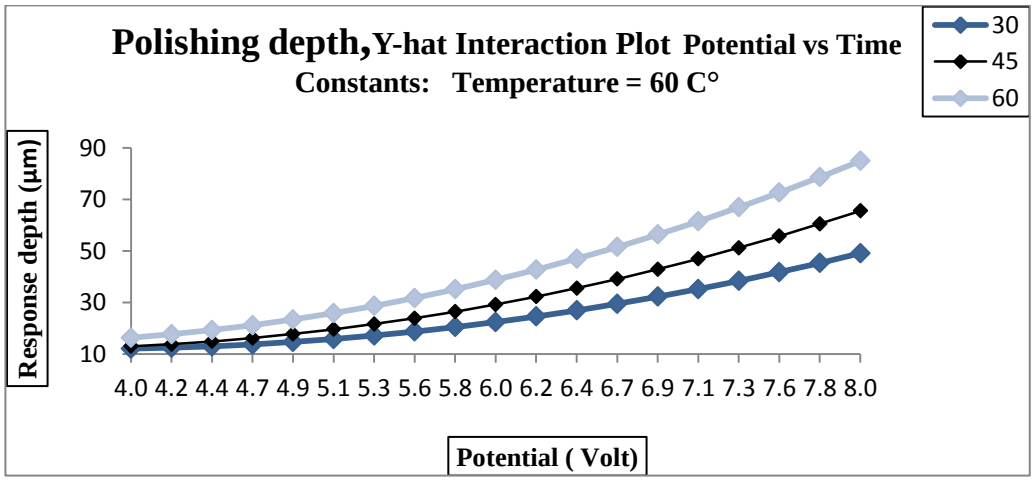

Figure 8-16 : Response values of depth, Y-hat Interaction at constant temperature 60C.

Figure 8-16 above shows the polishing depth response value against the potential for various process durations at a temperature of 60C°. In general, the lowest response values observed are for the lowest time interval (30 minutes) and least current density. On the other hand, the highest response values were obtained for the highest current density and highest time interval (60 minutes).

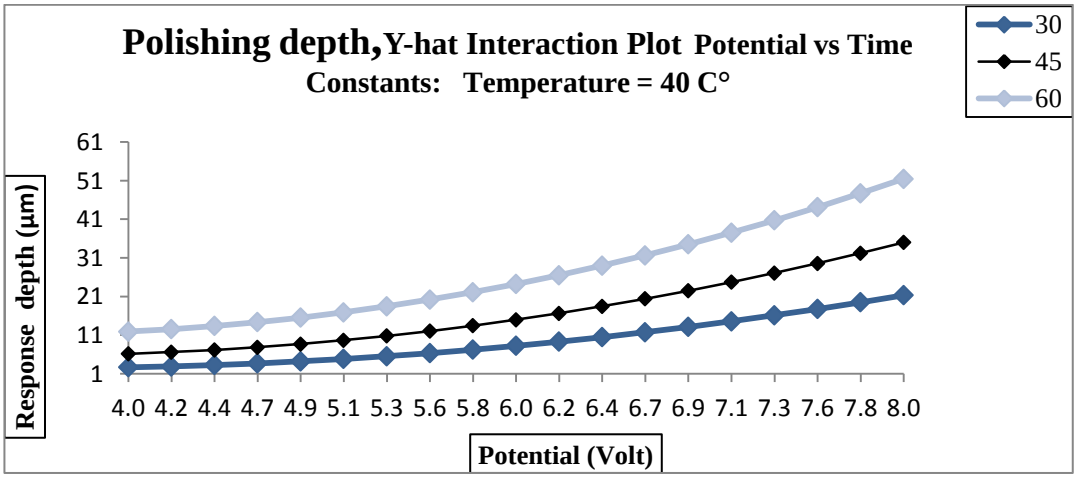

Figure 8-17: Response values of depth, Y-hat Interaction at a constant temperature of 40 C.°

Figure 8-17 above shows the variation of polishing depth response value against potential at a temperature of 40C°. Similar patterns can be seen as with the previous graph **Figure 8-16**; the response values for the polishing depth keep increasing as the time and potential increase (linear interaction).

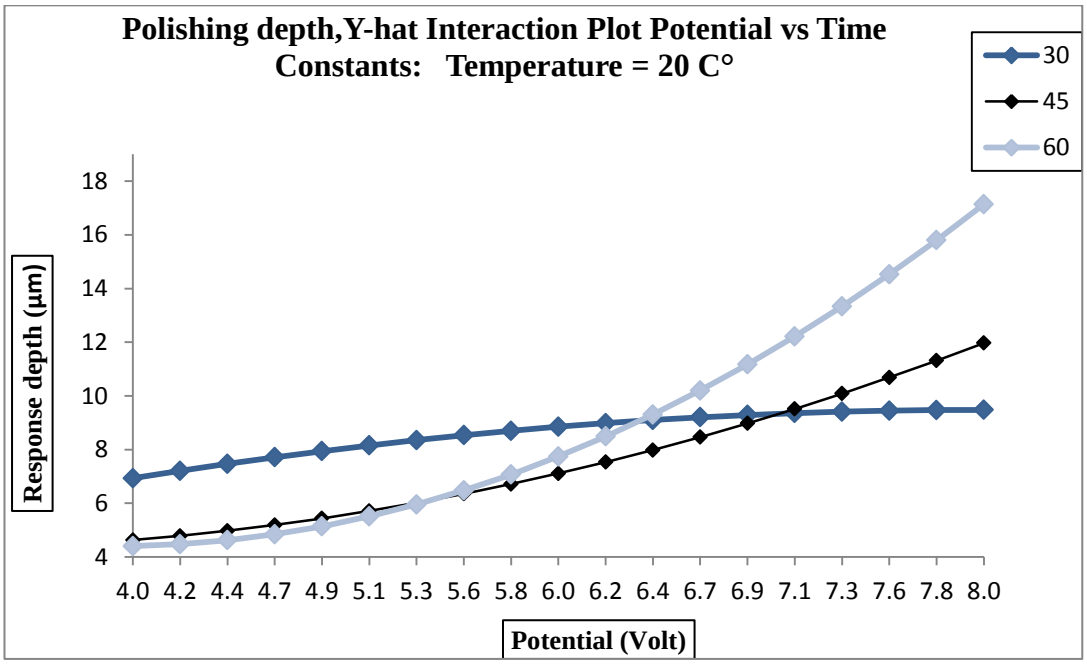

Figure 8-18: Response values of depth, Y-hat Interaction at a constant temperature of 20 C.°

Figure 8-18 above is a graph showing the variation of polishing depth against potential for a constant temperature of 20C°. This graph shows a different variation in comparison to the two previous graphs (**Figure 8-16 and Figure 8-17**). The lowest response value of 3.9µm was observed at a potential of 4.0 volts for the 60 minute process duration. The response value increased most as a response to the increase in potential for the 60 minute process duration. Results for the 45 minutes process duration show a similar behaviour to that of the 60 minute duration, but with a lower rate of increase in the response values, whereas the response values (polishing depth) for the 30 minutes duration were much higher than that of the other two durations (45 and 60 minutes). Furthermore, an increase in response values was observed with the lowest potential for the 30 minute process duration. Thus, in this case it can be stated that the predicted results of the response value after DOE analysis coms to against the results on **Table 8:2** (see the bottom results at 4 V) due to the potential and temperature decrease.

8.1.3.1.5 Overall statistical results

The results obtained from the DOE showed that the ranges of selected factors (potential, time and temperature) are in the good range to effect on the response factors.

The overall analysis shows that the potential and the temperature have the highest impact on the response factors (surface roughness and polishing depth), whereas the third factor (time) showed less effects as demonstrated in the Y-hat Pareto diagrams.

The best results were achieved with a potential between 4 and 5.5volts, process duration of 30 minutes and at a constant temperature of 40C°. This range of parameters may have enough authority to control the metal dissolution, current density ranges between 10 mA/cm^2 to 20 mA/ cm^2, leading the surface more planer. This range may facilitate maintaining accuracy of part dimensions and give less than 0.4 µm *Ra* as a final surface roughness. **Figure 8-19** below shows a comparison of the results of samples subjected to two stages of surface roughness improvement, namely laser re-melting followed by electropolishing.

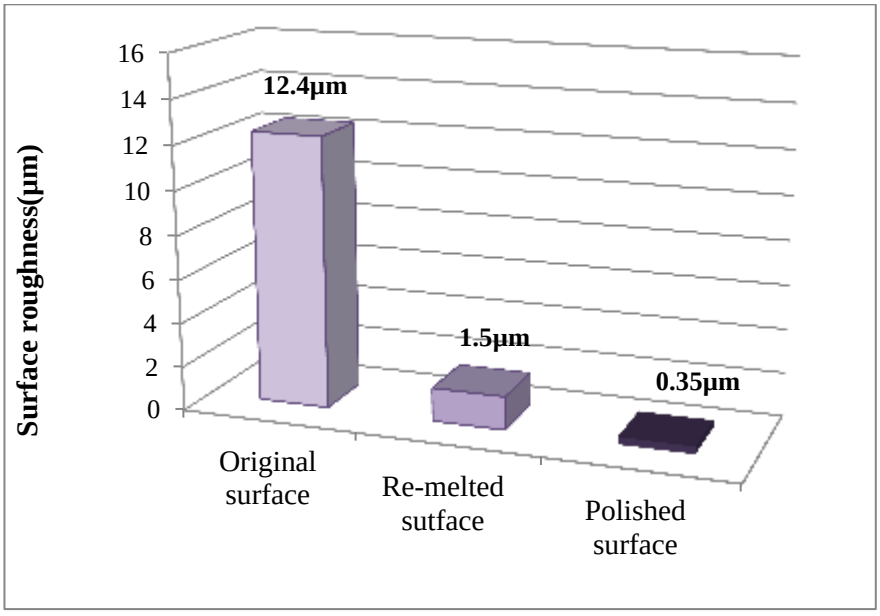

Figure 8-19: Comparison results of the three stages of surface roughness (Ra) results.

8.1.3.1.6 Surface topography

Surface topography was obtained by using SEM combined with EDX analysis. SEM was used to understand the feature defects remaining after the process, whereas EDX was exploited to report the percentage elemental composition of each sample surveyed before and after the polishing experiment. In this work the characterization of the surfaces surveyed varied, due to the variation in cell parameters. This parameter variation has a significant effect, and the relation between the parameters needs to be optimised to control the current density, which in turn determines whether homogeneous metal/ alloy dissolution is achieved.

Most surveyed samples showed good surface finish, but some pitting was detected, connected with exposures to high voltages and temperatures (8 volt at 60C° and different process durations) as shown in the following figure, **Figure 8-20.**

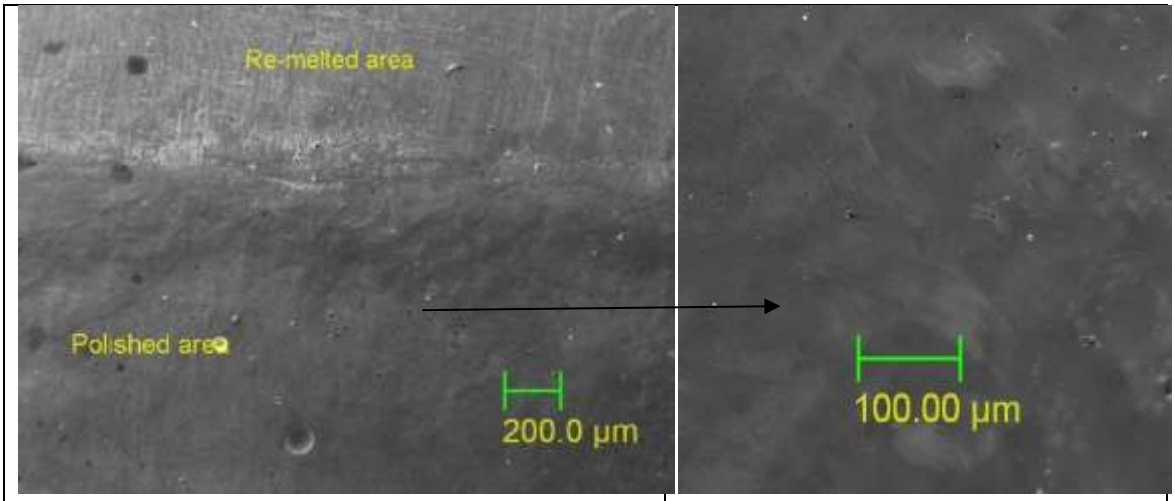

Figure 8-20: SEM micrograph result of polished sample obtained at 60C°, 8 volt and 45minutes.

It is well known that the key to the electropolishing method is the difference in current density across the microscopic surface profile (peaks and valleys), and that the current density is greater on the peaks than in the valleys. Also, the rates of metal/alloy dissolution are proportional to current density. In this case (8 volt at 60C°) the rate of current density was too high and fluctuated (see **Figure 8-6**) leading to faster metal dissolution (non-homogenous dissolving), and an increase in the viscous layer interface of the polished surface. This phenomenon (high rate dissolution) tends to leave the surface with pitting and poor surface finish as well as increasing the depth of the

polished area to more than 65µm, which is not desirable due to the negative effect on the dimensional accuracy of the parts.

In this case, there are only two ways which can be used to overcome the problem (of excessive current density). The first method is to reduce the source potential or the temperature, see **Figure 8-7**. The second method is to increase the resistance of the liquid by reducing the proportion of oxalic acid (which was not within the scope of this study).On the other hand, at various process durations between 30 and 60 minutes, the reduction of both source potential from 8 to 6 volt and of temperature from 60 C° to 40C° demonstrated a significant effect, due to the change of current density properties (less fluctuation and value as shown in **Figure 8-7**). The control of these properties is critical to achieving good control of mass transport, which is required for homogenous metal/alloy dissolution during the electropolishing process which in turn results in a good surface finish, as shown in the following **Figure 8-21**.

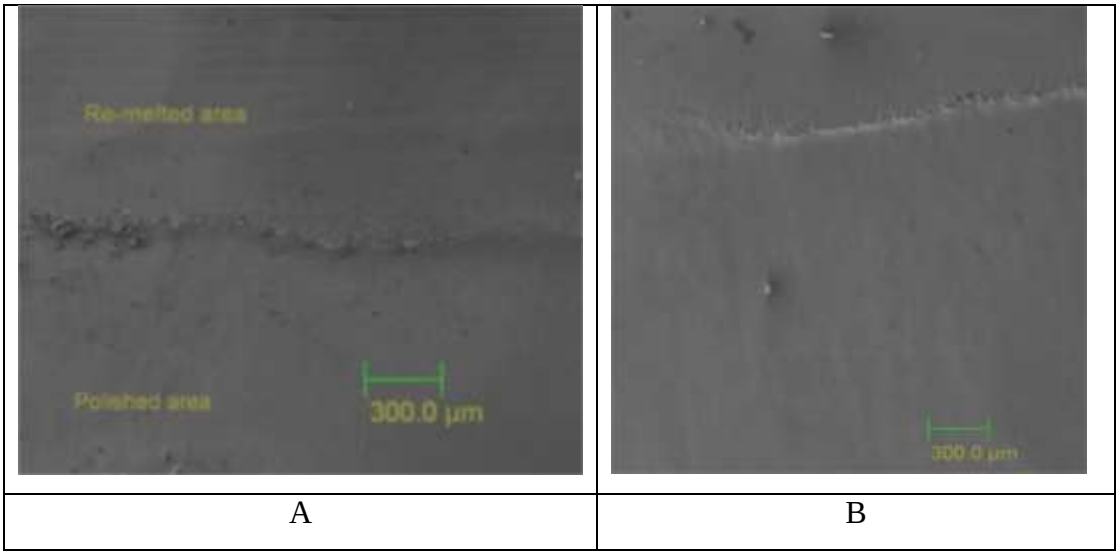

A B

Figure 8-21: SEM micrograph result of polished sample obtained at 40C°, A6 volt and B4 volt, time interval 45mint.

As show in **Figure 8-21** a reduction of current density may be favourable, by making the surface more planer and free of defects in comparison with the previous case. Some samples showed depth of polished area raised more than the required depth (less than 10 µm). In these cases, the required dimensional tolerance is not maintained.

In addition, the samples exposed to polishing at a constant 20C° and 4 volts with processing times between 30 and 60 minutes demonstrated pitting on the polished area as showed in **Figure 8-22**.

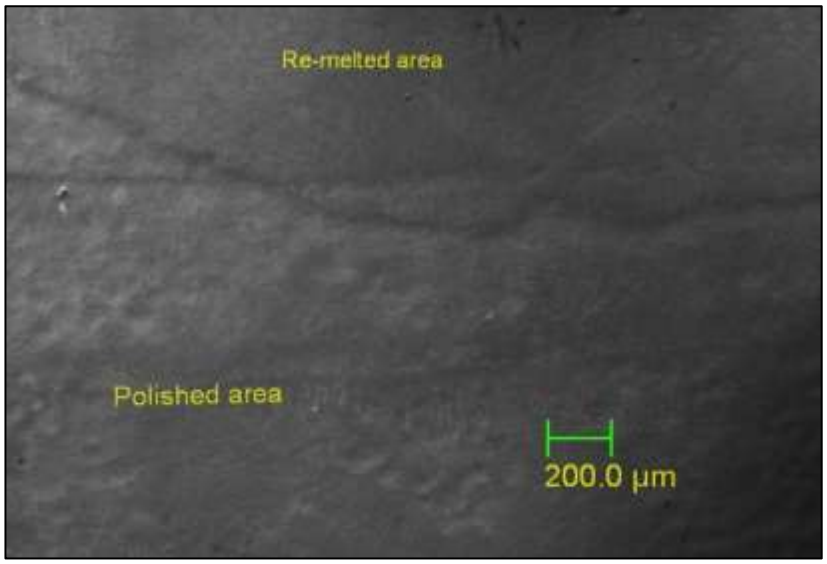

Figure 8-22 : SEM micrograph result of a polished sample obtained at 20C°, 4 volts and 45minutes.

The explanation of this phenomena (pitting) can be attributed to two different mechanisms. One possibility is that applying a potential that is less than the required potential (in this case 4 volts or less) leads to the formation of a thin viscous film on the part's surface during electropolishing. At the beginning of the process (high current density, see **Figure 8-8**) the dissolution of material results in the formation of cations that move through the viscous film to the solution, leaving vacancies at the metal-film interface. When the vacancy concentration rises too much due to the low current density, it could lead to the detachment of the ion-conducting film from the surface, due to the cations merging and forming voids. This phenomenon could be avoided by keeping the potential as high as possible, ensuring that anions in the film are kept pressed against the interface of metal-film (polished surface).

The second explanation is that pitting could be occurring by development of gas bubbles on the polished surface. In such cases, the surface could be blocked by bubbles, resulting in more dissolution of the surrounding surface, thus forming pitting defects. This problem can be overcome by preventing the bubbles from sticking to the surface, by increasing the liquid agitation (stirring), or increasing the temperature in order to improve the liquid's conductivity. However, agitation should be very carefully controlled in order to avoid disturbing the viscous layer; otherwise the problem stated earlier would apply here as well.

8.1.3.1.7 Surface brightness

The degree of surface brightness (lustre) is a useful way to determine if the electropolishing was successful in making the surface more planer and defect free.

The non-uniform thickness of the viscous layer over the material surface results in a different ohmic resistance from the cathode to the anode. This causes greater dissolution of protruding features than of features that are recessed; this allows creation of a uniform surface profile. [188]

In the case of the stainless steel (SS 316L) samples, EDX was used to track the metal /alloy surface composition before and after polishing, as shown in the following figure, **Figure 8-23**.

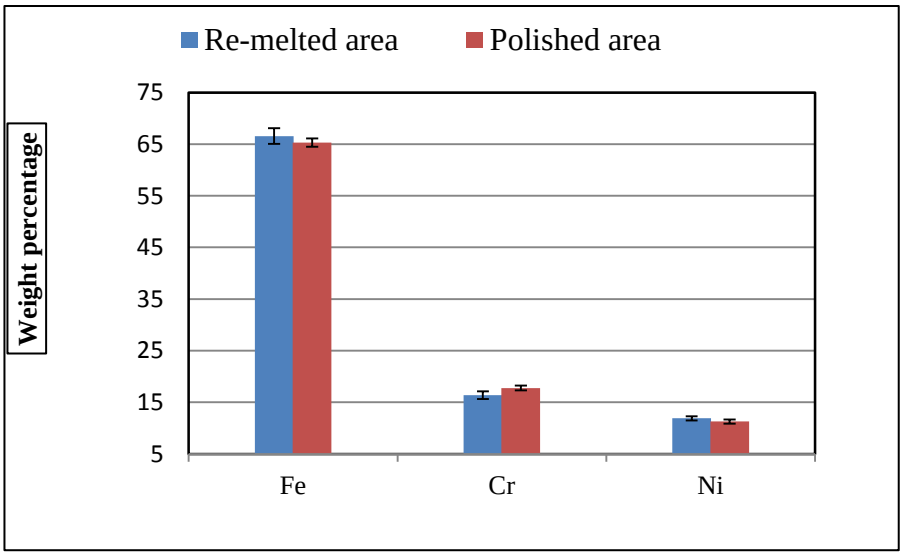

Figure 8-23: EDX spot analysis for the metal component before and after polishing (weight percentage).

The results demonstrate that the removal of the metal/alloy components from the anodic surface is non-uniform, and this produces a significant effect. The iron and nickel atoms are more easily removed from the crystal cell than the chromium atoms. Thus, it is possible to say that the electropolishing process is directed preferentially to iron and nickel, leaving the surface rich in chromium. Furthermore, the created surface with high chromium content is beneficial in some applications, especially where corrosion resistance, friction and mechanical strength are a primary concern.

.

8.1.4 Section summary

Electropolishing of SLM stainless steel parts (after re-melting) can achieve a surface texture with less than 0.5 micron *Ra*.

The significant feature of the process is its efficiency in eliminating/or suppressing a number of defects on the surface (peaks and valleys). The dissolution results for surface improvement are different due to differ of surface texture and it's in the peaks faster than the valleys, which also are proportions of the cell parameters.

Factorial investigation (DOE analysis) showed that the best results for surface roughness and minimal defects were obtained when the specimens were kept anodically at current densities associated with potential ranges between (4 to5.5 volt), maintained at (40 C°).

The overall finding through electropolishing of SLM stainless steel parts in DES type III (choline Chloride based) ionic liquids are as follows:

- It is a reliable process for polishing additive manufactured stainless steel parts and improves their surface finish more than 65% compared to the re-melted samples.
- Polishing is possible with the full range of tested process variables, but high current density can lead to non-homogeneous dissolution.
- It is a very effective process for removing the residual oxide scale formed during the re-melting process.
- The addition of a small amount of oxalic acid facilitates improving the liquid's conductivity and this encourages polishing with less potential and temperature (cyclic voltammeters results).
- The results showed that the electropolishing process is directed preferentially to iron and nickel, leaving a surface rich in chromium, which beneficial to the mechanical and chemical properties of the surfaces.
- Homogenous dissolution (when use optimum parameters) and very encouraging results to polish another metal of additive manufacture parts such as Al and Al alloys, Ti and Ti alloys, various cobalt chrome alloys etc.
- This process offers significant advantages over the current practice due to the fact that the raw materials are cheap, have high performance efficiency and are environmentally friendly.

8.2 Fatigue test

In scientific material, it is clear that metals of all kind have natural properties such as mechanical strength, strain, hardness etc. Surface roughness however, can be defined as an element of the surface's texture, which appears as peaks and valleys on the part's surface, but which also affects both product quality and mechanical performance. In such a case, surface roughness has an effect on many physical and chemical properties, such as fatigue behaviour, creep strength, corrosion resistance, light reflection, wear resistance, friction, electrical conductivity, lubrication flow, heat transmission etc. Additive manufacturing technologies such as SLM offer a new design possibility for applications in industrial sectors, but the products still suffer from drawbacks such as poor surface quality or roughness that ranges from 10-30microns. Hence, good control of the SLM process and post-processing is necessary to decrease these ranges of surface roughness. [4,189,190] Moreover, although "many results have been published regarding material options and their static mechanical properties, the knowledge about their dynamic mechanical behaviour is still low."[43]

8.2.1 Aim and objective

The aim of this study was to assess the performance (fatigue life) of SLM stainless steel (316L) parts subjected to two different stages of surface finishing method, namely laser re-melting and electropolishing. The samples had a range of surface roughness values and the importance the above stages of surface finishing in developing the parts' fatigue performance was assessed by comparing the fatigue test results.

The main objectives of these experiments were as follows

1. Implement the Fatigue tester HSM 20 to perform a fatigue test on the surveyed samples to evaluate the fatigue life.
2. Plot the S-N curve for the specimens at various amplitudes, after exposures to two stages of surface improvement (re-melting and polishing), evaluate compare the results.

8.2.2 Experimental procedure

The SLM 125 at De Montfort University was used to generate the test specimens in a vertical orientation, starting with a CAD model (created in Solidworks) to define the sample which had a specific dimension of (100 x 10 x 1) mm. Manufacturing was done following the specific steps described in section **6.1.1.** The following figures, **Figure 8-24** and **Figure 8-25** show the CAD model and the final manufacturing results.

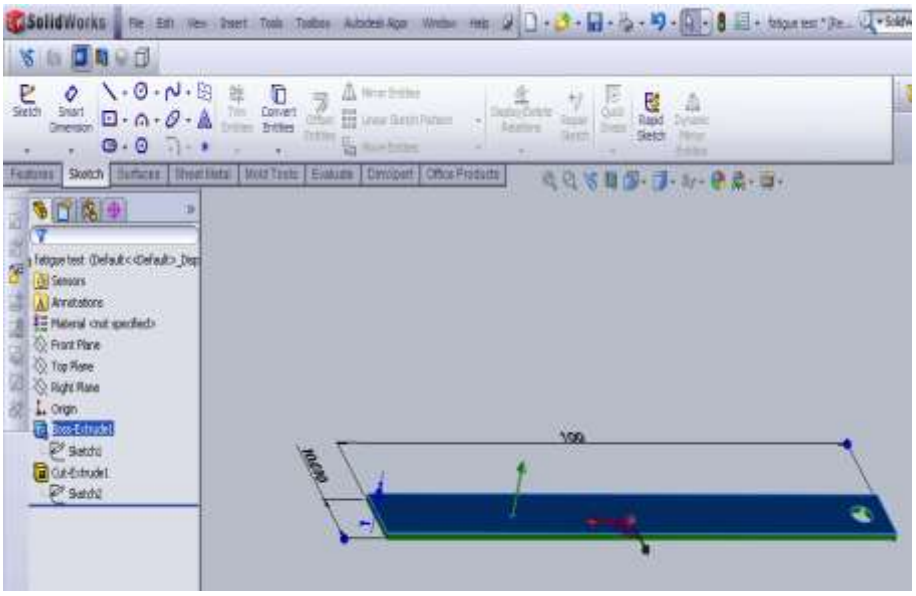

Figure 8-24: Shows the CAD model part.

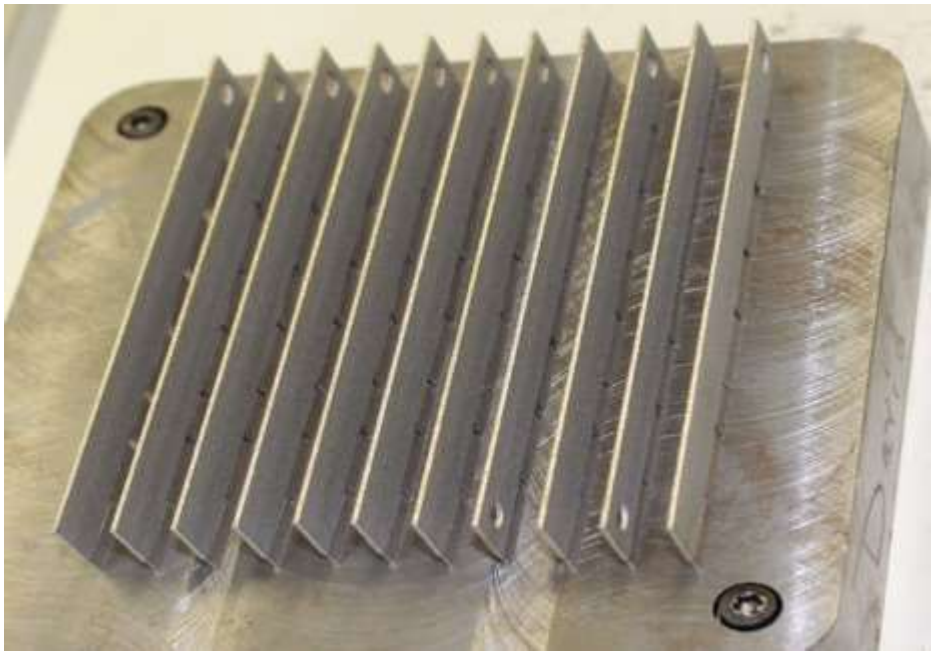

Figure 8-25: Shows the fatigue samples fabricated by SLM (125).

The samples were made and then divided into three groups. Surface roughness was measured for the three sets of SLM samples: as fabricated, re-melted samples and electropolished samples, in order to detect the manner in which the fatigue life is affected by the surface roughness. **Table 8:5** presents the details of the fabricated samples through the different stages of surface improvement.

	Part	Process parameters & Comments
As fabricated		• Laser power 200 watt • Scan speed 480mm/s • Layer thickness 50 µm • Exposure time 100 µs • Average roughness (Ra) 10 µm ± 10%
Re -melted		• Grid scanning method • Laser power 180 watt • Scan speed 400 mm/min • Beam spot size 1mm • Hatch spacing 0.4mm • Focal distance 128 mm • Average roughness(Ra) 1.4 µm ± 15%
Polished		• Cell potential 4 volts • Ethaline 5% oxalic acid as solution • Process duration 45 min • Temperature 40 C° • Average roughness(Ra) 0.4 µm ± 15%

Table 8:5: Shows the specimens' profile **(1x 10 x100)** *with the most important parameters of the surface finish improvement processes.*

The experiment was carried out through three stages as follows:

1- Generate a fatigue test on SLM samples (as fabricated material)
2- Generate a fatigue test after re-melting (as the first stage of surface roughness improvement)
3- Generate a fatigue test after re-melting and electropolishing (as a final finishing stage)

The effects of the rough surface quality on the specimen's fatigue life were studied through this experiment. Cyclic cantilever bending was imposed on the samples at 1400 rpm, when loaded. In order to simplify this process, the cyclic cantilever bending conditions were applied along the Y-axis to generate reversing stresses on each sample. The recorded results were then taken for the total number of cycles to the failure of each applied amplitude stress. Not all the samples showed fatigue failure; especially those exposed to less than 500 MPa amplitude stress. The test was usually terminated after approximately $2x10^5$ cycles.
The S-N relationship was then ascertained for the various specific loading amplitudes and created for the materials tested under the varying stress amplitude. The stress amplitude is denoted by 'S', while the number of cycles are denoted by 'N'.

As fatigue performance is severely affected by the amplitude of the cyclic load, the minimum peak stress divided by the maximum peak stress is the R ratio value, used to express the amplitude, as showing in the followed figure.

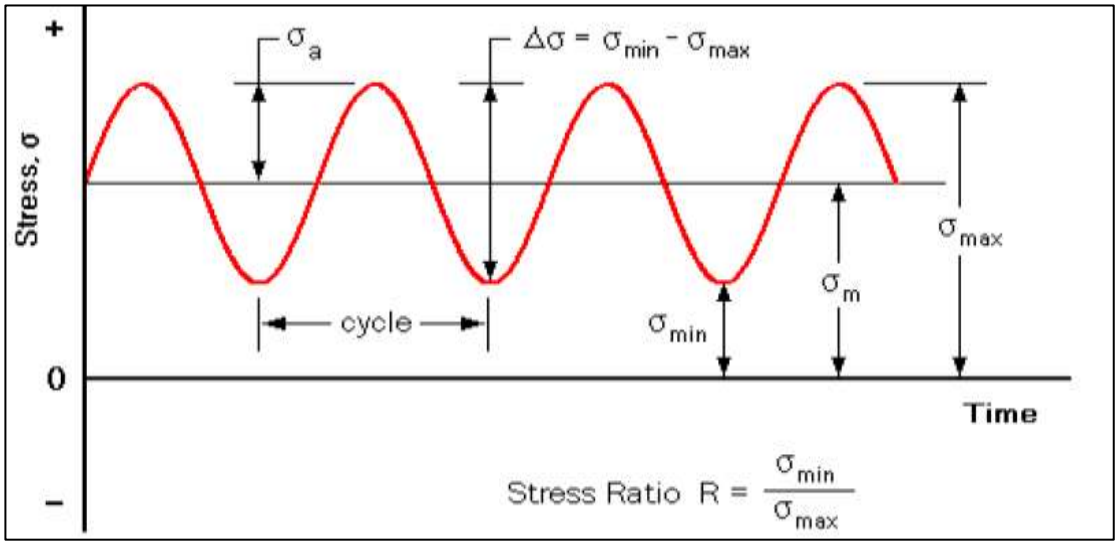

Figure 8-26 : Schematic of cyclic loading[191].

- Stress ratio $R = \sigma_{min} / \sigma_{max}$ **Equation 8-2**

It is most common to test at an R value of -1 and kept constant.

- Stress range $\Delta\sigma = \sigma_{max} - \sigma_{min}$. **Equation 8-3**

- The mean stress $\sigma_m = \frac{\sigma_{max} + \sigma_{min}}{2}$ **Equation 8-4**

The schematic of the fatigues test configuration is presented in **Figure 8-27**.

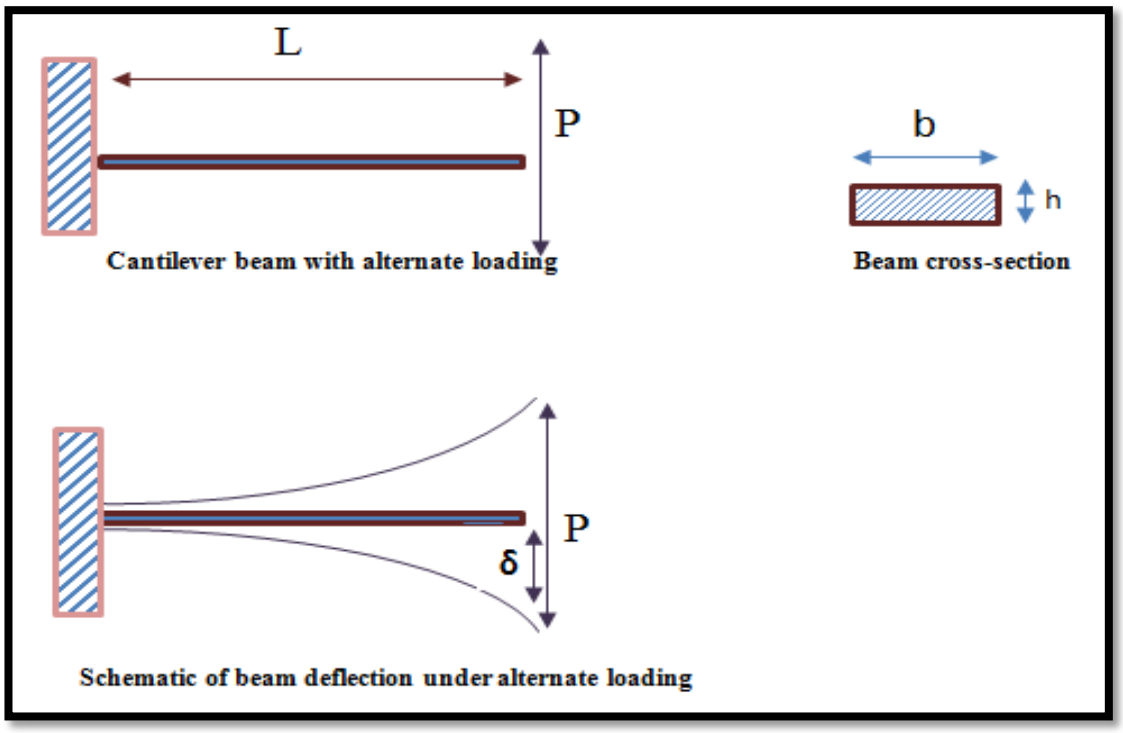

Figure 8-27: Schematic of the fatigue test configurations.

The following table, **Table 8:6** presents the fixed conditions that were set for the cantilever beam in this experiment:

Specifications	samples
The length of beam (L) = mm	40
The width of cross-section (b) = mm	10.1
The height of cross section (h) = mm	1.02
The second moment of area $I = \frac{b\,h^3}{12}$ = mm^4	0.9197

Table 8:6: Specification of tested samples.

The beam cantilever analysis uses the following equations

A) Beam deflection $\boldsymbol{\delta = \frac{P\,L^3}{3EI}}$ $(\boldsymbol{mm})$ **Equation 8-5**

Where δ is the cantilever beam deflection, E is the Young's Modulus (200MPa for stainless steel) and P is the load applied to generate the specific deflection.

B) The maximum bending moment, which occurs at the fixed end is

$\mathbf{M_{max}} = PL$ (Nm) **Equation 8-6**

C) The maximum bending stress at the fixed end is [192]

$$\boldsymbol{\sigma_{max} = \frac{M_{max} Y_{max}}{I} = \frac{M_{max}\left(\frac{h}{2}\right)}{I} = \frac{6PL}{bh^2}} \quad \textbf{(MPa)} \qquad \textbf{Equation 8-7}$$

The first specimen was tested at a high peak stress. This is the usual procedure, carried out with stresses where a failure is expected in a short number of cycles. The test stress was reduced for each successive specimen by reduction of the cantilever deflection as shown in the **Table 8:7**. The failure time of each specimen was also recorded and repeated three times in order to determine the effect of specimens' surface quality when subjected to two different stages of surface improvement. The results are shown in **Table 8:8**.

8.2.3 Experimental results

The recorded results of the cantilever data analysis are shown in the table below.

No, S	L(mm)	h(mm)	b(mm)	I(mm)^4	δ(mm)	P(N)	M max(Nm)
1	40	1.03	10.1	0.9197	9	77.599	3.10398
2	40	1.03	10.1	0.9197	8	68.978	2.75913
3	40	1.03	10.1	0.9197	7	60.356	2.41424
4	40	1.03	10.1	0.9197	6	51.733	2.06935
5	40	1.03	10.1	0.9197	5	43.111	1.72445
6	40	1.03	10.1	0.9197	4	34.489	1.37956
7	40	1.03	10.1	0.9197	3	25.866	1.03467
8	40	1.03	10.1	0.9197	2	17.244	0.68978

Table 8:7: Shows the beam cantilever data analysis.

The average recorded results of the fatigue life for each specimen are shown in the table below.

Sample number	**δ (mm)**	**σ max (MPa)**	**Fatigue life time (number of cycles)**					
			As fabricated material		Re-melted material		Polished material	
			No of cycles	Error	No of cycles	Error	No of cycles	Error
1	9	1738.2	1618	110	2046	258	2272	319
2	8	1554	3302	231	4274	408	4843	556
3	7	1351.9	5476	175	7572	746	7733	781
4	6	1158.8	9623	387	11575	979	12706	877
5	5	965.6	19067	454	24913	2328	29009	3499
6	4	772.5	42028	1787	55738	4136	63601	5305
7	3	579.4	81329	2618	103503	7551	123928	8706
8	2	386.6	200000		200000		200000	

Table 8:8 : The average results of fatigue lifetime of specimens at various amplitudes, subjected to varying surface finish techniques.

8.2.4 Discussion of results

It is important to expand the knowledge relating to the material properties of AM parts, in order to broaden the field of component application. The dynamic mechanical behaviour (fatigue life) of the SLM components was surveyed through different three stages of surface roughness as shown in the following figure, **Figure 8-28**.

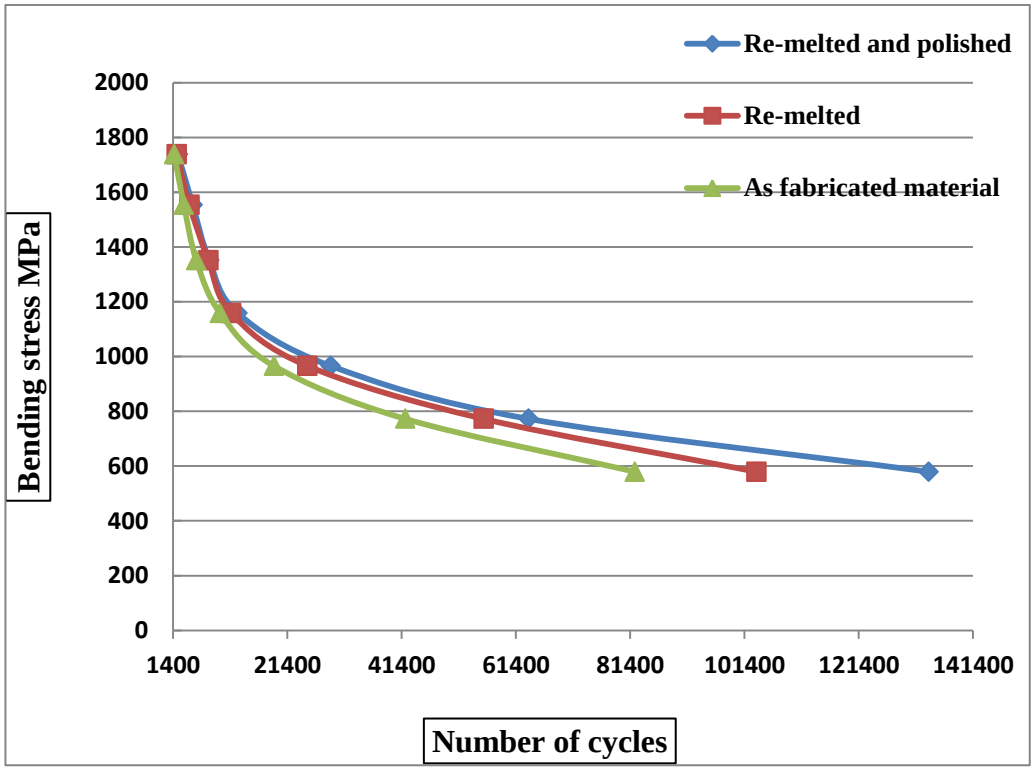

Figure 8-28: Stress-fatigue life curve for tested the material after different post-processing.

The S-N relationship was ascertained for the various loading amplitudes for the materials tested and the results showed various drawbacks in the S-N fatigue data.

The actual performance of the test specimens is not identical, but showed scattering of the fatigue lifetime even though all the specimens were made using the same parameters (see **Table 8:5**) and exposed to the same stages of surface finish improvement. The results of the surface condition (surface roughness) associated with the manufacturing process and with the post processing treatments differ from sample to sample. These differences caused an important change in the fatigue performance generated among the samples. This demonstrates that the fatigue test is highly sensitive to the number of test material.

Also, the results showed a considerable amount of scatter in the fatigue life data especially at lower stress, but recorded less scatter at high stress (see error in **Table 8:8**); this occurred in spite of the fact that the specimens were carefully made and handled.

As the results in the above plotted (S-N) relationship show, the increase of fatigue life is associated with a decrease of the loading of the specimens. At higher stress, the lifetimes are significantly lower for these materials irrespective of surface roughness, and show significant scattering for the three tests. On the other hand, the re-melted samples with surface roughness (*Ra*) 1.4 μm demonstrated significant fatigue life at lower stress and recorded about 30% improvement, in comparison with the samples fabricated by SLM and not post-processed.

In this case it is possible to say that laser re-melting plays a significant role in improving the fatigue life of SLM components, due to its ability to supress any dendrites, pitting, porosity and residual stress that may be initiated during the manufacturing process. Also, re-melting provides a homogenous surface with fine microstructure.

For the re-melted and polished specimens with surface roughness (*Ra*) 0.4μm±15%, the effect of surface quality failed to produce significant affects in the fatigue life at higher amplitudes stress, when compared to the behaviour of the re-melted material. The reason behind this may be that the fatigue life to failure is dependent on two periods, the crack initiation period and the crack growth period. The high stress of the applied load would lead to a reduced crack growth period. In the case of polished surfaces, the crack nucleation on the metal surface is very small leading to an increased initiation period at lower stress. Also, the period of crack growth will be larger extended from the period of crack initiation. An improvement in the fatigue life was recorded at lower stresses. The results presented an approximately 20% improvement compared to the re-melted samples.

8.2.4.1 Macroscopic characteristics

Initial observations of fatigue failure of SLM components can be made by the naked eye or with small magnification. This is in order to clarify details regarding crack nucleation and surface damage during loading. The details of the defects may be important for estimating the cause of fatigue failure.

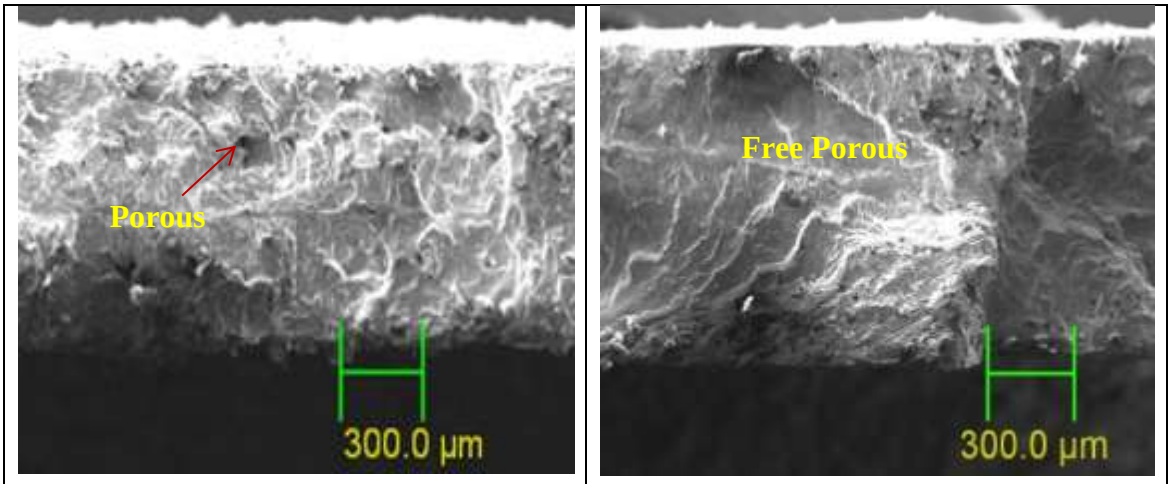

(A) As fabricated sample	(B) Re-melted sample

Figure 8-29: Micrographs of different fracture surfaces of different specimens at high stress 1350 MPa, for SLM part as fabricated (Ra= 10µm) and re-melted samples (1.5 µm).

Figure 8-29 shows the fracture surfaces of specimens observed by SEM at low magnification. The appearance of the fracture surfaces of the two specimens are different due to the different surface treatments applied. For the specimen in (
Figure 8-29-A) with surface roughness (As fabricated and Ra~10 µm) the high number of defects on the surface (roughness and pores) raise stresses at the loading point, demonstrating the reason for fast failure. In such cases cracks can be initiated at any point where high stresses are increase.

On the other hand, the possible sites for crack initiation are less for re-melted and polished samples (**Figure 8-29-B**) which had a surface roughness of (Ra~1.4 µm and 0.4 µm). Because the surfaces are flatter with reduced porosity, leading to almost equally for cracks start and also a decrease of stress raisers due to the surfaces roughness improvement.

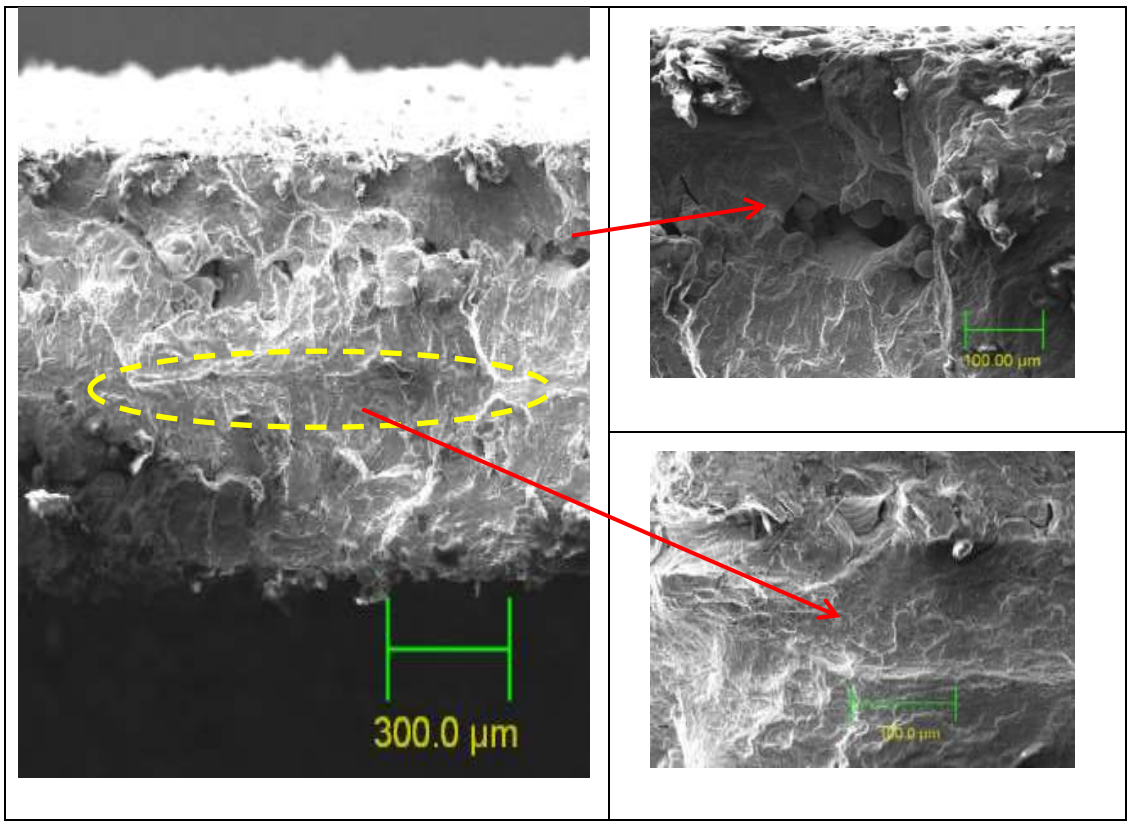

Figure 8-30 : Micrograph of fatigue fracture surfaces at high stress (1350 MPa) for SLM parts as fabricated (Ra= 10µm) demonstrating different regions of the fatigue fracture surfaces.

Figure 8-30, clearly shows that there are two regions in the fracture of the as fabricated specimen. The first region is caused by the fatigue crack growth occurring in each cycle. As a result, the fatigue occurs by micro crack growth due to the very rough surface and a number of micro-cracks can be developed successfully on the surfaces, which generate a large size of deformation. This could explain the reason for the rapid failure.

The second region of fracture surfaces occurs when the final cross section of the specimen can no longer carry the final increased load, leading to final fracture (elliptical area in **Figure 8-30**).

In case of SLM components, failures associated with fatigue and stress are commonly initiated by the roughness of the surface and porosities together with the intensity of externally applied load. These problems can be minimised by laser re-melting leading to extend the material lifetime. [193]

Alternatively, many conventional surface engineering techniques are available to solve this issue. However, unlike the rest, laser re-melting is regarded as the most suitable method due to its flexibility to improve surface roughness, eliminate porosity,

increasing fatigue and minimizing residual stress. [194, 195] This is the reason why the cracks are not easily initiated in a properly re-melted surface.

Vollertsen and co-authors have reported an improved wear and friction resistance of stainless steel material surfaces mostly attributed to residual compressive stress and porosity removal from the material, achieved through a re-melting process. [70] Furthermore, laser re-melting is considered more effective in improving the stainless steel material's surface roughness, compared to attempts to enhance corrosion and wear resistance.

8.2.5 Section summary

The effect of the surface finish on the fatigue life of the surveyed samples showed various responses. This variation are associated with the difference of surface roughness due to the stages of improvement (both re-melting and electropolishing processes).

A list of the major findings from this study can be concluded as follows:

1. The change in the deflection amplitude influenced the variability in the fatigue life of the samples.
2. The residual defects (high surface roughness and porosity) associated with manufactured 316L stainless steel specimens made by SLM, are a major determinant of fatigue life.
3. Laser re-melting improved the fatigue life of SLM stainless steel 316L parts by about 30% at lower stress (570 MPa). The reasons for this are its ability to supress surface roughness and porosity issues and to reduce residual stress.
4. Electropolishing after laser re-melting further improved fatigue life by approximately 20% at lower stresses.
5. Both re-melted and electropolished samples failed to produce a significant effect on lifetime at higher deflection amplitudes when compared with the behaviour results of the as-fabricated samples.
6. The improvement of fatigue life by laser re-melting followed by electropolishing can be attributed to reduced porosity, surface roughness and residual stress.

9.0. Conclusions

Surface finish improvement is a vital requirement for many additive manufacturing applications and it remains a challenge with most conventional methods. Proper implementation and selection of post-processing is a key factor in achieving the intended goal. The SLM technique can produce fully functional parts with several advantages, due to the possibility of producing complex shapes, with acceptable dimensional accuracy. However, the remaining porosity and poor surface roughness of SLM parts are considered major drawbacks of this technology. Therefore, the study of surface finishing methods is very important because each method has its own side effect on both the physical and chemical properties of the parts.

The main aim of the project was to improve the surface finish of Stainless Steel 316L parts produced by SLM through a novel combination of two stages of optimization. SS-316L was chosen because the AM material development has been completed on this material to obtain parameters (for a range of particle size 15 to 45μm) for part construction. The two stages of optimisation are laser re-melting followed by electropolishing, to achieve better surface roughness while maintaining dimensional tolerance. The overall conclusions can be summarized and divided into three sections:

9.1 Machine and parts characterization

From the manufacture process and analysis of results, several points can be noted as follows:

- In the case of the Renishaw SLM 125 machine, the obtained results confirmed that the machine can produce fully functional parts with repeatability, having ranges of surface finish between 10 and 20 μm.
- The simple objects (cubes) investigated in the initial stage of this work demonstrated a small increase of the top surface roughness at the right side of build area, due to the direction of argon flow from right to left.
- The density of the manufactured cubes ranged from 95% to 99%. The effect of the argon flow on the density was also assessed and the density demonstrated a decrease in value in the direction facing the argon flow.
- It was found that in the case of the inclined surfaces, an increase in build angle caused a decrease of surface roughness.

- Also, an increase in build angle led to a decrease of density. It is suggested that this is due to the increased side wall area and the porosities which are concentrated under this surface as a result of the scanning method used.
- Surface topography of SLM components showed some topographical defects and dendrites, including, balling, open porosities, peaks, valleys, powder particle agglomeration and partially melted areas. The variations of these features depend on the build process parameters and parts' build orientation.

9.2 Laser re-melting work

Through the investigation, the laser re-melting technique (as a post-process) has shown versatile capabilities for modification of the surface roughness of stainless steel 316L components made by SLM. The alterations of the response values (surface roughness) are related in the first instance to the laser energy absorbed by the modified surface. The overall findings during the experimental results can be summarised as follows:

- Laser re-melting is a capable process for metal surface modification, because it is flexible, controllable and a green process (clean for the environment).
- The microstructural dendrites, such as balling, agglomeration, waviness and the shrinkage cavities (open and closed pores) can be substantially eliminated, when employing optimal parameters, as shown by the statistical analysis of the experimental data.
- Laser re-melting is a promising technique; the results showed that an improvement of about 80% of the average roughness (*Ra*) value was obtained, in comparison to the original SLM part surface.
- In addition, external and internal (open and closed) porosity was completely eliminated by the laser re-melting; the process can provide a surface of almost 100 % density and the re-molten zone does not show any pores.
- The best surface roughness result was about1.4 μm±10% and connected with implementation of medium to low scan speeds and 180 W of laser power, to give energy density ranges between 2160 and 2700 J/cm^2.
- DOE analysis predicts that a reduction of beam spot size with a 50% overlapping factor can be expected to provide a more satisfactory surface finish.
- Laser re-melting is one of the best options, not just for surface modification, but also for improving mechanical properties. The re-melting process shows an

improvement in fatigue life of approximately 30% compared to the as-fabricated material, at low stress levels.

9.3 Electropolishing work

An improvement in surface finish of re-melted SS316L SLM parts was achieved by optimizing the parameters of a 'green' electropolishing process, for minimal environmental impact (DES type III ,Choline Chloride based ionic liquids). Based on the investigation, the overall findings can be summarized as follows:

- The results show that further improvement of the response values (*Ra*) can been obtained by electropolishing after re-melting, to about 75% improvement compared to the as-built *Ra*.
- The best response value (*Ra*) result was less than 0.5µm, obtained with a potential of 4 volt, maintained for 30mins at 40C°.
- Electropolishing is very effective at removing the residual oxide film formed during the re-melting process.
- Material dissolution is not homogenous during the process and is directed preferentially towards the iron and nickel, leaving the surface rich in chromium; this result is expected to facilitate improvement of the chemical and mechanical properties of the part's surface.
- The effects of the re-melted and polished samples' surface finish on fatigue life was positive, and showed approximately 20% improvement in fatigue life at low stresses (approximately 570MPa); this was linked to the surface improvement.
- The obtained results showed that the selected two stages (re-melting and electropolishing) are flexible methods for surface texture improvement; they are also capable of keeping the dimensional accuracy of parts within an acceptable range.

9.4 Future work

The overall aims of this project have been reached through the research and post-processing carried out. The final result (less than Ra= 0.5µm), obtained by a combination of two methods (re-melting and electropolishing) is very encouraging and competitive compared to conventional methods.

Due to the unique aspect of this combination process, it's possible to say that the results are very promising, attributable to the high capacity of the first stage of surface improvement (laser re-melting) to suppress any defects connected with SLM SS 361L manufactured parts. Also in this stage the tolerance accuracy was maintained, but there is still room for future work that can be suggested in this stage (re-melting) as follows.

- Try out laser re-melting on a multi axis machine to re-melt real components with curved surfaces, not just flat ones.
- Try with other materials such as Al and Ti alloys, various cobalt chrome alloys, other stainless steels etc.
- Try out laser re-melting with parts made by recycled powder, effect of oxides, contaminants etc.
- Try out laser re-melting with other AM parts such as SLS and EBM.

In the second stage of surface improvement, electro chemical polishing based on ionic liquid showed another potential process that can be used in AM parts to improve surface finish. It has been found that the process is very reliable on processing SS 316L when using optimal parameters. A reduction of surface finish of less than 0.5 micron is achievable, but there is still room for further work to be done, due to a number of factors that can affect the process efficiency and can be summarized as follows.

- Try different acidity concentration, type of ionic liquid and number of agitation.
- Obtain numbers for Ra for various material removals, so the user has a choice.
- These encouraging results open the door to new materials being utilized for surface improvement, such as Al and Al alloys, Ti and Ti alloys, various cobalt chrome alloys and various stainless steels etc.

The unique aspect of these applications will provide novel development applications, made possible with this technique's capability.

10.0.References

[1] T. Wohlers, Additive manufacturing state of the industry. Colorado, USA: Wohlers Associates, 2010.

[2] T. Wohlers, Additive manufacturing state of the industry. Colorado, USA: Wohlers Associates, 2012.

[3] P. Venuvinod, P. K, and M. Weiyin, "Rapid Prototyping, Laser-Based and other technologies, USA," Kluwer Acad. Publ., p. 135, 2004.

[4] E. Yasa, J.-P. Kruth, and J. Deckers, "Manufacturing by combining Selective Laser Melting and Selective Laser Erosion/laser re-melting," CIRP Ann. - Manuf. Technol., vol. 60, no. 1, pp. 263–266, Jan. 2011.

[5] K. Senthilkumaran, P. M. Pandey, and P. V. M. Rao, "Influence of building strategies on the accuracy of parts in selective laser sintering," Mater. Des., vol. 30, no. 8, pp. 2946–2954, Sep. 2009.

[6] J. Steyn, K. Naidoo, and K. Land, "Improvement of the Surface Finish obtained by Laser Ablation with a Nd : YAG Laser on Pre-ablated Tool Steel .," in International Conference on Competitive Manufacturing, 2007.

[7] E. Yasa and J. Kruth, "Applecation of laser re-melting on selective laser melting parts," Prod. Eng., vol. 6, no. 4, pp. 259–270, 2011.

[8] G. N. Levy and R. Schindel, "rapid manufacturing and rapid tooling with layer manufacturing (lm) technologies, state of the art and future perspectives," cirp ann. - manuf. technol., vol. 52, no. 2, pp. 589–609, 2003.

[9] J. Munguia, C. Riba, and J. Lloveras, "in the search of design for rapid manufacturing strategies to solve functional and geometrical issues for small series production," in international conference on engineering design, on 28 - 31 august 2007, cité des sciences et de l'industrie, paris, france.

[10] D. Thomas, "The Development of Design Rules for Selective Laser Melting," University of Wales Institute . Cardiff, 2009.

[11] G. N. Levy, R. Schindel, and J. P. Kruth, "rapid manufacturing and rapid tooling with layer manufacturing (lm) technologies, state of the art and future perspectives," cirp ann. - manuf. technol., vol. 52, no. 2, pp. 589–609, jan. 2003.

[12] N.Karapatis, J. P. S. Griethuysen, and R.Glardon, "Direct rapid tooling: A review of current research," Rapid Prototyp. J., vol. 4, no. 2, pp. 77–89, 1998.

[13] W. Meiners, "Selective Laser Melting – Additive Manufacturing for series production of the future?," 2011.

[14] K. A. Mumtaz, P. Erasenthiran, and N. Hopkinson, "High density selective laser melting of Waspaloy®," J. Mater. Process. Technol., vol. 195, no. 1–3, pp. 77–87, Jan. 2008.

[15] P. Hopkinson, N., Hague, R., & Dickens, "Rapid Manufactureing An industrial revolution the digital age," Chichester John Wiley Sons. Ltd, 2006.

[16] J.-P. Kruth, G. Levy, F. Klocke, and T. H. C. Childs, “Consolidation phenomena in laser and powder-bed based layered manufacturing,” CIRP Ann. - Manuf. Technol., vol. 56, no. 2, pp. 730–759, Jan. 2007.

[17] K. . Karunakaran, S. Suryakumar, U. Chandrasekhar, and A. Bernard, “Hybrid rapid manufacturing of metallic objects,” Int. J. Rapid Manuf., vol. 1, no. 4, pp. p. 433–455, 2010.

[18] J. Cherng, X. Shao, and C. Y, “Feature-Based Part Modeling And Process Planning For Rapid Response Manufacturing,” Comput. Ind. Eng., vol. 34, no. 2, pp. 515–530, 1998.

[19] N. Waterman and P. Dickens, “Rapid product development in the USA, Europe and Japan,” World Cl. Des. To Manuf., vol. 1, no. 3, pp. 27–36, 1994.

[20] S. L. Campanelli, N. Contuzzi, A. Angelastro, and A. D. Ludovico, “Capabilities and Performances of the Selective Laser Melting Process,” in In New Trends in Technologies, Devices, Computer, Communication and Industrial Systems, Rijeka: Sciyo, 2010, pp. 223 – 252.

[21] T. Wohlers, Additive manufacturing state of the industry. Colorado, USA: Wohlers Associates, 2009.

[22] P. M. D. Neil Hopkinson, R. J. M. Hague, Rapid Manufactureing An industrial revolution the digital age. Chichester: John Wiley & Sons. Ltd, 2006.

[23] K. Monroy, J. Delgado, and J. Ciurana, “Study of the Pore Formation on CoCrMo Alloys by Selective Laser Melting Manufacturing Process,” Procedia Eng., vol. 63, pp. 361–369, Jan. 2013.

[24] G. N. Levy and R. Schindel, “rapid manufacturing and rapid tooling with layer manufacturing (lm) technologies, state of the art and future perspectives,” vol. 52, no. 2, pp. 589–609, 2003.

[25] G. I. Gheorghe and I. Drstvensek, “The New Generation of Rapid Prototyping Technology in Selective Laser Sintering for Metal Powders,” in International Conference on Innovations, Recent Trends and Challenges in Mechatronics, Mechanical Engineering and New High-Tech Products Development,Bucharest, 8-9 October 2009.

[26] D. Buchbinder, H. Schleifenbaum, S. Heidrich, W. Meiners, and J. Bültmann, “High Power Selective Laser Melting (HP SLM) of Aluminum Parts,” Phys. Procedia, vol. 12, pp. 271–278, Jan. 2011.

[27] K. A. Ghany and S. F. Moustafa, “Comparison between the products of four RPM systems for metals,” Rapid Prototyp. J., vol. 12, no. 2, pp. 86–94, 2006.

[28] P. Rochus, J.-Y. Plesseria, M. Van Elsen, J.-P. Kruth, R. Carrus, and T. Dormal, “New applications of rapid prototyping and rapid manufacturing (RP/RM) technologies for space instrumentation,” Acta Astronaut., vol. 61, no. 1–6, pp. 352–359, Jun. 2007.

[29] G. N. Levy, R. Schindel, and J. P. Kruth, “rapid manufacturing and rapid tooling with layer manufacturing (lm) technologies, state of the art and future perspectives,” cirp ann. - manuf. technol., vol. 52, no. 2, pp. 589–609, jan. 2003.

[30] J.-P. Kruth, M. C. Leu, and T. Nakagawa, “Progress in Additive Manufacturing and Rapid Prototyping,” CIRP Ann. - Manuf. Technol., vol. 47, no. 2, pp. 525–540, Jan. 1998.

[31] ConceptLaser, “laser systems/concept-lasere.” [Online]. Available: http://www.estechnology.co.uk/lasersystems/concept-laser?gclid=CPebh4_Y3bsCFZPItAodWBIA4g. [Accessed: 28-Dec-2013].

[32] Renishaw, “Selective Laser Melting.” [Online]. Available: http://www.renishaw.com/mtt-group/us/selective-laser-melting.html. [Accessed: 29-Dec-2013].

[33] Directindustry, “phenix systems and rapid prototyping machines by laser sintering.” [Online]. Available: http://www.directindustry.com/prod/phenix-systems/rapid-prototyping-machines-by-laser-sintering-13610-311742.html. [Accessed: 15-Dec-2013].

[34] EOS, “Metal laser sintering systems.” [Online]. Available: http://www.eos.de/en/products/systems-equipment/metal-laser-sintering-systems.html. [Accessed: 18-Dec-2013].

[35] E. Yasa, J. Deckers, T. Craeghs, M. Badrossamay, and J.-P. Kruth, “Improving productivity rate in SLM of Commercial Steele Powders,” RAPID. Schumberg, IL, USA, pp. 1–13, 2009.

[36] A. B. Spierings, N. Herres, G. Levy, and C. Buchs, “Influence of the particle size distribution on surface quality and mechanical properties in additive manufactured stainless steel parts,” pp. 1–10.

[37] J. Kruth, M. Badrossamay, E. Yasa, J. Deckers, L. Thijs, and J. Van Humbeeck, “Part and material properties in selective laser melting of metals,” in 16th International Symposium on Electromachining (ISEM XVI). shanghai-china.19-23 April 2010.

[38] S. L. Campanelli, N. Contuzzi, A. Angelastro, and A. D. Ludovico, “Capabilities and Performances of the Selective Laser Melting Process,” 1994.

[39] D. Thomas, “The Development of Design Rules for Selective Laser Melting,” University of Wales. Cardiff Institute, 2009.

[40] S. A. McKelvey and A. Fatemi, “Surface finish effect on fatigue behavior of forged steel,” Int. J. Fatigue, vol. 36, no. 1, pp. 130–145, Mar. 2012.

[41] E. S. Gadelmawla, M. M. Koura, T. M. A. Maksoud, I. M. Elewa, and H. H. Soliman, “Roughness parameters,” J. Mater. Process. Technol., vol. 123, no. 1, pp. 133–145, Apr. 2002.

[42] B. P. Novovic D, Dewes RC, Aspinwall DK, Voice W, “Effect of machined topography and integrity on fatigue life,” Int J Mach Tools Manuf, vol. 44, pp. 125–34, 2004.

[43] A. B. Spierings, T. L. Starr, and K. Wegener, “fatigue performance of additive manufactured metallic parts,” Rapid Prototyp. J., vol. 19, no. 2, pp. 88 – 94, 2013.

[44] P. Properties and L. S. Parts, “Mechanical and Physical Properties – A Way to assess quality of Laser Sintered Parts,” Energy, vol. 2200, pp. 239–251, 2011.

[45] W. Morgan, R., Sutcliffe, C.J., O’Neill, “Density analysis of direct metal laser re-melted 316L stainless steel cubic primitives,” J. Mater. Sci., vol. 39, no. 4, pp. 1195–1205, 2004.

[46] W. Zhao, H.D., Wang, F., Li, Y.Y., Xia, “Experimental and numerical analysis of gas entrapment defects in plate ADC12 die castings,” J. Mater. Process. Technol., vol. 219, no. 9, pp. 4537– 4542, 2009.

[47] L. C. Zhang, D. Klemm, J. Eckert, Y. L. Hao, and T. B. Sercombe, “Manufacture by selective laser melting and mechanical behavior of a biomedical Ti–24Nb–4Zr–8Sn alloy,” Scr. Mater., vol. 65, no. 1, pp. 21–24, Jun. 2011.

[48] J. Parthasarathy, B. Starly, S. Raman, and A. Christensen, “Mechanical evaluation of porous titanium (Ti6Al4V) structures with electron beam melting (EBM),” J. Mech. Behav. Biomed. Mater., vol. 3, no. 3, pp. 249–259, 2010.

[49] C. Sanz, V. G. Navas, O. Gonzalo, and G. Vansteenkiste, “Study of surface integrity of rapid manufacturing parts after different thermal and finishing treatments,” Procedia Eng., vol. 19, pp. 294–299, Jan. 2011.

[50] S. Kumar and J. Kruth, “Effects of bronze infiltration into laser sintered metallic parts,” Mater. Des., vol. 28, pp. 400–4007, 2007.

[51] L. Z. Wang RJ, Wang L, Zhao L, “Influence of process parameters on part shrinkages in SLS,” Ant J Adv Manuf. Technol., vol. 33, pp. 498–504, 2007.

[52] K. Zhang, W. Liua, and X. Shanga, “Research on the processing experiments of laser metal deposition shaping,” Opt. Laser Technol., vol. 39, pp. 549–557, 2007.

[53] O. Rehme and C. Emmelmann, “Reproducibility for properties of Selective Laser Melting products,” in Proc. III International WLT-Conference on Lasers in Manufacturing, Munich, 2005.

[54] Y. Yang and J.-Y. Huang, “Direct manufacturing of Cu-based alloy parts by selective laser melting,” Chin. Opt. Lett, vol. 5, pp. 37–40, 2007.

[55] K. O. and M. Shiomi, “Flexible manufacturing of metallic products by selective laser melting ofpowder,” Int. J. Mach. Tool Des. Res, vol. 46, pp. 1188–1193, 2006.

[56] L. E. Murr, S. a Quinones, S. M. Gaytan, M. I. Lopez, a Rodela, E. Y. Martinez, D. H. Hernandez, E. Martinez, F. Medina, and R. B. Wicker, “Microstructure and mechanical behavior of Ti-6Al-4V produced by rapid-layer manufacturing, for biomedical applications.,” J. Mech. Behav. Biomed. Mater., vol. 2, no. 1, pp. 20–32, Jan. 2009.

[57] R. Boyer and W. Collings, Materials Properties Handbook: Titanium Alloys, ASM International. 1994.

[58] K. Kempen, E. Yasa, L. Thijs, J.-P. Kruth, and J. Van Humbeeck, “Microstructure and mechanical properties of Selective Laser Melted 18Ni-300 steel,” Phys. Procedia, vol. 12, pp. 255–263, Jan. 2011.

[59] K. Zhang, S. Wang, W. Liu, and X. Shang, “Characterization of stainless steel parts by Laser Metal Deposition Shaping,” Mater. Des., vol. 55, pp. 104–119, Mar. 2014.

[60] R. Hasan, R. Minesa, and P. Fox, “Characterisation of selectively laser melted Ti-6A1-4V micro-lattice strut, Procedia Engineering,” vol. 10, pp. 536–541, 2011.

[61] D. Thomas, “The Development of Design Rules for Selective Laser Melting,” University of Wales Institute, Cardiff, 2009.

[62] F. Vollertsen, “Mechanisms and models for laser forming, in: Proc. of the LANE’94,” pp. 345 – 359, 1994.

[63] M. Shiomi, K. Osakada, K. Nakamura, T. Yamashita, and F. Abe, “Residual Stress within Metallic Model Made by Selective Laser Melting Process,” CIRP Ann. - Manuf. Technol., vol. 53, no. 1, pp. 195–198, 2004.

[64] J.-P. Kruth, J. Deckers, E. Yasa, and R. Wauthle, “Assessing and comparing influencing factors of residual stresses in selective laser melting using a novel analysis method,” Proc. Inst. Mech. Eng. Part B J. Eng. Manuf., vol. 226, no. 6, pp. 980–991, Mar. 2012.

[65] X. R. Zhang Y, Chen J, Lei W, “Effect of laser surface melting on friction and wear behaviour of AM50 magnesium alloy,” Surf. Coatings Technol., vol. 202, no. 14, pp. 3175–3179, 2008.

[66] K. P. Karunakaran, S. Suryakumar, V. Pushpa, and S. Akula, “Robotics and Computer-Integrated Manufacturing Low cost integration of additive and subtractive processes for hybrid layered manufacturing,” Robot. Comput. Integr. Manuf., vol. 26, no. 5, pp. 490–499, 2010.

[67] H. Schleifenbaum, W. Meiners, K. Wissenbach, and C. Hinke, “CIRP Journal of Manufacturing Science and Technology Individualized production by means of high power Selective Laser Melting,” CIRP J. Manuf. Sci. Technol., vol. 2, no. 3, pp. 161–169, 2010.

[68] T. Mushambadope, “Improving Surface Finish of SLM Metal Parts,” De-Montfort University, Leicester, 2011.

[69] D. Lacalle, A. Lamikiz, J. A. Sa, and L. N. Lo, “Improving the surface finish in high speed milling of stamping dies,” J. Mater. Process. Technol., vol. 123, pp. 292–302, 2002.

[70] F. Vollertsen, K. Partes, and J. Meijer, “State of the art of Laser Hardening and Cladding,” in Proc. of the Third Int. WLT-Conf. on Lasers in Manufacturing, Munich, AT-Verlag, Munich, AT-Verlag, 2005.

[71] A. Temmler, E. Willenborg, and K. Wissenbach, “Design Surfaces by Laser Remelting,” Phys. Procedia, vol. 12, pp. 419–430, Jan. 2011.

[72] E. Yasa, J. Deckers, and J.-P. Kruth, “Experimental investigation of Laser Surface Re-melting for the Improvement of Selective Laser Melting Process,” in Proc. of 14èmes Assises Européennes du prototypage Rapide ,Paris,France, 2009.

[73] A. Lamikiz, J. A. Sánchez, L. N. López de Lacalle, and J. L. Arana, “Laser polishing of parts built up by selective laser sintering,” Int. J. Mach. Tools Manuf., vol. 47, no. 12–13, pp. 2040–2050, Oct. 2007.

[74] J. A. Ramos, J. Murphy, K. Wood, D. L. Bourell, and J. J. Beaman, “Surface Roughness Enhancement of Indirect-SLS Metal Parts by Laser Surface Polishing,” Mech. Eng., pp. 28–38, 2001.

[75] A. Lamikiz, J. A. Sánchez, L. N. López de Lacalle, and J. L. Arana, “Laser polishing of parts built up by selective laser sintering,” Int. J. Mach. Tools Manuf., vol. 47, no. 12–13, pp. 2040–2050, Oct. 2007.

[76] J. A. Ramos, J. Murphy, K. Wood, D. L. Bourell, and J. J. Beaman, “Surface Roughness Enhancement of Indirect-SLS Metal Parts by Laser Surface Polishing,” Mech. Eng., pp. 28–38, 2001.

[77] P. Kruth, B. Vandenbroucke, I. Vaerenbergh, and I. Naert, “Rapid Manufacturing of Dental Prostheses by means of Selective Laser Sintering/Melting,” in in Proceedings of the AFPR,S4, 2005.

[78] E. Tolksdorf and N. Westkamper, “Developments in Precision Product Manufacturing for Laser-Sintering,” in presentation, Third International Conference Multiscale Materials Modeling, Freiburg, Germany, September, 2006.

[79] K. A. Mumtaz, P. Erasenthiran, and N. Hopkinson, “High density selective laser melting of Waspaloy®,” J. Mater. Process. Technol., vol. 195, no. 1–3, pp. 77–87, Jan. 2008.

[80] K. Murali, a. . Chatterjee, P. Saha, R. Palai, S. Kumar, S. . Roy, P. . Mishra, and A. R. Choudhury, “Direct selective laser sintering of iron–graphite powder mixture,” J. Mater. Process. Technol., vol. 136, no. 1–3, pp. 179–185, May 2003.

[81] M. Ashok, S. Biswajit, M. Jibitesh, T. Ghosh, S. Sengupta, P. K. Dan, E. Yasa, J. Kruth, T. Rajmohan, K. Palanikumar, A. Ammeri, W. Hachicha, H. Chabchoub, F. Masmoudi, D. I. B, and G. K. Purohit, “Advances in Production Engineering & Management,” vol. 6, no. 4, 2011.

[82] W. Morgan, R., Sutcliffe, C. J. and O’Neill, “Density analysis of direct metal laser remelted 316L stainless steel cubic primitives,” J. Mater. Sci., vol. 39/4, pp. 1195– 1205, 2004.

[83] E. Tolksdorf and N. Westkamper, “Developments in Precision Product Manufacturing for Laser-Sintering,” in presentation, Third International Conference Multiscale Materials Modeling, Freiburg, Germany, September, 2006.

[84] F. Braga, R. Marques, E. Filho, and A. Guastaldi, “Surface modification of Ti dental implants by Nd:YVO4 laser irradiation,” Appl. Surf. Sci., vol. 253, pp. 9203–9208, 2007.

[85] R. Freeman, “The flowability of powder-an empirical,” in International conference on powder and bulk solides handling, london 13-15.06.2005.

[86] J. Karlsson, A. Snis, H. Engqvist, and J. Lausmaa, “Characterization and comparison of materials produced by Electron Beam Melting (EBM) of two different Ti–6Al–4V powder fractions,” J. Mater. Process. Technol., vol. 213, no. 12, pp. 2109–2118, Dec. 2013.

[87] B. Zhang, H. Liao, and C. Coddet, “Effects of processing parameters on properties of selective laser melting Mg–9%Al powder mixture,” Mater. Des., vol. 34, pp. 753–758, Feb. 2012.

[88] B. Engel and D. L. Bourell, “Titanium alloy powder preparation for selective laser sintering,” Rapid Prototyp. J., vol. 6, no. 2, pp. 97–106, 2000.

[89] N. Raghunath and P. M. Pandey, “Improving accuracy through shrinkage modelling by using Taguchi method in selective laser sintering,” Int. J. Mach. Tools Manuf., vol. 47, no. 6, pp. 985–995, May 2007.

[90] P. M. Lonardo and a. a. Bruzzone, “Measurement and Topography Characterisation of Surfaces Produced by Selective Laser Sintering,” CIRP Ann. - Manuf. Technol., vol. 49, no. 1, pp. 427–430, Jan. 2000.

[91] A. Jhon, C.Ion, Laser processing of ingineering material, prenciples,provedure and industryal application. Oxford: Elsevier Butterwoth-Heinemann, 2005.

[92] K. Shahzad, J. Deckers, S. Boury, B. Neirinck, J.-P. Kruth, and J. Vleugels, “Preparation and indirect selective laser sintering of alumina/PA microspheres,” Ceram. Int., vol. 38, no. 2, pp. 1241–1247, Mar. 2012.

[93] W. M. Steen, Laser material processing, Second Edi. London: Springer- Verlag, 1998.

[94] E. Yasa and J.-P. Kruth, “Investigation of laser and process parameters for Selective Laser Erosion,” Precis. Eng., vol. 34, no. 1, pp. 101–112, Jan. 2010.

[95] C. Hu and T. N. Baker, “Overlapping Laser Tracks to Produce a Continuous Nitrided Layer in Ti–6Al–4V Alloy,” J. Mater. Sci., vol. 32, no. 11, pp. 2821–2826, 1997.

[96] N. B. Harimkar and P. D. Sandip, LASER FABRICATION AND MACHINING OF MATERIALS. Springer Science + Business Media, LLC, 2008.

[97] E. Yasa and J.-P. Kruth, “Investigation of laser and process parameters for Selective Laser Erosion,” Precis. Eng., vol. 34, no. 1, pp. 101–112, Jan. 2010.

[98] T. Sudarshan and J. Stiglich, Surface Modification Technologies. ASM International Surface Engineering, 2006.

[99] B. Benhabib, Manufacturing Design, Production,Atumationand integration. New York: Marcl Dekker,Inc, 2003.

[100] B. Robert and Ross, Handbook of Metal Treatments and Testing, 2 Edi. London,UK: Chapman and Holl, 1988, p. 592.

[101] R. Thompson, Manufacturing Processes For Design Professionals. London,UK: Thames & Hudson, 2007, p. 192.

[102] C. Accelerated, V. Surface, F. Cavsf, and E. Juergenfischermailundedu, “Basic studies concerning chemically accelerated vibratory surface finishing (cavsf),” pp. 1–23.

[103] L. J. Durney, Grahams Electroplating Engineering Handbook, 4th ed. New York: Springer, New York, 1984, p. 790.

[104] J. D. Spencer, R. C. Cobb, and P. M. Dickens, “vibratory finishing of stereolithography parts,” pp. 27–39.

[105] J. Thomas, T. Drozda, and C. Wick, Tool and Manufacturing Engineers Handbook, 4th Editio. Society of Manufacturing Engineers, 1983.

[106] Campbellmachinery, “MEDIBLAST 1400,” 2013. [Online]. Available: http://www.campbellmachinery. [Accessed: 21-Nov-2013].

[107] S. Siddique, “Investigation of High Cycle Fatigue Behavior of Laser Additive Manufactured Ti-6Al-4V,” pp. 1–2.

[108] J. V. Skoff, “Understanding Residual Stress Effects and Corrective Action for Die Casting Tools,” Badger Met. Tech Inc, 2007.

[109] A. Yoshida, Y. Ohue, and M. Seki, “INFLUENCE OF SHOT PEENING ON SURFACE DURABILITY,” pp. 1–8, 2003.

[110] A. H. Shinohara and P. L. Guzzo, “A Comparative Study on Ultrasonic Machining of Hard and Brittle Materials,” vol. 26, no. 1, pp. 18–21, 2004.

[111] D. Shi and I. Gibson, “Surface Finishing of Selective Laser Sintering Parts with Robot,” pp. 27–36.

[112] B. Paul, F. M. Cmfge, S. P. Manager, R. Systems, and A. Manufacturing, “Robotic Finishing Applications.”

[113] R. Noorani, Y. Farooque, and T. Ioi, “Improving Surface Roughness of CNC Milling Machined Aluminum Samples Due to Process Parameter Variation,” pp. 1–7.

[114] Tct-magazine, “Matsuura-lumex-avance-25-laser-sintering-milling-hybrid.” [Online]. Available: http://www.tctmagazine.com/additive-manufacturing/matsuura-lumex-avance-25-laser-sintering-milling-hybrid/. [Accessed: 03-Dec-2013].

[115] K. Boivie, K. Sørby, V. Brøtan, and P. Ystgaard, “development of a hybrid manufacturing cell ; integration of additive manufacturing with cnc machining background : industrial case studies case 1 : insert for a bracket to an office chair,” pp. 153–163, 2011.

[116] M. Rivette, J.-Y. Hacoët, and P. Mognol, “A graph-based methodology for hybrid rapid design,” Proc. Inst. Mech. Eng. Part B J. Eng. Manuf., vol. 221, no. 4, pp. 685–697, Jan. 2007.

[117] P. Mognol, L. Jégou, M. Rivette, and B. Furet, “High speed milling, electro discharge machining and direct metal laser sintering: A method to optimize these processes in hybrid rapid tooling,” Int. J. Adv. Manuf. Technol., vol. 29, no. 1–2, pp. 35–40, Dec. 2005.

[118] Kennametal Extrude Hone, “Machining Processes,” 2013. [Online]. Available: http://www.kennametal.com/kennametal/en/products/precision-surface-management/machining-processes.html. [Accessed: 20-Nov-2013].

[119] M. R. Sankar, V. K. Jain, and J. Ramkumar, “Abrasive flow machining (AFM): An Overview 2 . Classification of AFM machine,” pp. 1–9.

[120] BEST in CLASS, “Micro Machining Process,” 2013. [Online]. Available: www.MMPtechnology.comp, pdf . [Accessed: 22-Nov-2013].

[121] M. Jobin, R. Foschia, and G. Vansteenkiste, “Topography and optical properties of polished laser melted Maraging Steel , Cobalt Chromium and Inconel 718,” 2009.

[122] C. Gohn and Ion, Laser Processing Of Engineering Materials: Principles, Procedure and Industrial Application. Elsevier B.H.Uk, 2005.

[123] D. Rajiv Asthana, Ashok Kumar, Narendra B, Material Processing and Manufacturing Science. Springer, New York, 2006, p. 363.

[124] H. Dong, Laser surface modification of Surface Engineering of Light Alloys - Aluminium, Magnesium and Titanium Alloys. Woodhead Publishing Ltd, 2010, p. 680.

[125] E. Yasa, J. Deckers, and J.-P. Kruth, "The investigation of the influence of laser re-melting on density, surface quality and microstructure of selective laser melting parts," Rapid Prototyp. J., vol. 17, no. 5, pp. 312–327, 2011.

[126] E. Ukar, a. Lamikiz, L. N. López de Lacalle, D. del Pozo, and J. L. Arana, "Laser polishing of tool steel with CO2 laser and high-power diode laser," Int. J. Mach. Tools Manuf., vol. 50, no. 1, pp. 115–125, Jan. 2010.

[127] K. Vutova and V. Donchev, "Electron Beam Melting and Refining of Metals: Computational Modeling and Optimization," Materials (Basel)., vol. 6, no. 10, pp. 4626–4640, Oct. 2013.

[128] R. Sautebin, H. Froidevaux, and D. Landolt, "theoretical and experimental modeling of surface leveling in ecm under primary current distribution conditions," j. electrochem. soc., vol. 27, no. 5, p. . 1096–1100, 1980.

[129] C. Clerc, M. Datta, and D. Landolt, "On the theory of anodic levelling: model experiments with triangular nickel profiles in chloride solution," Electrochim. Acta, vol. 29, no. 10, pp. 1477–1486.`, 1984.

[130] D. Landolt, "Fundamental aspects of electropolishing. Electrochimica Acta," Electrochim. Acta, vol. 32, no. 1, pp. 1–11, 1987.

[131] M. Datta and D. Landolt, "Surface Brightening during High Rate Nickel Dissolution in Nitrate Electrolytes," J. Electrochem. Soc., vol. 122, no. 11, pp. 1466–1472, 1975.

[132] M. Datta and D. Landolt, "On the role of mass transport in high rate dissolution of iron and nickel in ECM electrolytes—I. Chloride solutions," Electrochim. Acta, vol. 25, no. 10, pp. 1255–1262, 1980.

[133] A. P. Abbott, I. Dalrymple, F. Endres, and D. R. Macfarlane, "Why use Ionic Liquids for Electrodeposition ?," vol. 01, 2008.

[134] H. Jacquet, Figous P, and A, "in French Patent, F. patent, Editor," 1930.

[135] T. Welton, "Room-temperature ionic liquids. Solvents for synthesis and catalysis," Chem. Rev., vol. 99, no. 8, pp. 2071–2083, 1999.

[136] M. C. Buzzeo, R. G. Evans, and R. G. Compton, "Non-haloaluminate room-temperature ionic liquids in electrochemistry--a review.," Chemphyschem, vol. 5, no. 8, pp. 1106–20, Aug. 2004.

[137] A. P. Abbott, G. Capper, K. J. McKenzie, and K. S. Ryder, "Voltammetric and impedance studies of the electropolishing of type 316 stainless steel in a choline chloride based ionic liquid," Electrochim. Acta, vol. 51, no. 21, pp. 4420–4425, Jun. 2006.

[138] A. P. Abbott, G. Capper, K. J. McKenzie, A. Glidle, and K. S. Ryder, "Electropolishing of stainless steels in a choline chloride based ionic liquid: an electrochemical study with surface characterisation using SEM and atomic force microscopy.," Phys. Chem. Chem. Phys., vol. 8, no. 36, pp. 4214–4221, Sep. 2006.

[139] J. A. Whitehead, G. A. Lawrance, and A. McCluskey, "?Green? leaching: recyclable and selective leaching of gold-bearing ore in an ionic liquid," Green Chem., vol. 6, no. 7, p. 313, 2004.

[140] S. Zhang and Z. Conrad, "Novel properties of ionic liquids in selective sulfur removal from fuels at room temperature. Green Chemistry," vol. 4, pp. 376–379, 2002.

[141] C. Zhao and X. Qu, "Recent progress in G-quadruplex DNA in deep eutectic solvent.," Methods, vol. 64, no. 1, pp. 52–8, Nov. 2013.

[142] Q. Zhang, K. D. Vigier, S. Royer, and F. Jerome, "Deep eutectic solvents: syntheses, properties and applications," Chem. Soc. Rev, vol. 41, pp. 7108–7146, 2012.

[143] A. P. Abbott, D. Boothby, G. Capper, D. L. Davies, and R. Rasheed, "Deep Eutectic Solvents Formed Between Choline Chloride and Carboxylic Acids," J. Am. Chem. Soc, vol. 126, p. 9142, 2004.

[144] M. H. Chakrabarti, F. Sabri, and M. Inas, "Prospective of applying ionic liquids and deep eutectic solvents for renewable energy storage by means of redox flow batteries& quot," in Renewable and Sustainable Energy Reviewes,2014.

[145] A. P. Abbott, G. Capper, D. L. Davies, R. Rasheed, and V. Tambyrajah, "Novel Solvent Properties of Choline Chloride/ Urea Mixtures," Chem. Commun, vol. 70, 2003.

[146] A. P. Abbott and K. J. McKenzie, "Physical Chemistry Chemical Physics," vol. 8, pp. 4265 – 4279, 2006.

[147] S. Mohan, D. Kanagaraj, R. Sindhuja, S. Vijayalakshmi, and N. Renganathan, "Electropolishing of stainless steel - a review," Inst Met Finish, vol. 79, pp. 140–142, 2001.

[148] K. S. Ryder, "Introduction to Ionic Liquids," 2008.

[149] K. S. Ryder, "New Sustainable Electrolytes for Metal Finishing and Electropolishing (aerospace investment castings)."

[150] A. . Abbott, K. . Ryder, and U. Konig, "Electrofinishing of metals using eutectic based ionic liquids," Inst. Met. Finish, vol. 86, pp. 196–204, 2008.

[151] G. Beddoes, J . Parr, Introduction to Stainless Steels, 3 ed. Ohio, USA: ASM International, Materials Park., 1999.

[152] R. Lula and et al, Stainless steel. American Society for Metals, 1986.

[153] K. H. Lo, C. H. Shek, and J. K. L. Lai, "Recent developments in stainless steels," Mater. Sci. Eng. R Reports, vol. 65, no. 4–6, pp. 39–104, May 2009.

[154] Y. Wang, J. Bergstrom, and C. Burman, "Characterization of an iron-based laser-sintered material," J. Mater. Process. Technol., vol. 172, no. 1, pp. 77–87, 2006.

[155] S. Kumar, "SELECTIVE LASER SINTERING : RECENT ADVANCES," in In: Proceedings of the CSIR National Laser Centre, 2008.

[156] O. Rehme, "Selective Laser Melting of Honeycombs with Negative Poisson's Ratio," J. Laser Micro/Nanoengineering, vol. 4, no. 2, pp. 128–134, Aug. 2009.

[157] Renishaw, “Laser melting systems,” 2013. [Online]. Available: http://www.renishaw.com/en/laser-melting-systems--15240. [Accessed: 15-Dec-2013].

[158] R. Tosi, “Re-manfacture of high value products by combining laser cladding, inspection and machining system,” De Montfort University, 2012.

[159] J. Jones, P. Mcnutt, R. Tosi, C. Perry, and D. Wimpenny, “Remanufacture of turbine blades by laser cladding , machining and in-process scanning in a single machine,” in 23rd Annual International Solid Freeform Fabrication Symposium, 2012 Austin, TX, USA. : University of Texas, pp. 821-827.

[160] MTC, “RECLAIM MACHINE,” 2013. [Online]. Available: http://www.the-mtc.org/case-studies/reclaim. [Accessed: 01-Oct-2013].

[161] M. Antoni. N.Vaxevanidis, “Multi-parameter Identification and control of turned surface textures, International Journal of,” Int. J. Adv. Manuf. Technol., vol. 29, no. 1&2, pp. 118–128, 2006.

[162] B. Mac Donald, “Components & Elements of Surface Topography.” [Online]. Available: http://www.bcmac.com/PDF_files/Surface Finish 101.pdf. [Accessed: 20-Nov-2013].

[163] M. Badrossamay and et al, “layer formation studies in selective laser melting of steel powder,” Univ. Leeds, UK.

[164] M. Zecchino et al, “Characterizing Surface Quality : Why Average Roughness is Not Enough,” pp. 1–4.

[165] G. Bradshaw, “Non-Contact Surface Geometry Measurement Techniques,” 1999.

[166] M. Visscher and K. G. Struik, “Optical profilornetry and its application to mechanically inaccessible surfaces Part I : Principles of focus error detection,” vol. 16, no. 3, 1994.

[167] Zeta Instruments, “Zeta-20 True Color 3D Optical Profiler,” 2013. [Online]. Available: http://www.zeta-inst.com/page/zeta-20-optical-profiler. [Accessed: 10-Nov-2013].

[168] H. Warriner, “Veeco Optical Profilers,” pp. 1–6, 2008.

[169] J. Goldstein, Scanning electron microscopy and x-ray microanalysis. Kluwer Academic/Plenum Publishers, New York, 2003.

[170] Nanomicroscopy Center, “Zeiss EVO HD15,” 2013. [Online]. Available: http://nmc.aalto.fi/en/instruments/sem/evo-hd/. [Accessed: 03-Dec-2013].

[171] H. Limited, “Alternating Bending Fatigue Machine instruction manual HSM20.”

[172] P. Sciences, “Microstructure , Texture and Mechanical Property Evolution during Additive Manufacturing of Ti6Al4V Alloy for Aerospace Applications School of Materials,” 2012.

[173] S. A. McKelvey and A. Fatemi, “Surface finish effect on fatigue behavior of forged steel,” Int. J. Fatigue, vol. 36, no. 1, pp. 130–145, Mar. 2012.

[174] K. A. Mumtaz and N. Hopkinson, “Journal of Materials Processing Technology Selective Laser Melting of thin wall parts using pulse shaping,” vol. 210, pp. 279–287, 2010.

[175] Z. Yang and E. Al, Convention machining method for rapid prototyping direct manufacture. 2009.

[176] A. H. Nickel, D. M. Barnett, and F. B. Prinz, “Thermal stresses and deposition patterns in layered manufacturing,” Mater. Sci. Eng. A, vol. 317, no. 1–2, pp. 59–64, Oct. 2001.

[177] M. Elsen, V. F. Al-Bender, and J. Kruth, “Application of dimensional analysis to selective laser melting,” Rapid Prototyp. J., vol. 14, no. 1, pp. pp.15–22, 2008.

[178] W. Zhao, H. D., Wang, F., Li , Y. Y. and Xia, “Experimental and numerical analysis of gas entrapment defects in plate ADC12 die castings,” J. Mater. Process. Technol., vol. 219/9, pp. 4537–4542, 2009.

[179] C. B. Roundy and D. Ph, “Current Technology of Laser Beam Profile Measurements 2 . Laser Beam Properties 2 . 1 Unique Laser Beam Characteristics,” no. 435, pp. 1–43.

[180] K. J.-P. Yasa E, Deckers J, “The Investigation of the Influence of Laser Re-Melting on Density, Surface Quality and Microstructure of Selective Laser Melting Parts,” Rapid Prototyp. J., vol. 17, no. 5, pp. 312–327, 2011.

[181] D. B. Evans Chikarakara, Sumsun Naher, “process mapping of laser surface modification of aisi 316l stainless steel for biomedical applications evans chikarakara, sumsun naher, dermot brabazon,” pp. 1–5.

[182] E. Yasa and J. Deckers, “Experimental investigation of Laser Surface Re-melting for the Improvement of Selective Laser Melting Process,” in Proc. of 14èmes Assises Européennes du prototypage Rapide ,Paris,France, 2009.

[183] F. Endres, Douglas MacFarlane, and Andrew Abbott, Electrodeposition from Ionic Liquids. John Wiley & Sons. Copyright., 2008, p. 410.

[184] A. P. Abbott, N. Dsouza, P. Withey, and K. S. Ryder, “Electrolytic processing of superalloy aerospace castings using choline chloride-based ionic liquids,” Trans. Inst. Met. Finish., vol. 90, no. 1, pp. 9–14, Jan. 2012.

[185] E.-S. Lee, “Machining Characteristics of the Electropolishing of Stainless Steel (STS316L),” Int. J. Adv. Manuf. Technol., vol. 16, no. 8, pp. 591–599, Jul. 2000.

[186] G. R. Kamat, “Pitting and its Control During Electropolishing of Stainless Steel,” Trans. Indian Inst. Met., vol. 40, no. 4, p. page 343–345, 1987.

[187] C.-C. Shih, C.-M. Shih, Y.-Y. Su, L. H. J. Su, M.-S. Chang, and S.-J. Lin, “Effect of surface oxide properties on corrosion resistance of 316L stainless steel for biomedical applications,” Corros. Sci., vol. 46, no. 2, pp. 427–441, Feb. 2004.

[188] D. Landolt, P. . Chauvy, and O. Zinger, “Electrochemical micromachining, polishing and surface structuring of metals: fundamental aspects and new developments,” Electrochim. Acta, vol. 48, no. 20–22, pp. 3185–3201, Sep. 2003.

[189] T. R. Thomas, Surface roughness,Imperial College Press, 2nd ed. London, 1999.

[190] U. Khandy, “optimization of surface roughness removal, department of mechanical engineering, national institute of technology. India.,” 2009.

[191] N. E. Dowling, “Mean Stress Effects in Stress-Life and Strain-Life Fatigue,” Tech. Pap., no. 2004–01–2227, Apr. 2004.

[192] J. M. Gere and B. J. Goodno, Mechanics of Materials, 8th ed. Canada: Cengage Learning, 2012.

[193] J. a. Francis, H. K. D. H. Bhadeshia, and P. J. Withers, “Welding residual stresses in ferritic power plant steels,” Mater. Sci. Technol., vol. 23, no. 9, pp. 1009–1020, Sep. 2007.

[194] D. S. Mankar and P. V Jadhav, “effect of surface roughness on fatigue life of machined component of inconel 718,” Int. J. Fatigue, vol. 41, no. 6, pp. 141–149, 2007.

[195] G. Haijun, R. Khalid, and S. Thomas, “Effect of Defects on Fatigue Tests of As-Built Ti-6Al-4V Parts Fabricated By Selective Laser Melting,” in Solid Freeform Fabrication Symposium, 2012, pp. 499–506.

11.0.Appendixes

11.1 Appendix (1)

Material in use (Stainless steel 316L powder)

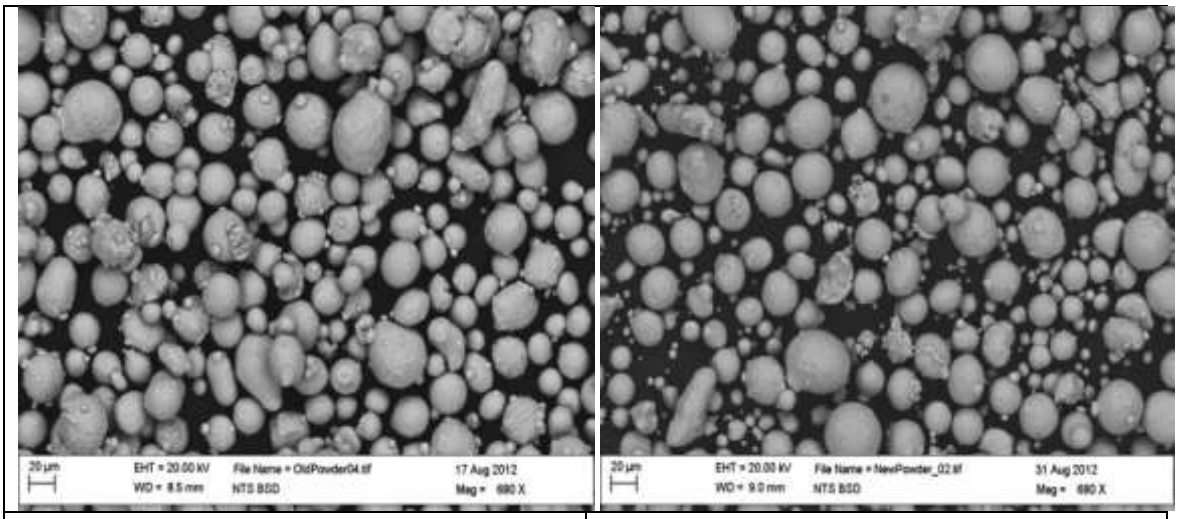

New powder	Recycle powder

SEM results show the different between new and recycle powder

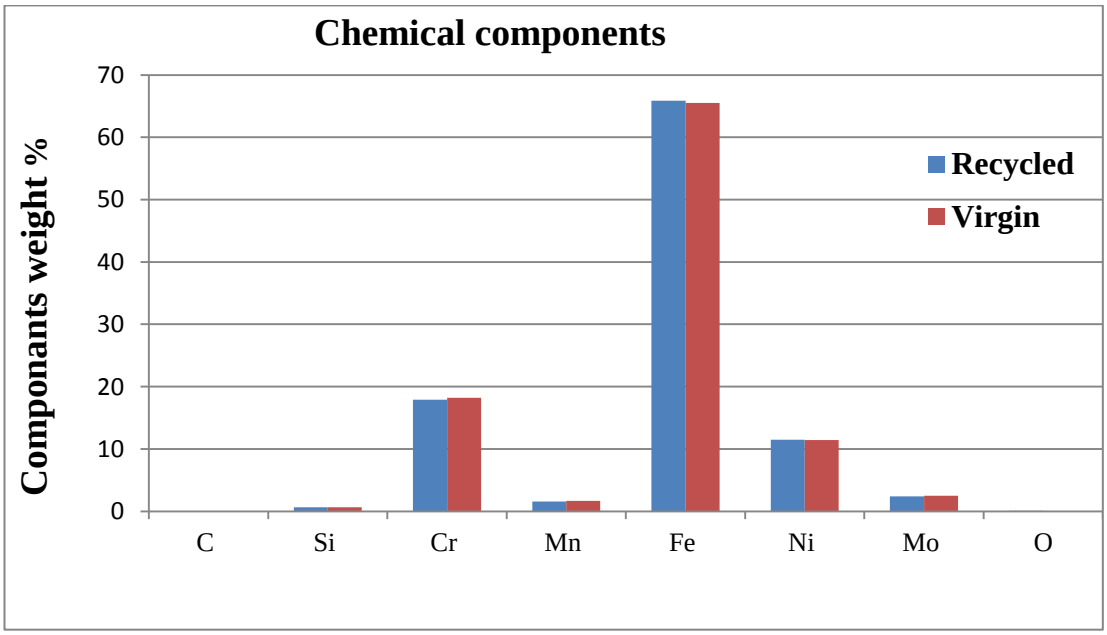

Show the different between new and recycle powder

Preliminarily experimental trail

Cubes results

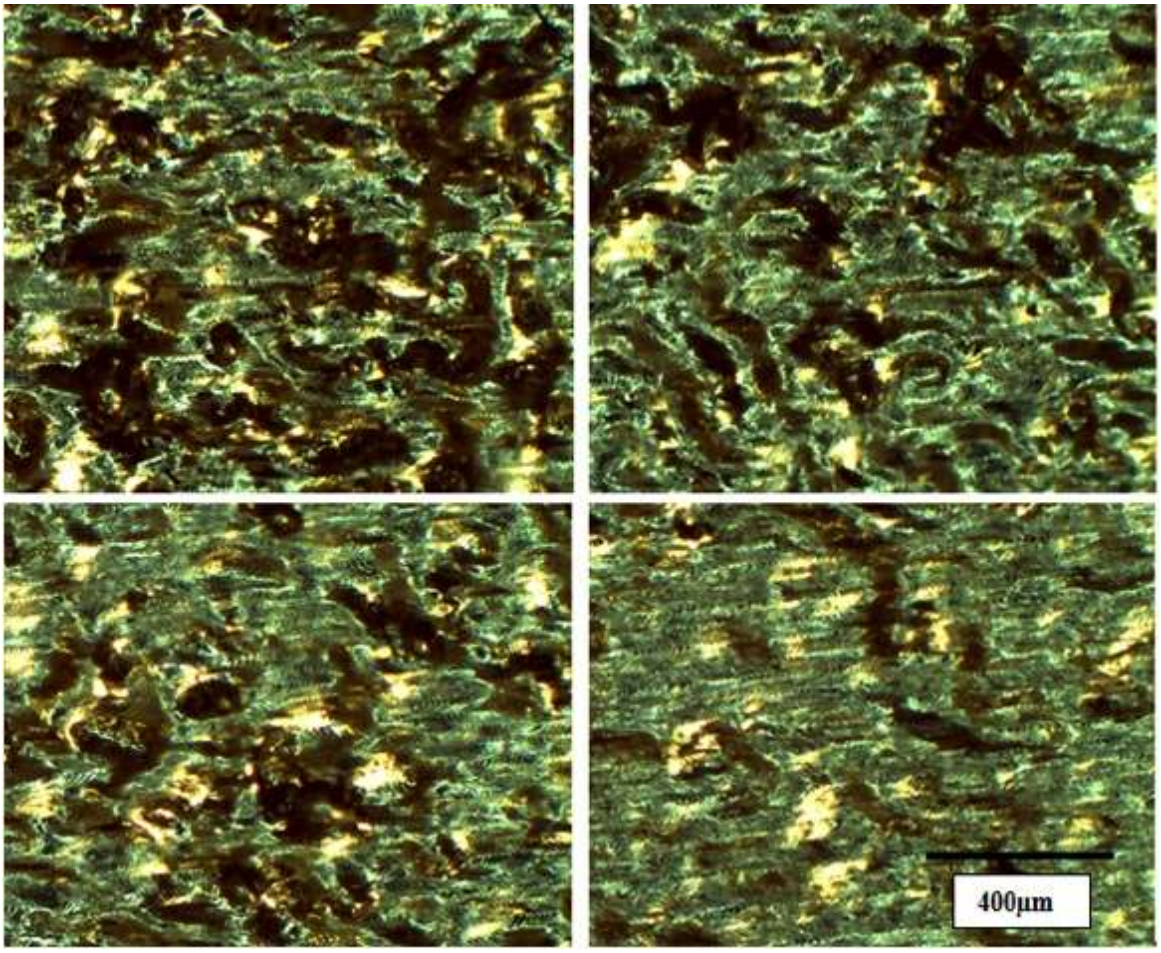

Surface topography of cubes

No, substrate	A	B	C	D	E	Average	Error
substrate 1	15.208	15.6396	16.0166	15.822	16.1498	15.7672	0.367618
substrate 2	15.3392	15.808	15.6308	15.826	16.0352	15.72784	0.260283
substrate 3	15.2248	16.078	15.8006	15.52	16.2946	15.7836	0.427149
substrate 4	15.1092	15.5066	15.648	16.167	16.324	15.75096	0.495891
substrate 5	15.096	15.0502	15.292	16.1992	16.43	15.61348	0.651574

Average surface roughness of cubes (μm)

Sub	A1	B1	C1	D1	E1	A3	B3	C3	D3	E3
Row1	7.515	7.524	7.581	7.721	7.584	7.638	7.429	7.634	7.466	7.545
Row2	7.712	7.478	7.486	7.471	7.432	7.693	7.4915	7.606	7.716	7.612
Row3	7.615	7.703	7.657	7.727	7.612	7.709	7.653	7.682	7.559	7.422
Row4	7.658	7.628	7.531	7.468	7.642	7.472	7.612	7.573	7.572	7.487
Row5	7.613	7.663	7.624	7.486	7.429	7.561	7.497	7.482	7.491	7.559
Average	7.622	7.599	7.575	7.574	7.539	7.614	7.536	7.595	7.560	7.525
Error	0.072	0.094	0.069	0.136	0.101	0.098	0.092	0.074	0.097	0.0723

Density measurement of cubes (gm/cm^3)

Second Experimental trail (Bench marks results)

	A1	B1	C1	D1	A2	B2	C2	D2	B3	C3	D3
Top (16)mm	15.62	15.67	14.40	15.62	13.73	13.89	14.75	16.53	15.56	16.54	15.66
Top (12)mm	14.52	15.60	14.67	16.53	15.67	15.19	16.71	14.60	16.40	16.53	14.87
Top (8)mm	15.09	13.75	13.80	15.5	15.08	15.67	14.21	15.57	15.76	15.63	14.72
Top (4)mm	14.60	14.31	15.19	15.42	13.96	15.4	13.94	16.66	15.02	14.76	14.15

Average surface roughness (Ra) results of top surface with different hight

	A1	B1	C1	D1	A2	B2	C2	D2	B3	C3	D3
Angle 60°	10.93	10.97	12.62	12.61	10.91	11.38	12.27	12.21	11.66	11.97	11.97
Angle 45°	12.48	12.68	13.05	13.91	11.53	12.93	12.81	13.11	13.23	12.90	13.11
Angle 30°	12.68	12.41	13.56	14.72	13.04	13.62	13.83	13.57	13.22	13.91	14.75
Angle 15°	15.65	14.80	15.05	15.63	15.18	15.67	17.02	15.47	15.44	16.02	15.54

Average surface roughness (Ra) results of different inclination surfaces

METAL POWDER INDUSTRIES FEDERATION

Method for

Determination of Density of Compacted or Sintered Powder Metallurgy (PM) Products

MPIF Standard 42
Issued 1980, Revised 1986, 1997, 2004, 2008
(Formerly included in Standards 08, 13, 16 and 35)

STANDARD 42

1. SCOPE

1.1 This standard describes a method using Archimedes' principle for measuring the density of powder metallurgy products having interconnected porosity. It is applicable to both green specimens and sintered parts. The density of PM products is expressed in grams per cubic centimeter.

1.1.1 For a test method to determine the density of impermeable materials, see MPIF Standard 54.

1.2 Green Density, (ρ_g), is the mass per unit volume of an unsintered PM part or test specimen. Normally the green density is determined on PM parts for quality control tests and for determining the compressibility of powders and mixes.

1.3 Dry Density, (ρ_d), is the mass per unit volume of a sintered, non-oil-impregnated PM part. This term is synonymous with sintered density.

1.4 Wet Density, (ρ_l), is the mass per unit volume of a sintered PM part impregnated with oil or other non-metallic lubricant. This term is synonymous with impregnated density. Normally the density of sintered bearings are reported in this way since they are supplied and used fully oil-impregnated.

1.5 *This standard may involve hazardous materials, operations and equipment. This standard does not purport to address all of the potential safety problems associated with its use. It is the responsibility of the user of this standard to establish appropriate safety and health practices and to determine the applicability of regulatory limitations prior to use.*

2. APPARATUS

2.1 Analytical Balance - A precision analytical balance that will permit readings within 0.01% of the test specimen mass as shown in Table 1.

Table 1. Balance Sensitivity

Specimen Mass (g)	Minimum Balance Sensitivity (g)
1 to < 10	0.0001
10 to < 100	0.001
100 to < 1,000	0.01
1,000 to <10,000	0.1

2.2 Container: A beaker or vessel, suitable for holding water, of sufficient capacity to immerse specimens of various sizes as illustrated in Figure 1.

2.3 Test Specimen Support for Weighing in Water: Two typical arrangements are shown in Figure 2. The suspension wire may be twisted around the test specimen or the test specimen may be supported in a wire basket. For either arrangement, a single corrosion resistant wire, e.g. austenitic stainless steel, copper, or nichrome should be used for the basket and suspension wire. The recommended diameter of suspension wire to be used for various mass ranges is shown in Table 2.

Table 2. Wire Diameter Recommendations

Specimen Mass	Wire Diameter
1 to < 50 grams	0.12 mm [48 gauge] (0.005 inch)
50 to < 200 grams	0.25 mm [35 gauge] (0.010 inch)
200 to < 600 grams	0.40 mm [28 gauge] (0.015 inch)
600 grams & above	0.50 mm [25 gauge] (0.020 inch)

2.4 Water: Distilled or deionized and preferably degassed water to which 0.05 to 0.1 volume % of a wetting agent has been added.

The values, ρ_w, shown in Table 3 should be used for the density of distilled water.

2.5 Thermometer: To determine water temperature to the nearest 1 °C (2 °F).

2.6 Impregnating oil with a kinematic viscosity of 65 cSt maximum (300 SUS) at 38 °C (100 °F). In the case of oil impregnated PM bearings or parts, match the oil that was used to impregnate the part originally.

3. TEST SPECIMEN

3.1 The test specimen shall be a PM part or a group of parts or a section of a part with a minimum mass of 1 gram.

4. DETERMINATION OF GREEN DENSITY

4.1 This procedure is used to determine the green density of unsintered specimens. In order to determine accurately the volume of the test piece by water displacement in conducting this test the specimens are oil impregnated or the pores are filled with a suitable material. The density determined is an average of the metal and any solid lubricant originally present.

4.2 Determine the mass of the green test specimen

Table 3. Effect of Temperature on Water Density

Temperature	ρ_w	Temperature	ρ_w
°C	g/cm³	°F	g/cm³*
15	0.9991	60	0.9990
15.5	0.9990	61	0.9989
16	0.9989	62	0.9988
16.5	0.9988	63	0.9987
17	0.9988	64	0.9986
17.5	0.9987	65	0.9985
18	0.9986	66	0.9984
18.5	0.9985	67	0.9983
19	0.9984	68	0.9982
19.5	0.9983	69	0.9981
20	0.9982	70	0.9980
20.5	0.9981	71	0.9978
21	0.9980	72	0.9977
21.5	0.9979	73	0.9975
22	0.9978	74	0.9974
22.5	0.9976	75	0.9973
23	0.9975	76	0.9972
23.5	0.9974	77	0.9970
24	0.9973	78	0.9969
24.5	0.9972	79	0.9967
25	0.9970	80	0.9966
25.5	0.9969	81	0.9964
26	0.9968	82	0.9963
26.5	0.9966	83	0.9961
27	0.9965	84	0.9959
27.5	0.9964	85	0.9958
28	0.9962	86	0.9956
28.5	0.9961		
29	0.9959	*Interpolated from °C data	
29.5	0.9958		
30	0.9956		

The values of ρ_w shown are taken from, "Metrological Handbook 145, Quality Assurance for Measurements", 1990, NIST, pp. 9,10, and represent the values in air at one atmosphere pressure.

in grams to the precision stated in Table 1. This is mass A.

4.3 Oil impregnate the part by either of the following procedures:

4.3.1 **Preferred Procedure:** Immerse the specimen in the impregnating oil at room temperature. Reduce the pressure over the specimen to 7 kPa (1 psi) or less for 30 minutes, then increase the pressure back to atmospheric pressure for a period of at least 30 minutes keeping the specimen immersed during the entire period.

4.3.2 **Alternative Procedure:** Immerse the specimen, for at least 4 hours, in the impregnating oil that has been heated to a temperature of 82 ° ± 5 °C (180 ° ± 10 °F). Cool by immersing in oil held at room temperature for at least 10 minutes.

4.4 Remove excess surface oil by wiping gently with an absorbent, lintless medium. Take care not to extract the oil absorbed within the part. Determine the mass of the oil impregnated test specimen in grams to the accuracy stated in Table 1. This is mass B.

4.5 Support the container of water over the pan of the balance using a suitable bridge as shown in Figure 1a. Take care to ensure that the bridge does not restrict free movement of the balance pan. The container of water may also be supported below the balance for weighing larger specimens if the balance has a lower beam hook for this purpose. See Figure 1b. If this arrangement is used, shield the weighing system, including the wire, from the effect of air drafts.

4.6 Suspend the test specimen support with the test specimen from the beam hook of the balance. The water should cover any wire twists and the specimen support basket by at least 6 mm (0.25 inch) to minimize the effect of surface tension forces on the weighing. Take care to ensure that the test specimen and specimen support hang freely from the balance beam hook, are free of air bubbles when immersed in the water and are at the same temperature as the water and balance. Take care to ensure that the surface of the water is free of dust particles.

4.7 Weigh the test specimen and the specimen support immersed in water. This is mass C.

4.8 Remove the test specimen. Weigh the test specimen support immersed in water at the same depth as before. This is mass E. Take care to ensure that the suspension support is free of air bubbles and that the suspension wire is not immersed below its normal hanging depth as a change in depth will change the measured mass.

4.9 Measure the temperature of the water to the nearest 1 °C (2 °F) and record its density ρ_w at that temperature, from Table 3.

4.10 Calculate the green density from the following formula:

$$\text{Green Density, } (\rho_g), = \frac{A\rho_w}{B-(C-E)}$$

5. DETERMINATION OF DRY DENSITY

5.1 This procedure is used to determine the dry density of PM components. In order to determine accurately the volume of the test piece by water displacement, the specimens are oil impregnated or the pores are filled with a suitable material.

5.2 Determine the mass of the dry test piece in grams to the precision stated in Table 1. This is mass A.

NOTE 1—Oil impregnated specimens are to be free of lubricant for determining mass A. Remove the oil in a Soxhlet apparatus using a suitable solvent, such as petroleum ether. After extraction, residual solvent shall be removed by heating specimens at 120 °C (250 °F) for 1 hour. Alternate extraction and drying shall be continued until the dry mass, A, is constant to 0.05%

NOTE 2—A practical and fast method of oil removal for most materials is to heat the specimen in a protective atmosphere in the temperature range of 426 to 648 °C (800 to 1200 °F). This method, which results in values in close agreement with those obtained using the Soxhlet apparatus, may be used if agreed upon by both parties. This method also is applicable to sintered aluminum materials if the temperature does not

exceed 540 °C (1000 °F).

5.3 Oil impregnate the part by either of the following procedures:

5.3.1 **Preferred Procedure:** Immerse the specimen in the impregnating oil at room temperature. Reduce the pressure over the sample to 7 kPa (1 psi) or less for 30 minutes, then increase the pressure back to atmospheric pressure for a period of at least 30 minutes keeping the specimen immersed during the entire period.

5.3.2 **Alternative Procedure:** Immerse the specimen, for at least 4 hours, in the impregnating oil that has been heated to a temperature of 82 ° ± 5 °C (180 ° ± 10 °F). Cool by immersing in oil held at room temperature for at least 10 minutes.

5.4 Remove excessive oil by wiping gently with an absorbent, lintless medium. Take care not to extract oil absorbed within the part. Determine the mass of the oil impregnated test specimen in grams to the accuracy stated in Table 1. This is mass B.

5.5 Support the container of water over the pan of the balance using a suitable bridge as shown in Figure 1a. Take care to ensure that the bridge does not restrict free movement of the balance pan. The container of water may also be supported below the balance for weighing larger specimens if the balance has a lower beam hook for this purpose. See Figure 1b. If this arrangement is used, shield the suspension wire between the container of water and the bottom of the balance from the effect of air drafts.

5.6 Suspend the test specimen support with the test specimen from the beam hook of the balance. The water should cover any wire twists and the specimen support basket by at least 6 mm (0.25 inch) to minimize the effect of surface tension forces on the weighing. Take care to ensure that the test specimen and specimen support hang freely from the balance beam hook, are free of air bubbles when immersed in the water and are at the same temperature as the water and balance. Take care to ensure that the surface of the water is free of dust particles.

5.7 Weigh the test specimen and the specimen support immersed in water. This is mass C.

5.8 Remove the test specimen. Weigh the test specimen support immersed in water at the same depth as before. This is mass E. Take care to ensure that the suspension support is free of air bubbles and that the suspension wire is not immersed below its normal hanging depth as a change in depth will change the measured mass.

5.9 Measure the temperature of the water to the nearest 1 °C (2 °F) and record its density ρ_w, at that temperature, from Table 3.

5.10 Calculate the dry density from the following formula:

$$\text{Dry Density, } (\rho_s), = \frac{A\rho_w}{B-(C-E)}$$

6. DETERMINATION OF WET DENSITY

6.1 This procedure is used to determine the wet or oil impregnated density of PM bearings or parts. The density determined is the average of the solid material and the oil present in the voids.

NOTE 3—Ensure that the specimen is fully oil impregnated.

6.2 Oil impregnate the part by either of the following procedures:

6.2.1 **Preferred Procedure:** Immerse the specimen in the impregnating oil at room temperature. Reduce the pressure over the sample to 7 kPa (1 psi) or less for 30 minutes, then increase the pressure back to atmospheric pressure for a period of at least 30 minutes keeping the specimen immersed during the entire period. If the oil that had been used originally to impregnate the part had a viscosity higher than 65 cSt (300 SUS) then the oil shall be heated to a temperature of 82 ° ± 5 ° C (180 ° ± 10 °F).

6.2.2 **Alternative Procedure:** Immerse the specimen, for at least 4 hours, in the impregnating oil that has been heated to a temperature of 82 ° ± 5 ° C (180 ° ± 10 °F). Cool by immersing in oil held at room temperature for at least 10 minutes.

6.3 Remove excess surface oil by wiping gently with an absorbent, lintless medium. Take care not to extract the oil absorbed within the part.

6.4 Determine the mass of the oil impregnated test piece in grams to the precision stated in Table 1. This is mass B.

6.5 Support the container of water over the pan of the balance using a suitable bridge as shown in Figure 1a. Take care to ensure that the bridge does not restrict free movement of the balance pan. The container of water also may be supported below the balance for weighing larger specimens if the balance has a lower beam hook for this purpose. See Figure 1b. If this arrangement is used, shield the weighing system, including the wire, from the effect of air drafts.

6.6 Suspend the test specimen support with the test specimen from the beam hook of the balance. The water should cover any wire twists and the specimen support basket by at least 6 mm (0.25 inch) to minimize the effect of surface tension forces on the weighing. Take care to ensure that the test specimen and specimen support hang freely from the balance beam hook, are free of air bubbles when immersed in the water and are at the same temperature as the water and balance. Take care to ensure that the surface of the water is free of dust particles.

6.7 Weigh the test specimen and the specimen support immersed in water. This is mass C.

6.8 Remove the test specimen. Weigh the test specimen support immersed in water at the same depth as before. This is mass E. Take care to ensure that the suspension support is free of air bubbles and that the suspension wire is not immersed below its normal hanging depth as a change in depth will change the measured mass.

6.9 Measure the temperature of the water to the nearest 1 °C (2 °F) and record its density, ρ_w, at that temperature, from Table 3.

6.10 Calculate the wet density from the following formula:

$$\text{Wet Density, } (\rho_s) = \frac{B\rho_w}{B-(C-E)}$$

7. REPORT

7.1 Density as calculated from the appropriate formula to the nearest 0.01 g/cm³.

8. PRECISION

8.1 The repeatability (r) and reproducibility (R) measurements were determined according to ASTM E691, Practice for Conducting an Interlaboratory Test Program to Determine the Precision of Test Methods and are listed below for ten materials and a range of density values. On the basis of test error alone, the difference in absolute value of two test results obtained in the same laboratory will be expected to exceed (r) only 5% of the time. If such a difference is found to be larger than (r) there is reason to question one or both results. Similarly, the difference in two test results obtained in different laboratories will be expected to exceed (R) only 5% of the time. If the difference is found to be greater than (R) there is reason to question one or both measurements.

Table 4. Precision of Dry (Sintered) Density

Material	Powder Type	Treatment	Number of Labs	Density g/cm³	(r) g/cm³	(R) g/cm³
FC-0205	S	sintered	18	6.21	0.03	0.06
F-0005	S	sintered	23	6.22	0.04	0.05
FN-0208	A	sintered	23	6.95	0.04	0.06
FL-4405	A	sintered	18	7.04	0.03	0.06
FC-0208	S	HT	24	6.43	0.04	0.08
F-0008	A	HT	17	6.68	0.05	0.06
FD-0205	A	HT	23	6.79	0.03	0.06
FLN4-4408	A	HT	23	6.98	0.05	0.07
FC-0205	A	HT	17	7.03	0.05	0.06
FLN-4205	A	HT	24	7.12	0.04	0.07

Notes—A = atomized powder; S = sponge powder; HT=heat treated. The (r) and (R) values were determined from the testing of three transverse rupture test specimens by each participating laboratory.

APPENDIX

A1. COMPARABLE STANDARDS
ASTM B328
ISO 2738

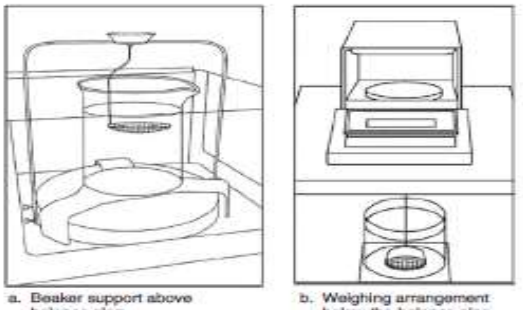

a. Beaker support above balance plan b. Weighing arrangement below the balance plan

FIGURE 1: Methods for Weighing in Water

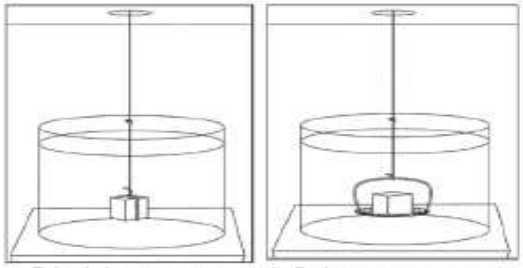

a. Twisted wire arrangement b. Basket support arrangement

FIGURE 2: Methods for Holding the Test Specimen When Weighing in Water

The metric system conversion factors used in this standard are in accordance with IEEE/ASTM SI 10, "Standard for Use of the International System of Units (SI): The Modern Metric System". Recognized as an American National Standard (ANSI), the standard is published by the following organizations: ASTM International, 100 Barr Harbor Drive, West Conshohocken, PA 19428-2959, USA; and Institute of Electrical and Electronics Engineers, Inc., 345 East 47th Street, New York, NY 10017, USA.

This Standard, prepared by the Metal Powder Industries Federation, is subject to periodic revision. Suggestions for revision should be addressed to the Metal Powder Industries Federation, 105 College Road East, Princeton, N.J. 08540-6692. Users of Standards are cautioned to secure the latest editions. Complete edition of standards may be obtained from the Federation at the above address.

Third experimental trail

	Top surface	Angle 15°	Angle 30°	Angle 45°	Angle 60°
Original benchmark	16.54	16.026	13.91	12.9	11.97
Sand blasting	7.21	6.53	6.03	4.56	3.93
Electropolishing	3.06	2.87	3.56	2.03	1.69
Improvement %	0.81	0.82	0.74	0.84	0.85

Comparison results of two stage of post processing, mainly Vapour blasting and Electropolishing

11.2 Appendix (2)

Inclined surface results

Sample	S1	S2	S3	S4	S5
	Ra	Ra	Ra	Ra	Ra
Angle 90°	7.59	8.12	8.53	7.36	7.85
Angle 75°	8.85	9.14	9.813	10.13	8.94
Angle 60°	10.93	10.97	12.62	12.62	10.91
Angle 45°	12.48	12.68	13.05	13.91	11.53
Angle 30°	12.68	12.41	13.56	14.73	12.04
Angle 15°	15.65	14.80	15.05	15.63	15.18
Angle 0°	16.46	16.23	16.14	17.18	16.29

Surface roughness (Ra) of inclined surfaces (µm)

Sample	Ra	Error	Rq	Error	Rz	Error
Angle 90°	7.89	0.457	9.15	1.03	35.21	2.52
Angle 75°	9.37	0.565	11.31	1.722	43.86	2.79
Angle 60°	11.6	0.918	14.86	1.549	50.31	3.16
Angle 45°	12.73	0.866	15.36	2.01	53.28	3.09
Angle 30°	13.08	1.073	16.18	1.906	67.8	3.9
Angle 15°	15.26	0.372	20.24	2.05	71.92	5.22
Angle 0°	16.46	0.420	21.09	2.336	73.97	5.09

Average results of Ra, Rq and Rz with the error

S, No	Angle 90°	Angle 75°	Angle 60°	Angle 45°	Angle 30°	Angle 15°	Angle 0°
S1	7.515	7.524	7.581	7.7821	7.584	7.638	7.629
S2	7.592	7.678	7.486	7.571	7.632	7.693	7.795
S3	7.615	7.503	7.657	7.527	7.612	7.709	7.753
S4	7.658	7.628	7.596	7.568	7.642	7.732	7.612
S5	7.613	7.663	7.624	7.686	7.729	7.661	7.797
Average	7.598	7.599	7.588	7.626	7.639	7.686	7.717
Error	0.0525	0.0806	0.0643	0.1051	0.0545	0.0374	0.0902

Density results of inclined surfaces

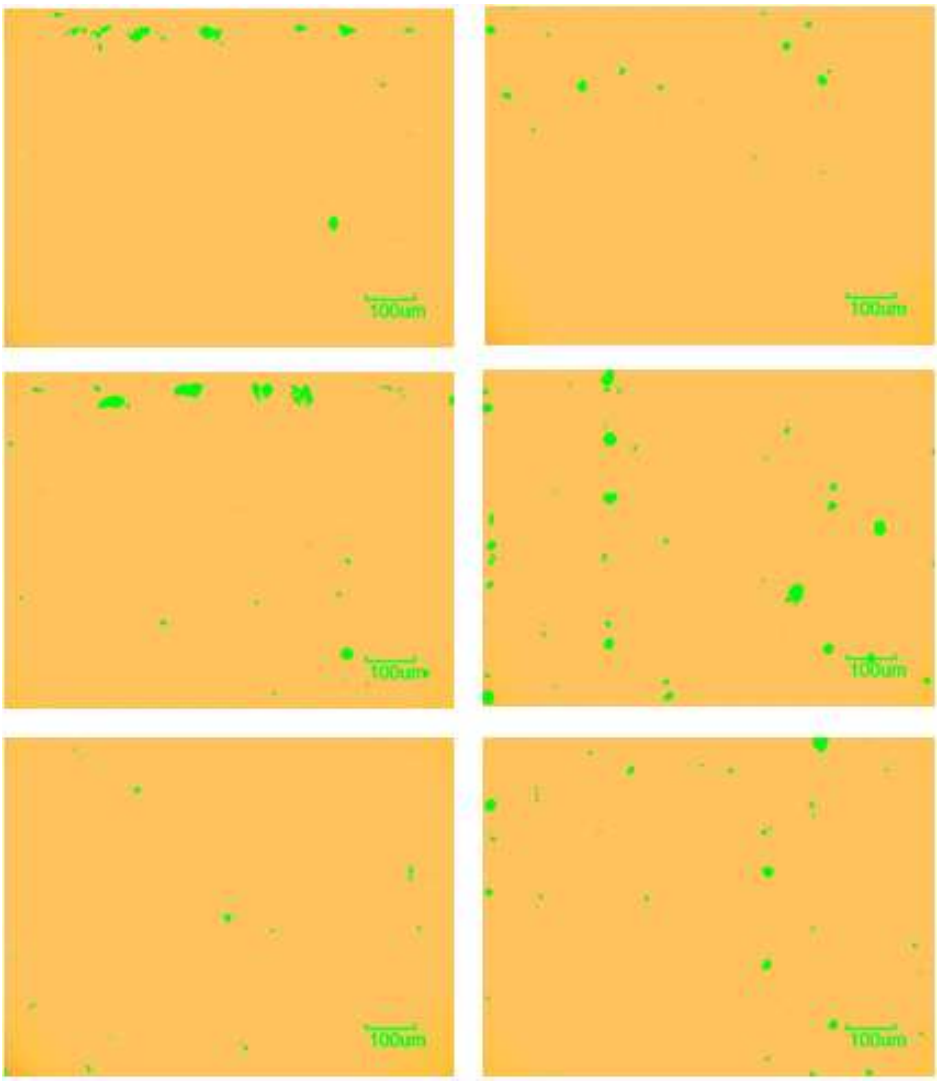

2D micrograph, demonstrated random distribution of porosities and mostly located adjacent to wall side

Laser re-melting setup

Setup the beam diameter at the substrate

		Laser power percentage, requested from 200Watt				
		50%	60%	70%	80%	90%
Nozzle stand-of distance (mm)	124	352	493	620	718	815
	125	274	462	602	705	850
	126		363	511	687	835
	127		321	462	608	821
	128			387	581	789
	129			303	519	717
	130			241	444	674

Beam diameter results (μm) at different stand-of and laser power

		Laser power percentage, requested from 200Watt				
		50%	60%	70%	80%	90%
Nozzle stand-of distance (mm)	124	32	48	91	123	151
	125	25	42	70	106	138
	126		26	55	91	125
	127			38	69	109
	128			26	58	95
	129				42	67
	130				28	45

Depth of re-melted tracks (μm) at different stand-of and laser power

Setup inert gas environment

Area tested	**Nozzle**			**Shielding**			**Nozzle & shielding**		
	2L/min	**4L/min**	**6L/min**	**2L/min**	**4L/min**	**6L/min**	**2L/min**	**4L/min**	**6L/min**
Area1	39	31	17	34	20	14	28	17	14
Area2	43	34	15	27	21	16	31	17	13
Area3	38	25	17	33	19	13	29	15	17
Area4	35	27	18	35	17	15	25	18	13
Average	38.75	29.25	16.75	32.25	19.25	14.5	28.25	16.75	14.25
Error	3.304	4.031	1.258	3.593	1.707	1.290	2.5	1.258	1.899

The amount of oxygen atomic ratio obtained through three different setup of argon flow methods

Effect of laser power and scan speed on the surface finish

	50%	60%	70%	80%	90%
200 mm/min	11.75	5.63	2.83	2.74	2.37
300 mm/min	12.24	7.12	3.74	1.982	2.45
400 mm/min	13.83	11.64	5.36	1.75	1.62
500 mm/min	14.62	14.67	6.32	1.81	1.47
600 mm/min	14.503	13.1966	6.51	2.01	1.67

Surface roughness (Ra) results as function of different speed and laser power

	50%	60%	70%	80%	90%
200 mm/ min	3000	3600	4200	4800	5400
300 mm/min	2000	2400	2800	3200	3600
400 mm/min	1500	1800	2100	2400	2700
500 mm/min	1200	1440	1680	1920	2160
600 mm/min	1000	1200	1400	1600	1800

Energy density (J/cm^2) results as function of different speed and laser power

		Scanning speed (mm/ min)			
		400	500	600	700
Hatch spacing (µ m)	500	1.55	1.49	1.58	1.75
	600	1.72	1.87	2.17	2.63
	700	2.54	2.96	2.81	3.28

Surface roughness results (µm) as results of different feed rate and hatch spacing

Optimizing parameters for re-melting (DOE design and results)

Power	Speed	Hatch spacing	Initial	Response factors							
			Ra(0) ±15%	Ra1	Ra2	Ra3	Ra4	Ra5	Average	Error	Energy density
200	600	600	10	2.19	2.36	2.23	2.41	2.09	2.256	0.129	2000
200	600	500		1.87	2.08	1.74	2.01	1.93	1.926	0.131	2000
200	600	400		1.57	1.76	1.59	1.62	1.72	1.652	0.083	2000
200	500	600		2.49	2.12	2.42	2.46	2.31	2.36	0.151	2400
200	500	500		2.32	1.98	2.21	1.96	2.11	2.116	0.153	2400
200	500	400		1.81	1.69	1.64	1.74	1.51	1.678	0.113	2400
200	400	600		2.49	2.63	2.56	2.32	2.71	2.542	0.149	3000
200	400	500		1.96	1.93	2.13	2.05	2.24	2.062	0.127	3000
200	400	400		1.58	1.51	1.66	1.71	1.61	1.614	0.076	3000
180	600	600		2.1	2.33	2.17	2.28	2.11	2.198	0.103	1800
180	600	500		1.66	1.72	1.77	1.82	1.57	1.708	0.097	1800
180	600	400		1.53	1.56	1.56	1.48	1.71	1.568	0.086	1800
180	500	600		1.86	2.23	1.92	1.81	2.12	1.988	0.179	2160
180	500	500		1.48	1.39	1.62	1.51	1.57	1.514	0.088	2160
180	500	400		1.42	1.47	1.49	1.37	1.46	1.442	0.048	2160
180	400	600		1.92	1.83	2.03	1.85	2.23	1.972	0.164	2700
180	400	500		1.67	1.58	1.62	1.48	1.71	1.612	0.089	2700
180	400	400		1.33	1.49	1.38	1.42	1.45	1.414	0.062	2700
160	600	600		2.18	2.38	2.06	2.25	2.17	2.208	0.118	1600
160	600	500		1.91	2.03	2.17	2.03	1.87	2.002	0.119	1600
160	600	400		1.58	1.98	1.68	1.71	1.63	1.716	0.156	1600
160	500	600		2.15	2.43	2.13	2.32	2.03	2.212	0.161	1920
160	500	500		1.89	1.82	2.12	1.92	1.97	1.944	0.112	1920
160	500	400		1.78	1.66	1.67	1.73	1.56	1.68	0.083	1920
160	400	600		2.14	1.91	2.26	2.02	2.24	2.114	0.148	2400
160	400	500		1.86	1.89	1.75	1.69	1.76	1.79	0.084	2400
160	400	400		1.65	1.41	1.61	1.51	1.54	1.544	0.093	2400

Results data for the response factor Ra obtained after re-melting

(DOE), Statistical analysis

Y-hat Model

Factor	Name	Ra Coeff	P(2 Tail)	Tol	Active
Const		1.682	0.0000		
A	Laser power	0.05900	0.0565	0.2000	X
B	scan speed	0.07633	0.0141	0.2000	X
C	Hatch spacing	0.27444	0.0000	0.2000	X
AB		-0.07183	0.0000	1	X
AC		0.05167	0.0026	1	X
BC		-0.02750	0.1039	1	X
ABC		-0.03075	0.1372	1	X
AA		0.25467	0.0000	1	X
BB		0.00167	0.9441	1	X
CC		0.04500	0.0603	1	X
AAB		-0.07150	0.0153	0.3333	X
ABB		0.00350	0.9043	0.3333	X
AAC		0.02833	0.3316	0.3333	X
ACC		-0.00900	0.7573	0.3333	X
BBC		0.02183	0.4540	0.3333	X
BCC		0.00450	0.8772	0.3333	X

R^2	0.8532
Adj R^2	0.8333
Std Error	0.1300
F	42.8755
Sig F	0.0000
F_{LOF}	3.1185
Sig F_{LOF}	0.0016

Source	SS	df	MS
Regression	11.6	16	0.7
Error	2.0	118	0.0
$Error_{Pure}$	1.5	108	0.0
$Error_{LOF}$	0.4	10	0.0
Total	13.6	134	

Factor	Name	Low	High	Exper
A	Laser power	160	200	180
B	scan speed	400	600	500
C	Hatch spacing	400	600	500

Multiple Response Prediction

	Y-hat	S-hat	99% Confidence Interval Lower Bound	Upper Bound
Ra	1.6818	0.1038	1.371	1.993

S-hat Model

Factor	Name	Ra Coeff	P(2 Tail)	Tol	Active
Const		0.10376	0.0000		
A	Laser power	0.02409	0.0184	0.2000	X
B	scan speed	0.00152	0.8631	0.2000	X
C	Hatch spacing	0.05507	0.0001	0.2000	X
AB		-0.00622	0.2144	1	X
AC		0.00505	0.3072	1	X
BC		-0.01706	0.0046	1	X
ABC		0.00840	0.1748	1	X
AA		0.01956	0.0146	1	X
BB		-0.00896	0.2070	1	X
CC		0.00591	0.3938	1	X
AAB		0.00971	0.2599	0.3333	X
ABB		-0.01182	0.1767	0.3333	X
AAC		-0.02090	0.0278	0.3333	X
ACC		-0.02095	0.0275	0.3333	X
BBC		-0.01989	0.0344	0.3333	X
BCC		-0.00945	0.2721	0.3333	X

R^2	0.9146
Adj R^2	0.7781
Std Error	0.0163
F	6.6967
Sig F	0.0021
F_{LOF}	NA
Sig F_{LOF}	NA

Source	SS	df	MS
Regression	0.0	16	0.0
Error	0.0	10	0.0
$Error_{Pure}$	NA	0	NA
$Error_{LOF}$	NA	0	NA
Total	0.0	26	

Regression table of full factorial results

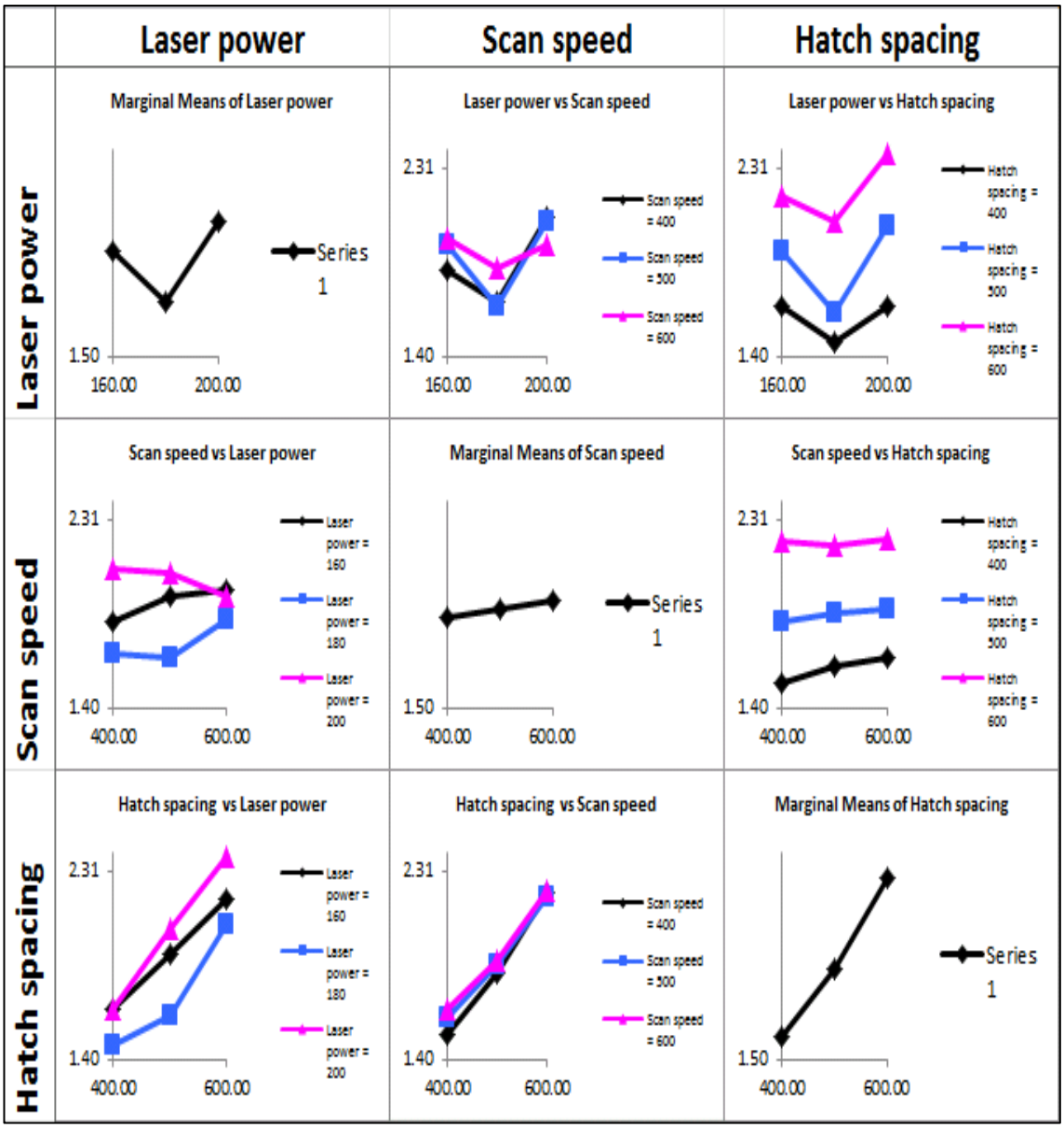

Graphical matrix illustrating factor interactions.

Predicted results of model during reducing of hatch spacing (DOE analysis)

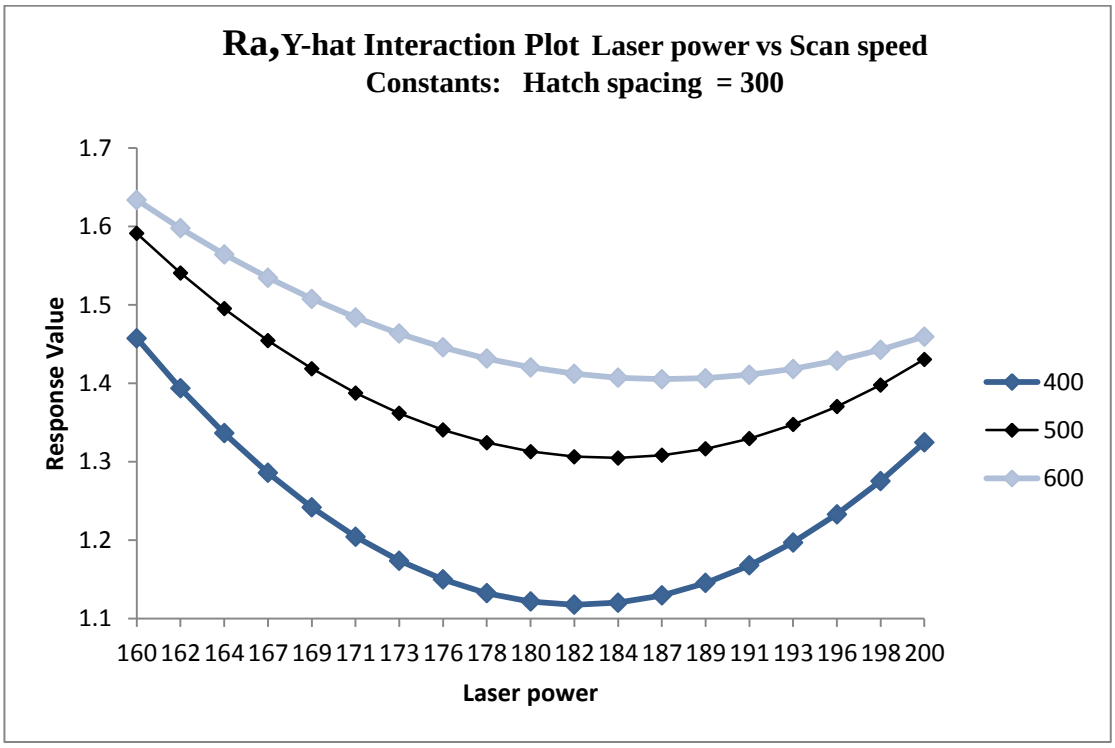

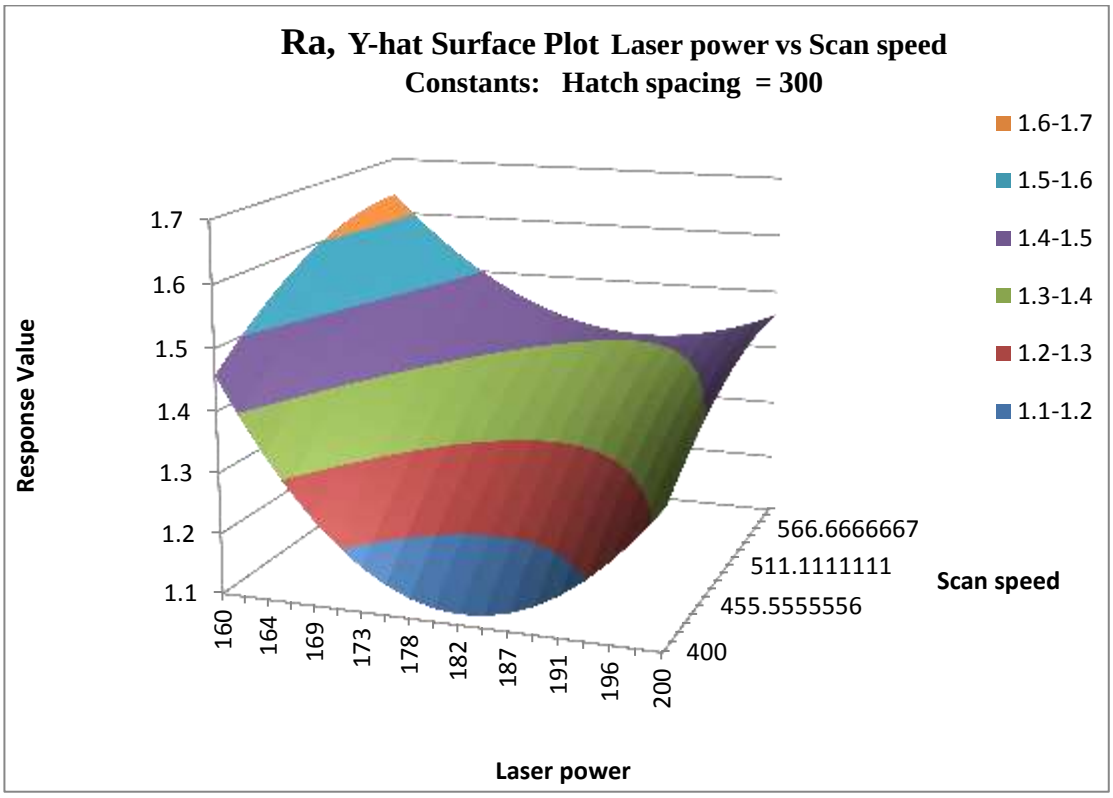

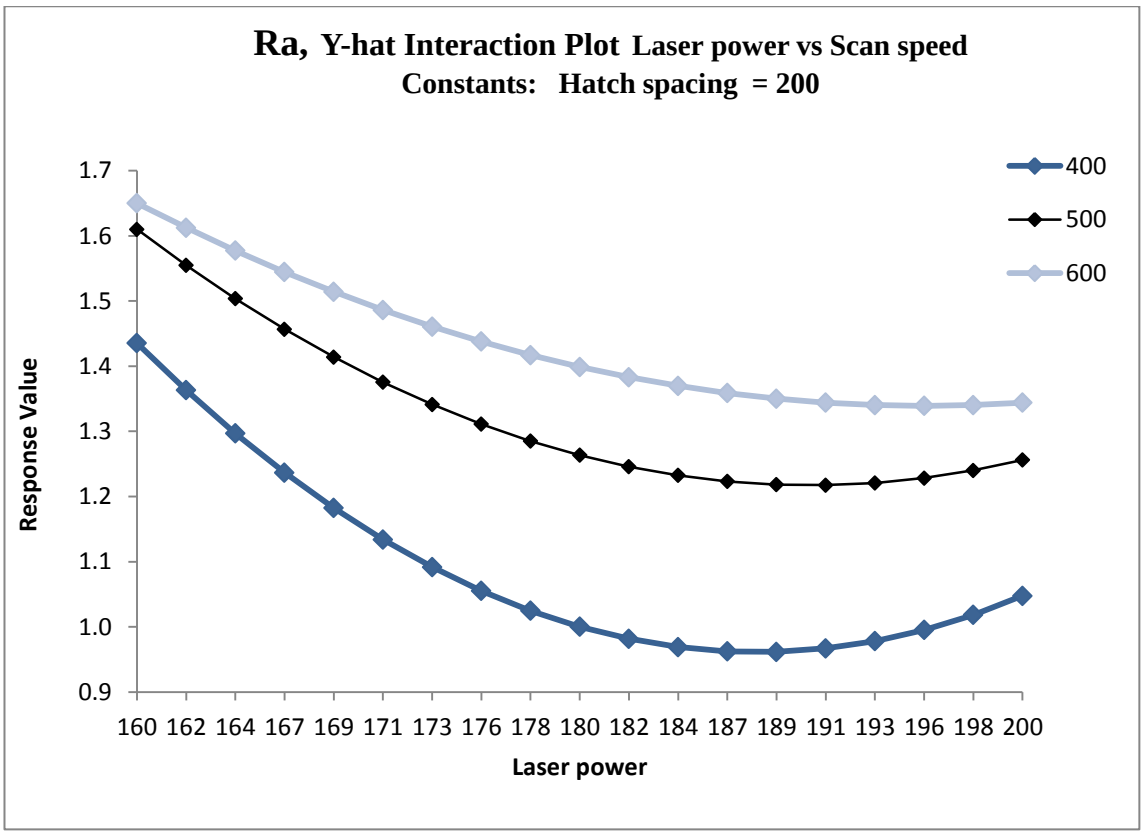
Ra, Y-hat Interaction Plot Laser power vs Scan speed
Constants: Hatch spacing = 200
Response Value
1.7
1.6
1.5
1.4
1.3
1.2
1.1
1.0
0.9
160 162 164 167 169 171 173 176 178 180 182 184 187 189 191 193 196 198 200
Laser power
400
500
600

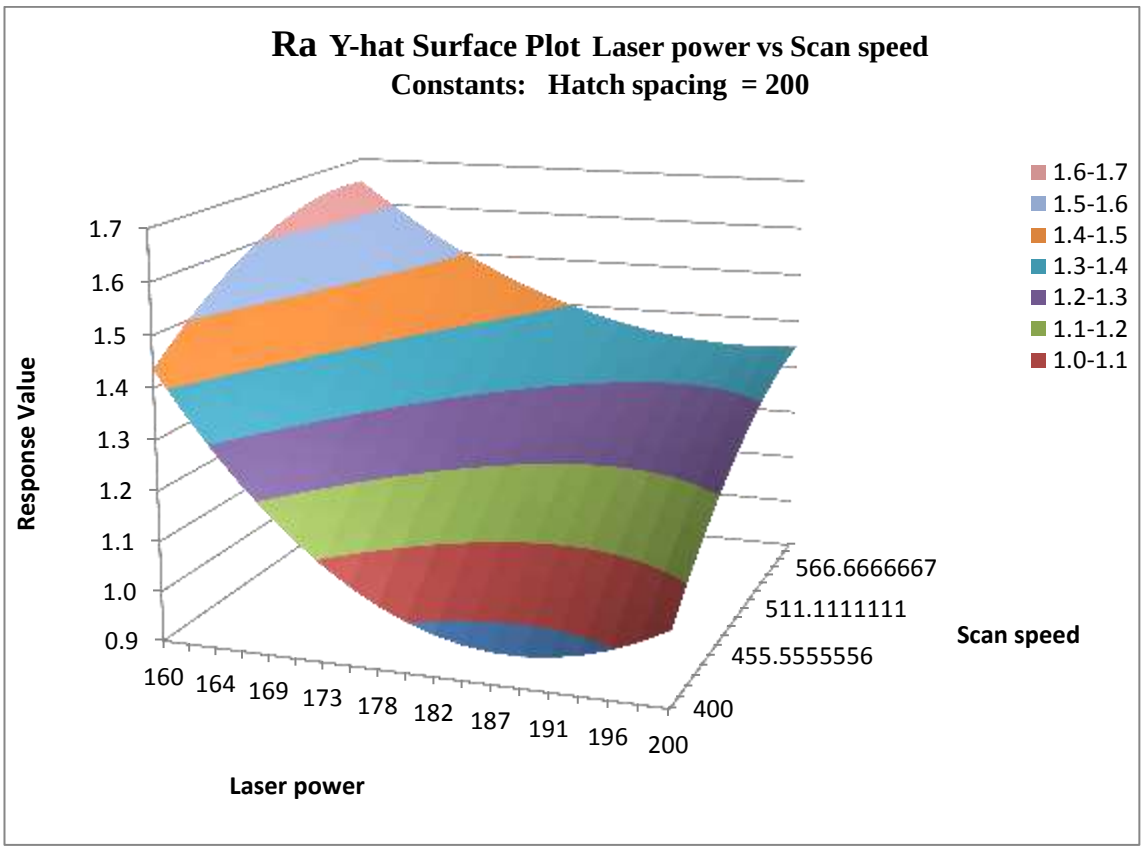
Ra Y-hat Surface Plot Laser power vs Scan speed
Constants: Hatch spacing = 200
Response Value
1.7
1.6
1.5
1.4
1.3
1.2
1.1
1.0
0.9
160 164 169 173 178 182 187 191 196 200
Laser power
566.6666667
511.1111111
455.5555556
400
Scan speed
1.6-1.7
1.5-1.6
1.4-1.5
1.3-1.4
1.2-1.3
1.1-1.2
1.0-1.1

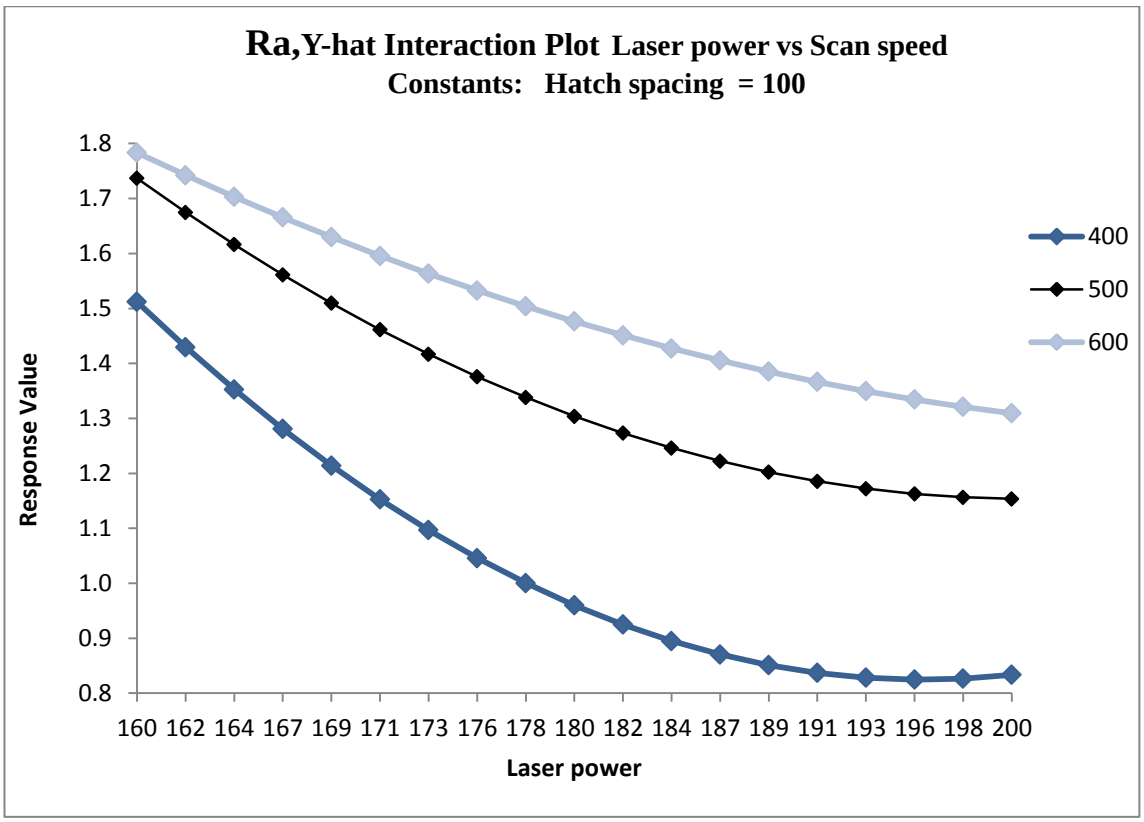
Ra,Y-hat Interaction Plot Laser power vs Scan speed
Constants: Hatch spacing = 100
Response Value
1.8
1.7
1.6
1.5
1.4
1.3
1.2
1.1
1.0
0.9
0.8
160 162 164 167 169 171 173 176 178 180 182 184 187 189 191 193 196 198 200
Laser power
400
500
600

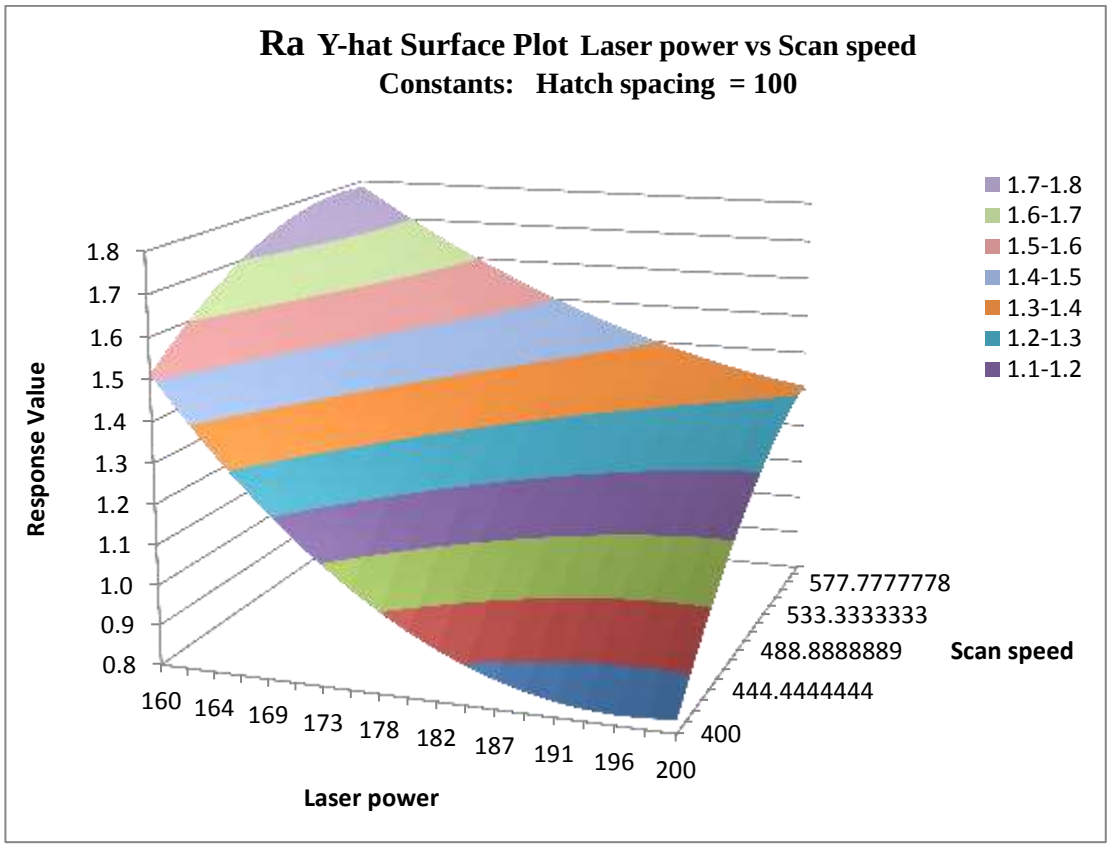
Ra Y-hat Surface Plot Laser power vs Scan speed
Constants: Hatch spacing = 100
Response Value
1.8
1.7
1.6
1.5
1.4
1.3
1.2
1.1
1.0
0.9
0.8
160 164 169 173 178 182 187 191 196 200
Laser power
577.7777778
533.3333333
488.8888889
444.4444444
400
Scan speed
1.7-1.8
1.6-1.7
1.5-1.6
1.4-1.5
1.3-1.4
1.2-1.3
1.1-1.2

Re-melting on different inclined surfaces with optima parameters

Sample angle	Tested sample Ra (μm)			Average	Error
	Ra1	Ra2	Ra3		
Angle 90°	1.63	1.37	1.48	1.49	0.1305
Angle 75°	1.53	1.57	1.49	1.53	0.04
Angle 60°	1.45	1.58	1.67	1.56	0.1106
Angle 45°	1.65	1.46	1.53	1.54	0.096
Angle 30°	1.42	1.49	1.65	1.52	0.1178
Angle 15°	1.55	1.53	1.48	1.52	0.036
Angle 0°	1.49	1.45	1.35	1.43	0.072

Average roughness (Ra) with error obtained on all sample after SLR

Angle	Ra results of re-melted surfaces	Ra of Initial Surfaces
0	1.43	16.46214
15	1.52	15.266
30	1.52	13.086
45	1.546	12.73267
60	1.56	11.612
75	1.53	9.37711
90	1.49	7.89594

Dependence of re-melted Ra and initial Ra on angle of build

11.3 Appendix(3)

Electropolishing

Optimizing parameters for electropolishing (DOE design and results)

Factors			Response factors									
Volt	Time mints	Temperature	**Polished depth (microns)**					**Surface roughness Ra(microns)**				
			Test 1	Test 2	Test 3	**Average**	Error	Ra 1	Ra 2	Ra 3	**Average**	Error
8	60	60	80.964	83.706	75.182	79.951	4.351	0.96	0.72	0.83	0.836	0.120
8	60	40	58.366	61.699	57.195	59.087	2.336	0.73	0.65	0.68	0.686	0.040
8	60	20	13.168	11.371	15.776	13.438	2.214	0.51	0.37	0.43	0.436	0.070
8	45	60	66.438	70.483	66.214	67.712	2.402	0.91	0.84	0.77	0.84	0.07
8	45	40	33.424	35.371	30.587	33.127	2.405	0.69	0.81	0.73	0.743	0.061
8	45	20	13.141	11.549	12.623	12.437	0.811	0.49	0.38	0.41	0.426	0.056
8	30	60	50.928	54.474	48.007	51.136	3.238	0.89	0.75	0.84	0.826	0.070
8	30	40	17.326	18.148	16.631	17.368	0.759	0.57	0.66	0.54	0.59	0.062
8	30	20	11.3031	10.435	9.250	10.328	1.03	0.63	0.47	0.53	0.543	0.080
6	60	60	45.467	43.282	40.687	43.145	2.393	0.43	0.45	0.36	0.413	0.047
6	60	40	20.070	21.464	18.295	19.943	1.588	0.28	0.35	0.38	0.336	0.051
6	60	20	8.798	9.249	7.180	8.409	1.088	0.36	0.42	0.35	0.376	0.037
6	45	60	27.913	30.946	25.873	28.244	2.552	0.42	0.35	0.38	0.383	0.035
6	45	40	12.607	11.760	15.004	13.124	1.682	0.37	0.43	0.35	0.383	0.041
6	45	20	6.2156	6.455	8.358	7.009	1.174	0.43	0.38	0.39	0.4	0.026
6	30	60	21.545	23.987	17.087	20.873	3.498	0.41	0.37	0.45	0.41	0.04
6	30	40	10.728	11.271	10.430	10.810	0.426	0.31	0.33	0.39	0.343	0.041
6	30	20	6.867	7.280	11.490	8.545	2.558	0.39	0.35	0.42	0.386	0.035
4	60	60	15.093	18.422	15.008	16.175	1.947	0.35	0.38	0.31	0.346	0.035
4	60	40	9.497	12.286	9.026	10.270	1.761	0.34	0.3	0.38	0.34	0.04
4	60	20	5.282	3.944	6.039	5.088	1.061	0.36	0.43	0.41	0.4	0.036
4	45	60	13.822	11.523	15.575	13.640	2.032	0.37	0.32	0.39	0.36	0.036
4	45	40	7.064	6.329	6.089	6.494	0.507	0.43	0.35	0.33	0.37	0.052
4	45	20	4.515	4.928	3.909	4.451	0.512	0.42	0.36	0.38	0.386	0.030
4	30	60	11.630	10.089	10.783	10.834	0.771	0.34	0.35	0.4	0.363	0.032
4	30	40	5.396	4.521	7.240	5.719	1.388	0.37	0.34	0.35	0.353	0.015
4	30	20	4.233	3.028	4.861	4.032	0.945	0.48	0.43	0.39	0.433	0.045

Results of two response factors with the error

DOE result analysis

Y-hat Model		Surface roughne				Polishing depth			
Factor	Name	Coeff	P(2 Tail)	Tol	Active	Coeff	P(2 Tail)	Tol	Active
Const		0.37728	0.0000			14.966	0.0000		
A	Potential	0.16519	0.0000	0.2000	X	14.416	0.0000	0.2000	X
B	Time	0.01481	0.3949	0.2000	X	8.009	0.0000	0.2000	X
C	Temperature	0.01389	0.4249	0.2000	X	11.334	0.0000	0.2000	X
AB		0.00528	0.5794	1	X	5.225	0.0000	1	X
AC		0.10389	0.0000	1	X	11.293	0.0000	1	X
BC		0.01222	0.2016	1	X	4.367	0.0000	1	X
ABC		0.01250	0.2853	1	X	2.678	0.0005	1	X
AA		0.13426	0.0000	1	X	5.616	0.0000	1	X
BB		-0.00907	0.5006	1	X	1.260	0.1383	1	X
CC		0.01537	0.2555	1	X	2.976	0.0007	1	X
AAB		-0.00306	0.8529	0.3333	X	1.838	0.0786	0.3333	X
ABB		-0.00861	0.6015	0.3333	X	0.15073	0.8839	0.3333	X
AAC		0.07167	0.0000	0.3333	X	4.423	0.0001	0.3333	X
ACC		-0.02444	0.1412	0.3333	X	0.54883	0.5953	0.3333	X
BBC		-0.01000	0.5444	0.3333	X	0.07304	0.9436	0.3333	X
BCC		-0.02556	0.1243	0.3333	X	-4.196	0.0001	0.3333	X
	R^2	0.9095				0.9760			
	Adj R^2	0.8869				0.9700			
	Std Error	0.0568				3.5612			
	F	40.2154				162.4714			
	Sig F	0.0000				0.0000			
	F_{LOF}	2.0099				14.7299			
	Sig F_{LOF}	0.0502				0.0000			
	Source	**SS**	**df**	**MS**		**SS**	**df**	**MS**	
	Regression	2.1	16	0.1		32967.2	16	2060.5	
	Error	0.2	64	0.0		811.6	64	12.7	
	$Error_{Pure}$	0.2	54	0.0		217.7	54	4.0	
	$Error_{LOF}$	0.1	10	0.0		593.9	10	59.4	
	Total	2.3	80			33778.9	80		

Regression table of full factorial results of response factors

Predicted results of the response factors at different temperature (DOE analysis)

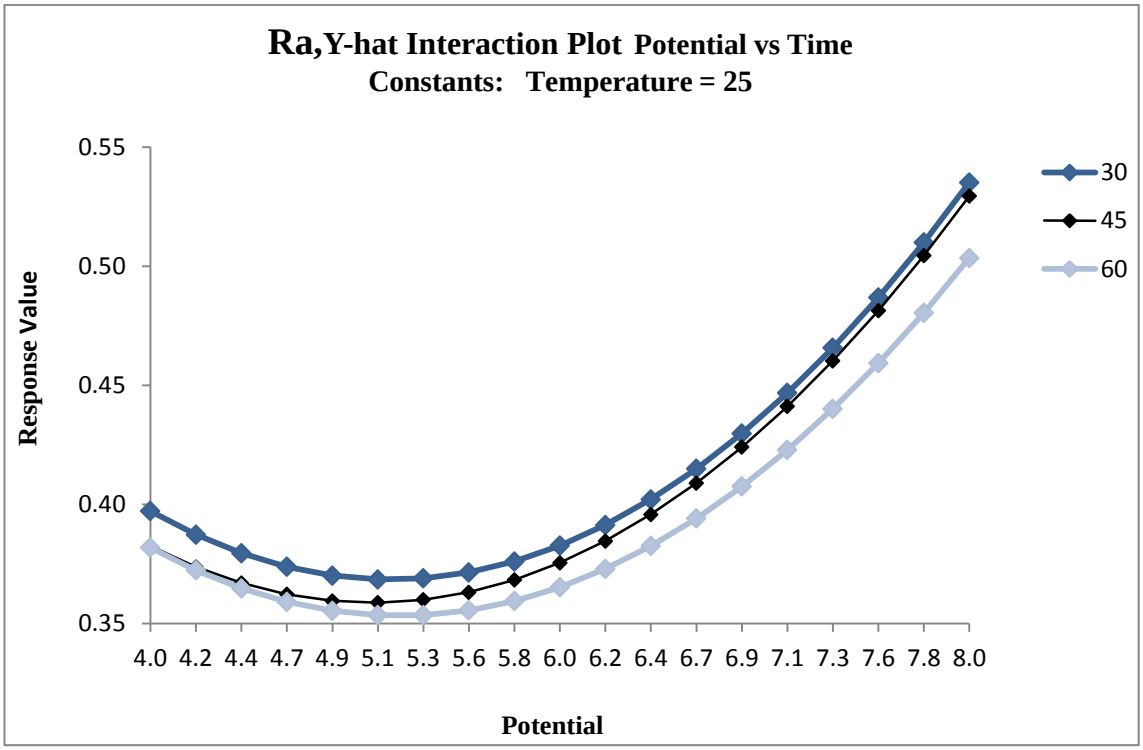

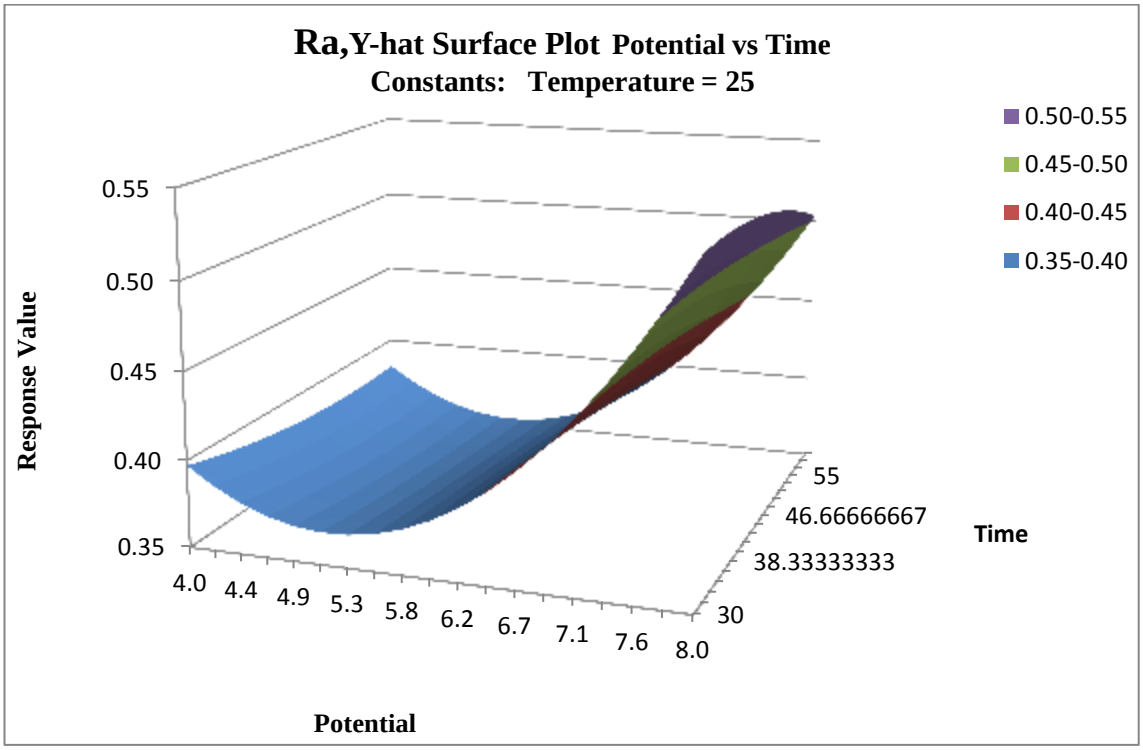

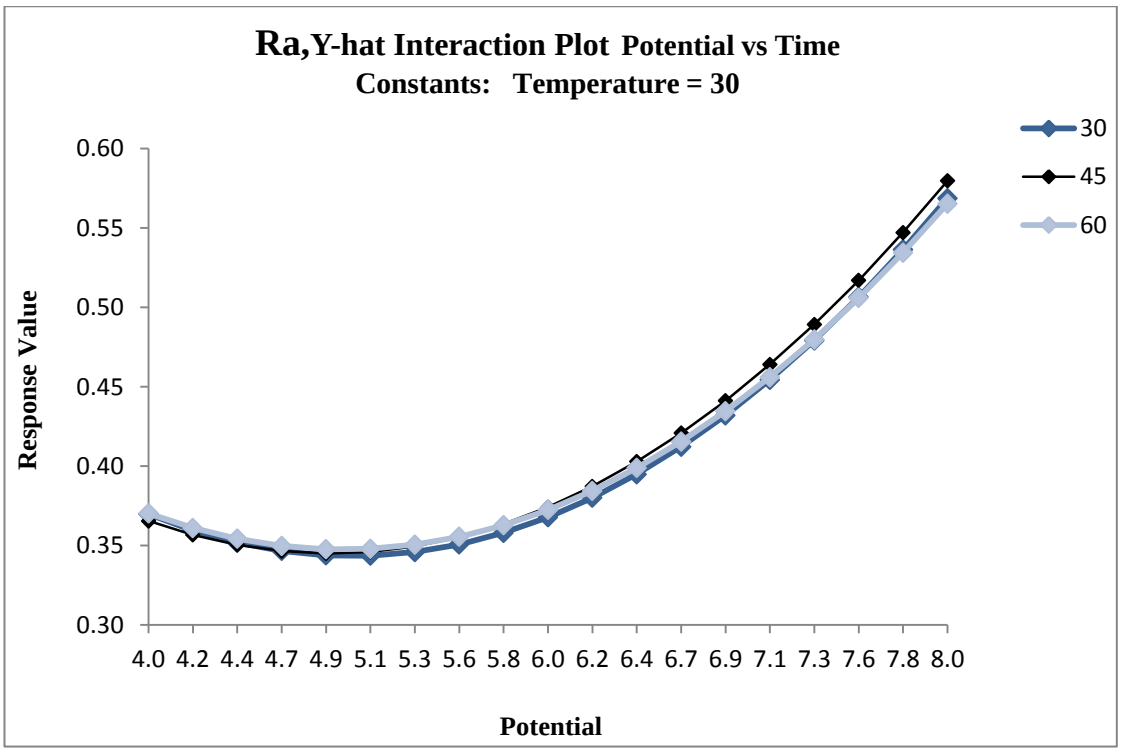
Ra,Y-hat Interaction Plot Potential vs Time
Constants: Temperature = 30
Response Value
0.60
0.55
0.50
0.45
0.40
0.35
0.30
4.0 4.2 4.4 4.7 4.9 5.1 5.3 5.6 5.8 6.0 6.2 6.4 6.7 6.9 7.1 7.3 7.6 7.8 8.0
Potential
30
45
60

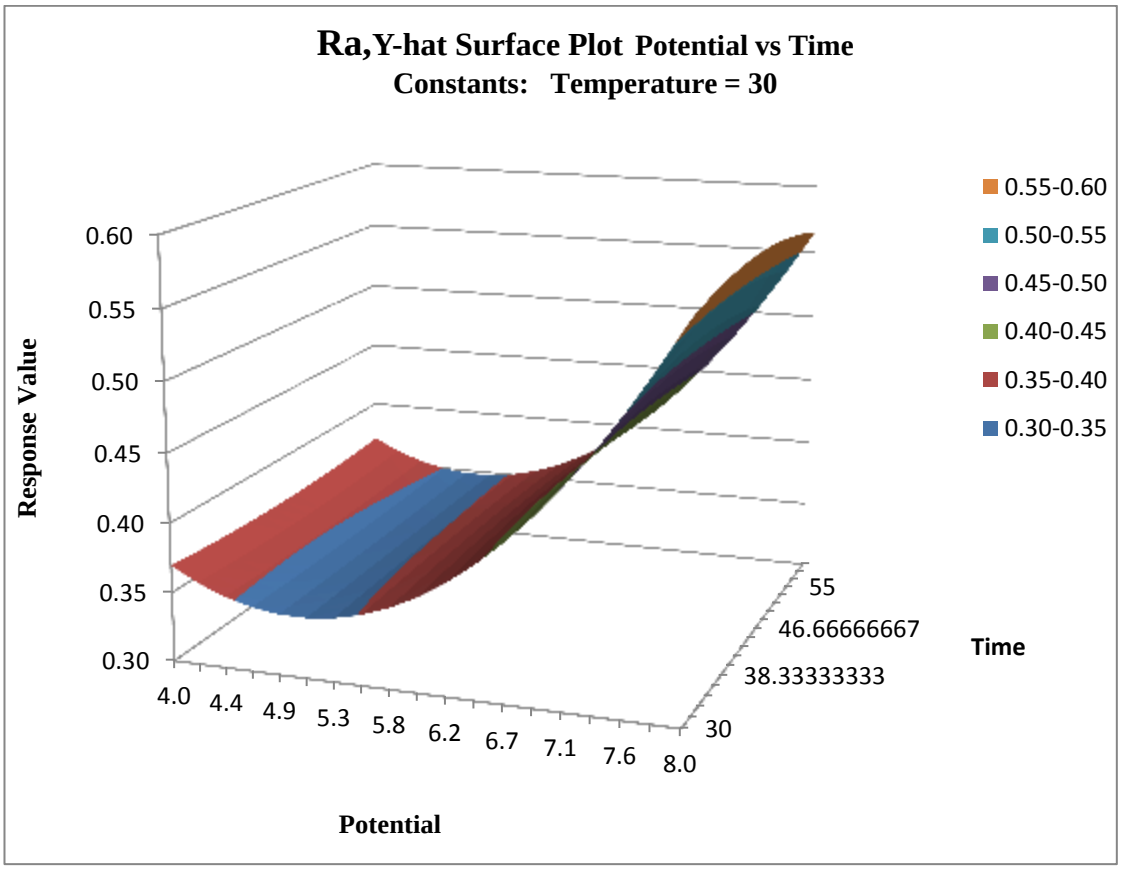
Ra,Y-hat Surface Plot Potential vs Time
Constants: Temperature = 30
Response Value
0.60
0.55
0.50
0.45
0.40
0.35
0.30
4.0 4.4 4.9 5.3 5.8 6.2 6.7 7.1 7.6 8.0
Potential
55
46.66666667
38.33333333
30
Time
0.55-0.60
0.50-0.55
0.45-0.50
0.40-0.45
0.35-0.40
0.30-0.35

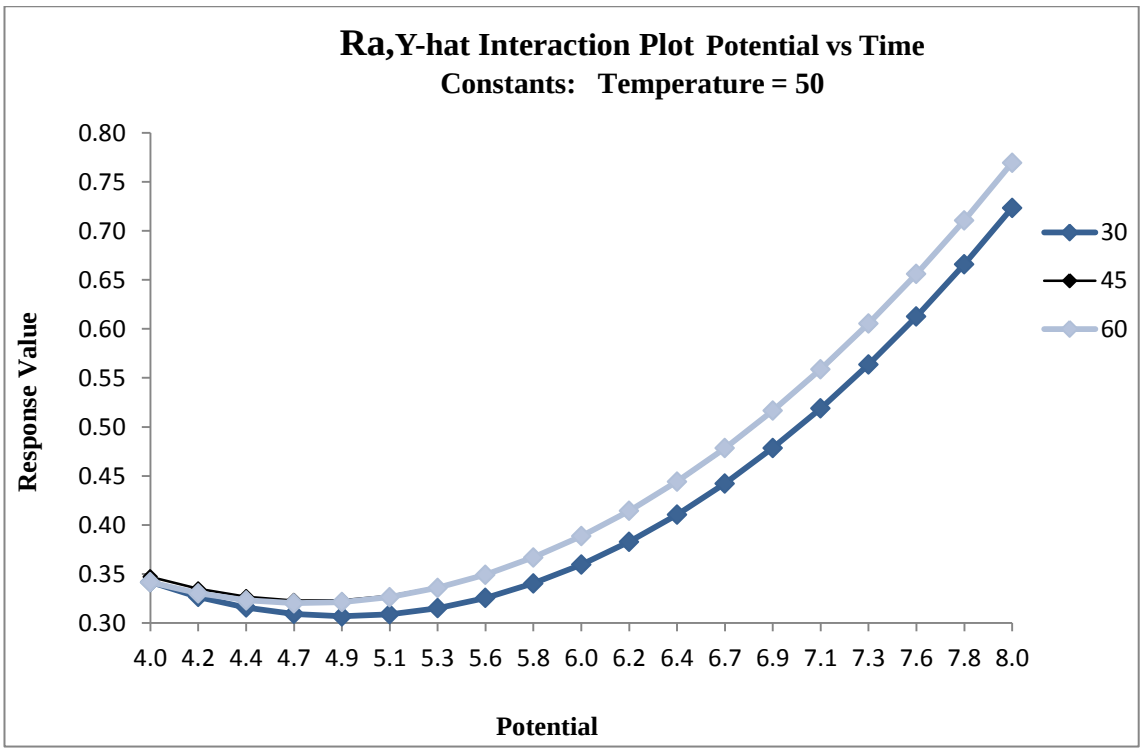
Ra,Y-hat Interaction Plot Potential vs Time
Constants: Temperature = 50
Response Value
0.80
0.75
0.70
0.65
0.60
0.55
0.50
0.45
0.40
0.35
0.30
4.0 4.2 4.4 4.7 4.9 5.1 5.3 5.6 5.8 6.0 6.2 6.4 6.7 6.9 7.1 7.3 7.6 7.8 8.0
Potential
30
45
60

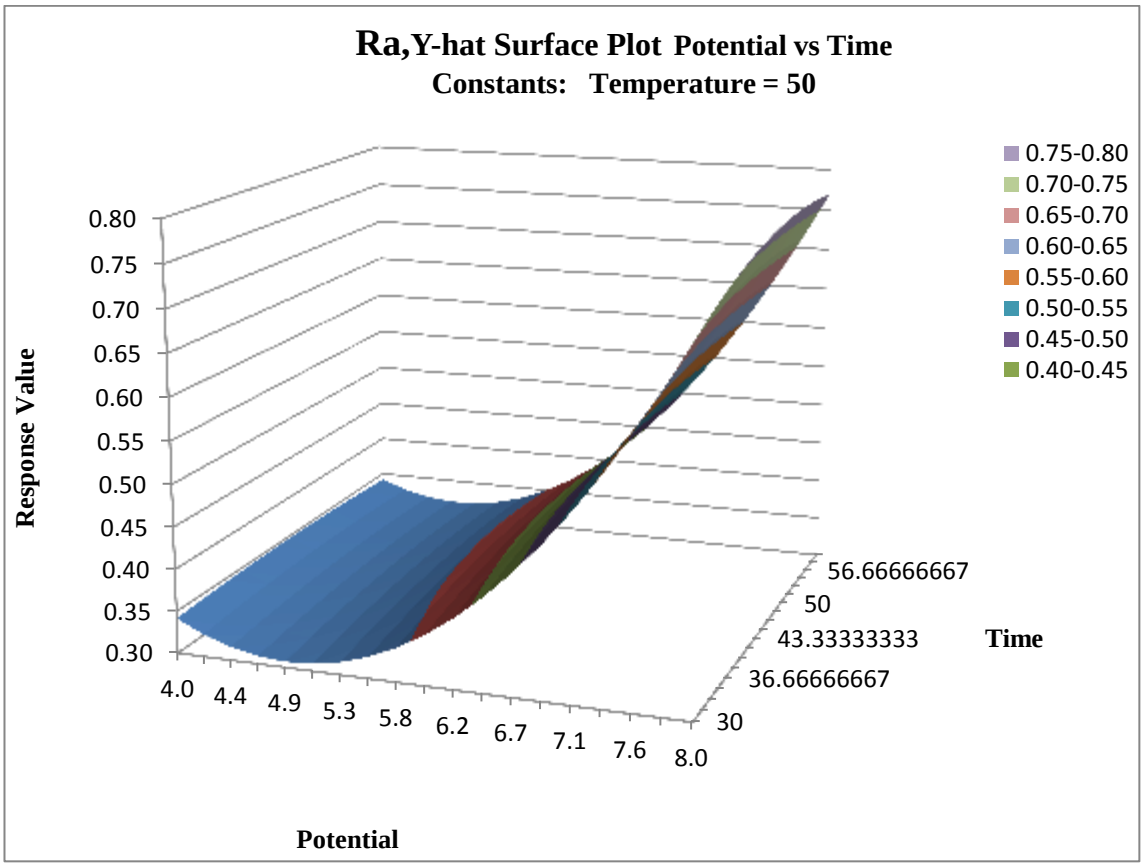
Ra,Y-hat Surface Plot Potential vs Time
Constants: Temperature = 50
Response Value
0.80
0.75
0.70
0.65
0.60
0.55
0.50
0.45
0.40
0.35
0.30
4.0 4.4 4.9 5.3 5.8 6.2 6.7 7.1 7.6 8.0
Potential
56.66666667
50
43.33333333
36.66666667
30
Time
0.75-0.80
0.70-0.75
0.65-0.70
0.60-0.65
0.55-0.60
0.50-0.55
0.45-0.50
0.40-0.45

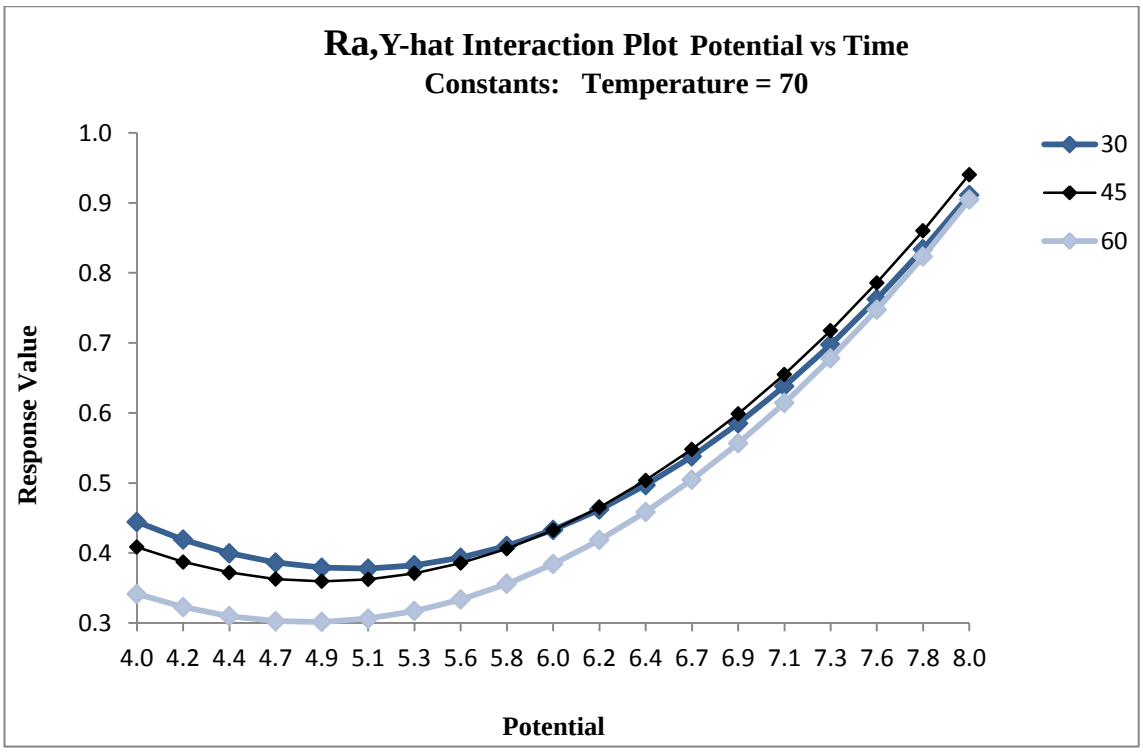
Ra, Y-hat Interaction Plot Potential vs Time
Constants: Temperature = 70
Response Value
1.0
0.9
0.8
0.7
0.6
0.5
0.4
0.3
4.0 4.2 4.4 4.7 4.9 5.1 5.3 5.6 5.8 6.0 6.2 6.4 6.7 6.9 7.1 7.3 7.6 7.8 8.0
Potential
30
45
60

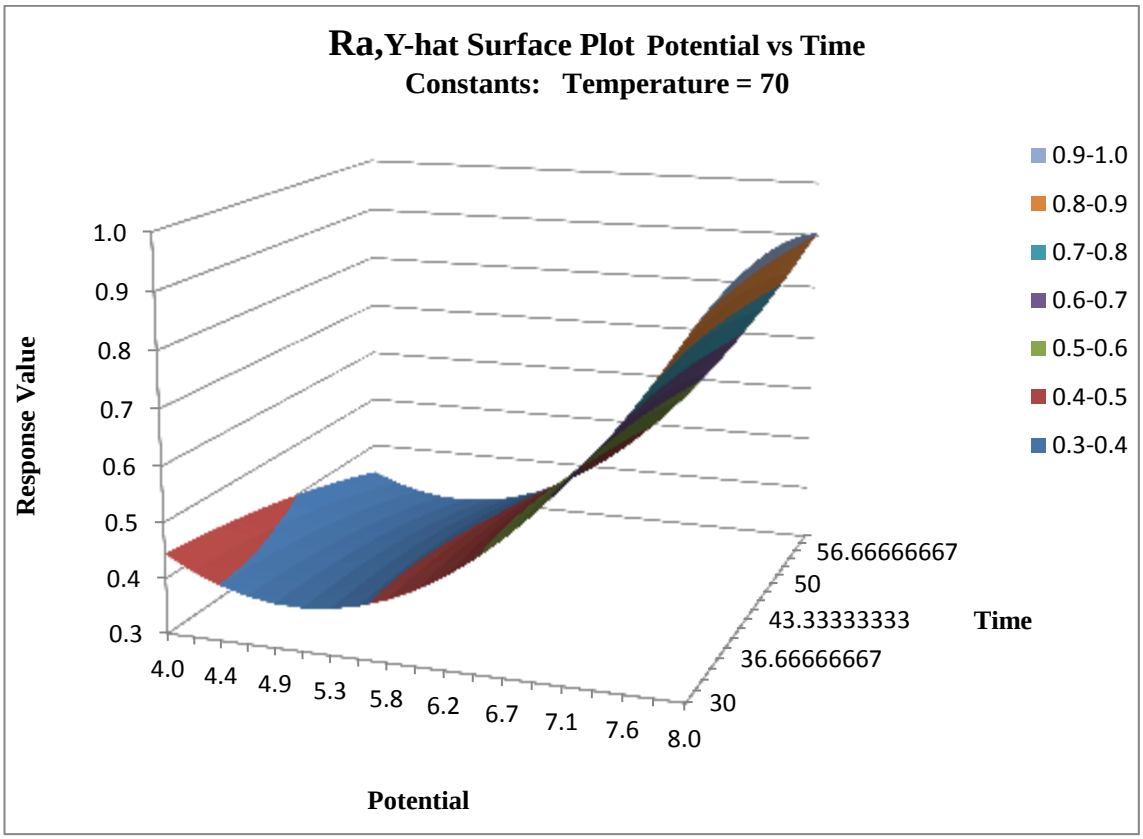
Ra, Y-hat Surface Plot Potential vs Time
Constants: Temperature = 70
Response Value
1.0
0.9
0.8
0.7
0.6
0.5
0.4
0.3
4.0 4.4 4.9 5.3 5.8 6.2 6.7 7.1 7.6 8.0
Potential
56.66666667
50
43.33333333
36.66666667
30
Time
0.9-1.0
0.8-0.9
0.7-0.8
0.6-0.7
0.5-0.6
0.4-0.5
0.3-0.4

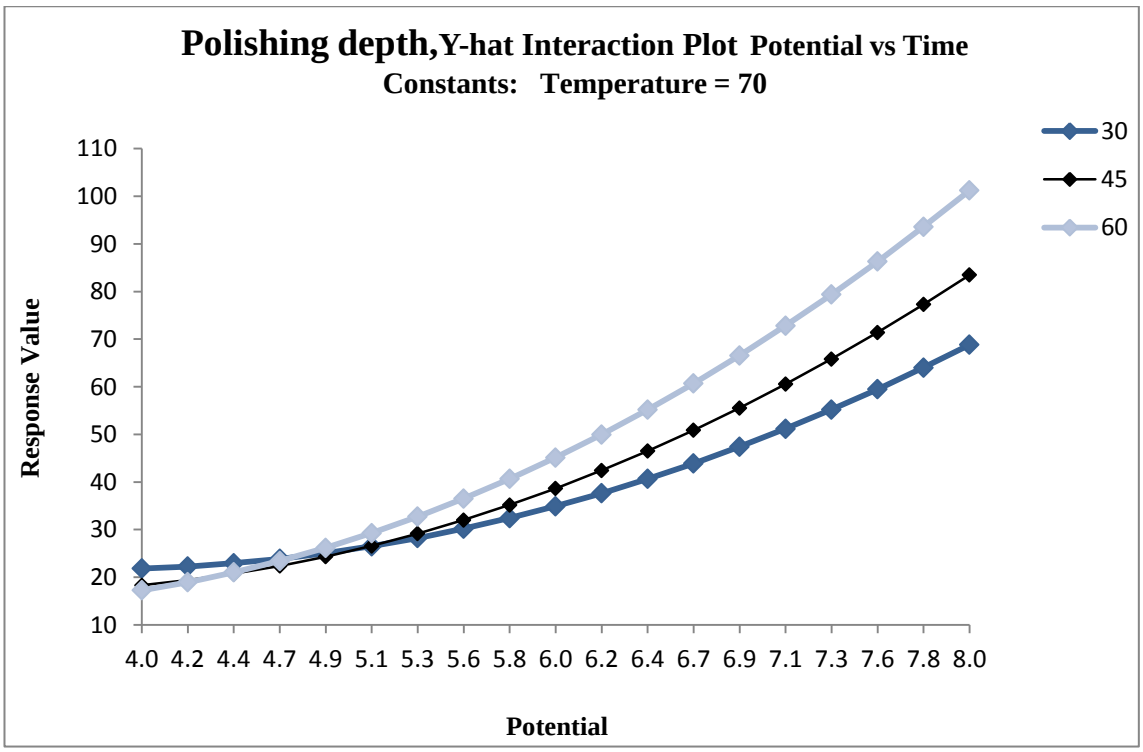
Polishing depth,Y-hat Interaction Plot Potential vs Time
Constants: Temperature = 70
Response Value
110
100
90
80
70
60
50
40
30
20
10
4.0 4.2 4.4 4.7 4.9 5.1 5.3 5.6 5.8 6.0 6.2 6.4 6.7 6.9 7.1 7.3 7.6 7.8 8.0
Potential
30
45
60

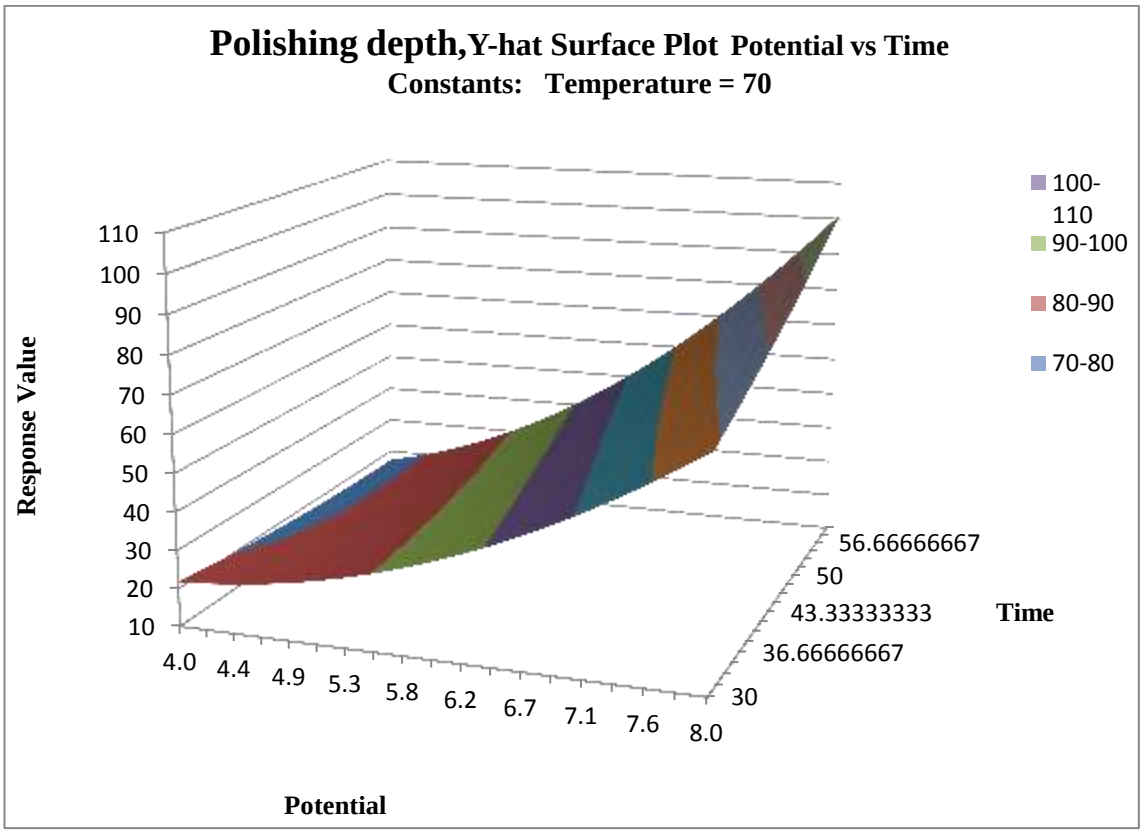
Polishing depth,Y-hat Surface Plot Potential vs Time
Constants: Temperature = 70
Response Value
110
100
90
80
70
60
50
40
30
20
10
4.0 4.4 4.9 5.3 5.8 6.2 6.7 7.1 7.6 8.0
Potential
56.66666667
50
43.33333333
36.66666667
30
Time
100-110
90-100
80-90
70-80

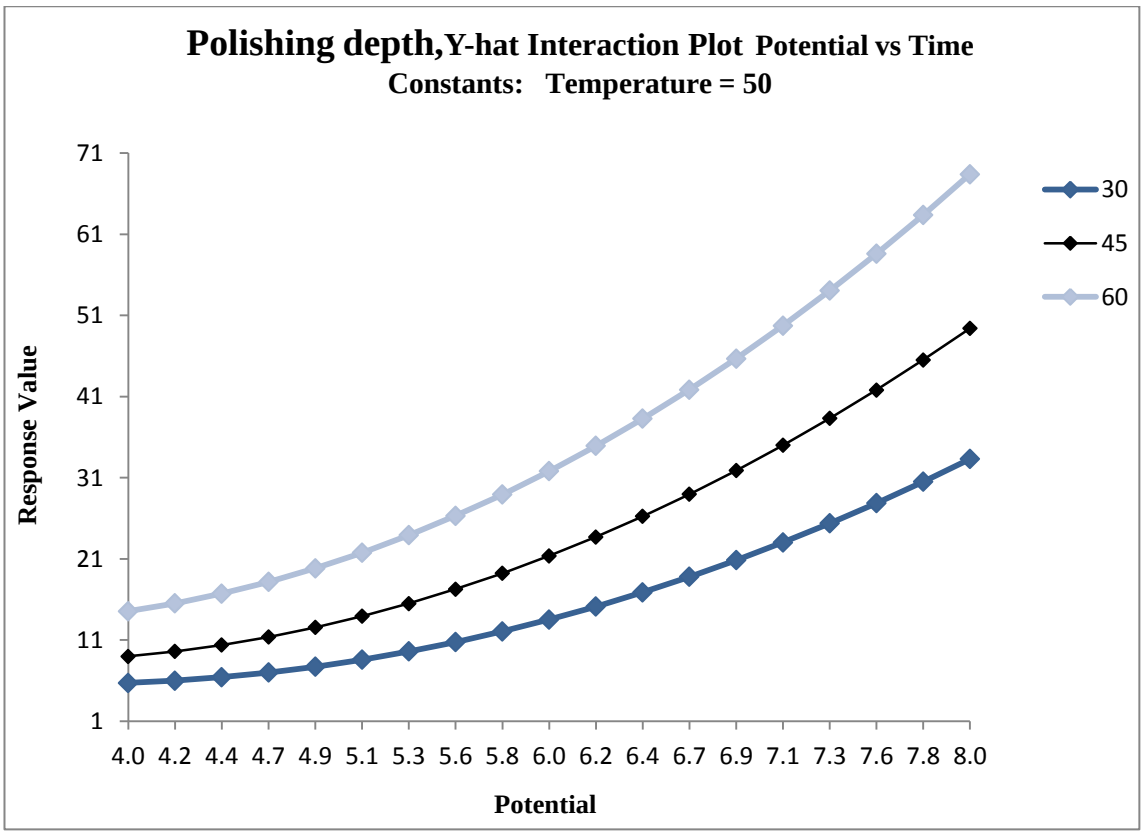
Polishing depth,Y-hat Interaction Plot Potential vs Time
Constants: Temperature = 50
Response Value
71
61
51
41
31
21
11
1
4.0 4.2 4.4 4.7 4.9 5.1 5.3 5.6 5.8 6.0 6.2 6.4 6.7 6.9 7.1 7.3 7.6 7.8 8.0
Potential
30
45
60

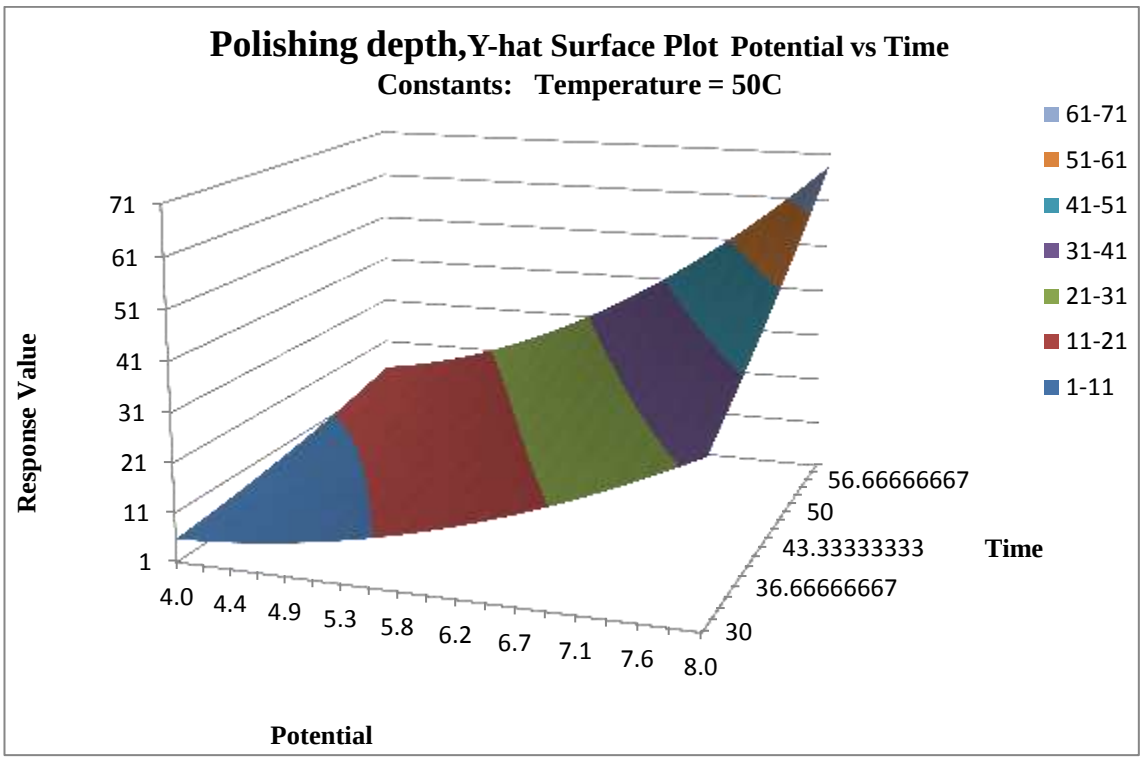
Polishing depth,Y-hat Surface Plot Potential vs Time
Constants: Temperature = 50C
Response Value
71
61
51
41
31
21
11
1
4.0 4.4 4.9 5.3 5.8 6.2 6.7 7.1 7.6 8.0
Potential
56.66666667
50
43.33333333
36.66666667
30
Time
61-71
51-61
41-51
31-41
21-31
11-21
1-11

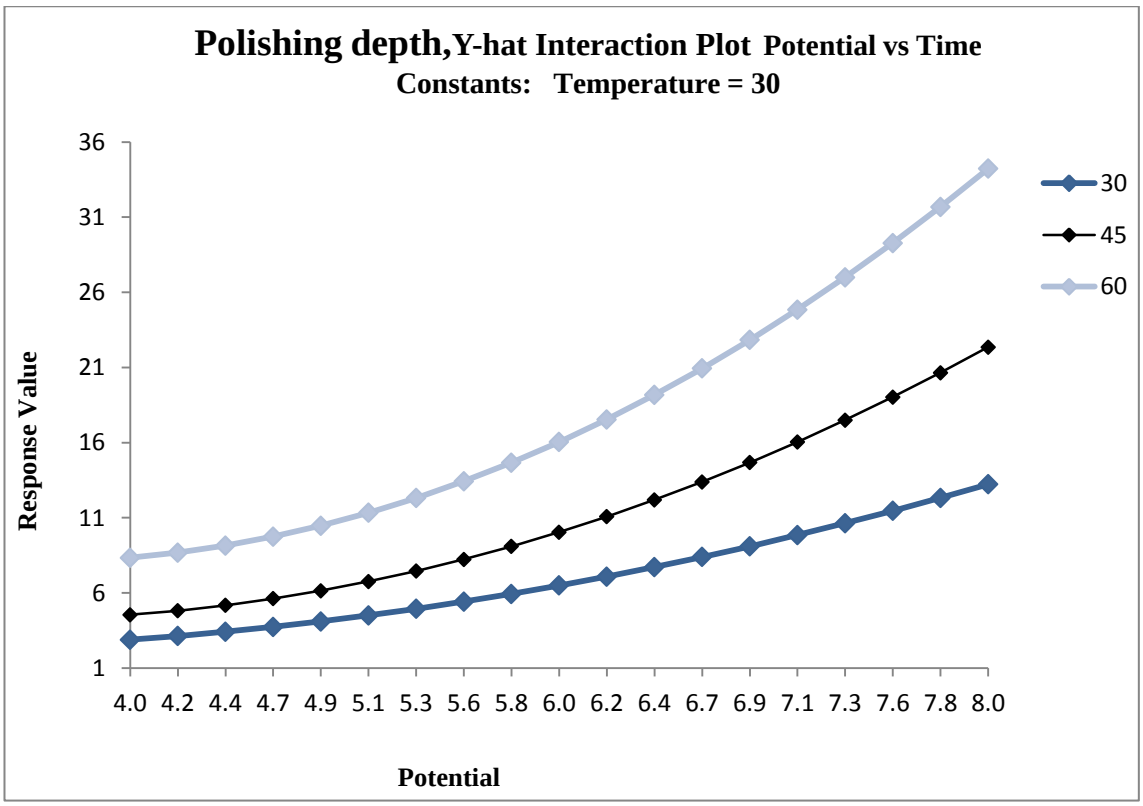
Polishing depth,Y-hat Interaction Plot Potential vs Time
Constants: Temperature = 30
Response Value
36
31
26
21
16
11
6
1
4.0 4.2 4.4 4.7 4.9 5.1 5.3 5.6 5.8 6.0 6.2 6.4 6.7 6.9 7.1 7.3 7.6 7.8 8.0
Potential
30
45
60

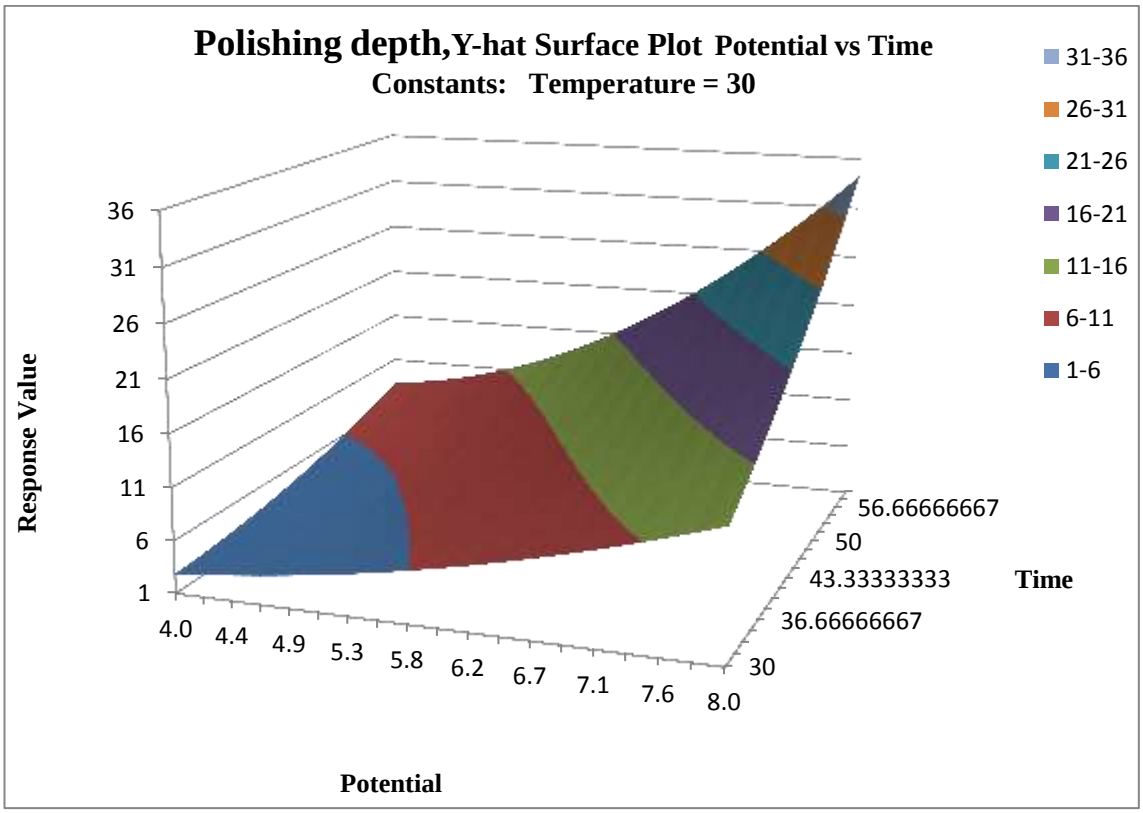
Polishing depth,Y-hat Surface Plot Potential vs Time
Constants: Temperature = 30
Response Value
36
31
26
21
16
11
6
1
4.0 4.4 4.9 5.3 5.8 6.2 6.7 7.1 7.6 8.0
Potential
56.66666667
50
43.33333333
36.66666667
30
Time
31-36
26-31
21-26
16-21
11-16
6-11
1-6

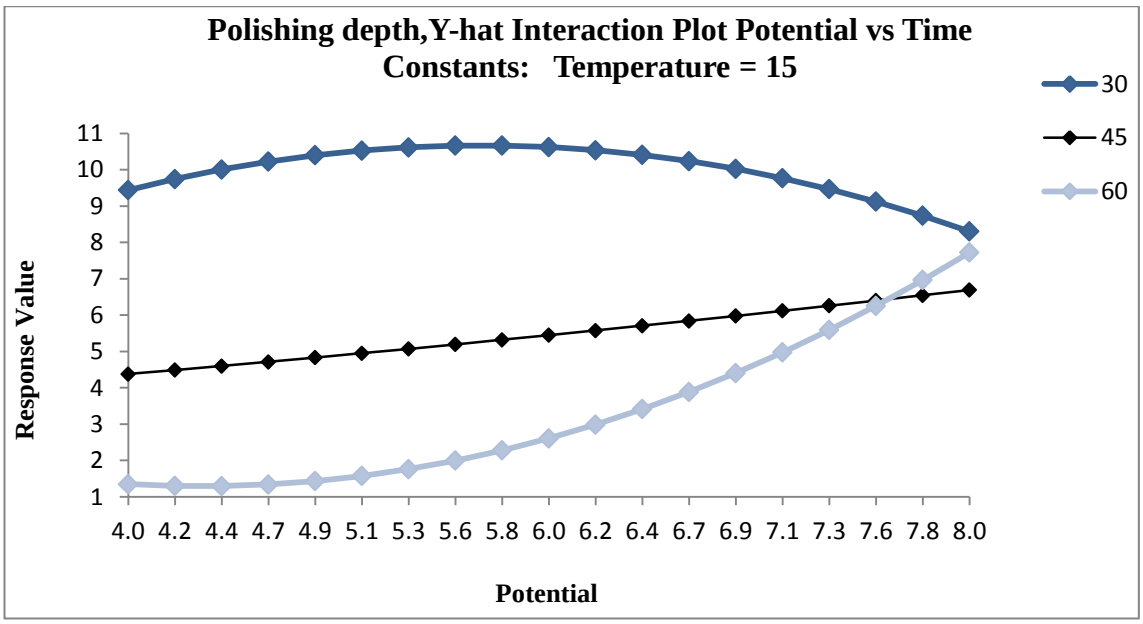

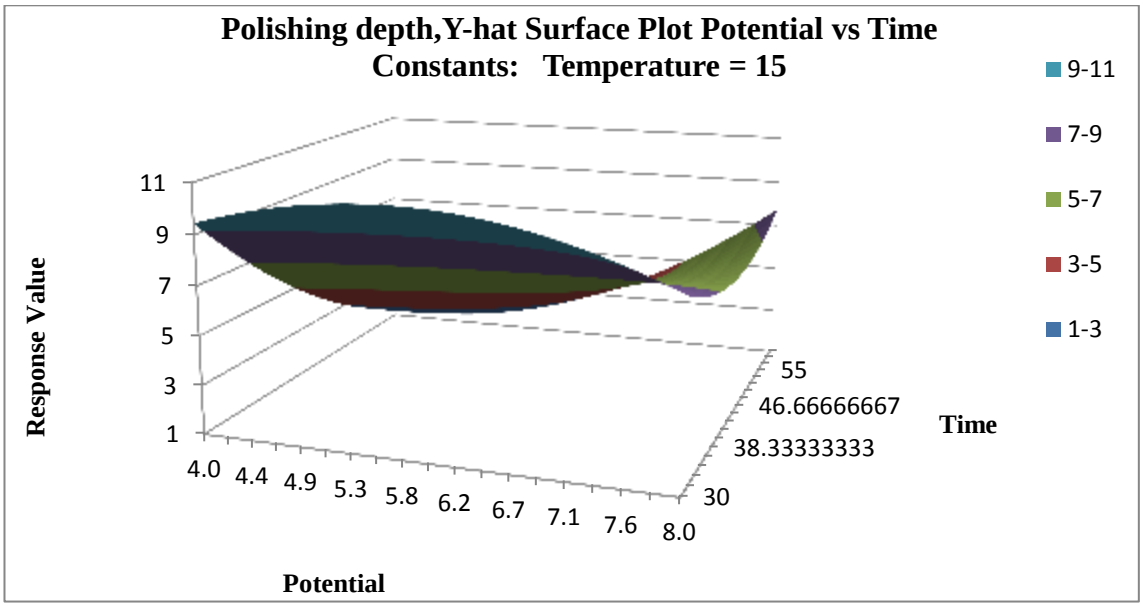

Re-melted	NO, of samples						
Component	1	2	3	4	5	Average	Error
Fe	65.25	68.33	66.92	64.74	67.52	66.552	1.517587
Cr	15.36	16.91	15.74	17.01	16.83	16.37	0.763184
Ni	12.41	11.35	11.86	11.71	12.12	11.89	0.402554
Polished	NO, of samples						
Component	1	2	3	4	5	Average	Error
Fe	66.13	64.87	65.17	64.28	66.05	65.3	0.789557
Cr	17.91	18.35	17.36	17.97	17.28	17.774	0.448364
Ni	11.16	11.94	11.08	11.19	10.97	11.268	0.385188

Chemical component comparison between re-melted and polished samples

Beam results									Fatigue lifetime (number of cycle)				
No,s	L	h	b	I	δ	P	M max	σ max	As fabricated material	Re-melted material	Polished material	Improvement 2-1	Improvement 3-2
1	40	1.03	10.1	0.9197	9	77.599	3.103	1738.10	1618	2046	2272.667	0.26452	0.11078527
2	40	1.03	10.1	0.9197	8	68.977	2.759	1544.98	3302	4274	4843.667	0.29437	0.13328654
3	40	1.03	10.1	0.9197	7	60.355	2.414	1351.85	5476.667	7572	7733.667	0.38259	0.02135059
4	40	1.03	10.1	0.9197	6	51.733	2.069	1158.73	9623.667	11575.7	12706.33	0.20283	0.09767616
5	40	1.03	10.1	0.9197	5	43.110	1.724	965.61	19067.67	24913.3	29009	0.30657	0.16439657
6	40	1.03	10.1	0.9197	4	34.488	1.379	772.49	42028	55738.3	63601	0.32622	0.1410639
7	40	1.03	10.1	0.9197	3	25.866	1.034	579.36	81329.33	103503	123927.7	0.27264	0.1973302
8	40	1.03	10.1	0.9197	2	17.244	0.689	386.24	200000	200000	200000		

Results of fatigue lifetime of samples subjected in stages of surface roughness improvement

As fabricated material			Average	Error	Re-melted samples			Average	Error	polished samples			Average	Error
1497	1765	1592	1618	110.944	2095	1767	2276	2046	258.014	1953	2591	2274	2272.67	319.00209
3520	3405	2981	3302	231.785	3864	4680	4278	4274	408.015	5463	4386	4682	4843.67	556.403
5270	5698	5462	5476.667	175.037	8420	7284	7012	7572	746.876	7412	8625	7164	7733.67	781.813
10072	9126	9673	9623.66	387.775	10726	12647	11354	11575.6667	979.496	13568	11813	12738	12706.3	877.928
19664	18563	18976	19067.6	454.130	27564	23198	23978	24913.3333	2328.44	26394	32985	27648	29009	3499.937
44160	39786	42138	42028	1787.371	52648	60438	54129	55738.3333	4136.85	57982	68524	64297	63601	5305.351
82761	77656	83571	81329.33	2618.403	94846	108736	106928	103503.333	7551.77	115948	133213	122622	123928	8706.240

Beam analysis results and improvement results